Increasing the Efficiency of the Rankine Cycle using a Thermoelectric Heat Pump

Jonathan Peter Siviter

M.Eng

Submitted in fulfilment of the requirements for the

Degree of Doctor of Philosophy

Supervisor: *Prof. Andrew R. Knox*

Academic Year 2013-2014

Abstract

Thermal plants operating on the Rankine cycle are by far the most common method of global electrical power generation. The Rankine cycle, first developed in the late 19th century, continues to this day to be one of the most important practical implementations of a heat engine. Innovation and enhancement of the cycle continues and today's emphasis is directed towards reduced carbon emissions from the combustion of fossil fuel as well as improvement of the absolute efficiency. This thesis presents an increase in the Rankine cycle efficiency through reducing the waste heat rejected from the process by the use of a thermoelectric heat pump.

A thermoelectric heat pump converts a flow of electrical charge carriers to a flow of thermal energy via phonon transport through a semiconductor lattice, described by the Peltier effect. The heat flux through the device can be modulated by varying the electrical voltage and current applied to the semiconductor. Unlike a conventional heat pump, however, the direction of heat transport is determined by the direction of migration of the charge carriers. The efficiency with which the device operates is determined by complex relationship amongst the differential temperature across the device, the geometry of the semiconductor pellets forming the device and the electrical current flow. Peltier effect devices are typically used in small-scale refrigerators, on high-power lasers to aid cooling and to maintain the wavelength stability of optical communications networks.

In this thesis the application of a heat pump to recover a portion of the waste thermal energy normally rejected from the Rankine cycle process after the re-condensation of feed-water in the condenser of a steam turbine is considered. Firstly, a theoretical statement of the required Coefficient of Performance for economic operation of such a system is derived. This is followed by an experimental investigation to determine if the calculated performance is available using today's thermoelectric technology point. The thesis then presents a rigourous analysis of novel experimental apparatus used to characterise the impact of redirecting enthalpy normally rejected from the process to instead reducing the fuel load to the plant and concludes with an assessment of the economic benefits such a heat pump system would bring.

Contents

List of Tables

List of Figures

Acknowledgments

First I would to thank my supervisor Prof. Andrew Knox for his guidance and mentorship throughout this project.
I would like to thank Andrea Montecucco who has been my PhD pal throughout my time, long days and nights in the lab and in the pub.
Thanks to Paul Mullen for the last year of sharing the lab and the jokes.
Thanks to Peter Miller whose help was vital in getting the test apparatus running.
Thanks to James Buckle for his valuable discussions and sanity-checking from the start.
Thanks to Euan McCulloch for his support and in bringing my PhD project together initially.
Thanks to my other colleagues Craig Clanachan, Liam Macisaac, Graham Morton, Matthias Willig, Jeremiah Matthey and Ed Pratt for the distractions and squash games.
Thanks to friends at European Thermodynamics Ltd Kevin Simpson, Mark Robbins and Ashley Fullham for the conference laughs. I would also like to thank my fantastic friends and also my girlfriend Felicity Lumb for her support and patience especially during the 'writing-up' phase.

Finally and above all, I would reserve my greatest thanks for my family Peter, Michael and Jill for their love and support.

Declaration

I declare that, except where explicit reference is made to the contribution of others, this thesis is the result of my own work and has not been submitted for any other degree at the University of Glasgow or any other institution.

Jonathan Peter Siviter
May 2014

List of Acronyms

AC Alternating Current

ASU Air Supply Unit

CAD Computer Aided Design

CAGR Compound Annual Growth Rate

CAPEX Capital Expenditure

CCS CO_2 Capture and Storage

COP Coefficient Of Performance

DC Direct Current

EPRI Electric Power Research Institute

ESP Electro-static Precipitator

FGD Flue Gas Desulphurisation

GDP Gross Domestic Product

GHG Greenhouse Gas

HPT High Pressure Turbine

IGCC Integrate Gasification Combined Cycle

IPT Intermediate Pressure Turbine

LPT Low Pressure Turbine

MPP Maximum Power Point

MPPT Maximum Power Point Tracking

OECD Organisation for Economic Co-operation and Development

ORC Organic Rankine Cycle

PCCC Post Combustion CO_2 Capture

PID Proportional Integral Derivative

PSU Power Supply Unit

PV Photo-voltaic

PWM Pulse Width Modulation

SCR Selective Catalytic Reduction

TE Thermoelectric

TEC Thermoelectric Cooler

TEG Thermoelectric Generator

THP Thermoelectric Heat Pump

TRL Technology Readiness Level

List of publications

Conferences

1. A. Montecucco, J. Siviter, and A. Knox, "Simple, fast and accurate maximum power point tracking converter for thermoelectric generators," *ECCE 2012*, pp. 2777–2783, 2012

2. J. Siviter, A. Knox, J. Buckle, A. Montecucco, and M. Euan, "Megawatt scale energy recovery in the Rankine cycle," in *ECCE2012*, pp. 1374–1379, 2012

Journals

1. J. Siviter, A. Montecucco, and A. Knox, "Rankine Cycle efficiency gain using Thermoelectric Heat Pumps," *Applied Energy*

2. A. Montecucco, J. Siviter, and A. Knox, "Practical Design Considerations for Automotive Thermoelectric Exhaust Energy Recovery Systems," *Applied Energy (under review)*

3. J. R. Buckle, a. Knox, J. Siviter, and a. Montecucco, "Autonomous Underwater Vehicle Thermoelectric Power Generation," *Journal of Electronic Materials*, vol. 42, pp. 2214–2220, Apr. 2013

4. A. R. Knox, J. Buckle, J. Siviter, A. Montecucco, and E. McCulloch, "Megawatt-Scale Application of Thermoelectric Devices in Thermal Power Plants," *Journal of Electronic Materials*, 2013

5. O. Maganga, N. Phillip, K. J. Burnham, A. Montecucco, J. Siviter, A. Knox, and K. Simpson, "Hardware Implementation of Maximum Power Point Tracking for Thermoelectric Generators," *Journal of Electronic Materials*, Feb. 2014

6. A. Montecucco, J. Buckle, J. Siviter, and A. R. Knox, "A New Test Rig for Accurate Nonparametric Measurement and Characterization of Thermoelectric Generators," *Journal of Electronic Materials*, vol. 42, pp. 1966–1973, Mar. 2013

Reports and Patents

1. J. Siviter, "Stirling Engines and Thermoelectric Devices for Heat Scavenging in Oxyfuel and PCCC," tech. rep., 2010

2. A. R. Knox, E. McCulloch, and J. Siviter, "Method and Apparatus for Improvement of Efficiency of Thermal Cycles WO 2012 085551 A2," 2011

Chapter 1

Introduction

There is a growing focus on the environmental impact of rapidly increasing energy consumption in both developed and developing countries. According to the International Energy Agency (IEA) World Energy Report 2013 the demand for energy is set to increase from 87mb/d (million barrels of oil per day) to 102 mb/d by 2035. It is estimated that 80% of this energy will come from fossil fuels with a quarter from the combustion of coal. Thermal power plants are the world's single biggest coal user and improving the cycle efficiency of such plants forms part of a long-term strategy to reduce the carbon footprint of energy production.

The weight of evidence now suggests observed climate changes are anthropogenic in original. The amount of CO_2 released to the atmosphere has come under increased pressure from a legislative standpoint and as such, there is a global imperative to combat, or at least mitigate, the extent to which the climate may change. Current UK Government policy aims to lead the way by setting a target of 60% reduction in CO_2 emissions by 2050. This legislative requirement has spurred the development of CO_2 Capture and Storage (CCS) technologies to lower emissions from these power plants, despite the detrimental impact such technology has on plant efficiency.

An impending 'energy gap' is of concern with many power plants reaching the end of their operating life and therefore to assure an adequate future supply of electricity new plants must be built or existing plants must be upgraded. However, future plant must meet new CO_2 emissions targets enforced by legislation. In combination with plant

cycle efficiency reduction associated with implemention of CCS technologies there is a significant incremental cost factor to be considered on top of what is already turning into a highly political issue. Any additional power generation by heat scavenging technologies such as thermoelectric devices that do not impact CO_2 emissions is of particular interest if it can reduce the cost impact to the plant.

A thermoelectric material is simply a semiconductor which has specific thermal and electrical properties that enables direct conversion of energy between electrical and thermal forms. Devices or modules are comprised of a number of n- and p-type semiconductor pellets connected electrically in series and thermally in parallel. Most current thermoelectric devices are formed by a pair of thin ceramic plates that act as a thermal conductors but an electrical insulator, thereby preserving the series electrical connections of the device.

This thesis examines the ability of thermoelectric devices to capture energy rejected as waste heat from a Rankine cycle thermal power plant. Throughout the thesis, 'thermoelectric heat pump' or 'TEG' refers to a generic device and although BiTe-based devices are used in this work, it is not limited to this material. The Rankine cycle applied to electrical power generation by extracting work from high pressure and high temperature steam is by far the most common method world-wide, and is equally applicable to coal, gas, nuclear and biomass combustion.

1.1 Thesis structure

The following chapters investigate the viability of the addition of a thermoelectric heat pump (THP) to the condenser stage of the Rankine cycle and attempt to quantify the cycle efficiency improvement that this is achievable using technology presently available.

- Chapter 2

In this chapter a brief history of the literature of the Rankine cycle theory and waste heat applications is provided before detailing the literature associated with heat pumping and thermoelectric modules and applications. Initially the motivations for maintaining

development of Rankine cycle thermal power plants are explored in the context of an ever increasing population and resultant demand for more energy. This is developed to show the need for innovations to increase the efficiency of such thermal power plants as these plants are now operating under severe emission restrictions from Governments internationally. The application of a heat pump to the condenser of the Rankine cycle is explored by detailing current use of heat pump applications and other methods of improving the thermal power plant efficiency. Finally, a review of thermoelectric literature including past and present applications.

- Chapter 3

In Chapter 3 thermoelectric device theory is presented, specifically the Seebeck, Peltier effects and Kelvin relationships. These relationships provide the basis to understand the complexities of these small devices as they are applied to large scale applications. A theoretical model of a THP is then introduced. In order to verify predicted theoretical operation, a THP module is characterised and the test apparatus used is presented in this chapter. A drive mechanism for THP devices is described and specifically the advantages of a constant electrical drive being used to maximise the heat and cooling power. A MATLAB model is developed to show the relationship between the coefficient of performance and the pellet dimensions and how this impacts the performance of the THP.

From this, conclusions are drawn about the current capabilities of thermoelectric devices while providing a test-bed for studying the impact of any other thermoelectric device independent of the materials selected. Further, this apparatus is now being used to define international standards for thermoelectric devices by the National Physical Laboratories (NPL).

- Chapter 4

In Chapter 4 the Rankine cycle is detailed with the proposed adjustments and the thermodynamic viability is presented. Of utmost importance in assessing the technical and economic viability of a condenser heat pump is determining the performance needed to achieve break-even or net gain for the process. In this chapter the mathematical model that describes this condition is developed and includes the overall plant energy balance

equations for steady-state operation. This is extended to the Benson Load calculations at the end of the chapter.

The chapter focuses analysis on the Ratcliffe-on-Soar power plant, North East England. Each stage of the Rankine cycle is analysed from an efficiency viewpoint and the impact of adding a thermoelectric device is considered in the reheating of the process fluid returning to the boiler. Specific detail is included in relation to the conditions in the condenser and the necessity to mimic this when developing the test apparatus detailed in Chapter 5.

In order to determine the thermodynamic viability of a heat pump application to the Rankine cycle thermal power plant, a break-even COP is defined and this sets the benchmark for operation of the test apparatus. Chapter four concludes with a Benson load analysis for a thermal power plant and specific operating regimes that can be adopted with a view to improving the thermal efficiency and fuelling requirements.

- Chapter 5

This chapter presents the experimental apparatus required to verify the theoretical model presented in preceding chapter. Each stage of the small-scale Rankine cycle is detailed and calibration data is presented. An important aspect of the experimental apparatus is its ability to reproduce actual plant condenser entry conditions and the use of low temperature and low pressure steam exactly as found in much larger plants. By doing this the apparatus is suitable for use in developing accurate models of the steam process which can be used for calibrated measurements that would form the basis of new standards and specifications.

The boiling unit and associated thermal losses are experimentally validated; the designs of the condensing coils are analysed to ensure the maximum surface area to meet the required cooling capacity; the pump selection is justified and characteristics are experimentally verified; the various mounting configurations of the THP are described and the optimised system is presented in §5.4.

- Chapter 6

Chapter 6 presents the system results and analysis with respect to the theoretical model developed in chapter 4. A MATLAB model is developed to describe the system thermodynamically. Properties interpolated from steam tables is used to calculate the increase in feedwater energy. The experimental results of the Rankine cycle small-scale experiment are described and analysed. The results are calibrated against baseline measurements from the returning feedwater loop to give an accurate estimate of the improvement in thermal performance that a heat pump can make.

The results show that the minimum COP has not been achieved due to intrinsic properties of the test system at the small scale. However, this work represents a first attempt to validate the process and while the result was not conclusive there remains the opportunity to develop an experimental setup to achieve the desired break-even COP.

The discussions and conclusions in chapter 6 reflect on the principal reasons that the experimental apparatus was not able to reproduce the performance expected from larger plant and ways to overcome these difficulties are suggested.

- Chapter 7

The main thrust of the thesis is to present experimental work, however it was identified that there are several other aspects to this work. As such, chapter 7 represents the future work and visions of the project as a whole. The implications of the work contained in this thesis are discussed in this chapter, and a potential exploitation route is briefly discussed.

A cascaded heat pump system is detailed that applies various amount of heat pumping power to achieve a greater feedwater temperature. Various parallel and series configurations of THP devices are considered that are able to achieve the cascade THP system. The electrical requirements for a large scale THP are introduced and the final system integration is described including the use of a 12-pulse AC/DC rectifier to sufficiently power a THP chain. Further, an economic argument is presented over a 4 year payback period using that is independent of the device technology but sensitive to the large number of devices that are required to achieve the cascaded THP system.

- Chapter 8

This chapter summarises the conclusions and provides a thesis review. The outcomes and contributions of the research project are highlighted including the application of a THP to the Rankine cycle; the break-even COP calculation and detail of the test apparatus. The research contribution is detailed which includes the development of a thermoelectric characterisation apparatus and the use of this system for thermoelectric testing standards by NPL (National Physics Laboratory); a design guide for the building of the Rankine cycle test apparatus and a summary of the total saving the THP application would have on a modern Rankine cycle thermal power plant by exploiting the plant availability.

1.2 Original contributions

The following is a list of original contributions to the research presented in this thesis, published in peer-reviewed journals, a patent and in the conference proceedings listings at the start of this thesis.

- The test apparatus to determine the heat pumping performance of a thermoelectric device. This test apparatus is being used as part of work by NPL to develop thermoelectric testing standards. (Chapter 3)
- Testing apparatus that is independent of thermoelectric material composition, and can be applied to any thermoelectric device comprising new and advanced materials. (Chapter 3)
- Experimental apparatus and analysis to determine the low power coefficient of performance using isothermal masses. (Chapter 3)
- Identification of the condenser as a location of potential for large scale energy scavenging technology (Chapter 4)
- The development of a break-even coefficient of performance when applying a generic heat pump to the Rankine cycle. (Chapter 4)
- Engineering of the thermoelectric heat pump and Rankine cycle in to a single test setup and control programme. (Chapter 5)

- The capability of the small-scale Rankine cycle test apparatus to simulate condenser entry conditions. (Chapter 5)

- Use of thermoelectric heat pump in the horizontal position in the Rankine cycle condenser to ensure preferential condensation and efficient removal of condensate droplets (Chapter 5)

- Determination of the minimum economically viable coefficient of performance of the heat pump when applied to the Rankine cycle (Chapter 7)

- Application of a thermoelectric heat pump to reduce the fuel input when the thermal power plant is operating at the Benson load (Chapter 7)

Chapter 2

Literature Review

2.1 Energy consumption

The global population is rising and the energy consumption per capita is also increasing. By 2030, the world population is projected to be 8.3 billion people in data presented by the United Nations Department of Economic and Social Affairs [33]. This equates to a 1.6% compound annual growth rate (CAGR) resulting in a 36% increase by 2030. In real terms, over one billion people more than the world currently has will need energy in the form of thermal energy for heating, 'portable' energy for transport and electrical energy.

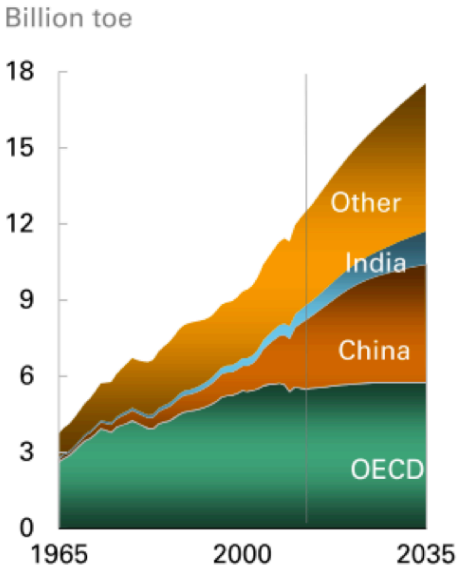

Figure 2.1: Primary energy consumption by region [1]

Figure 2.1 shows the energy increase in billion-tonnes of oil equivalent, where one

tonne of oil equivalent equals 11.63MWh.

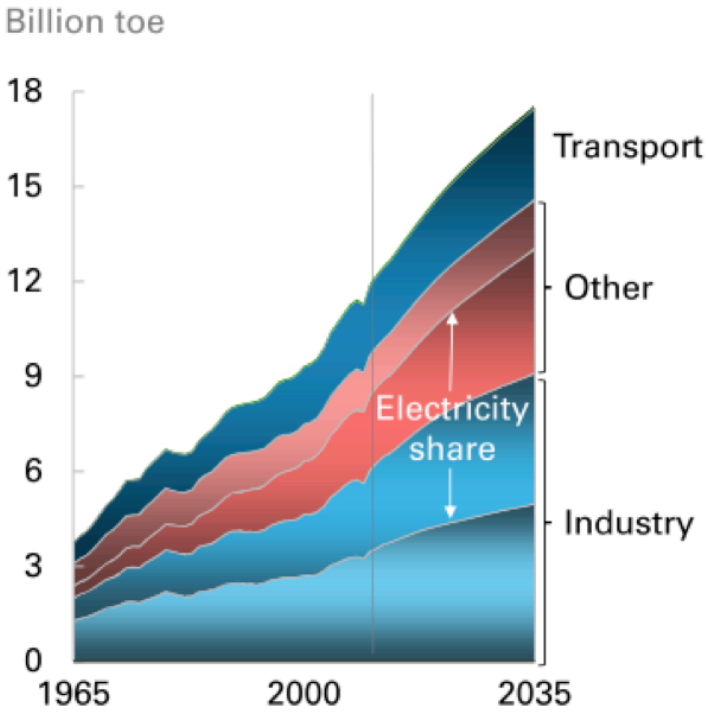

Figure 2.2: Energy consumption by sector [1]

The energy growth in the non-OECD countries of India, China, etc. reflects the population expansion. Further, the breakdown of energy use per sector is shown in Figure 2.2. This predicts the levels of energy use for transport and electricity generation are set to increase to at least 2035.

2.2 Energy demand in infrastructure, transport and electricity

Energy demand can be split in to three primary categories: buildings, transport and electricity. Zhao et al. [34] note that energy consumed in buildings accounts for 40% of energy use including air conditioning, heating and lighting in China. This energy is set to increase despite efficiency improvements due to complexity of being able to predict the actual energy consumption and the large number of influencing factors such as the variance of the occupancy of a building over its lifetime.

The use of energy for transport in China is examined by Wang et al. [2] by focusing

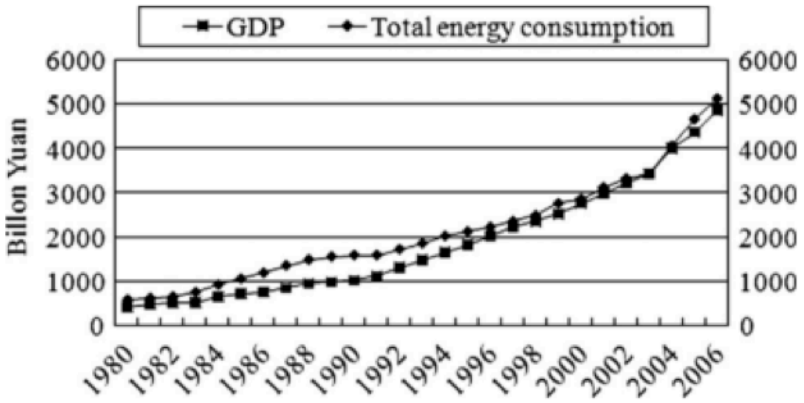

Figure 2.3: Energy consumption in China with increasing GDP [2]

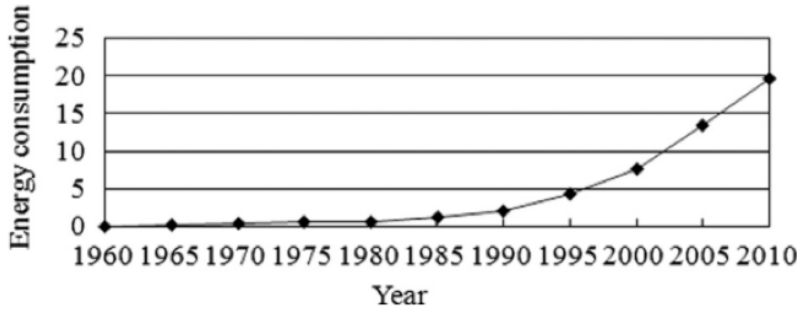

Figure 2.4: Energy consumption in China, compared between 1986 and 2006 [2]

on the wide-ranging transport use from aviation, road and rail. The rate of population growth closely matched the rate of energy consumption across the transport sector (shown in Figure 2.3 and Figure 2.4), and the paper concludes that efficiency improvements mitigate, but do not halt the growth in energy demand. The relationship between growth and transport energy demand is shown in statistics released by the UK Government Department for Energy and Climate Change [3]. These state that energy demand for transport accounts for 36% of all energy consumed in 2011-2012 shown in Figure 2.5. In the long term, the energy consumption in the transport sector is increasing as shown by Figure 2.6. The picture is similar across the world where a review conducted by Weijermars et al. [5] found that 71% (Natural gas and coal shown in Figure 2.7) of the United States of America electricity was generated by fossil-fuels and the electricity consumption accounted for over 20% of energy supplied to residential and commercial users (shown in Figure 2.8). The substantive portion is natural gas (63%) used for heating. Emphasising the widespread use of fossil-fuels to generate heat and electricity over other

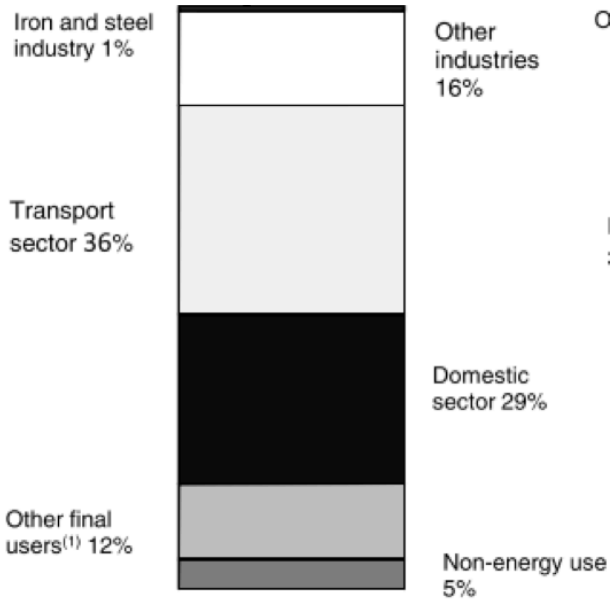

Figure 2.5: Energy consumption in the UK by sector [3]

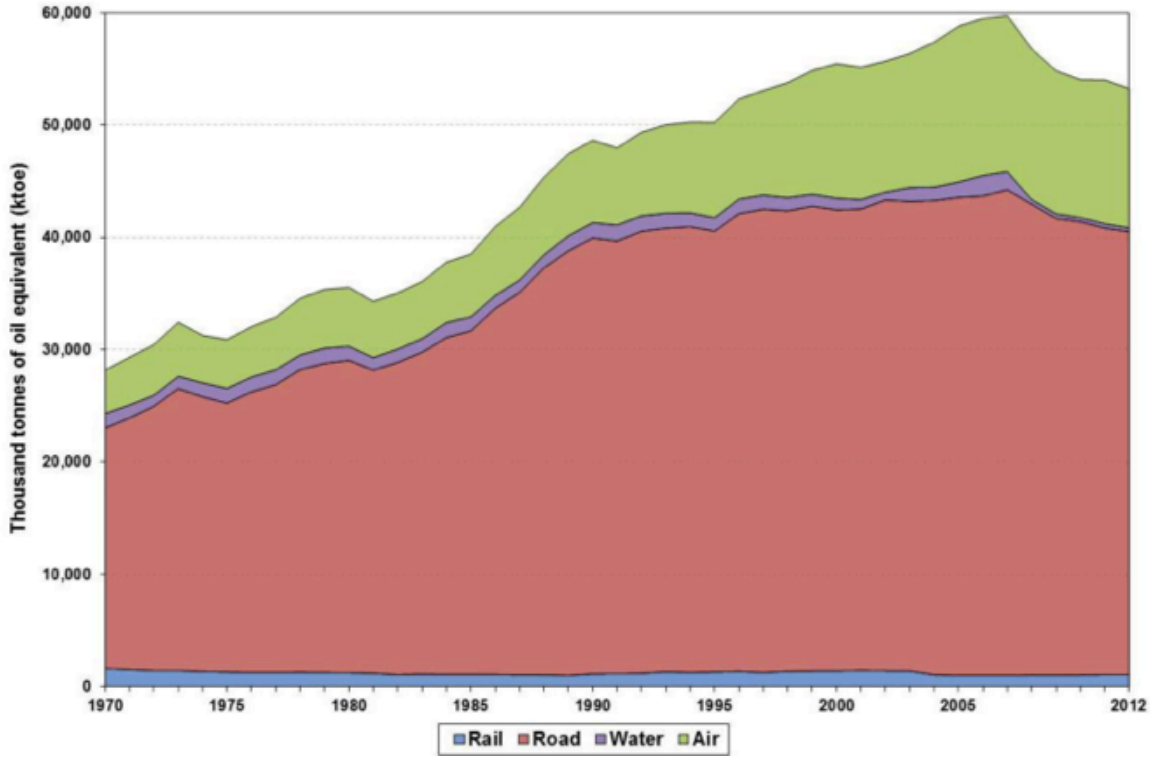

Figure 2.6: Energy consumption in the transport sector of the UK from 1970 to 2012 [4]

all other technology.

BP Energy Projections reports [35] and [1] to the year 2013 shows the energy spectrum diversifies away from fossil-fuels to make way for renewable technology growth. However coal, oil and gas will remain major sources of fuel for electricity generation and these

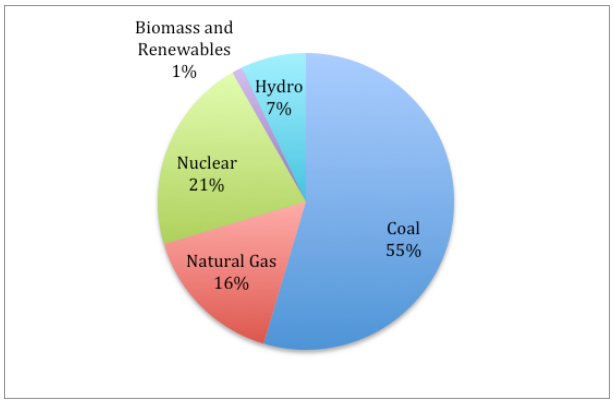

Figure 2.7: Energy sources in the USA [5]

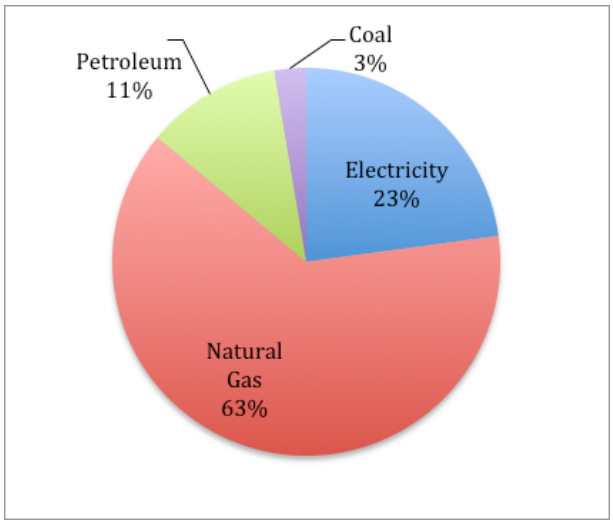

Figure 2.8: Residential and commercial use of energy in the USA [5]

resources are clearly contributors to CO_2 emissions. The reports go on to estimate that the world power generation market will grow by 61%, and with that the CO_2 emissions will increase by 1.2% CAGR per annum. This level of increase is above the levels that are acceptable to mitigate a rise in global temperature, data which is further reinforced by Arora et al. [36]. The authors conclude that if the levels of CO_2 and greenhouse gas (GHG) emissions continue there would be severe consequences; a view that the media often focus on. Increasing levels of GHG and CO_2 emissions, and methods of mitigating these increases has been the subject of a review by Pacala et al. [6]. The world's GHG emissions are split up in to fifteen topics (shown in Figure 2.9), each topic details a section of society that could have the level of GHG emitted reduced. The release of CO_2 is the focus of EU policy and the European Commission's report "Roadmap for moving to a low carbon economy in 2050" [7] presents the motivations to achieve an 80% reduction in green

Option	Effort by 2054 for one wedge, relative to 14 GtC/year BAU	Comments, issues
	Energy efficiency and conservation	
Economy-wide carbon-intensity reduction (emissions/$GDP)	Increase reduction by additional 0.15% per year (e.g., increase U.S. goal of 1.96% reduction per year to 2.11% per year)	Can be tuned by carbon policy
1. Efficient vehicles	Increase fuel economy for 2 billion cars from 30 to 60 mpg	Car size, power
2. Reduced use of vehicles	Decrease car travel for 2 billion 30-mpg cars from 10,000 to 5000 miles per year	Urban design, mass transit, telecommuting
3. Efficient buildings	Cut carbon emissions by one-fourth in buildings and appliances projected for 2054	Weak incentives
4. Efficient baseload coal plants	Produce twice today's coal power output at 60% instead of 40% efficiency (compared with 32% today)	Advanced high-temperature materials
	Fuel shift	
5. Gas baseload power for coal baseload power	Replace 1400 GW 50%-efficient coal plants with gas plants (four times the current production of gas-based power)	Competing demands for natural gas
	CO_2 Capture and Storage (CCS)	
6. Capture CO_2 at baseload power plant	Introduce CCS at 800 GW coal or 1600 GW natural gas (compared with 1060 GW coal in 1999)	Technology already in use for H_2 production
7. Capture CO_2 at H_2 plant	Introduce CCS at plants producing 250 MtH_2/year from coal or 500 MtH_2/year from natural gas (compared with 40 MtH_2/year today from all sources)	H_2 safety, infrastructure
8. Capture CO_2 at coal-to-synfuels plant	Introduce CCS at synfuels plants producing 30 million barrels a day from coal (200 times Sasol), if half of feedstock carbon is available for capture	Increased CO_2 emissions, if synfuels are produced without CCS
Geological storage	Create 3500 Sleipners	Durable storage, successful permitting
	Nuclear fission	
9. Nuclear power for coal power	Add 700 GW (twice the current capacity)	Nuclear proliferation, terrorism, waste
	Renewable electricity and fuels	
10. Wind power for coal power	Add 2 million 1-MW-peak windmills (50 times the current capacity) "occupying" 30×10^6 ha, on land or offshore	Multiple uses of land because windmills are widely spaced
11. PV power for coal power	Add 2000 GW-peak PV (700 times the current capacity) on 2×10^6 ha	PV production cost
12. Wind H_2 in fuel-cell car for gasoline in hybrid car	Add 4 million 1-MW-peak windmills (100 times the current capacity)	H_2 safety, infrastructure
13. Biomass fuel for fossil fuel	Add 100 times the current Brazil or U.S. ethanol production, with the use of 250×10^6 ha (one-sixth of world cropland)	Biodiversity, competing land use
	Forests and agricultural soils	
14. Reduced deforestation, plus reforestation, afforestation, and new plantations.	Decrease tropical deforestation to zero instead of 0.5 GtC/year, and establish 300 Mha of new tree plantations (twice the current rate)	Land demands of agriculture, benefits to biodiversity from reduced deforestation
15. Conservation tillage	Apply to all cropland (10 times the current usage)	Reversibility, verification

Figure 2.9: Greenhouse gas emissions targets [6]

house gas emissions by 2050. Figure 2.10 shows a breakdown of various CO_2 producing sectors of society and the challenges facing them to reach the desired reduction.

Electricity demand and greenhouse gas emissions across the world is the focus of work by Khan et al. [37]. The authors surmise that the increasing energy consumption is leading to increased levels of green house gas emissions. However they note that there is a negative correlation between government and international bodies sanctioning GHG emission reductions and a decline in that countries GDP. The trade off therefore becomes meeting the GHG emissions deadlines while allowing the gross domestic product of the affected country to naturally develop. GHG emissions targets by the EU and UK Government should not be reduced, driven by short-term economic benefits to recover from recession.

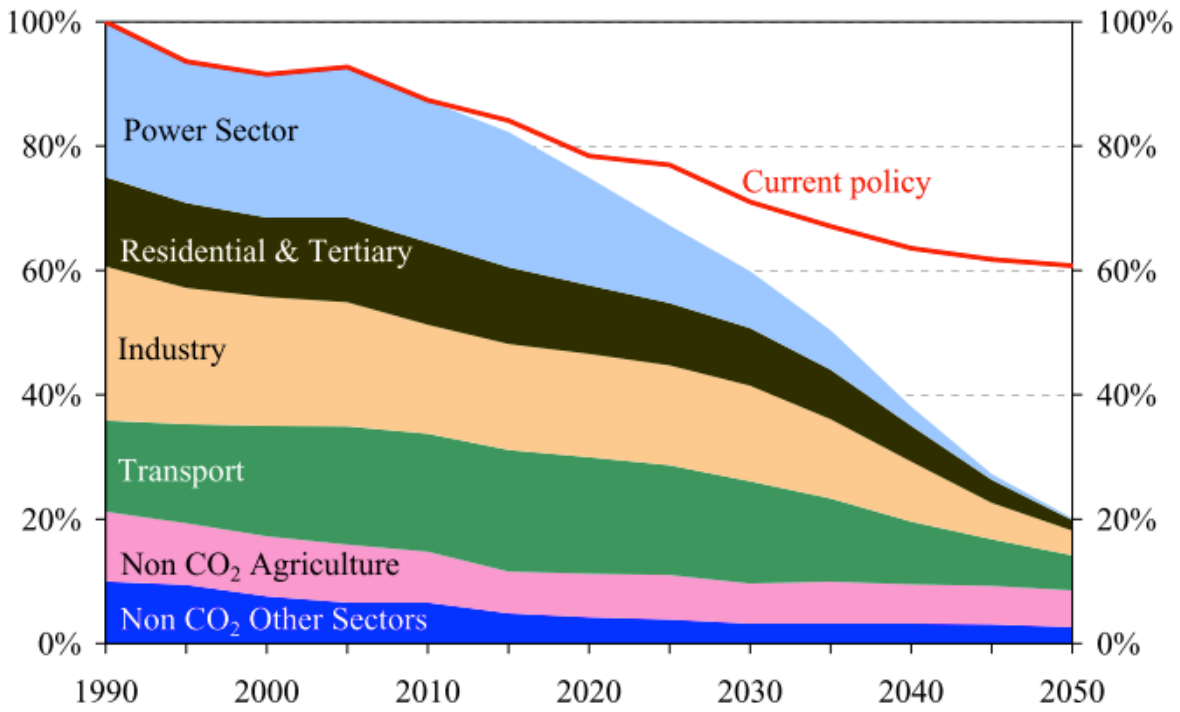

Figure 2.10: Emissions by sector from 1990 to 2050 to reach 80% reduction in GHG ([7])

The Intergovernmental Panel on Climate Change (IPCC) produced a report in 2007 [38] that detail the average growth of energy consumption and electricity generation sources, and the respective growth in CO_2 emissions. The report goes on to detail the impact of these emissions, and methods of mitigation. For more detail please see §2.3.2. The latest report from the IPCC [39] acknowledges that steps have been taken to adopt policies and strategies that penalize emissions of pollutants. Despite this, the GHG emissions levels have grown to 49 billion Gigatonnes of CO_2 equivalent, being the highest ever level of CO_2 emissions.

Increase in CO_2 capture for fossil fuel supplied thermal power plants features in study by Capros et al. [40] as they explore the methods of achieving the 80% reduction in GHG emissions set out by the EU Commission.

Eight scenarios are presented and detail the assumptions on EU climate change policies and target being met or delayed. The first scenario is defined as the reference scenario: the 2020 policies defined in the Energy and Climate Policy Package are adopted by the EU. After 2020 there is a linear annual reduction of the emissions trading scheme cap, and no renewable energy targets or efficiency plans are required. Scenario two sees the

EU roadmap carbon budget imposed and all emissions reduction options are included. The adoption of these reduction options follows the least cost approach.

Scenario three implements the same strategy of scenario two but higher efficiencies of renewable systems lead to low uptakes of CCS and nuclear technologies leading to phase-outs. Scenario four and five see the same adoptions of scenario three, but with no phase-out of nuclear power stations and renewable technologies achieve maximum efficiency. Scenarios six, seven and eight detail varying levels of transport electrification adoption meaning that carbon emissions have been stabilized and the restrictions of the 2050 roadmap can be eased as early as 2030.

A comprehensive review by Ghoniem et al. [41] deals with various methods of meeting the world's current demand in energy while maintaining the CO_2 and GHG emissions levels set out by the Kyoto protocol [42]. The authors conclude that supply-side efficiency improvements must be coupled with reducing end-user waste energy is the path to achieving the required GHG reductions.

In the past the intention has been to meet the energy demand of increasing economies and populations by any means necessary. This has been achieved by exploiting fossil fuel resources to supply thermal power stations, transportation and heating. The current situation is such that the amount of CO_2 emitted to the atmosphere is now having a detrimental impact on the planet's climate. The global aim is now to reduce the CO_2 emissions from contributors across the spectrum. The focus of this work is the potential reduction in CO_2 emissions possible from Rankine cycle thermal power plants and is described in more detail in §2.3.2.

2.2.1 Setting the context for this programme of research

It is clear that Rankine cycle thermal power plants dominate the electricity generation market and the work detailed in this thesis is applicable to any steam cycle, such as those operating on gas, coal, biomass and nuclear. There are numerous methods of reducing the CO_2 emissions of Rankine plants namely attempting to capture the emissions, or reducing the rate at which they are produced by increasing the cycle efficiency. Once the CO_2 is

captured the prevailing opinion is to store the CO_2 underground in aquifers that once were mined for their fossil fuel content. Ironically, in doing so, a greater portion of the residual hydrocarbon content of these reserves can be extracted.

2.3 Electricity generation

The primary method of electricity generation as previously noted is via the Rankine cycle. This is emphasized by a report on the monthly electricity generation statistics by the International Energy Agency [43]. The study notes that combustible fuels and nuclear operating on the Rankine cycle are the dominant source of electrical power generation globally. Therefore the details of the thermodynamic cycle are important in order to understand how the cycle has developed since its inception and why it is so critical to the emissions targets set out across the world.

2.3.1 Rankine cycle technology

The Rankine cycle was devised by Lord William Rankine in the early half of the 1800's to describe the operation of a steam engine. In recent history, the application of these steam engines has transferred from driving locomotives and winding engines for mines to driving electrical machines in thermal power stations. The principles behind the operation are the boiling of water to generate steam, injected at high pressure to turbines that efficiently convert it to rotation. This rotation is coupled to an alternator to generate electrical power. Once the steam has been passed through the turbines, it is condensed and pumped back to the boiler in a closed loop cycle with the latent heat of evaporation rejected from the process. The mechanical implementations of the Rankine cycle have remained similar as the cycle itself has become synonymous with electricity generation on a large scale.

Countries across the world have implemented numerous Rankine cycle-based power stations to provide a reliable base of electricity generation. As such, there have been numerous enhancements to the system and the mechanical components it encompasses. Thermal plants built in the UK in the late 1960's are still in use today as a testament to the robustness and reliability of the Rankine cycle. Although the plants built at that time

were based on the best current technology, that is now considered unacceptably poor in the current climate of low-carbon emissions and efficiency improvements.

Current large thermal power plants utilise high pressure and high temperature steam to maximise the system thermal to electrical energy conversion efficiency which is now 50%, studied by Bugge et al. [44] and Kjaer [45]. However, these thermal plants are driven by fossil-fuels and emit large amounts of CO_2 as shown in a study by Yang et al. [46].

In light of the previously discussed CO_2 emission reduction legislation previous generation thermal power plants are now the focus of retrofits that would make them suitable for the aspirations of a low carbon age. To examine this in more detail, three existing plants are described and the proposed changes are discussed in this thesis.

The largest UK electricity generation plant is 'Drax' in the North-East of England. It is capable of generating $3960MW_e$ from six $660MW_e$ generating units. These units were initially coal-fired from 1974 but in the past few of years one unit has been converted to fire biomass. The station burns 10 million tonnes of solid fuel each year with 1.3 million tonnes biomass. Operation on such a massive scale is evidence of the installed capacity invested in Rankine cycle thermal power plants. Technology that can be beneficial to both the cycle efficiency and result in CO_2 emission reduction is highly desirable given the legislative requirements that are on the horizon or have already been implemented.

The second largest UK plant at Longannet is another coal-fired power station with an installed capacity of $2400MW_e$ provided by eight $300MW_e$ turbine units. In 2009 it became the first plant to implement Carbon Capture and Storage technology. After two years of operation the CCS portion was shut down as it was no longer economically viable as the necessary UK Government subsidy funding was not forthcoming. The tribulations of operating CCS at Longannet have made clear that for CCS to be competitive with other CO_2 reduction technologies it must be cost effective. At current energy prices this is not the case, without heavy subsidy.

The third UK coal plant, Ratcliffe-on-Soar, has been the subject of a review by the UK Government's Technology Strategy Board (TSB) to upgrade the plant to have a higher Rankine cycle thermal efficiency. This plant has a rated output of $2000MW_e$ from four

$500MW_e$ turbines. The TSB report outlines an aim to increase the cycle efficiency from 38.7% to 44.9% and hence generate $625MW_e$ per unit resulting in an increased installed capacity of $2.5GW_e$. The plans for this are still in progress with little announcement in the press.

One conclusion that can be drawn from examining these three plants is that the Rankine cycle thermal plants in operation across the UK are going to be in use for the foreseeable future and that a CO_2 emission-reduction solution is needed that will suitably scale to these plants. The biomass project at Drax is built on proven technology, and co-firing means that the risk of the scheme not working both technologically and economically is minimized. However, it is key in noting that the scheme only proceeded with the help with further UK Government financial subsidy. There remains a question over the sustainability of co-firing given it will necessitate the import of many millions of tonne of biomass per annum, for decades to come.

Despite the CCS project at Longannet being halted, it shows that there is a market incentive to continue to use coal-fired power stations use for baseload generation. The benefit of the CCS solution is the adaptability to coal-fired plants as Post-Combustion CCS can be retrofitted on to the existing plant. However, there are other significant drawbacks in CCS technology due to the reduction in cycle efficiency, and large capital cost. These factors are examined in more detail in subsequent sections of this thesis.

The aim of the retrofit discussed for the Ratcliffe-on-Soar thermal power plant is to indirectly reduce the emissions of the plant by increasing the electrical output. In terms of fuel input, this will not alter but the amount of electricity generated would increase from $500MW_e$ to $625MW_e$. The net result is: while no less CO_2 is emitted, there is a CO_2 neutral benefit by improving the fuel to electricity efficiency ratio.

It is clear that the thermal plants must have a combination of the three points noted: be scalable, be economical and importantly: reduce CO_2 emissions.

2.3.2 CO_2 capture and storage technologies for thermal power plants

Use of the Rankine cycle is not restricted to fossil-fuelled power stations, as it can be applied to any power station that operates a steam cycle. The prime example is a nuclear power station. The nuclear reactor core emits a very large amount of heat when a Uranium-235 atom is split. This fission process is used to raise the temperature of water to steam as per the cycle in a conventional power station. The main merit of the nuclear plant is that it is CO_2-free but the public perceptions of the risks that nuclear fission plants bring are negative, apparently limiting their widespread use. It is interesting to note, however, that whilst the Scottish government will prevent new Nuclear build in Scotland via the planning system (energy is not a devolved Policy), the UK government is pressing ahead with several new reactors around England and Wales. Therefore, CO_2 emissions reduction technology is explored with a view to either being retrofitted or applied as part of newly built plants, regardless of the heat source

In order to achieve the reductions in CO_2 required, CO_2 capture and storage (CCS) technologies will almost certainly be employed in fossil-fuelled thermal power plants and their widespread use is documented in a patent review conducted by Li et al. [47]. Three methods of CCS are suitable for this purpose and at scale: pre-combustion capture, post-combustion capture and combustion in oxygen. A short review of each technology now follows. As a prelude to these different techniques, the cycle efficiency and plant

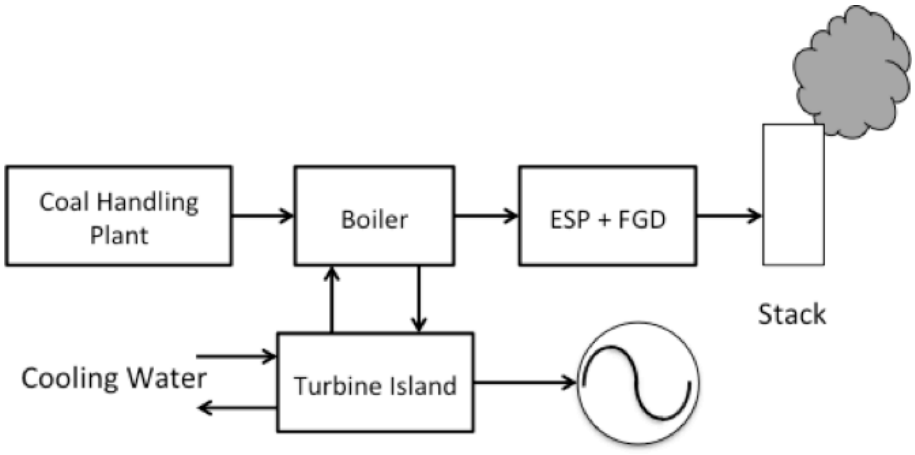

Figure 2.11: Rankine cycle thermal power plant

type are defined. Each of the following plant configurations with the exception of Pre-Combustion Capture are assumed to be retrofitted to an existing plant. The existing plant is presented in a report to the UK Government Technology Strategy Board (TSB) by Panesar et al. [48]. The report details a UK power plant "Ratcliffe-on-Soar", which is currently a subcritical plant with an installed capacity of $2GW_e$ comprising four $500MW_e$ generating units. (Figure 2.11). These units generate superheated steam at 160 bar and 566°C. The boiler uses pulverized bituminous coal as a fuel source from the handling plant.

Superheated steam is passed to the steam turbine unit in order to drive the generators. These consist of five stages: one high-pressure turbine (HPT), one intermediate pressure turbine (IPT) and three low-pressure turbines (LPT). Various extraction points along the turbine plant allow for steam to be bled off providing regenerative heating of feed water and condensate. The feed system comprises of seven feed water heater stages (two LPT heaters, a de-aerator to remove excess Oxygen, four HPT heaters). The Electrostatic Precipitator (ESP) uses a high voltage electrode to attract and remove dust and fly ash as the flue gas leaves the boiler before passing to the Flue Gas Desulphurisation (FGD) plant. The FGD reduces the amount of Sulphur Oxides in the flue gas which is then cooled before being passed to the stack column for expulsion to the atmosphere[1]. The overall thermal net efficiency of the subcritical plant is calculated at 38.9%.

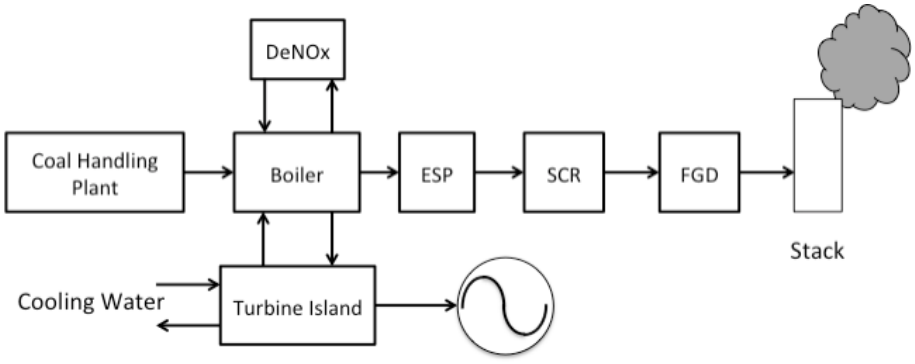

Figure 2.12: Ratcliffe-on-Soar upgraded with $DeNO_x$ and to handle supercritical steam

A supercritical retrofit is under consideration for the plant at Ratcliffe-on-Soar. The work will comprise a boiler and turbine unit upgrade, installation of a new selective

[1]In the Ratcliffe-on-Soar plant, the mass flow and thermal energy of the flue gas is sufficient as to ensure the gas rises and disperses.

catalytic reduction unit (SCR) to reduce Nitrogen Oxides, and the installation of an upgraded FGD. The proposed retrofitted plant (Figure 2.12) will increase the pressure and temperature of the superheated steam to 290 bar at 600°C. Work detailed by Goidich [49]; [50]) shows the Once-Through Benson boiler configuration used to achieve the supercritical conditions required and the resultant improvement in plant heat rate.

The rate of superheated fluid is passed to the boiler is controlled by the condensate pump, but the fuel firing rate determines the temperature and pressure of the steam. The turbine island is retrofitted to include more feed water heater stages and modified turbines to cope with higher-pressure steam. The overall thermal net efficiency of the plant with the supercritical retrofit (shown in Figure 2.12) is estimated at 44.9%.

2.3.2.1 Pre-combustion capture

As opposed to pulverizing the coal in a conventional power plant configuration, the coal is gasified by heating it in the presence of steam and Oxygen resulting in a syngas mixture of H_2 and CO. CO_2 is separated by reacting CO with steam. The resultant CO_2 is transported to the compression plant while the Hydrogen syngas is sent to an open cycle gas turbine and fired to produce electricity. Due to the nature of the chemical process that converts the coal to a syngas, the resultant gas can be purified to remove Sulphur and around 90% of the CO_2. The overall net efficiency is expected to be over 40%.

A study compiled by Klara et al. [51] supports the notion of an Integrated Gasification Combined Cycle (IGCC) as the preferred way of reducing CO_2 emissions when compared to PCC and Oxygen combustion. However, for the coal to be gasified the process requires pure oxygen which is an expensive process accounting for 15% of the IGCC plant capital costs. An article by Bhutto et al. [52] noted an often-overlooked consideration of IGCC is separation of the other chemicals released when the CO_2 is removed. Arsenic, Mercury and Selenium are released and must be retained and disposed of correctly.

2.3.2.2 Post-combustion carbon capture (PCCC)

The coal is pulverized in the coal plant, transported to the boiler and burned to produce supercritical steam. The carbon dioxide in the flue gas can be removed by using an

amine-based solvent that scrubs the gas. The flue gas is passed through a Flue Gas Desulphurisation (FGD) plant and cooled before going to the Absorber. An amine based solvent flows over the packing in the Absorber column and mixes with the flue gas. In a counter-current configuration, the CO_2 is absorbed in the Amine solution and removed from the resultant gas. The flue gas, now with CO_2 removed, is sent to the stack and vented to the atmosphere. The amine solvent now rich in CO_2 is pumped to the stripper column where the CO_2 is removed by heating. The Amine solvent, free from CO_2, is then reused in the process. The CO_2 now liberated from the solution exits the Stripper column to the CO_2 compression plant via indirect coolers to condense the entrained water vapour.

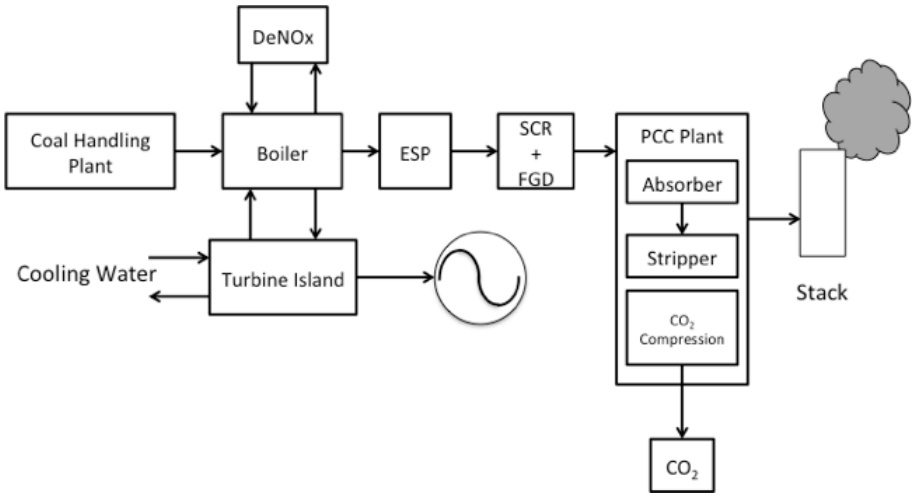

Figure 2.13: Ratcliffe-on-Soar thermal power plant retrofitted with PCCC

This is shown in Figure 2.13. The overall thermal net efficiency of the plant with a supercritical retrofit and Amine Post Combustion CO_2 Capture is calculated at 35.7%.

The significant loss in energy from the traditional supercritical Rankine plant to the PCCC plant requires additional thermal energy for the reheating of the amine solvent. Oexmann et al. [53] explore fluids that reduce the heat duty on the reboiler, typically these fluids have a low heat of absorption meaning that they require less input energy to raise the temperature. However a major drawback of these fluids is the need for near vacuum pressure levels for fluid regeneration and with this comes the penalty of requiring higher CO_2 compression which ultimately results in increased power demands from the

power plant, in turn nullifying the effects originally desired.

A study by Bhown et al. [54] found that the technology readiness levels of the current research of PCCC is estimated at EPRI-graded TRL 7, meaning that significantly more work is required in order to progress this technology to a state at which it can be fitted the numerous large scale power plants across the world.

2.3.2.3 Combustion in Oxygen

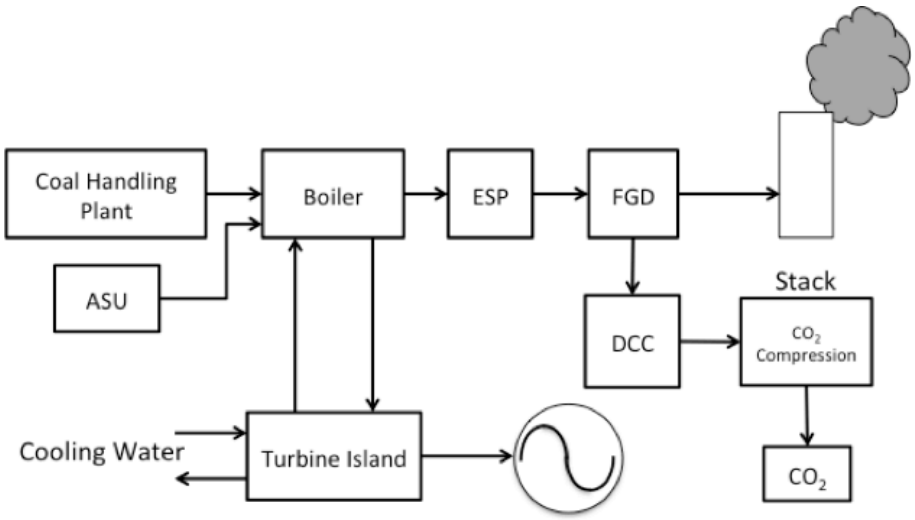

Figure 2.14: Ratcliffe-on-Soar thermal power plant with Oxygen firing retrofit

The Oxygen combustion process (Figure 2.14) burns coal in pure Oxygen, as opposed to firing in air for the other configurations. Burning coal in pure Oxygen results in a flue gas with a high concentration of CO_2, inerts (such as Nitrogen) and water vapour. The Nitrogen is removed prior to combustion and therefore the flue gases require less filtration and no NO_x removal is needed. Flue gas recycling is used to control the flame temperature and optimize boiler thermal performance[2]. The water vapour and inerts are removed in a condenser as part of the CO_2 purification and compression plant. The use of Oxygen combustion CCS technology will require the addition of several components. These include an Air Separation unit (ASU), flue gas heat recovery units, CO_2 purification and Compression plant. The overall thermal net efficiency of the plant with a supercritical retrofit and Oxygen Combustion CO_2 Capture is calculated at 34.8%.

[2]Exhaust gas recycle is a common concept in petrol and diesel engines. In diesel engines the CO_2 heavy exhaust gas is used to reduce the NO_x emissions by reducing the O_2 levels in combustion as referenced by [55]

Plant Configuration	Pre-CCS Efficiency	Post-CCS Efficiency	Relative Cost of Electricity Implications ($/MWh$)	Efficiency of CO_2 Capture
Supercritical retrofit of subcritical plant	38.7% [48]	44.9% [48]	46 [59]	–
Pre-combustion CO_2 Capture	38.1% [60]	32.9% [60]	73 [59]	90% [60]
Post-combustion CO_2 Capture	44.9% [48]	35.7% [48]	62 [59]	$85 - 90\%$ [61]
Oxy-Combustion	44.9% [48]	34.8% [48]	62 [59]	85% [48]

Table 2.1: Comparison of CO_2 Reduction Technologies

This net reduction in cycle efficiency when compared to the original Supercritical Rankine plant is supported by a review by Mousavian et al. [56] and Chen et al. [57] who also document the development of other plant across the world developing plant-scale oxygen-combustion CCS. Further research by Hong et al. [58] details the potential for a cycle efficiency increase of 3% when the flue gas recirculation pressure is increased from 1.2 bar to 10 bar.

2.3.2.4 CCS conclusions

It is clear that all forms of CCS are a parasitic load to the thermal power plant.

This is shown in Table 2.1. The thermal efficiency impact creates a challenge in that there will be a shortfall in electricity generated by the plant that is sacrificed to the auxiliary components required by the CO_2 capture process. The final cost of electricity also increases and these costs must be absorbed by utility operators, the consumer, or offset using some form of carbon levy (for which the end users ultimately pay).

2.3.3 Energy efficiency

Due to the impact CCS technologies have on net cycle efficiency, it is now worthwhile to investigate heat scavenging technologies that historically were considered economically unviable. Reducing waste energy is a basic requirement to improving the net cycle efficiency of plants both with and without CCS technology. Any heat losses that can be recovered and converted to electrical power will have a direct impact on fuel consump-

tion and plant net cycle efficiency. An internal[3] Doosan Babcock report by Siviter [31] found this to be the case and explored two options to improving the cycle efficiency by scavenging waste heat from the CCS systems. The report concluded that there is a significant case for investing in energy scavenging technologies as the pay back time proved favourable to the utility owner and typically could yield a net benefit within a decade.

CO_2 capture technologies aim to achieve efficiencies close to the Carnot cycle limit. The Carnot cycle describes the theoretical relationship between the temperature difference in the heat process and the amount of work that can be extracted from the process as shown by Bejan [62]. However, there are supplementary methods of improving the electrical output and thermal efficiency of a power plant that have evolved over many decades. In one such technique Geete et al. [63] show that the cycle efficiency can be increased by varying the steam inlet temperature. The initial conditions at the exit of the boiler to the inlet of the high-pressure turbine are varied between 500°C and 570°C. If the inlet pressure is held constant then the amount of power the plant generates is directly proportional to this temperature.

The final LP turbine stage exhausts into a condenser in which the cycle feedwater is recondensed and pumped back to the boiler. The condenser pressure is known to be an important factor in influencing the amount of energy extracted by the turbines as demonstrated by e.g. Wang et al. [64]. The authors found that if a constant electrical output power is required then the fuel firing rate can be reduced as the condenser pressure conditions drops with mass flow rate and temperature of the cooling water. This was confirmed in work by Bekdemir et al. [65] as they show that an increase in pressure causes the effective heat transfer area to drop. This is due to the rate at which steam condensed on the condensing coils being proportional to the velocity of the cooling water. It is therefore important to ensure that condensing coils meet the required cooling capacity as it will result in an increase in condenser pressure, and reduce the thermal efficiency of the plant.

[3]Report titled: 'Stirling Engines and Thermoelectric Devices for Heat Scavenging in Oxyfuel and Post Combustion CO_2 Capture'. Report Number: RD-10-055. Date of Issue: 14/12/10. For details of the report please contact Doosan Power Systems (helen.waugh@doosan.com.

2.3.4 Reheat and regenerative cycles

The 'traditional' Rankine cycle has been presented and the relative efficiency improvements have been noted. The next major step in the advancement of the Rankine cycle was the advent of the reheat and regeneration cycles.

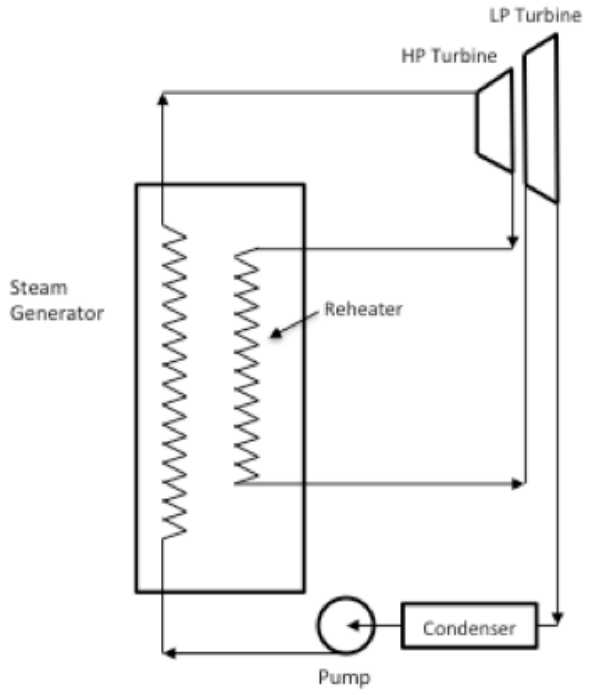

Figure 2.15: Rankine cycle with reheating stage between the high pressure turbine (HPT) and the low pressure turbine (LP) [8]

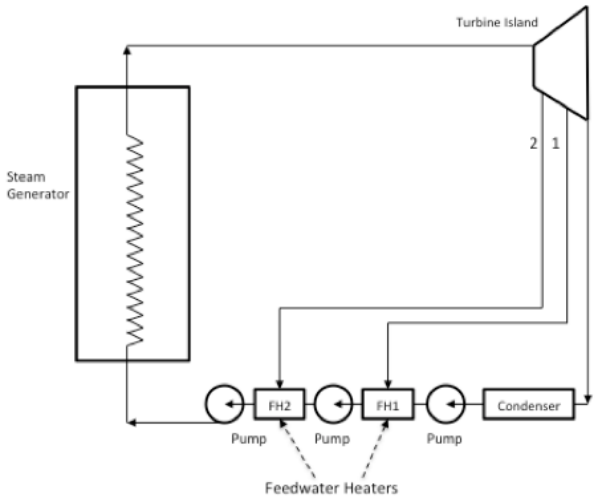

Figure 2.16: Rankine cycle with feedwater regeneration stages bled off various points in the turbine island [8]

Figure 2.15 shows the Rankine cycle with a reheat stage, and Figure 2.16 with two

regeneration stages. The use of reheat and regeneration cycles to increase the practically attainable efficiency is well documented by Badr et al. [8]. The software program developed by Badr et al. detailed both reheat and regenerative calculations for balancing the mass flow, temperature, pressure and enthalpy of each of plant configurations.

The reheat cycle shown in Figure 2.15 operates as follows: after the steam is generated in the boiler and expanded in the high-pressure turbine, it returns to the boiler where its temperature is increased again, resulting in drier steam and a higher cycle efficiency. The paper quotes a 2% increase in cycle efficiency compared to the basic Rankine cycle. The regeneration cycle follows a similar principle but rather than raising the steam temperature as in the reheating cycle, the feed-water returning to the boiler is heated, known as feed-water regeneration. In the regenerative Rankine cycle there are two benefits: the increase in average temperature that thermal energy is added to the water thus increasing the cycle efficiency and also increasing the net power generated by maximizing the enthalpy drop across the turbines. Again, 2% cycle efficiency increase is shown in the basic Rankine cycle, but it is coupled with a 2% increase in electrical power produced.

In practical plants both reheat and regeneration cycles are employed as shown in an exergy analysis by Yasni et al. [66]. The authors detail an exergy analysis of the fossil-fuelled power station in Huntly, New Zealand. The thermal plant was built in the early 1980's and consists of four $250MW_e$ generating units. Each generating unit includes seven feedwater regeneration stages and a single steam heating stage. The feedwater regeneration accounts for an additional 9% of the thermal energy supplied to the plant, and the reheat stage accounts for 7.57% of the thermal energy to be retained in the system. Therefore it can be concluded that both the reheat and regeneration cycles are ultimately a cycle efficiency gain by reducing thermal losses. A current power station detailed by Richardson et al. [67] is presented. The $800MW_e$ capacity boiler again features both reheat and regeneration cycles and reheat / regeneration stages are now considered an essential part of any high efficiency Rankine cycle plant.

2.4 Waste energy

The development of the Rankine cycle represents a path to the practical embodiment of the Carnot cycle, but the practical use of the cycle in a thermal power has limitations in thermodynamic availability and hence there are inherent irreversibilities.

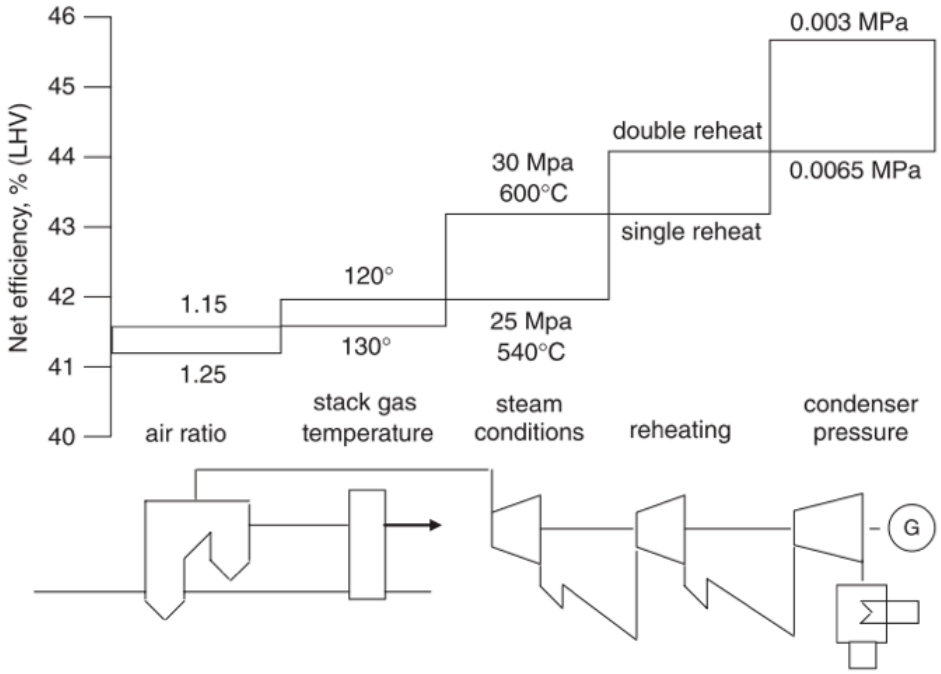

Figure 2.17: Efficiency of Rankine cycle thermal power plants and the effects on the efficiency at each stage [9]

Figure 2.17 describes the waste energy sources and details how they affect the overall plant efficiency.

Each stage of the Rankine cycle thermal power plant introduces an irreversibility. In the boiler there are irreversibilities inherent as the system is constantly losing energy to the environment. Typical boiler efficiency is 95% and can be characterised by two main factors: the ratio of excess air to the theoretical minimum required for combustion; and the amount of thermal energy in the exiting flue gas after combustion.

Reducing the excess air in the combustion is essential to reducing the amount of thermal energy wasted in the flue gas. The ideal situation is to have a low Oxygen content in the flue so to reduce SO_x contributions allowing Sulphuric acid to form. The

formation of the acid raises the condensation point of the exiting flue gas meaning not only that the emissions of the power plant increase, but the thermal efficiency of the plant decreases to remove the SO_x.

The temperature and pressure of condensation are inexplicably, and maintaining a low cooling water temperature will help keep the condenser pressure low, leading to a larger operating range for the turbines and greater plant efficiency. Plants in Northern Europe have access to lower temperature cooling water (seawater, rivers, etc.) and can maintain condenser pressures near to 30mbar-abs, compared with 67mbar-abs average in the USA. This reduction in condenser pressure can account for up to 3% efficiency.

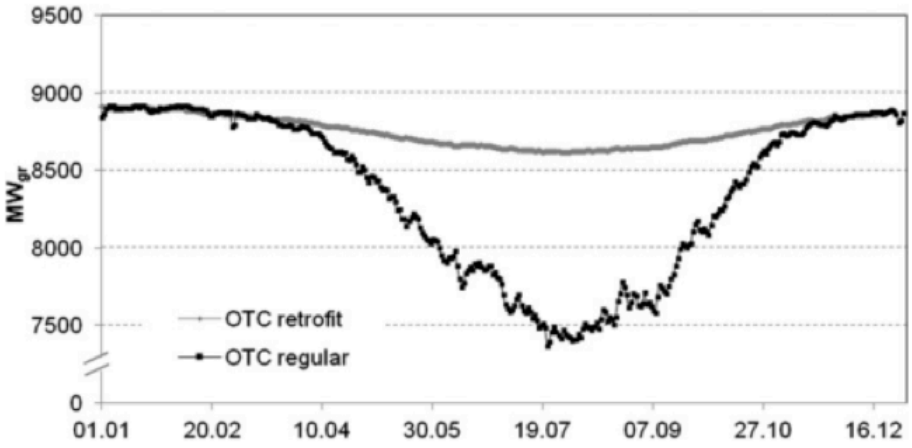

Figure 2.18: Mean daily performance values of a Once Through Cooling System (OTC Regular) and a Closed Circuit Cooling System (OTC retrofit)[10]

Hoffman et al.[10] investigate the performance losses of thermal power plants in Germany, concluding that performance of the cooling circuit directly impacted the up-time and availability of the plant. As temperatures of rivers rose during the summer months the amount of thermal energy that could be discharged reduced and so the plant had to reduce thermal load (and therefore electrical output) to account for this. Figure 2.18 shows the output power of the plant over the course of a year with both a Once Through Cooling circuit (OTC) and the improvement a closed circuit (OTC-retrofit) would bring for a power plant in central Germany. However, power plants near to the Alps suffer from a reduction in performance during the winter months as the rivers used as the source of cooling circuits are constrained due to reduced river run-off. This is caused by the

precipitation that would normally maintain a high river water level is reduced by the fact most is stored as snow in the mountains.

Work by Salazar et al. [68] reaches similar conclusions for thermal power plants operating in the United States. The study found that the capacity varies between $5-10\%$ depending on the relative humidity of the region and the effect on the condenser pressure. A day is modelled with temperatures varying from 288K to 299K, and relative humidity varying between 20% and 90%. The modelling shows the dependency of power plant performance and the humidity, temperature is shown to have almost no effect. There this study shows the importance of adjusting the cooling circuit depending on the humidity, rather than the ambient temperature.

The drop in cooling circuit performance due to either higher ambient temperatures, or other weather-related phenomena occur at times in the year when power demand may be at its highest. During the winter months, large amounts of power are required for heating systems. However, since there are other methods of obtaining heat (such as directly burning coal, wood or gas) the impact of the plant drop in electrical output power is not so heavily felt as during the summer months. During the summer months, brownouts (and less frequent blackouts) occur across the USA are common as the electrical load spikes as air-conditioning and refrigerating units are in widespread use.

Blackouts and brownouts are two types of electrical power outage, and both can occur as a result of mismatch between electrical supply and demand. One such example of this is the North-East American blackout in August 2003. Over 10 million people lost all power due to a series of failures at the management and fault-detection level of electrical power control.

A report by the USA and Canadian Governments [69] found that the initial cause was when data received by a power system operator was incorrect, and the software tools used to monitor the situation were disabled. The large power consumption required to power air conditioning units and refrigeration units on a hot day led to several high-voltage (345kV) lines being over-loaded and sagging[4] after the energy operator failed to correctly balance

[4]Power transmission line capacity is determined by the thermal expansion of the conductors, hence their height above ground and ground-connected obstacles.

the electricity supply from various power plants operating in the region. This ultimately led to the disruption in electricity supply. /par The progress of thermal power plants in

	2015			2020		
	High	Medium	Low	High	Medium	Low
GDP growth rate (%)	8.0	8.0	7.5	7.5	7.5	6.5
Elasticity of electricity	0.90	0.90	0.80	0.85	0.85	0.70
Electric growth rate (%)	7.2	7.2	6.0	6.4	6.4	4.6
Percentage of coal-fired electricity (%)	77	72	72	70	64	64
Total electricity (10^3 GWh)	6149	6149	5813	8376	8376	7261
Coal-fired electricity (10^3 GWh)	4723	4440	4197	5905	5352	4640
Coal-fired units (GW)	926	871	823	1230	1115	967
Coal consumption (Mt)	2281	2126	2009	2769	2510	2176

Figure 2.19: The projected growth of coal-fired thermal power stations in China in 2015 and 2020 [11]

China is the focus of work done by Wang et al. [70] and concludes the cost benefits that efficiency improvements bring will be a significant driver in developing current and future plants. The authors believe these improvements will be found in reducing CO_2 emissions. A study by Zhao et al. [11] investigates the pollutant levels of coal-fired power stations in China. In doing so, the current number of generating units is presented in Figure 2.19. The projections for 2015 and 2020 show a decline in the use of coal with a decline in GDP growth rate. However, these figures show an increase in electricity supplied by coal when going from 2015 to 2020 which underlines a present growth in such thermal power plants. Therefore the conclusions drawn by Yang et al. [70] are emphasized by the scale of power plant growth.

2.4.1 Alternative cycles for increasing efficiency including the organic Rankine cycle

Waste energy recovery has long been a topic of interest. A review by Al-Rabghi et al. [71] discusses several methods for improving efficiency of process plants and facilities. By extending known cycles, such as the Rankine cycle, energy can be recovered that would otherwise be wasted through the use of a separate cycle coupled to the original process.

The most commonly used heat transport fluid is pure H_2O for high temperature process plants, but for low temperature and low-grade waste energy organic fluids can be used instead of water as the working fluid and frequently referred to as Organic Rankine

cycle (ORC). Efficiency improvements can be achieved by coupling the ORC to a plant at specific locations where thermal energy is wasted or thermal energy must be removed as part of the main process.

Borrnet et al. [72] show the application of ORC to low grade heat sources in the temperature range 150°C - 400°C in a cement works. The cements works operates by heating a mixture of clay and limestone in a kiln to 1500°C to produce clinker. The clinker is then cooled before being ground down in a mill to produce a fine powder. The high temperatures required in the process and the thermal energy rejected to cool the process make this a suitable application for waste energy recovery. Two locations are selected: the first from the waste gas preheater; the second is in the clinker where it is cooled. Ultimately, the efficiency improvements brought by the ORC system resulted in a 20% net reduction in electricity costs to the cement works.

Angelino et al. [73] investigate the use of the ORC to recover waste heat from the Rankine cycle using the condensate entering the main cycle pump as the energy source and cooling loop as the energy sink. The authors have simulated a single stage and multistage ORC with multiple turbines operating at decreasing fluid pressures and attain efficiency improvements of $1.5-2.5\%$ above the original plant efficiency. Murugan et al. [74] report a 4% efficiency percentage improvement by taking advantage of the low grade heat in a similar location to [73], however Murugan et al. apply the Kalina cycle, also known as the combined cycle. The Kalina cycle operates by extracting heat from the steam turbine stage of the main Rankine cycle by interfacing a secondary loop with the high temperature steam flow in a heat exchanger. The heat is transferred into the working fluid and expanded in a turbine. The enthalpy of the working fluid is removed and transferred as latent heat to the condensate of the original Rankine cycle. The Kalina cycle addition to the Rankine cycle quotes a 2.1% efficiency percentage increase, from 38.1% to 40.2%. This efficiency gain is attributed to the condensing operation performed in the original cycle is now done by the Kalina-cycle ammonia-water in the evaporation. This means that the condensing operation is no longer sensitive to the atmospheric pressure and temperatures inside the condenser, as it is now constant in the Kalina cycle.

The application of the ORC to a process may initially be seen as a benefit, but there

may be other conclusions that can be drawn, namely the introduction of further thermodynamic irreversibilities. The energy sink for an ORC is often shared with the original process. Therefore, the energy rejected by the ORC will end up limiting the cooling capacity of the main process of the plant. If this is the case then the overall efficiency of the original process will drop as more energy is required to obtain the necessary conditions at the initial stages of the system.

The main aim of these plant additions is to extract an appreciable amount of energy from what is normally classed as waste. These innovations are successful when only measuring the efficiency gain but do not consider the impact on the plant reliability. Each use of a mechanical cycle adds complication to the balance of the plant, and there may be circumstances where the maintenance of the add-on cycle inadvertently harms the original cycle leading to outages that could have been avoided. Therefore the design of these systems should carefully consider the mechanical reliability impact on the overall system.

Wang et al. [75] investigate the application of the ORC to the flue gas exiting a thermal power plant[5]. The authors achieve a CO_2 emission reduction of 2.55 tonnes per hour as a result of less fuel needing to be burned to achieve the same power output. Borsukiewicz-Gozdur [76] shows an exergy analysis for the ORC. Mohamed et al. [77] investigate the ORC in a large scale plant where an increase in cycle efficiency of between 1.7-2.2 cycle efficiency percentage points were obtained. A further ORC adaption to the traditional Rankine cycle is presented by Lui et al. [78] where the authors implement a regeneration cycle in the traditional ORC in improve efficiency. However, they conclude through analysis of different working fluids that the fluid required to obtain the efficiency calculated is very expensive and not economic in the medium term.

The reduction of CO_2 by firing less fuel is beneficial as long as the same thermodynamic conditions are maintained in the main process. The steam flow into the turbines must be maintained in order to prevent the turbines entering a state that may lead to water droplets forming at earlier stages in the expansion process which has the potential

[5]There is a minimum flue gas energy content required to ensure sufficient dispersion. CO_2 is denser than air and asphyxiation near the plant can result if this is not done.

to destroy generating sets. Further, an ORC extracting energy from the flue gas will be detrimental to the environment as a minimum mass flow and temperature must be maintained in order to ensure the flue gas is dispersed correctly, otherwise asphyxiation can occur due to the heavier-than-air gases (e.g. CO_2) falling back to the plant area

The ORC and Kalina cycle can be considered as 'bolt-on' additions to the main Rankine cycle process. The aim of this thesis is to examine from first principles the opportunities to improve the Rankine cycle beyond increasing mechanical complexity through ORC or Kalina cycles. Although these cycles do result in a net gain in efficiency, the whole picture is not always present in the potential cooling capacity limitations or the necessity to preserve certain levels of thermal energy in the system.

Feed water heating using concentrated solar power was investigated by Hou et al. [12] as a means of injecting additional low-grade thermal energy into a standard power plant. The authors describe an ORC applied to a coal-fired thermal power plant where the evaporator stage is accomplished using an array of solar collectors. A working fluid is pumped to the feed water heater units, replacing the steam traditionally bled off from the HP, IP and LP turbines. The solar plant is theoretically applied to a $125MW_e$ coal fired power plant. In order to recover enough solar energy a field of photo-voltaic (PV) cells is calculated to be $4,710m^2$. Limited simulation data is presented so final correlation to the improvement of the overall cycle efficiency is unknown.

A similar plant is described by Ying et al. [79] shows an increase of 4.17% is attainable if all feed water heaters are included in a concentrated solar plant and ORC. Cost of installation and operation is expected to be a significant fact hampering development of these systems.

The size of the solar-collectors in these applications is likely to incur a large capital cost along with a large surface area. Further there has been little consideration of the potential dust and ash from the heavy-industry plant that will have a detrimental impact on the performance of the reflector. Whilst it is a conceptually attractive idea, little work as been done to consider the practical implementations of the solar-collector plants this will directly impact the performance of the Rankine cycle to which it is attached.

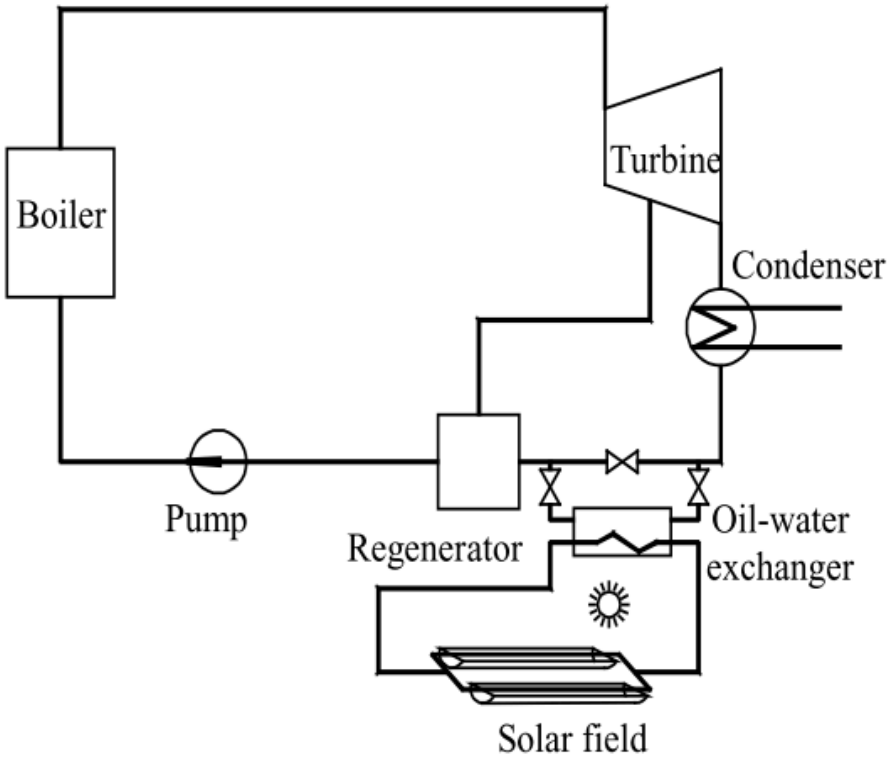

Figure 2.20: Example application of a solar field applied to a Rankine cycle to raise the temperature of the water returning to the main plant [12]

2.4.2 Waste energy summary

This section has examined the continuing motivation to investigate improvements to the Rankine cycle that result in reductions in CO_2 emissions when used with fossil fuels, and increases in thermal efficiency of plant using the cycle. Several techniques are in commercial use and all add mechanical complexity to the overall generation plant.

2.5 Energy scavenging

The regenerative cycle applied to the Rankine cycle has been shown to add thermal energy to the returning feedwater, resulting in increased plant efficiency.

This thesis investigates the potential of extracting recoverable energy in the condenser of the Rankine cycle and examines the use of a heat pump to capture a portion of the enthalpy released as low grade thermal energy in the isothermal conversion of the low pressure steam to liquid after the last turbine stage. By redirecting this energy back to

the process, rather than rejecting to the environment, the energy scavenged is used to raise the temperature of feedwater returning to the boiler. Both vapour-compression and thermoelectric based heat pumps are considered. The heat pump can be described and thought of as a reverse heat engine. Rather than converting thermal energy to mechanical or electrical power, the power is used in the conversion of thermal energy. The principal relies on the presence of a heat source and heat sink to pump energy from the former to the latter. Figure 2.21 describes the theoretical heat pump where Q_C represents the thermal energy source, W_{in} represents the applied power (mechanical or electrical) and Q_H represents the thermal energy sink combining W_{in} and Q_C at temperature T_H. The Coefficient of Performance of heating represents the efficiency at which energy is converted from the thermal energy source to the thermal energy sink by way of the applied power; and the COP of cooling is the efficiency at which the energy is extracted from the Q_C and is given in Equation 2.1.

$$COP_{heating} = \frac{Q_H}{W_{in}}; COP_{cooling} = \frac{Q_C}{W_{in}} \tag{2.1}$$

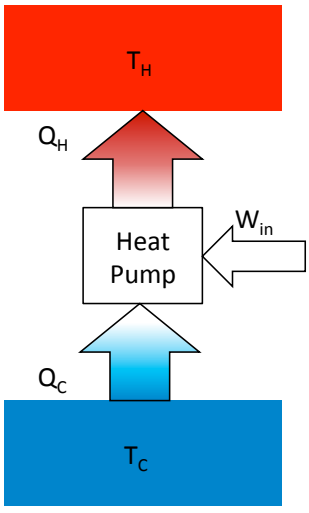

Figure 2.21: Diagram of a theoretical heat pump

2.5.1 Vapour-compression heat pumps

Vapour compression heat pumps are widely used and can be described by the temperature-entropy diagram (shown on the left) in Figure 2.22 and the system diagram (shown on the right). Heat pumps have been previously identified by Chua et al. [80] as a potential

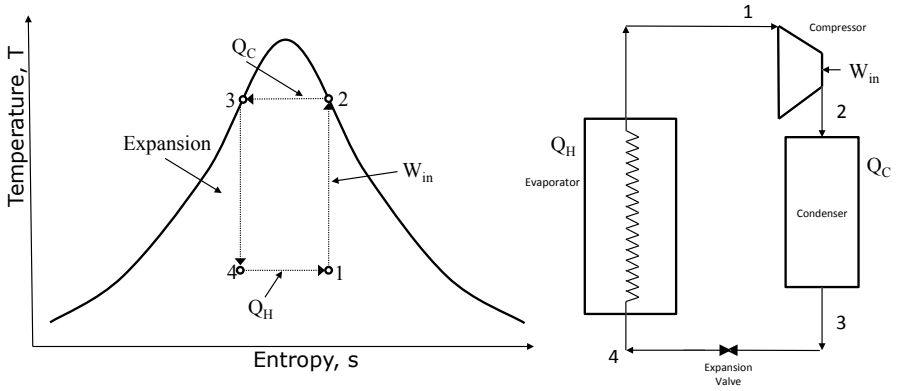

Figure 2.22: Diagram of the temperature-entropy diagram of a vapour-compression heat pump and the system diagram

technology that can aid the reduction in emissions, while improving the net efficiency of energy intensive processes such as in the process water heating in the paper manufacturing industry, or in the large-scale heating by using waste energy to supply a district heating network. Work done by Neal [81] initially explored potential applications for sources of low grade energy that would be suitable for heat pumps to operate. This included ground-, water- and air-sources. These applications are relevant to traditional vapour-compression cycles and an air source heat pump developed by Byrne et al. [82]; [83] details a large scale central heat unit that is capable of providing up to $7.4kW_{th}$ heating for hot water and cooling to a large building. Air source heat pumps have also been used to regulate greenhouse temperatures in varying climates, as discussed by Yang et al. [84]. Their paper presents a comparison between the winter months from November to March and shows that during the colder months the system is less efficient and has to be operated with a higher input power thus generating a lower COP when compared to February or March when ambient temperatures are higher.

When considering ground source heat pumps it is essential to note that the heat pump can be run in the reverse with the effect of cooling during the summer months. The heat

energy removed is stored underground. However, when running in heat pumping mode and using the ground as a source of 'cold' energy there is a risk of the surrounding ground freezing which may be the desired effect depending on the application[6].

Antonijevic et al. [85] present a heat pump for use in a vehicle where the energy source is the coolant used for the engine. The authors compare the use of the ORC heat pump to the standard heating and cooling system used in the car and find that the time to achieve the required temperature using heat pump improves by 50%. Despite having this advantage, the system weight is not specified in the paper, but, given the mechanical parts are sized to provide $1.9kW_{th}$ of heating it is likely to have significant mass. Further, the system is only of use during the start-up phase of the engine and no other use is detailed during the drive cycle. No cost information is provided therefore a balanced view of the true benefit of this system cannot be reached.

2.5.2 Thermoelectric power generation and heat pumps

Thermoelectric devices can be used in two operating modes: in heat pumping mode they utilize an electrical current to produce a thermal gradient according to the Peltier effect, while in power generating mode they generate an electrical current from a temperature difference, exploiting the Seebeck effect [86]. In the latter case they are usually referred to as thermoelectric generators (TEGs). In heat pumping mode the thermoelectric devices are termed thermoelectric heat pumps (THPs) or thermoelectric coolers (TECs) and their coefficient of performance (COP) is defined as the ratio of heat pumped to power input.

$$ZT = \frac{\alpha^2 \sigma}{\kappa} T \tag{2.2}$$

The metric used to compare the performance of a TEG is known as the figure-of-merit (ZT) and is based on the relationship between the electrical conductivity (σ), thermal conductivity (κ) and Seebeck coefficient (α), and T is the average temperature of the

[6]Freezing the ground using a ground source heat pump in reverse is one of the options the Japanese Government are considering around the recent Nuclear Power Plant incident in Fukushima Daiichi in 2011. By freezing the ground for an extended period of time at the site of the disaster they hope to stop the spread of radioactive groundwater in to the surrounding Pacific Ocean.

device (K). This is shown in equation 2.2.

The dimensionless ZT metric incorporates the key attributes of a thermoelectric device with the aim of comparing different devices on a like for like basis. The ZT value can also be used to evaluate the potential efficiency in a variety of ways, hence why it is often referred to as the device's 'Figure of Merit'. For reference, most commonly available thermoelectric modules today use Bismuth Telluride and have a ZT of approximately 1. An article presented by Zebarjadi et al. [87] details the physical effects of different thermoelectric structures from a ZT perspective. The Seebeck coefficient defines the boundary on the temperatures at which power can be extracted when the device is in generating mode (TEG), and limits the temperature difference when in heat pumping mode. The Seebeck coefficient can be manipulated by varying the doping of the n- and p-type semiconductor materials. The electrical conductivity determines the electrical current flow when the device is in both generating mode and heat pumping mode. The thermal conductivity defines how much heat is propagated through the device. It can be considered a parasitic effect in TEG mode: the ideal situation would be to keep the thermal energy at the source and have purely electrical power flow. However, in heat pumping mode electron migration enables heat flow in tandem and both are thus critical to ensuring an efficient heat pump.

A study by Meha et al. [88] describes the effect that new nano-materials will have when applied to the field of thermoelectricity. The article quotes a ZT value of 1.1 which is achieved by decreasing the thermal conductivity, while maintaining a high Seebeck value of 300μV/K and good electrical conductivity. A study by Biswas et al. [89] describes the practical realisation of nano-scale thermoelectric devices and the manufacturing techniques used to develop these nanoscale thermoelectric devices.

An application of thermoelectric generating devices to waste energy scavenging is presented by Felgner et al. [90] comparing the ORC with TEGs when fitted to a biogas production plant. The authors conclude that the TEG efficiency is lower than the ORC when extracting waste heat energy and converting it to electrical power. However, the TEG has no moving parts or fluid processes, therefore has can be considered lower maintenance than the ORC. Thermoelectric devices do not use any harmful refrigerants and

are shown to be reliable in work by Rowe et al. [91]. Their finding are not surprising given that for the temperature range available in this process they are unlikely to exceed $\eta = 3\%$ at best.

One of the few limitations to the reliability of thermoelectrics concerns the manufacture of the materials and their subsequent fabrication, described by Case [92]. The author presents the correlation between Young modulus of elasticity and the thermal expansion. At the individual pellet level, a TE module consists of two small pellets around 1mm in height, and $1.4mm^2$ area standing beside each other in a line. These pellets are placed on a thin layer of solder ($0.5\mu m$ thickness) with connects a series of pellets together before being mounted on a thin ceramic layer of 1mm thickness. Finally the top layer of solder connections is made and an optional ceramic layer is placed on top. Typical device sizes can range from 5mm x 5mm to 55 x 55mm with the number of pellets varying between 36 and 449 for the largest modules. However, there are far-reaching implications inherent in the manufacture of these devices that influence the ultimate mechanical packaging within a system.

Case [92] considers the effect of thermal fatigue by thermal shock to the brittle structure of the thermoelectric device, concluding that the most reliable materials have a high Young's modulus and high thermal expansion coefficient. However, these factors do not lend themselves to efficient thermoelectric devices - the thermal expansion coefficients place an upper limit on the module size for a given temperature excursion. There is a tradeoff between these factors and care must be taken when manufacturing devices for use in thermal cycling environments. The designer must also consider the transient temperature gradients likely to be encountered, as well as steady state operation.

The limits to the physical size of the TE device in thermal cycling applications for a power plant can be relaxed somewhat because of a constant low temperature difference. Thermal power plants seldom change temperature by more than a few °C once in full operation therefore a thermoelectric heat-pumping device could be physically considerably larger due to the low absolute temperature difference, which makes the thermal stress across the device manageable.

This view is supported in work by Hikage et al. [93]. Reliability of a thermoelectric

devices is analyzed by D'Angelo et al. [94]. The authors present test apparatus and measure the output power of the TEG when a constant temperature difference is imposed. This test is performed over a short term, 30 days and the best long term example of TEG operation is in the Voyager space system detailed by Ritz et al. [95] [7].

Traditionally, thermoelectric devices have been applied to refrigeration cycles as described by Min et al. [96]. An evaluation of prototypes of thermoelectric refrigerators is presented. These are: forced convection on both sides of the THP; forced convection and circulating liquid; liquid-circulation on both sides of the THP and a conventional vapour-compression refrigeration unit. Their study concluded that the liquid circulation on both sides of the THP (inside the chamber and outside to the atmosphere) was the closest in matching the performance of the vapour-compression refrigeration unit. This is

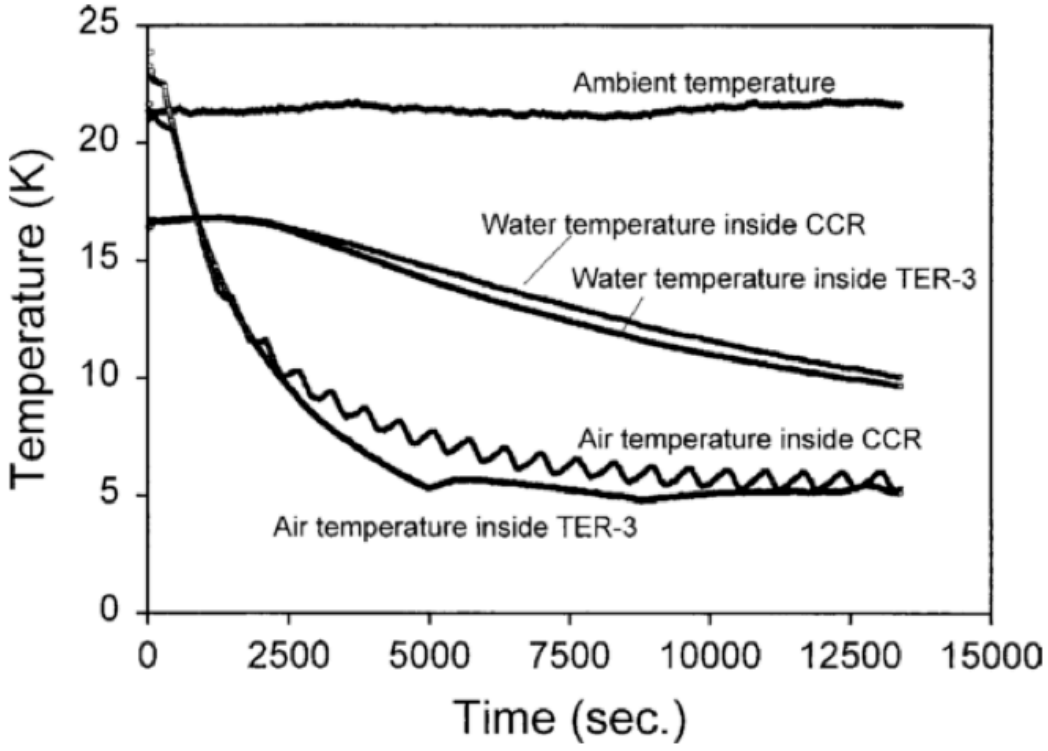

Figure 2.23: Comparison of temperatures inside and outside a refrigeration unit

shown in Figure 2.23 where TER-3 is the liquid circulation type and CCR is the vapour-compression refrigerator. Furue et al. [97] have investigated the performance of a TEG system placed in the flow of flue gas exiting the boiler of a $10MW_e$ Rankine cycle thermal

[7] A decade after this paper was published the system is still working – 40 years of continual operation which is a remarkable achievement.

power plant. The authors proposed placing the thermoelectric generators between two pipes, one carrying the exhaust gas from the boiler and the other containing the cooling liquid for to the condenser. Initial calculations show the TEGs recovered 1.84% of the electrical output. The main issue identified in this configuration is the rise in back-pressure due to the presence of the fins in the flue gas stream: this compromises the specific requirement that the flue gas must not suffer premature condensation inside the chimney.

Kyono et al. [13] have shown the application of TEGs to the condenser of the Rankine cycle, specifically on the surface of the pipes that are open to the exit of the low pressure turbines. The application is shown in Figure 2.24. The plant is capable of generating

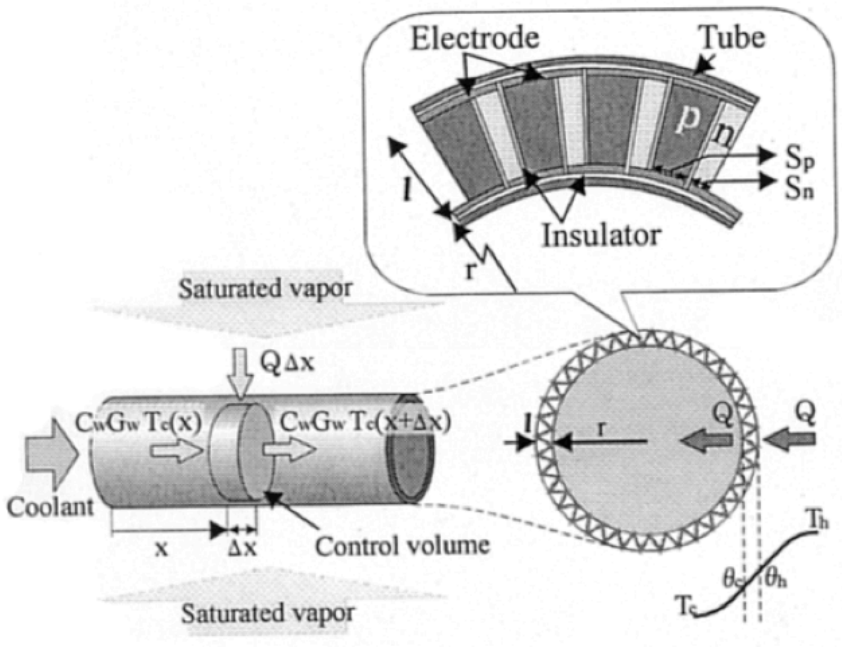

Figure 2.24: Thermoelectric generators applied to tubes of a condensing coils in a thermal power plant [13].

$700MW_e$, and condenses the steam from the low-pressure turbines at $33°C$. The authors assume that the temperature difference experienced across the TEG in the condensing pipe to be $27°C$. Since this is a low temperature difference, resulting in low output power per TEG, a very large number must be used in order to extract useful power. Despite the number of TEGs, the resultant electrical power generated remains low at around 0.78% additional electricity generated but requiring 131km of Copper tube with TEGs

in the condenser. This application is not considered economically viable in any way and illustrates the practical difficulty in extracting large amounts of energy from low grade heat sources.

Yazawa et al. [98] have demonstrated a thermoelectric generating device applied to the high temperature inlet of the Rankine cycle. The high temperatures at the top the steam cycle are interfaced with a TEG to generate electricity. The system considers the efficiency impact from a purely electrical standpoint and the inlet temperature of the steam is always assumed to be above the maximum operating temperature of the turbines. Therefore, in the analysis presented by the paper the TEG gives an efficiency improvement. However the TEG efficiency is lower than the Rankine cycle efficiency therefore combining the two techniques will result in a net reduction in the system because the original fuel input is not considered.

Yamaguchi et al. [99] propose extracting electricity using TEGs attached to the boiler of a thermal power station where they are exposed to 1500K. Traditional Bismuth Telluride (Bi_2Te_3) is not suitable for this application since the solder joints forming the module will melt at temperatures over 700K. SiGe and some Oxide compositions could be used at this temperature, however.

ZT for Bismuth Telluride drops as the temperature increases, summarised in Figure 2.25 from work by Kim et al. [14]. The Figure 2.24 shows that the various Figure-of-merit parameters, Seebeck coefficient and the power factor all decrease in value after 450K and the Power Factor drops off significantly towards 550K. As an aside, one practical point that is often overlooked in theoretical work is that even though for $BiTe$ the various important parameters describing the electrical output decrease above 450K, the power produced by the device is proportion to the output voltage squared, so with increasing temperature there is still a continually increasing power output, albeit at a rate slightly less than the square-law function.

To overcome the temperature limitations of $BiTe$, the authors propose using Silicon Germanium ($SiGe$) that can withstand the temperature levels experienced in a furnace. However, the study does not consider the impact on overall plant efficiency use of TEGs in the boiler would have: it is very likely more fuel would be required to meet the inlet

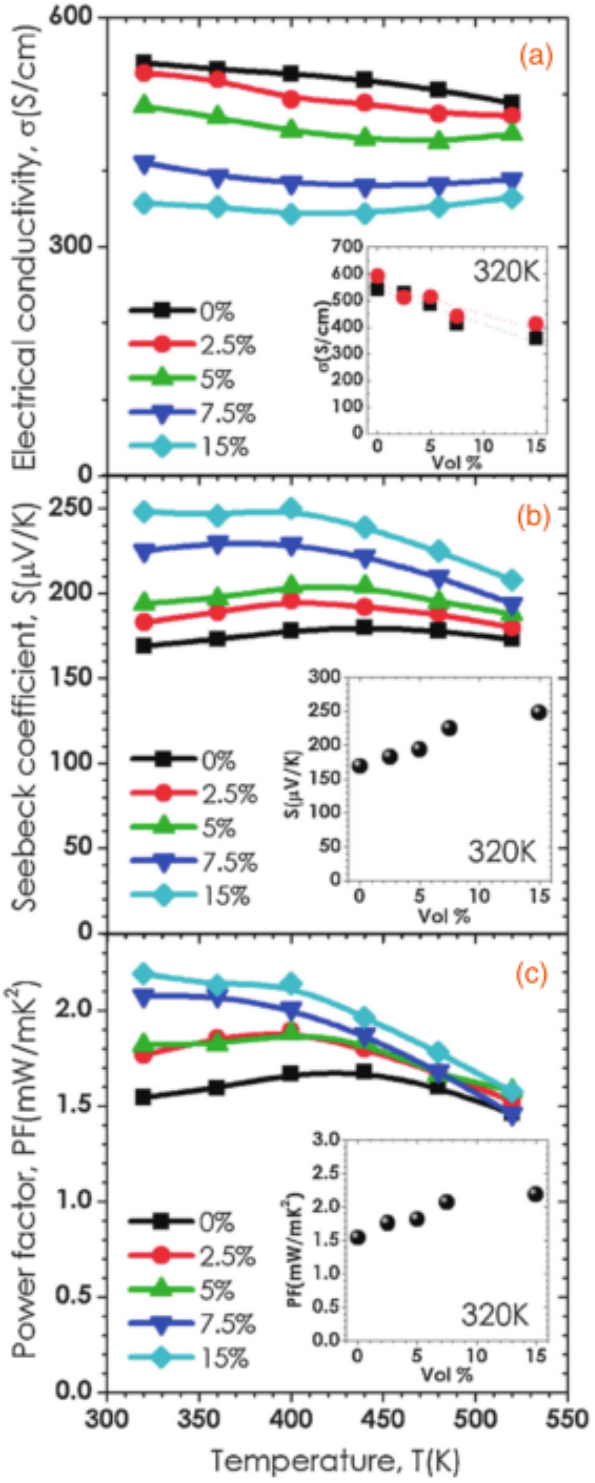

Figure 2.25: Figure-of-merit parameters and power factor for BiTe across a range over temperatures [14]

conditions of the high-pressure turbine. Once again the work fails to assess the impact on overall system efficiency. Further work by Kondo et al. [100] investigates applying TEGs in the heat exchangers of the feed water heaters. A $600 MW_e$ thermal power plant is selected as the base of this study where feedwater is rejected from the steam turbine

island at various stages to preheat the water returning to the boiler. This application only considers the electrical output that could be obtained by a 5% efficient TEG. No work is presented in considering the system efficiency forfeited as more energy is consumed by the boiler to raise the feedwater to the required temperature. The energy bled by the turbines for regenerative heating is defined by how much energy is required to maintain supercritical steam conditions using a fixed input fuel amount. Therefore extracting energy from this bleed using a TEG will reduce the amount of energy transferred to the feedwater by considerably more than the 5% electrical production from the TEG. Hence more fuel will be required by the boiler to obtain the same steam conditions as existed prior to the 'improvement'. The power plant Rankine cycle has benefited from continuous incremental improvement for many decades and consideration of overall system efficiency is essential to ensure that the addition of a thermoelectric device is beneficial to the overall cycle. Chapter 4 of this thesis presents a system level efficiency calculation assessing the break-even condition for thermoelectric devices applied to the plant condenser.

Work by Wu [101] introduces irreversibility concepts in heat transfer for TEGs stating that there is an inherent thermal resistance between the hot side and cold side reservoirs that must be accounted for. This work becomes particularly relevant when developing applications for TEGs, as careful consideration must be given to the thermal interface between the heat source and cold sink.

The study analyses the efficiency of the thermoelectric generator when in three operating situations and compares each to the idealised Carnot efficiency. The findings of the study show that the idealized TEG used in modelling has an overestimated efficiency. The study attributed the reason for this to little consideration of the thermal interfaces between the TEG and the heat sources and sinks. Therefore it is important when modelling a TEG, or indeed any thermoelectric device application, to consider the effect of the interface materials used. Buckle et al. [15] detail a novel application for an underwater vehicle that uses TEG's to supplement the electrical energy for a battery-powered autonomous ocean glider. The gliders dive and surface over large distances across oceans collecting environment data over extended time periods. They are self-powered using onboard batteries to alter the buoyancy of the glider to force diving or surfacing. In this

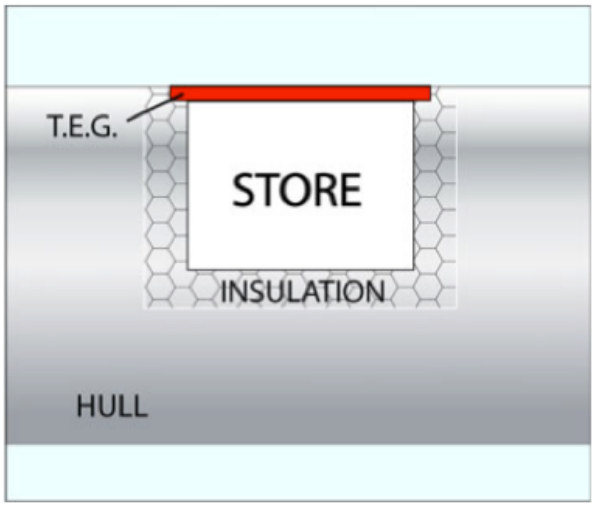

Figure 2.26: TEG applied to an ocean glider [15]

application the temperature difference for TEG operation is generated by the thermal gradient of seawater as the glider changes depth between the ocean floor and the surface. By placing the TEG on the top of an insulated enclosure (as shown in Figure 2.26) one side of the TEG is exposed to the ocean temperature and the other to a thermal store ('STORE' in Figure 2.26) that lags behind the ambient ocean temperature. The principal of operation of the thermal store makes use of the long duration of the glider's transition between temperature extremes. The thermal store must maintain a temperature difference for long enough to generate electrical power. The results of the simulations presented show that approximately 25 TEGs are required to power the glider. This application exploits the ability of the thermoelectric device to operate bi-directionally as the thermal store becomes the 'hot' side and then the 'cold' side depending if the glider is moving towards the ocean surface or ocean depths. The attraction of this approach is that the glider can operate autonomously for much greater periods than would be possible using only batteries.

The application of TEGs to a gas pipeline is presented by Xiao et al. [102]. The energy source is the hot fluid being transported by the pipeline and the power produced is used in autonomous sensors for temperature and other pipeline instrumentation.

A study by Leonov et al. [103] examines the applications for very low temperature difference thermoelectric generators. In particular, a TEG powered watch and an ECG

heart rate monitor are detailed. The TEG powered watch operates on a temperature difference of just $1°C$ to provide enough power to charge a capacitor to ensure the correct time is kept when the watch isn't worn. The ECG monitor consists of three TEGs mounted on various points around the chest to charge a small coin cell battery. Uses for flexible, wearable thermoelectric devices are explored by Francioso et al. [104]. The article quotes the ability to manufacture a TEG device with an open circuit voltage of 430mV and an electrical output power of 32nW at a temperature difference up to 40°C temperature difference. The flexible nature of these devices makes them attractive for body applications where the environment the device would be operating is unsuitable for brittle thermoelectric devices. Wearable thermoelectric devices provide a vast range of potential applications for supplying electrical power to low powered electronic devices, or supplementing a larger energy store or battery. However, the challenge with these applications is manufacturing a thermoelectric system that can operate at very small temperature differences. The TEG watch operating from 1°C temperature difference delivers a power of just 1μW but has a natural 'cold' side heatsink in the form of the body of the watch. The engineering challenge is not so much in the thermoelectric materials as the design of the system to give the required temperature gradient whilst retaining the necessary mechanical compliance for parts in contact with the body.

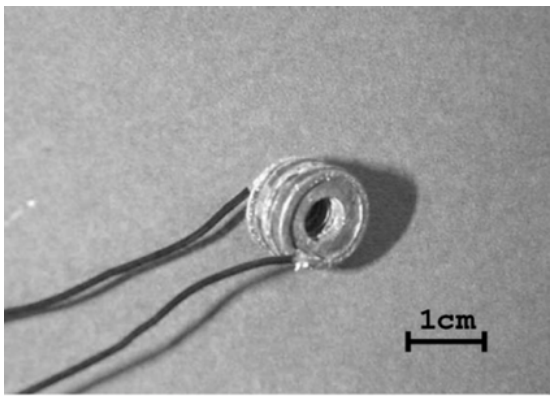

Figure 2.27: Ring-structured TEG [16]

A ring structure thermoelectric device is shown by Min et al. [16] which was developed with the aim of energy scavenging from cylindrical pipes. The device (pictured in Figure 2.27 and resulting power output shown in Figure 2.28) exhibited lower than expected performance, however. This was due to a mismatch in the device manufacture caused by

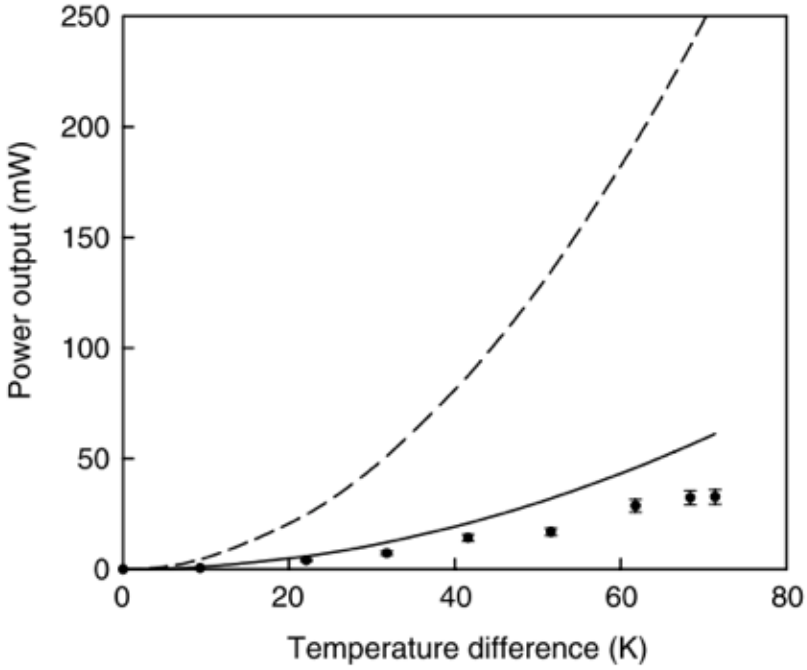

Figure 2.28: Output power of the ring-structured TEG and temperature difference [16]

the plane in which the TEGs are placed being perpendicular to the intended direction. Figure 2.28 shows the output power where the dots represent the experimentally obtained results, the solid line represents the expected results for the device manufactured, and the dashed line shows the theoretical results for the perpendicular manufactured device.

Despite the relatively poor performance, the device followed the correct trend and the paper concluded that the manufacturing process must be improved to achieve the efficiencies theoretically possible.

Suzuki et al. [17] develop a mathematical models for different 'thermoelectric tube' configurations (Figure 2.29) and show that the heat transfer surface area is a critical factor when designing these systems. The results presented in the paper show that largest output power is obtained when the TEGs are arranged in a helical path around the pipe, ensuring the maximum surface area and hence nearly doubling the length of the TEG chain when compared to the other linear configurations.

An application of recovering wasted heat energy from a vehicle is presented by Richter et al. [105] in a patent. No experimental or theoretical values are given, but the design shows the intention to scavenge the heat from the engine block directly. Heat from the engine is radiated to a metal plate which in turn conducts heat to the hot side of a TEG.

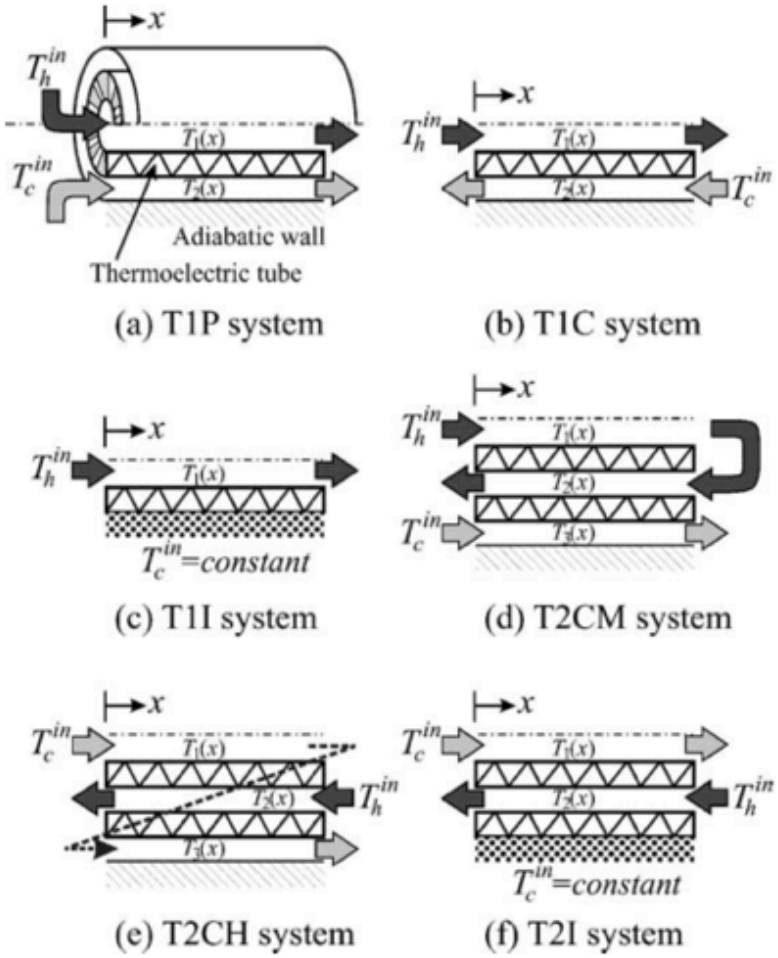

Figure 2.29: Thermoelectric tube configurations [17]

The cold side is then coupled to a heat-sink formed from either an air stream or liquid coolant stream. System efficiency is not quoted but is likely to be very low. Also, the accumulation of oil, dust and other contaminants would rapidly compromise heat transfer characteristics. Another patented vehicle application is suggested by Nakajima et al. [106] where a gas exhaust heat exchanger has TEGs integrated and the cold side is connected to the engine coolant system. This operates on the same principle as systems numerous automotive and heavy plant manufacturers are now developing.

There are two significant motivations for applying TEGs to a vehicle as presented by Stabler [18]: the first is the electrical power generated is supplied to the battery and that reduces the load the alternator puts on the engine. The second is that this reduction in load torque on the engine results in an increased crank efficiency and hence reduces fuel input to achieve the same crank power. The exhaust gas temperatures are ideal

for extracting waste energy as shown in Figure 2.30 for a 4-cylinder LD9 petrol engine. Stobart et al. [107] developed a TEG heat exchanger model simulation and experimental

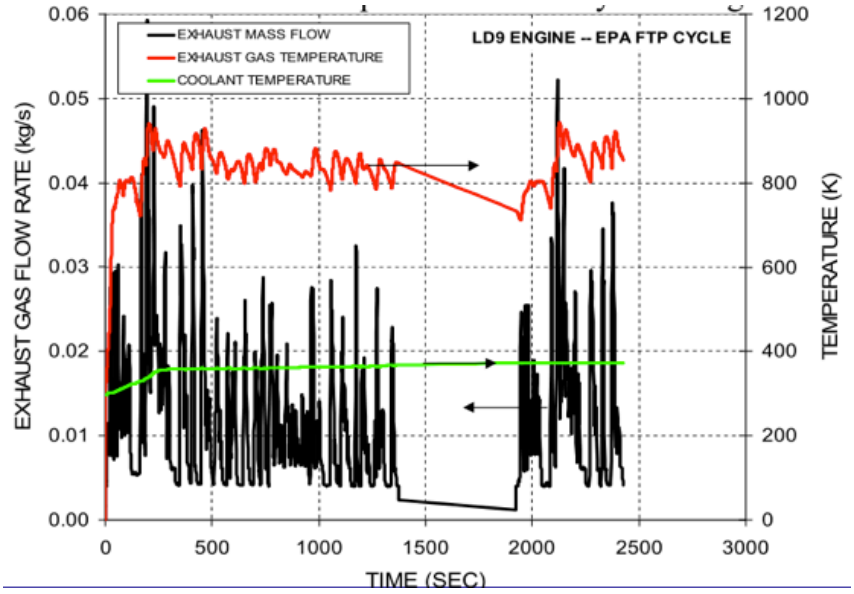

Figure 2.30: Plot of exhaust gas temperatures and coolant temperatures show a large temperature difference [18]

setup for TEGs in the vehicle exhaust for energy recovery. The paper projects fuel savings with a TEG system at varying performance levels. The system was modeled to maintain a hot side temperature of 800K and coolant flow of 288K, the 'cold' side interface to the TEG was effective, however, the highest temperature at the hot side of the TEG was obtained at lower exhaust gas flow rates. This shows that implementation in the IC exhaust requires careful design.

Work by Hsaio et al. [108] experimentally models a TEG system applied to the exhaust gas of a car. The thermal resistance of the exhaust gas heat exchanger is modelled then the experimental results are correlated to this model. The experimental results from the exhaust model show a lower efficiency than the simulation model which has no consideration of exhaust gas thermal resistance. The authors claim the simulation model is able to give a more precise efficiency estimate but does not detail how the system would perform in a gas flow system where the heat transfer mechanism is predominantly via radiation rather than conduction. More importantly perhaps, the evident disagreement between theoretical/simulation results and those actually measured indicates there are physical effects present that the models do not include. This view is supported by

anecdotal evidence from several exhaust gas energy recovery projects using TEGs which suggests that the simulation tools available to the system designer are not yet able to properly predict actual system efficacy. In practical applications the whole system from

Figure 2.31: Electrical model of a thermoelectric generator [19]

thermal to electrical conversion must be considered. As noted in the preceding discussion, significant effort has been expended in exploring the optimum heat transfer conditions but the electrical power production side must also be explored to ensure the maximum amount of electrical energy is converted from waste heat. To this end an electrical model presented by Lineykin et al. [19] has generally been accepted by the academic community and is shown in Figure 2.31. Their model comprises a voltage source and series resistance that changes with the temperature difference across the device. Using this model, the engineering challenge then becomes to simulate and experimentally validate an electrical power system that is able to convert the variable DC voltage from the TEG that is temperature dependent to a constant voltage that enables interfacing to other electrical components such as batteries and microprocessor systems. The maximum power transfer from the TEG circuit to an electrical load occurs when the external load resistance matches the internal resistance. Adherence to the Maximum Power Transfer Theorem for thermoelectrics as been shown by Nagayoshi et al. [109] and Tokumisu et al. [110].

Extraction of the maximum power from the TEG by load resistance matching is extensively examined in work by Montecucco et al. [24]. The authors present a maximum power point tracking (MPPT) algorithm for TEGs that measures the open circuit voltage periodically and then varies the current from the TEG to achieve precisely half the open-circuit output voltage. The energy extracted is used to charge a 12V battery. As the temperature difference across the TEG changes, the maximum power point will change and therefore the output current and effective resistance also changes. The benefit of MPPT is also reinforced by Yu et al. [111]. Crane et al. [20] investigates how the voltage

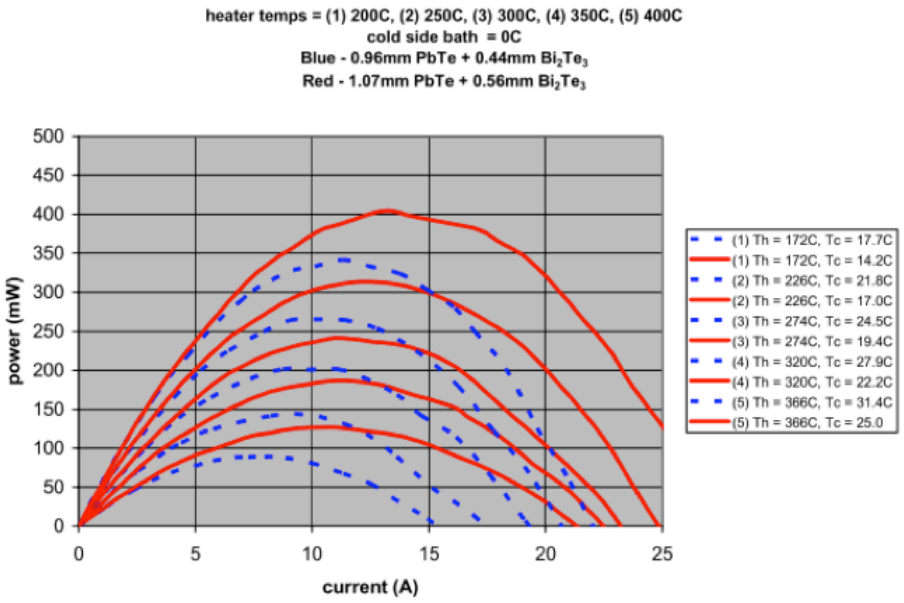

Figure 2.32: Power generation curves for changing temperature differences and different TEGs [20]

and power increases with changing TEG resistances at different temperature gradients across TEG devices with difference pellet leg lengths. Some of their results are reproduced in Figure 2.32. The peak of the parabolic curves corresponds to the MPP for each operating temperature.

Lesage et al. [112] investigate the required electrical load for a solar plant application. Due to the variable nature of the insolation the authors note the need to have a variable load resistance to ensure the maximum power is extracted but do not go into the details of how an electronic system might accomplish this.

Excellent mechanical connection of the thermoelectric device to the thermal sources and sinks is essential if good performance is to be achieved. Small modules, up to 25mm x 25mm, are available with metalised faces which permit soldering of the device directly to the rest of the system. This provides mechanical security and good thermal contact. Above this size, internal stresses caused by differential expansion and contraction exceed tolerable levels and therefore preclude soldering. The most common alternative method of mechanical connection is to clamp the module in a 'sandwich', with thermally conductive materials such as graphite sheet, carbon or copper grease used as gap filler at the interfaces. The metallic side of each interface should be highly polished for best results – unlike e.g. heat exchangers where turbulent flow improves energy transfer, for the

thermoelectric system a smooth surface yields the best result for heat conduction. Dry graphite is preferred where the system may have to be disassembled; often a module may be broken if trying to remove it from a system where grease has been used. Manufacturers recommend a minimum clamping pressure be applied to the module, usually in the range 1.0 to 1.5MPa. The importance of proper mechanical assembly, and the impacts likely to arise if this is inadequately performed have been investigated by a number of authors. However, a proper treatment of the topic is frequently omitted from much of the literature. In order to characterize the performance of a thermoelectric generator,

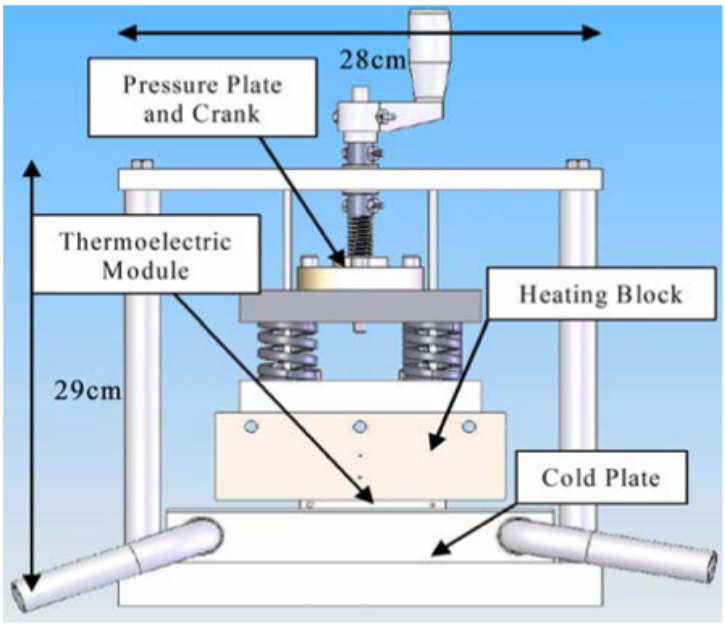

Figure 2.33: TEG test apparatus with variable mechanical pressure [21]

Sandoz-Rosado et al. [21] proposed test apparatus to apply a temperature difference to the TEG with a variable mechanical pressure shown in Figure 2.33. The test results note the impact of a heat leakage model and different temperature gradient on the electrical power output. Each temperature difference (100°C, 150°C and 200°C) is shown in Figure 2.34 with three associated data points (circles representing 100°C, triangles representing 150°C and diamonds representing 200°C). The heat leakage model is shown in the solid line, experimental data in the dotted line and the dashed line shows the analytical model. The authors do not comment on the effect of variable mechanical clamping pressure on the output power, despite their obvious intent from the fixture arrangement shown.

A similar apparatus is proposed by Gou et al. [22] focusing on low temperature waste

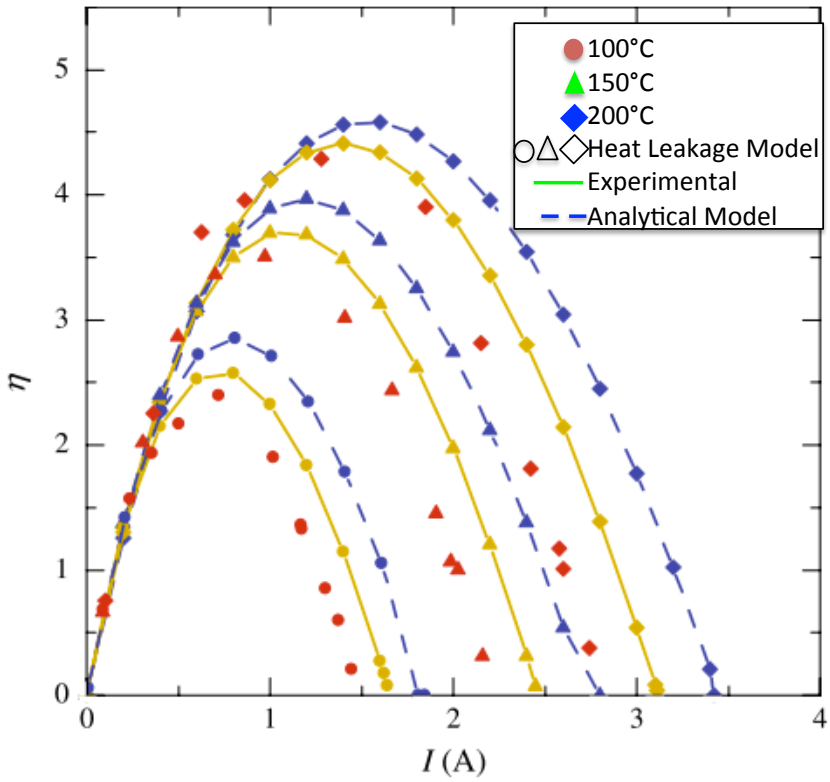

Figure 2.34: Electrical output power of a TEG system with varying ΔT's [21]

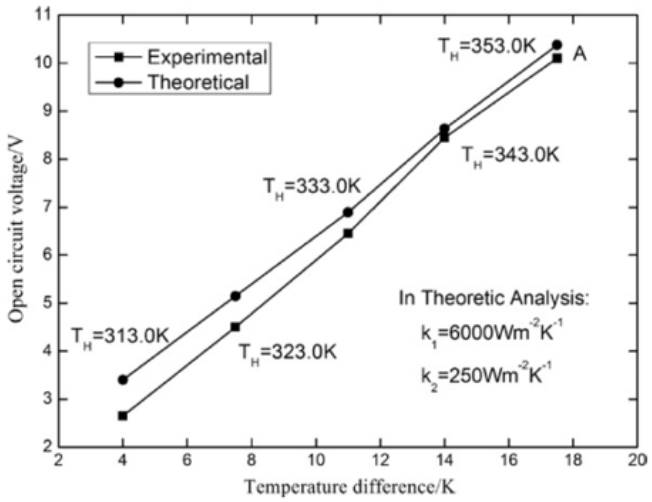

Figure 2.35: Measured open circuit voltage and temperature difference is lower for experimental values than theoretical [22]

heat. Again the authors note a difference in the experimentally obtained values (shown in Figure 2.35) and the theoretical values. The mechanical compliance of the test system is unknown, but it is likely to explain the difference in reported values. Another TEG setup is developed by Hsu et al. [23] where the hot side energy source is a gas at 500K and the cold side temperature is controlled by a heatsink and fan resulting in the system

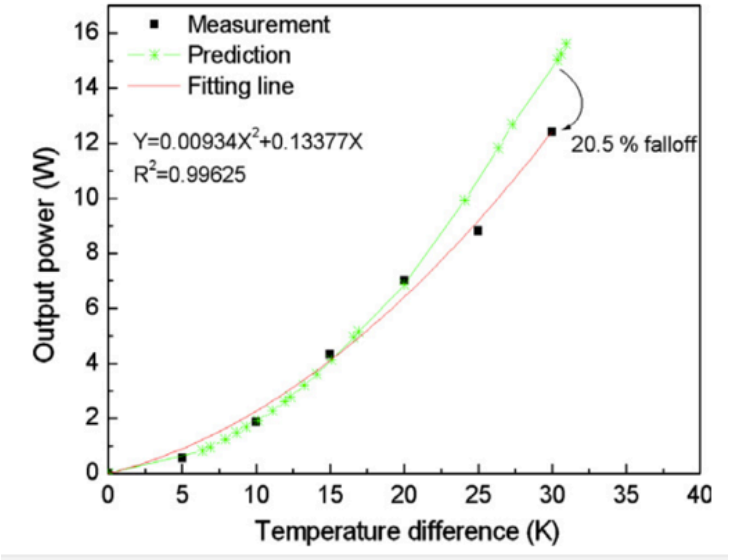

Figure 2.36: Output power at increasing temperature difference with a forced convection 'cold' side to the TEG [23]

being very sensitive to ambient temperature (Figure 2.36). Further, this system fixes the heatsink and fans to the TEG devices using thermal paste and no consideration has been given to the clamping pressure.

References [21], [22] and [23] present several different methods of testing TEGs, however, there is no common technique with authors measuring maximum efficiency or maximum power or specific tests cases for the system they intend to operate on. Therefore the datasheets produced often do not give a precise account of how the TEG may perform in other applications. A system designer is interested in the electrical performance where the output voltage or temperature difference is not specific to the thermal resistances or thermal time constants of a certain test configuration. Montecucco et al. [24] have developed a test system with minimised thermal losses through control of the conduction paths and insulation against radiative losses. This leads to an experimental apparatus to accurately compare the performance of two TEG devices at different mechanical clamping pressures. The results shown in Figure 2.37 demonstrate the impact of mechanical compliance as the pressure varies from 100kg to 200kg, showing the necessity of ensuring good thermal contact and the contribution made by the clamping force.

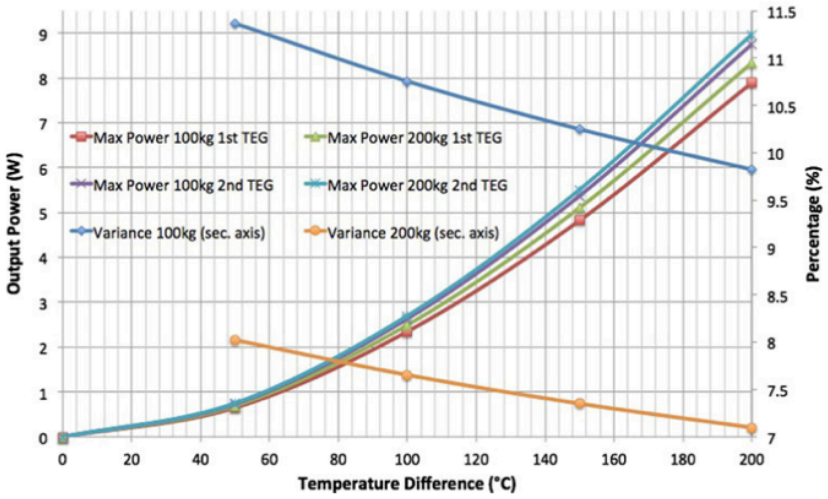

Figure 2.37: Maximum power and temperature difference across two TEGs at different pressures with a percentage variance between the TEGs [24]

2.5.3 Thermoelectric heat pumps

Thermoelectric heat pump operation depends on the Seebeck, Peltier and Joule effects. Under normal operating conditions the dominant behaviour of the THP is described by the Peltier effect: as electrical power is applied to the n- and p- couples it causes the movement of charge-carriers, driving heat transfer. Reversing the direction of the charge-carrier migration changes the heat transfer direction. In order to assess the thermoelectric device performance limits the maximum heat flux and the efficiency of converting electrical power to thermal energy transport are measured. Prior work by Min et al. [113] and Hodes et al. [114] has shown the impact that the pellets' cross-sectional area and length have on cooling performance. As the cross-sectional area of the thermoelectric element increases, its capacity to conduct current increases, leading to a larger heat flux. However, as the pellet height increases the electrical resistance increases and hence requires more electrical power to be drawn to attain the same levels of thermal performance. Therefore there is a trade off between maximizing the pellet cross-sectional area and its height. The way in which thermoelectric heat pumps can be employed is now examined.

2.5.4 Characterisation of heat pumps

The method of characterization of thermoelectric heat pumps and vapour compression heat pumps is broadly similar, and the development of a THP characterization system can be compared to that of the ORC heat pump. Work by Cho et al. [115] explores the measurement and performance of an ORC heat pump in the application of scavenging waste heat rejected by electric motors on an electric vehicle. The main performance criterion is the COP, therefore the input energies and output energy must be determined. The authors achieve this by measuring temperature and input electrical power. The experimental setup was modeled on the heating requirements of an electric bus and split in to three sections: the heat source is derived from the electronic devices and batteries, the heat sink is the passenger cabin requiring to be heated, and the heat pump is supplied with electrical power from the batteries. The system was rated to $30kW_{th}$ of heating power and this was obtained with a COP_h of 3 at an ambient temperature of 0°C.

The scalable nature of thermoelectric heat pumps permits their application in targeted areas for active heating or cooling. One of the first applications of these devices for active cooling was developed by Hava et al. [116]. The authors present a high power laser whose band-gap material is very sensitive to temperature therefore THP devices are employed to control this temperature. The device tested was built on to a device of 50μm width, 300μm length $x, 500\mu$m depth and a 2°C temperature reduction was measured on the diode at an input current of 6A. This is a very early adoption of a THP to a cooling application and is an example of the progression of the technology since then: nowadays virtually every laser used in optical communications systems is fabricated atop a Peltier cooler which is used to precisely adjust the wavelength of light produced, which is a function of the stresses in and therefore temperature of the optical material.

In a similar application, Li et al. [117] apply a thermoelectric heat pump to cool the substrate of a high power LED. The authors find that the THP is able to reduce the LED temperature by 17°C and its use improves the reliability of the device keeping the operating temperature below the maximum allowable for the LED.

Phelan et al. [118] assert that using a thermoelectric heat pump may be the only

method of maintaining high performance electronic chips whether lasers, LEDs or power amplifiers to operate at the optimal temperature. Work by Saucuic et al. [119] develop this argument further by investigating other methods of cooling and comparing them to a thermoelectric device. The THP is also applied to a data communication device in work presented by Tian et al. [120]. The speed of the communications link can be increased when the temperature of the substrate is decreased. In their paper a thermeoelectric heat pump of dimensions 40mm x 40mm is applied to the substrate of an optical sensor. The heat pump voltage and current are increased to 2.8V, 1A and various speeds of transmission are tested. The results show that the bit error rate on the link is reduced at a transmission rate of 40Gb/s when the THP is in use.

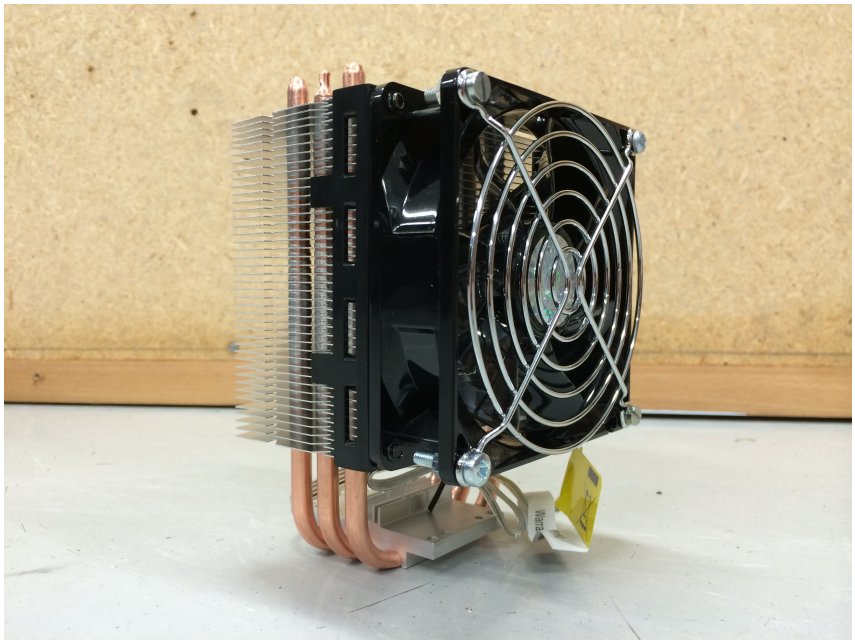

Figure 2.38: Heatsink

As microprocessor power and the number of instructions per second has increased so too has the amount of heat generated. In order to limit device degradation over time the microprocessors must be actively cooled as exemplified in work by Kondratiev et al. [121]. Assuming a perfect spherical light bulb of radius 25mm has a surface area of $7854mm^2$ and emits 100W, then the heat flux per mm^2 is $0.0127\frac{W}{mm^2}$. A thermoelectric device quoted by Zhang et al. [122] has a maximum cooling capacity of 330W for a 50mm x 50mm THP giving a heat pumping power of over $0.132\frac{W}{mm^2}$, i.e. it is able to exceed the cooling requirements for the most advanced CPUs. It is interesting to note that in these

very high performance applications invariably a secondary cooling system is employed to remove the heat from the hot side of the THP. Typically this involves the use of multiple heat pipes and a large fan-cooled heatsink, as shown in Figure 2.38. The visual appearance of the CPU cooler has also been the subject of much marketing and artistic design in an attempt to make the product look more desirable.

Chowdhury et al. [123] present active cooling of a computer processor chip using a THP based on superlattice thin-film Bi_2Te_3 technology. A superlattice consists of thin film layers of alternating materials laminated on top of each other to form a single thermoelectric pellet. The main benefits of these structures are their performance and figure of merit, specifically obtained by reducing thermal conductivity while maintaining or increasing electrical conductivity when compared to traditional manufacture using bulk materials. However, the long term thermal and electrical stability of the resulting devices is as yet unknown, as noted by Boettner et al. [124].

A patent by Letz [125] details a THP used to cool a microcontroller chip. Actual device dimensions and values attainable are not included but the principal concept described is to place a THP on the top of the microprocessor and use a large heatsink on the opposing side to remove the energy extracted by the THP. What is surprising about this patent is that it describes what has been widely available for many years and the narrowness of its claims suggests it is of little commercial value.

To further illustrate the breadth of use of thermoelectric devices, Jiang et al. [126] show how THP devices can be used in DNA amplification for biological research by thermally cycling the sample between temperatures around $45-65°C$. Kotlyarov et al. [127] present a glove-box cooler for a car using a thermoelectric heat pump. The THP is well suited to this application due to the size constraints and negligible added weight which would otherwise be incurred if a vapour-compression heat pump was used. Further, the system can also act as a heater if the outside temperature drops below the set temperature – something the mechanical system could not achieve.

Most THP applications described in the literature tend to focus on the cooling capacity and reduction in temperature that can be obtained. There is little research into their efficient heating capacity, which is of importance when investigating the improvements to

a thermal cycle and to be considered in this thesis. Work by Russel et al. [128] presents test apparatus that uses a heat pipe and chilled water loop to measure the performance of the THP. This particular test apparatus includes analysis of thermal losses such as the heat capacity of metal and resultant radiation losses of the heat pipe which are accounted for by the authors. The results of the system test show that by accounting for these losses the accuracy of the model improves but detracts from the overall COP predicted by calculation. The model accuracy when compared to the experimental values is improved, however. Accurately determining the COP of a thermoelectric heat pump is central to the work presented in this thesis and is a subject covered at length in subsequent chapters.

Perhaps surprisingly, there is little in the literature that has considered the use of thermoelectric devices operating as heat pumps in power plants. Patents have been filed with the aim of improving plant efficiency using thermoelectric devices. Yamaguchi [129] has patented work previously described [99]; [100]. The authors present a thermoelectric generator applied in the boiler of the thermal power plant. The authors claim being able to extract $35MW_e$ from a $700MW_e$ generating set. However they neglect to account for the thermal losses as a portion of the thermal energy from the boiler transferred to the 'cold' side of the device. The net impact of their invention is a considerable reduction in overall plant efficiency.

IHI Marine, a large shipbuilding manufacturer based in Japan, filed a patent [130] for a thermoelectric generator contained in a plate heat exchanger for use in a thermal power plant cooling water system. The cooling water acts as the 'hot' side to the TEG and the cold side is submerged in the sea at a deep level. The actual temperature difference across the device is very small, and hence the electrical power generated by the system will also be very small. A stove thermoelectric generating system is presented by Bass [131] where the electrical power extracted can be used to power a fan or charge a battery. A patent by Chakraborty et al. [132] describes potential industrial applications for a TEG and envisages a fluid flow with TEGs scavenging the thermal power in the fluid. Further work by Chakraborty et al. [133] details a pipeline with TEGs wrapped round the surface. A counter-current liquid-liquid heat exchanger with TEGs sandwiched between two thermal conductors is presented by Watts [134]. Taheer et al. [135] patented a TEG contained in

a gas-fluid cross flow heat exchanger. Such an application would be used in the flue gas of a thermal power plant by Jang et al. [136] or in the exhaust system of a car. A patent by Murata [137] details a thermoelectric generator applied to an exhaust of a vehicle.

The patents reviewed here show the great versatility of thermoelectric generators when applied to diverse waste heat processes.

2.6 Summary

The vast majority of thermoelectric device applications described in the literature concentrate on exploitation of the Seebeck effect for power generation. At the large scale, when applied to thermal power plants, their overall benefit to the process is, at best, dubious. In some cases there is clearly a disparity between technical accomplishment and commercial viability. In applications where exploitation of the Peltier effect is of primary importance, most papers focus on the ability to control temperature rather than pump heat and in these cases the absolute value of the COP is seldom considered. In instances where the COP is considered, other system aspects that affect device performance, for example mechanical mounting, are not examined in any great depth. One thing the literature teaches is that, although initially alluring, the exploitation of thermoelectric technology brings with it a host of engineering challenges the system designer needs to consider carefully.

In the spirit of these improvements to the Rankine cycle, a heat pump is applied to the condenser of a thermal power plant. There have been several publications on this concept by the author that form the basis of this work. Knox et al. [29] proposed the system initially and described the potential benefits of using THP's in the condenser. Siviter et al. [26] extend this work by presenting the results of commercial THPs for a condenser and further improved the analysis by combining the theoretical model and experimental results.

The remainder of this thesis explores the commercial and technical viability of the concept of the use of THPs in the condenser of a Rankine cycle plant. Chapter three details the THP model and characterization. Chapter four examines in more detail the proposed modifications to the Rankine cycle as implemented in the majority of power

plants. Chapter five describes the design of test apparatus used to perform the majority of the experimental research conducted as part of the work presented here. Chapter six then presents and critically assesses the results obtained from its use. Finally, in Chapter seven the further work necessary to scale up a THP system for application in a large scale thermal power plant is explored with a putative system design. The thesis concludes in Chapter 8 with the overall conclusions drawn from the work presented.

Chapter 3

Thermoelectric Theory and Characterisation

This chapter covers the basic physical effects that underpin the operation of thermoelectric devices and the physical structure of a thermoelectric device.

3.1 Effects

A thermoelectric device and its operation as a heat pump depends on three unique physical effects attributed to Seebeck, Peltier and Thomson. Other effects identified by Joule and Fourier that are common to all conductors and semiconductors are also covered in this chapter. Under normal operating conditions for a heat pump the dominant desired behaviour is described by the Peltier effect. The Seebeck and Joule effects are considered parasitic in this context.

3.1.1 The Seebeck effect

Discovered by Thomas Seebeck in the early 1900's this phenomenon becomes apparent when a temperature difference is applied to a semiconductor. Heat flow causes a charge-carrier migration that occurs at a molecular level within the semiconductor. Charge carriers are typically referred to as electrons in n-type material and holes in p-type material. The charge-carrier migration describes the rate that holes and electrons exchange

positions, causing an electrical current to flow. Placing two dissimilar semiconductors of different electron or hole concentration, e.g. Si and Ge, in parallel with the temperature gradient results in different levels of charge-carrier migration and hence an electrical current flows through both semiconductors. A potential difference develops at opposite ends of each of the semiconductors leading to the relationship between voltage (ΔV), temperature (ΔT) and the equivalent difference between the two current sources (α).

$$\alpha = \frac{\Delta V}{\Delta T} \tag{3.1}$$

Equation 3.1 defines ΔV as the open circuit voltage of the two semiconductors connected electrically in series, ΔT as the temperature difference applied across them and α as the Seebeck coefficient (V/K).

The Seebeck coefficient can be found for each semiconductor material given a measured voltage difference and applied temperature difference. The Seebeck coefficient for two dissimilar semiconductors joined as part of a thermoelectric device is the difference between the two Seebeck coefficients, hence the preferred use of n- and p- type materials in couples (i.e., thermocouples).

Pure metals have very small Seebeck coefficients: when a temperature gradient is applied, the voltage across the metal is proportional to the length of the pellet and its surface area. For semiconductors that are doped with excess electrons or holes (n- or p-type) the Seebeck coefficient is much larger with typical values in the hundreds of $\mu V/K$. The larger the Seebeck coefficient, the greater the resultant voltage for a given temperature gradient and hence the greater their potential for energy scavenging becomes.

3.1.2 The Peltier effect

The phenomenon associated with the Peltier effect can be thought of as complementary to the Seebeck effect. Also discovered in the early 1900's by French physicist Jean Charles Peltier, the effect concerns the magnitude of charge-carrier migration when a voltage is applied to a metal or semiconductor.

If two different semiconductor materials are electrically connected in series and a

current is caused to flow through the couple then the junction between the two devices will heat up and the opposing sides will be cooled. The effect occurs as the charge-carrier (holes and/or electrons) migration and complements the transport of phonons by lattice vibrations. Heating or cooling will occur at the device junction depending on the direction of current flow. Reversing the polarity of applied voltage reverses the heated / cooled ends of the materials.

Operability of a thermoelectric device depends on the ability of electrons and electron holes to exchange to enable electrical conduction. Fourier's law describes the change in heat flux during this process. An n-type semiconductor is usually made from a band IV element such as Silicon or Germanium and doped with a Band V element such as Antimony or Arsenic, which has a free valence band electron. Silicon is used as the substrate material with four valence electrons. When Silicon and Antimony (Sb) /Arsenic (As) are combined there is a single free valence electron.

In a p-type semiconductor the doping material selected should accept this free electron. This concept is known as an electronhole. Again Silicon is used as the Band IV substrate material and Band III elements such as Boron (B) or Aluminium(Al) are used as the dopants. These contain three valence electrons. When an n-type semiconductor and p-type are connected together, the electrons and electronholes can be combined above an applied voltage level, causing current to flow.

Typical materials used for thermoelectric devices are Bismuth Telluride (Bi_2Te_3) and Lead $Telluride(Pb_2Te_3)$, with the p- and n- type properties being established by doping with the III-V elements described. These exhibit many of the desirable properties such as high Seebeck voltage, good conductivity, and so on.

The Peltier relationship is defined as

$$\pi = \frac{P_{pelt}}{I} \tag{3.2}$$

where the amount of current and energy are related by the Peltier coefficient π, P_{pelt} is the heat transfer rate from the n- and p-type semiconductor junctions and I is the current flowing through the junction.

3.1.3 The Thomson effect and Joule heating

As current is passed through the thermoelectric device, heat is generated proportional to this current. The rate at which heat is generated is described by both the Thomson effect and the Joule heating effect.

The Thomson effect describes the heat transfer of a conductor and is dependent on the direction of current flow and temperature difference (equation 3.3).

$$P_{thomson} = \tau I \Delta T \tag{3.3}$$

where $P_{thomson}$ is the energy generated by the conductor from the current I flowing resulting in a temperature gradient (ΔT) across the conductor proportional to τ, the Thomson coefficient.

The Thomson coefficient is a function of a single conductor and therefore different from the Peltier and Seebeck coefficients which are dependent on the differences between two semiconductors.

The Joule-heating effect establishes the relationship between electrical current and resistance as a square power law (equation 3.4).

$$P_{joule} = I^2 R \tag{3.4}$$

where P_{joule} is the joule heating power in Watts, I is the current flowing through the semiconductor in Amps and R is the electrical resistance of the semiconductor in Ohms.

The pellets of n- and p-type materials that constitute a thermoelectric device will each exhibit slightly different Thomson coefficients and Joule-heating effects, influencing both their current carrying capability and therefore the thermal energy generated.

3.1.4 Kelvin relationships

The Seebeck, Peltier and Thompson effects can be related to one another using the Kelvin relationships. These were formulated by William Thomson (Lord Kelvin) in the late 19th

century.

The first relationship (Equation 3.5) states that the Peltier coefficient (π) and the Seebeck coefficient (α) are proportional to each other and related by the junction temperature (T_j).

$$\pi = \alpha T_j \tag{3.5}$$

Experimental evidence has demonstrated this relationship to hold true. Using (3.5), the expression for voltage can be rewritten to equation 3.6 as.

$$V = \pi \frac{\Delta T}{T_j} \tag{3.6}$$

The Thomson coefficient τ can be related to the Seebeck effect using the second Kelvin relationship as:

$$\tau = T_{avg} \frac{\Delta \pi}{\Delta T} \tag{3.7}$$

Where T_{avg} is the material's average temperature in Kelvin and the other variables have the same meaning as previously defined.

The implications of these relationships is that the absolute temperature of the thermoelectric junction is of critical importance to the magnitude of these effects. For a thermoelectric heat pump, the temperature at which it is operated will affect the amount by which the Seebeck, Thomson and Joule heating impact the overall performance and capacity for heat transfer.

3.2 Thermoelectric heat pumps

A thermoelectric device which transports heat is commonly referred to by two terms that depend on its application. The THP has been introduced previous and typically denotes when the heat pumping capabilities of the thermoelectric (TE) device are exploited. A thermoelectric cooler (TEC) is used to note when the cooling ability of the device is the dominant consideration. In this research the thermoelectric heat pump is of primary focus and therefore THP is the principal term used throughout this thesis.

3.2.1 THP module dimensions

A THP converts electrical power to a flow of thermal energy. A DC voltage applied to the device will give rise to a current flow through the materials, which in turn will cause the passage of thermal energy due to charge carrier migration. Assuming the THP is placed between finite thermal masses, this in turn develops a temperature difference between the surfaces of the device, resulting in thermal energy being removed from a source at one side of the device and being rejected as heat at the opposing end. The total energy at the "heated" side is the sum of the thermal energy transported from the "cooled" side and the electrical energy required to affect the transport.

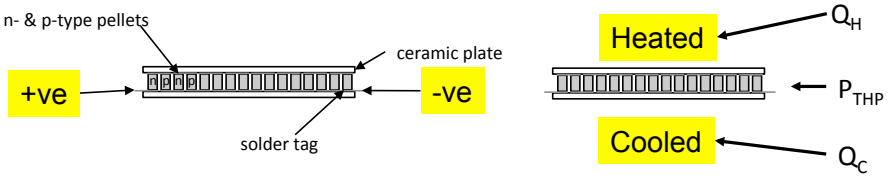

Figure 3.1: Module structure (left) of a thermoelectric device and the thermal structure (right)

The physical structure of a THP module is shown in 3.1. The semiconductor materials are manufactured into small cuboid-shaped pellets, which are electrically series-connected between a pair of alumina plates of standardised size. Table 3.1 lists these sizes between 4mm x 4mm and 50mm x 50mm. The cross-sectional area of the pellets varies between 0.75mm x 0.75mm and 5mm x 3mm: the smaller sections are usually used for power generation devices (TEGs) where large numbers of pellets in a module are required to yield a satisfactory output voltage whereas the larger sections are used in devices intended for heat pumping applications where the 'fill factor' (the ratio of the pellet area to total area of the device) and current flow are of primary importance. Since, for the THP, the quantity of heat pumped depends on the current flowing through the materials, this sensitivity to the electrical conductivity is to be expected. The height of all the pellets in a single module is nominally identical with any slight differences being accommodated for in the solder layer forming the pairs of couples. Equal numbers of n-type and p-type semiconductor pellets are used in each module. The height of the pellets strongly

Thermoelectric Device Dimensions (length x width) (mm)	Height (mm)	Number of Couples
4x4	3	7
6x6	3.8	7
9x9	3.8	17
15x15	3.8	17
20x20	3.6	71
25x25	3.8	127
30x30	3.6	127
40x40	3.8	127
55x55	3.6	241

Table 3.1: Various thermoelectric heat pump devices ranging from 20mm x 20mm to 55mm x 55mm

influences the thermal conduction properties of the module and this is described in §3.5.

The n- and p-type pellets are mounted on solders tags the width of two pellets to connect together one side of the n-type pellet and one side of the p-type pellet. Multiple n- and p-type pellets are connected in series to form single long chain.

It is common to find hundreds of pairs of such thermopiles comprising a thermoelectric device, usually 127, 254 or 449 depending on the required output voltage or physical size limitations. (Except for specialist devices, normally $2^N - 1$ couples formed in a square are used, with the space not occupied by the last pair of pellets used to attach wires. Figure 3.2 shows the cross section of a THP, 50mm x 50mm and containing 127 couples

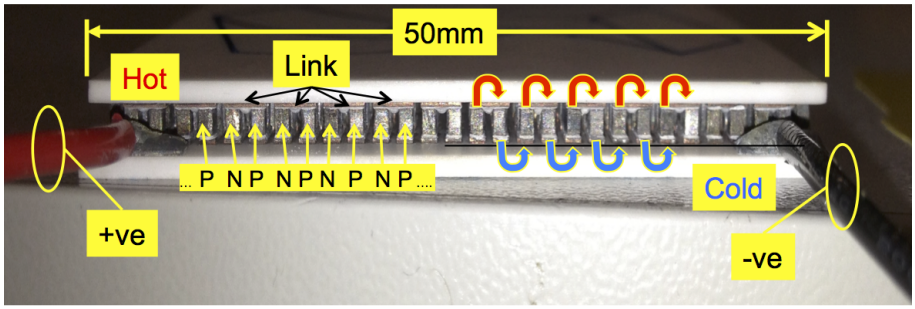

Figure 3.2: Mechanical structure and cross-section of THP

of 1.4mm (l) x 1.4mm (w) x 1.7mm (h).

Following the Seebeck effect (Equation 3.1), increasing the number of pellets connected in series will increase the open circuit voltage for a constant ΔT. Each pellet will have a small Seebeck voltage, between $200\mu V/K$ and $400\mu V/K$ for Bi_2Te_3 devices. In order for larger scale applications to be viable for thermoelectric devices a greater operating

voltage is required therefore numerous pellets are coupled together to obtain an operating potential of several volts per 100° C. The physical size of the pellets is small ($1mm^2$ or above), and larger applications introduce the need for larger thermoelectric device sizes up to a size limit of 65mm x 65mm. Above this limit, mechanical stresses induced as a consequence of the differential expansion of the 'hot' and 'cold' sides at high ΔT can easily cause mechanical failure of the module.

The Seebeck effect only describes the relationship between the voltage and temperature difference. In order to determine the complete performance of the device the electrical conductivity and thermal conductivity are also needed. The electrical conductivity determines the current flow characteristics and the thermal conductivity dictates how much heat is propagated through the device. The performance metric Z is shown in Equation 3.8, where (α) is the Seebeck coefficient (V/K), (σ) is the electric conductivity (S/m) and (κ) is the thermal conductivity (W/K).

$$Z = \frac{\alpha^2 \sigma}{\kappa} \tag{3.8}$$

The ideal device should be a good conductor of electricity but a poor thermal conductor meaning that the σ value should be large, but the thermal conductivity should be kept to a minimum to prevent unwanted heat transfer across the device. Thermal energy should remain at the respective sources in order to maximise the module temperature difference. Additionally, the Z figure-of-merit should be maximised.

The 'power factor' does not account for thermal conductivity and is defined as ($\alpha^2\sigma$). This parameter is often used in the literature in order to emphasis improvements in device electrical characteristics for new materials. The main benefit of using the figure-of-merit metric and the power factor is to easily compare many different thermoelectric devices as it is independent of the size or manufacturing technique used. It is not, however, independent of the measurement technique used, and there is considerable international effort underway to establish a standardised and consistent way of measuring the performance of different thermoelectric materials.

Bismuth Telluride is currently the most commonly used material for thermoelectric

devices: it boasts a large ZT over a wide temperature range and has proven to work reliably at high temperatures for extended periods of time without excessive degradation. With increasingly diverse application areas for thermoelectric devices there is a growing necessity to explore alternate materials that operate over larger temperature differences and higher absolute hot-side temperatures. In addition, Tellurium is a rare-earth material, which suffers from high extraction and processing costs, and therefore alternatives are being sought, especially for automotive applications where constrained supply will limit uptake of the technology and the market is particularly cost sensitive. Tellurium is also a critical element in composition of PV panels and the rapid expansion of this market is driving up material costs due to constrained supply. There are many as-yet unproven alternatives: Silicides have been developed to increase the figure of merit (ZT), have a lower thermal conductivity and are capable of operating up to $800°C$. Other common materials types include Skudderudites, Oxysulphides, Ti-S, Ni-Cr-S and Cobalt oxides. These materials are being developed for both specific markets in mind, e.g., for use in automotive exhaust gas energy recovery systems, or for their potential as replacement technologies for Bismuth Telluride. The work presented in this thesis uses current Bi_2Te_3 materials to form the THPs.

For large heat pumping powers the internal electrical resistance (i.e., Joule heating) should be low, therefore a small number of thermopiles and short pellet height are important. The current density of a conductor is given as the ratio of electric current to cross-sectional area. Maximising the area of the THP pellet and the fill factor in a module leads to higher heat pumping capability. Ultimately the performance of the THP is determined by the current passing through the module (i.e. the number of charge carriers), but this has to be balanced with the unavoidable I^2R losses in the physical wiring carrying electrical energy to the THP, the ΔT at which the desired heat transport occurs, and the operating voltage range of interest. Usually a THP module for a particular application is a compromise of many of the factors discussed above.

3.2.2 The THP coefficient of performance and its variation with ΔT

As previously noted, with larger pellets there can be a larger current flow and hence heat flux. Ideally the designer will maximise the heat flux over the operating temperature range of the THP. In order to experimentally assess the performance of a THP there are several parameters that require to be measured, including the variation of the heat pumping capacity of heating (or cooling) and the coefficient of performance (COP) with ΔT across the device.

A THP can be considered as a heat engine and hence is subject to the Carnot limit. The Carnot limit represents the maximum theoretical efficiency a heat engine can operate at: it assumes two isothermal processes and two isentropic processes, hence is completely reversible. In the 'standard' heat engine operation a temperature gradient is applied to an adiabatic fluid that expands to generate work. The Carnot limit for a THP as a 'reverse' heat engine is dependent solely on temperature difference and does not account for irreversibilities across the range of temperatures.

$$COP_h = \frac{T_h}{T_h - T_c} \tag{3.9}$$

where the suffix $_h$ denotes heating mode, T_h is the heated side temperature and T_c is the cold side temperature.

At low temperature difference the coefficient of performance is larger because less energy is required for a specific heat flux. At zero ΔT the denominator tends to zero and the COP tends to infinity. This relationship is shown in Equation 3.9 and Figure 3.3. At a low temperature difference the COP is large because of the low relative amount of power required to achieve the temperature increase. As the temperature difference increases, the amount of power required to shift the heat through the thermal gradient increases at a faster rate meaning that the relationship between input power and resultant thermal power is not linear, but follows an exponential decay. At an infinite temperature difference, COP_h is unity. The standard formula for COP for a practical heat pump is

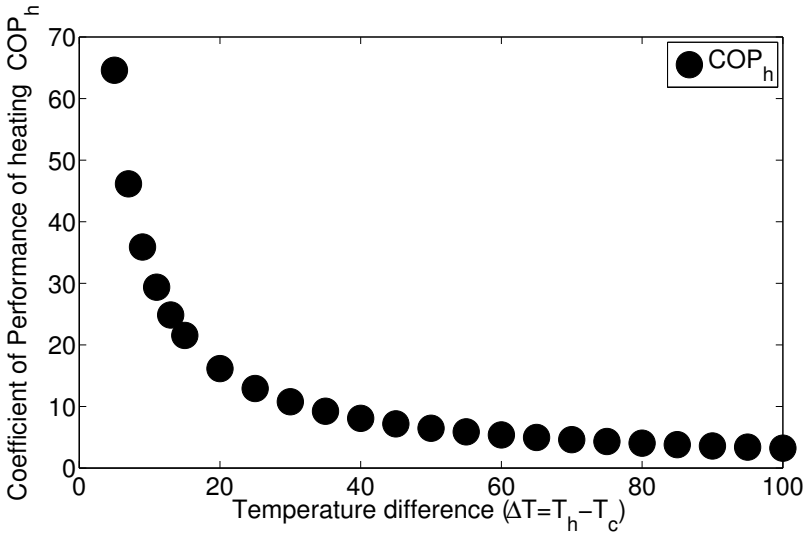

Figure 3.3: Carnot limit of COP_h with increasing temperature differences (ΔT)

given as the ratio of thermal energy (either heating or cooling) to the applied electrical power.

$$COP_h = \frac{Q_h}{P} = \frac{Q_c}{P} + 1 \tag{3.10}$$

where Q_h is the thermal energy delivered in heating mode for an applied electrical power to the heat pump P (the product of the applied voltage (V) and current (I)), and Q_c is the energy extracted from the cold side of the THP.

Although the coefficient of performance initially does not appear to have an absolute dependence on temperature, the quantity of heat converted by the THP does have this dependence and is shown in the Kelvin relationships. As the temperature difference across the device increases, the Carnot limit states that the COP_h should increase. However, for a practical THP is this not strictly true because of the additional energy contribution due to internal Joule heating of the device, which raises the average device temperature.

In the following sections detailed analyses of how the COP_h changes with temperature and the optimum driving power to maximize the available COP are presented.

3.2.3 Thermoelectric heat pumping driver requirements

When electrical power is applied to the thermoelectric device it behaves like a resistor. There is a small capacitance associated but since the device is driven with a DC source can be neglected for all practical purposes since the electrical resistance is of the order

of a few ohms at most, yielding time constants of the order of ns. The module leads will introduce some inductance and if the DC supply is pulsed, the resulting switching transients due to the reactive impedance components must be controlled. Good practice to minimize loop inductance by using twisted wires of equal length should also be adhered to.

Heat is pumped in the direction of electrical current flow, the corollary being that the direction of heat flow is determined by the polarity of the applied voltage. This feature makes the THP very different from the normal compression / expansion heat pump operation and is a feature unique to the thermoelectric device. If an alternating current is applied to the THP, the electrical polarity changes each half cycle and hence the direction of heat pumping also. If the period of the applied waveform is shorter than the response time of the thermal system then the result will be zero net heat flow between the 'hot' and 'cold' faces, and a net input of thermal energy from the THP to both faces equally due to the electrical power dissipated in the THP.

In a THP the Seebeck effect is parasitic, generating an opposing voltage that acts to reduce the current flowing through the module, thereby reducing the heat pumping. Thus as the module warms up it appears as if its electrical resistance increases.

The V_{max} rating of a THP device is the DC voltage which will deliver the maximum temperature difference (ΔT_{THP}) for a given hot side temperature (usually about $70°C$). For the condition that $V < V_{max}$, there is insufficient current flowing through the module to achieve the greatest ΔT_{THP}. For $V > V_{max}$ the power dissipated within the device due to electrical I^2R losses starts in increase the overall system temperature and therefore reduces ΔT_{THP}. For $V = V_{max}$ the maximum ΔT_{THP} is established. At this voltage I_{max} also occurs giving the maximum heat pumping effect as the largest migration of charge-carriers occurs. V_{max} is dependent on the temperature of the device but the current (I_{max}) remains essentially constant throughout the operating temperature range. V_{max} and I_{max} are not the maximum voltages and currents the module can withstand but they are the values that yield the greatest ΔT across the device. The maximum ΔT across the THP occurs when no heat is being pumped so the thermal load is zero.

It is common to use a Pulse-Width Modulated (PWM) drive regime with a THP. This

yields a system which is able to pump variable amounts of heat simply by varying the duty cycle. So long as the PWM supply voltage does not exceed V_{max}, whenever the drive is 'on' the device will pump heat. When 'off', the heat pumping stops. When using a PWM drive the switching frequency should be high enough to minimise thermal stresses in the module. Operation frequencies in the region of a few kHz are usually sufficient although this may be increased if audible effects are to be avoided. In a conventional PWM system driving a resistor at a higher voltage and reduced PWM duty cycle can be used to obtain the same average output power. This does not work with a THP and Figure 3.4 and Figure 3.5 illustrate the problem. For $V > V_{max}$, the 'on' phase I^2R losses in the module reduce the heat pumping ability. In the 'off' phase, no pumping occurs. By increasing the PWM drive voltage the thermoelectric system instead becomes highly inefficient. Even in the case of $V \leq V_{max}$, the system is not performing optimally because during the 'off' periods no heat is being pumped and hence the average COP_h is reduced compared to that which would be attainable from continuous pumping using an unmodulated DC supply.

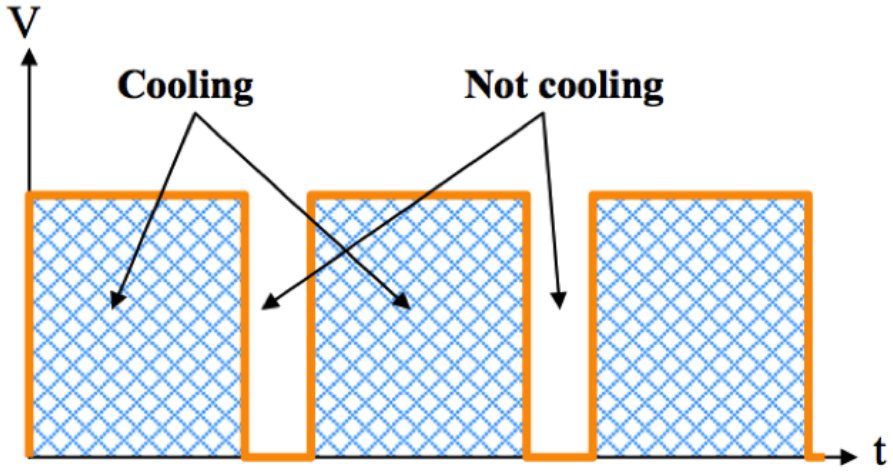

Figure 3.4: PWM driven THP for when $V \leq V_{max}$

In order to drive the THP most efficiently the device must be continually run (shown in Figure 3.6). For a given heat load on the thermoelectric module the efficiency with which the heat can be pumped is greater and the module is running at a higher average COP.

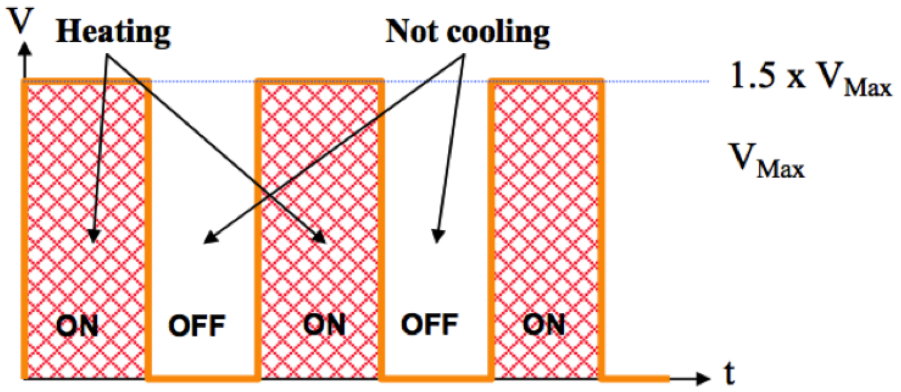

Figure 3.5: PWM driven THP where $V > V_{max}$

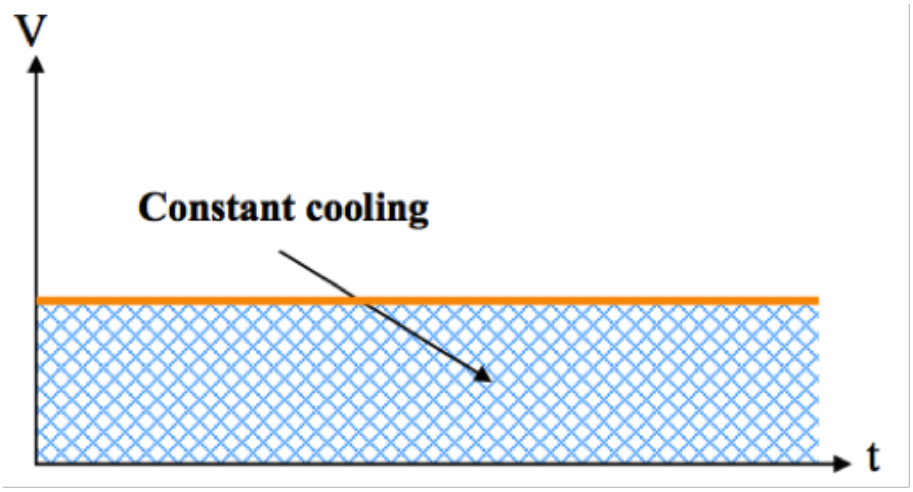

Figure 3.6: Constant driving power gives a constant cooling or heating ability

3.3 THP characterisation theory

In order to assess the performance of THPs in terms of the maximum heat flux that can be pumped and the efficiency of doing so, electrical input power and thermal energy transport were measured. Test apparatus was designed to facilitate these measurements. The thermal energy changes at either side of the THP characterise how the device performs. Figure 3.7 shows the schematic for the tests conducted. Q_h is the thermal energy removed at the 'heated' side, Q_c is the thermal input power available from energy supplied by electrical heaters and P_{THP} is the electrical power applied to the thermoelectric heat pump. Temperatures, pressures and fluid flow rate are measured at each 'T','P' and 'F' point(s) shown in the diagram.

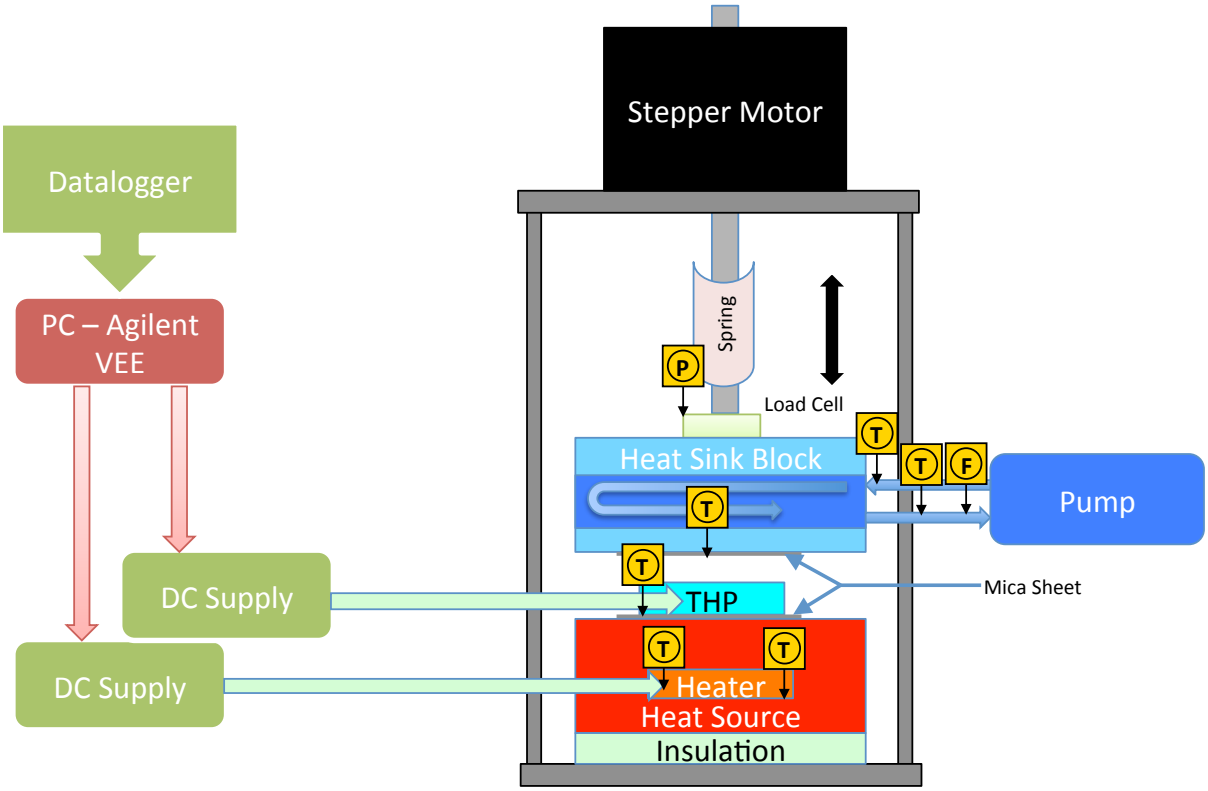

Figure 3.7: Test apparatus schematic for the characterisation of a THP

3.3.1 First iteration of measurement apparatus

This work is the result of significant previous efforts in characterising a THP which used 100W electrical power resistors as a heat source for the cold side of the THP: the thermal energy dissipated by the resistors was provided as the input for transport by the THP. The opposing 'hot' side of the device was in good thermal contact with a heat exchanger connected to a water chilling unit. The heat exchanger in this case was a simple aluminium block with three pipes passing through the device, through which the chilled water flowed. Thermocouples were placed at the water entrance and exit of the centre channel to measure the temperature difference acquired by flow through the block. The flow rate is measured using a hall-effect sensor that generates a frequency proportional to the rate of rotation of a turbine in the liquid. The measurement instruments were remotely controlled using Agilent's VEE Professional test automation software. This method enabled automatic, timed instrument control and data acquisition from the experiment with high accuracy and repeatability. The data acquisition unit measured the temperatures of each probe with

a resolution of one place after the decimal, and matched the probe accuracy of ±0.1°C. A multi-channel power supply was configured to independently control the voltage and current of both the heater pack and the THP device.

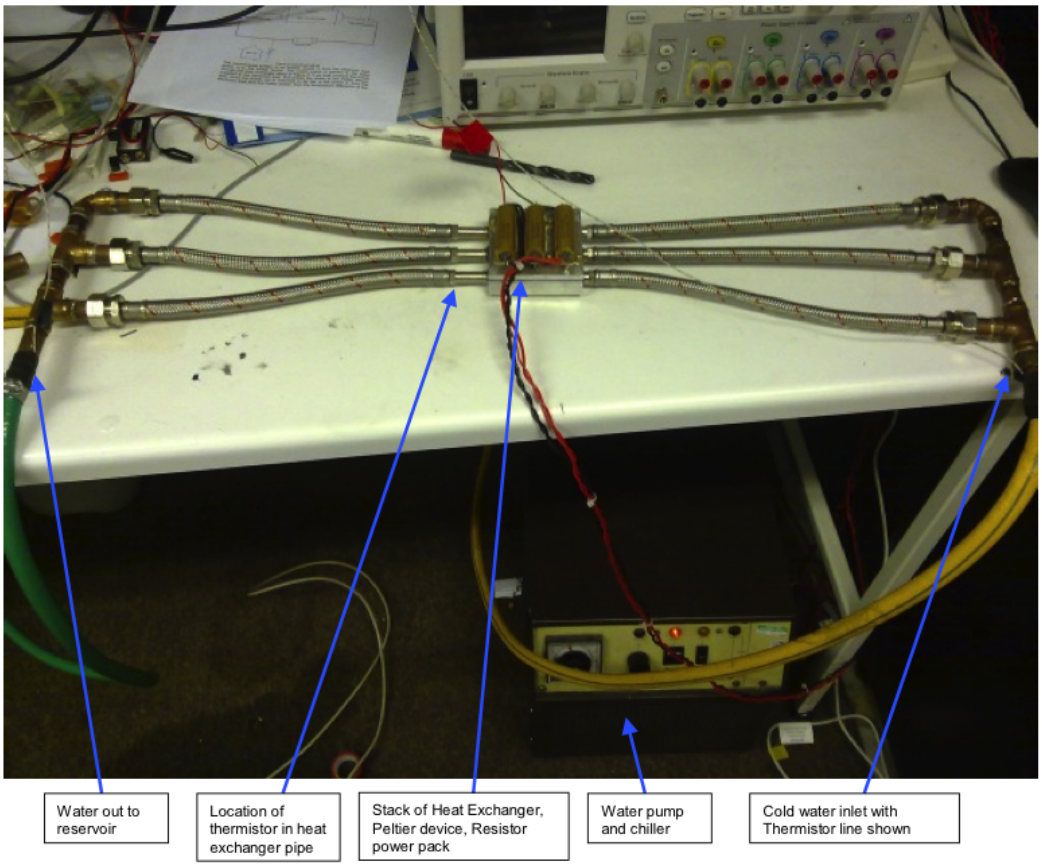

Figure 3.8: First test set up for characterisation of THPs

The quantity of thermal energy transferred from the electrical supplies to the chilled water via the THP was measured from a known mass flow rate and specific heat capacity of the chilling fluid. The COP was determined from the ratio of input electrical power to the THP and the temperature increase measured across the hot-side heat exchanger. The experimental apparatus is shown in Figure 3.8.

The COP of heat pumping is large when the device is transferring heat at a small temperature difference (0-5K). The results depicted in Figure 3.9 show that as the temperature difference across the THP increases, the COP decreases, indicating the ability of the THP to remove heat from one side of the pump to the other requires progressively more power (ultimately risking the THP operating as a heater rather than heat pump). For comparison with the Carnot limit a COP for a $\Delta T = 15°C$ ($T_h = 33°$C, $T_c = 18°$C)

that is achieved in the experiment is 19.85. The THP equivalent is a COP of 2.2, which is around 10% of the Carnot COP.

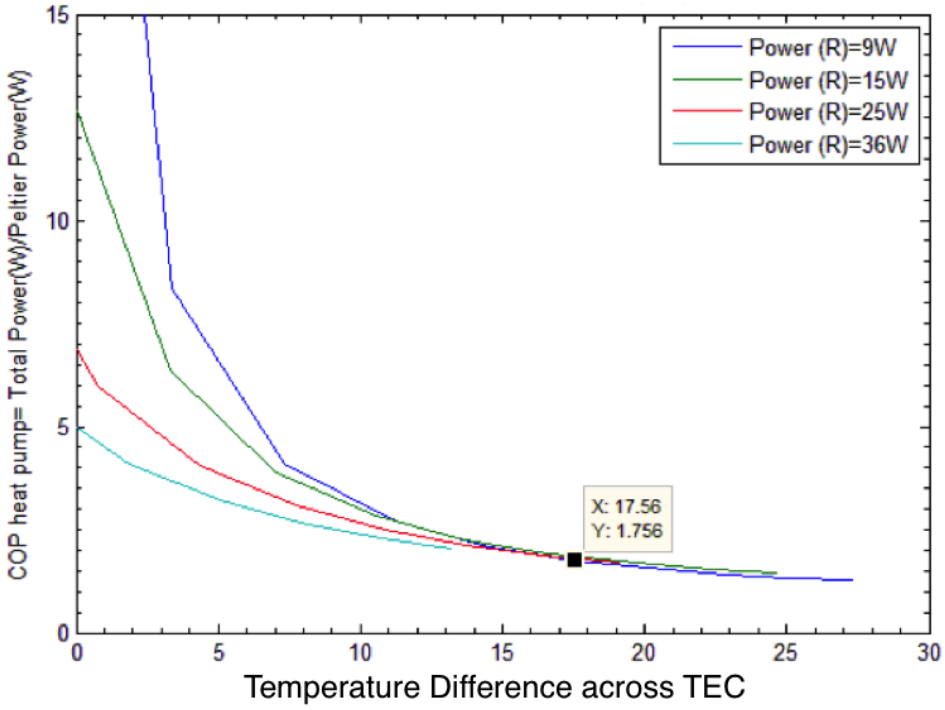

Figure 3.9: First THP Characterisation data showing temperature difference across the THP with COP of refrigeration

The COP was not calculated solely using the temperature measurement: as the temperature of the heater unit dropped below the ambient lab temperature condensation formed on the surface of the resistors, caused by the energy extracted by THP being greater than that delivered to the electrical heaters and thus causing the temperature at the cold side of the THP to drop below the dew point in the lab. This meant that the resultant heat removed by the water flow would have to include a factor to account for the energy removed from the atmosphere. In order to overcome this problem in future experimental setups, larger heater powers are required to prevent the temperature from dropping below the dew point.

The issues with the first iteration of the test system are summarised:

- Assumed all electrical energy is converted to heat. Convection and radiation losses are not accounted for
- Low electrical heater power resulting in cooling below the dew point

- Simple heat exchanger design leads to limited surface area for heat transfer to water.
- Limited mechanical compliance.
- Thermal short circuit across the screws leading to inaccurate energy flow across THP.
- Thermocouples placed on surfaces of the heaters and in the water, not in direct contact with the THP surfaces.
- Thermal shorts caused by condensation of water droplets as the THP dropped below the dew point of the room.

These points were addressed in the second iteration of the apparatus to improve the accuracy of the THP characterisation. The second version is still in use today.

3.3.2 Current test setup

The test fixture now in use allows for a single THP module up to 70mm x 70mm to be characterised. The fixture provides mechanical clamping pressure up to 250kg with very high impedance thermal paths for any thermal energy not flowing through the device under test. The heat pumped side can be supplied with up to 800W of input power with minimal thermal losses to ambient. Temperatures are sensed by thermocouples capable of 0.1°C accuracy and a computer program controls each measurement instrument to allow for averaging and accurate time stamping.

The revised experimental setup used a chiller unit to maintain a set temperature difference across the THP. However, at low input power the energy flux through the THP was too small to measure a rise in the fluid passing through the heat exchanger, despite throttling the fluid flow from the chiller unit to the lowest accurate reading available from the flow meter. This problem was overcome by the addition of a variable frequency inverter capable of accurately controlling the liquid flow rate of the heat pumped loop in the heat exchanger. In order to maximise the time the liquid was in contact with the heated surface of the THP, an advanced labyrinth design of heat exchanger was implemented.

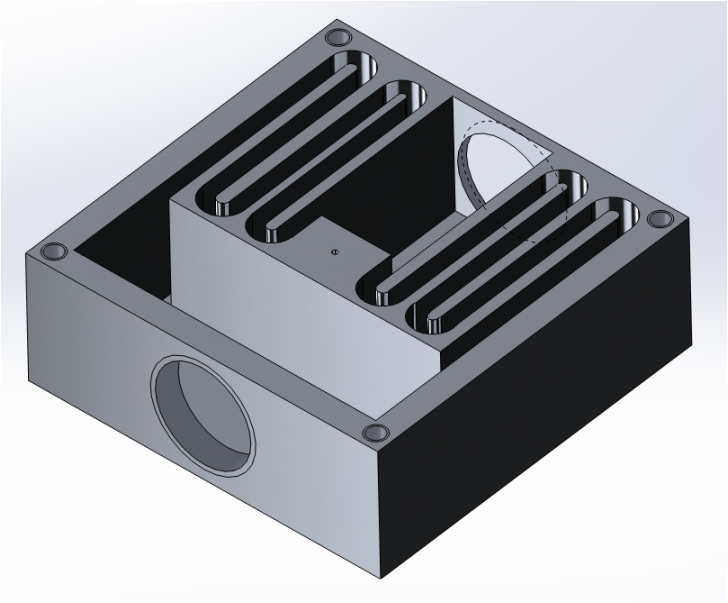

Figure 3.10: Labyrinth heat exchanger design

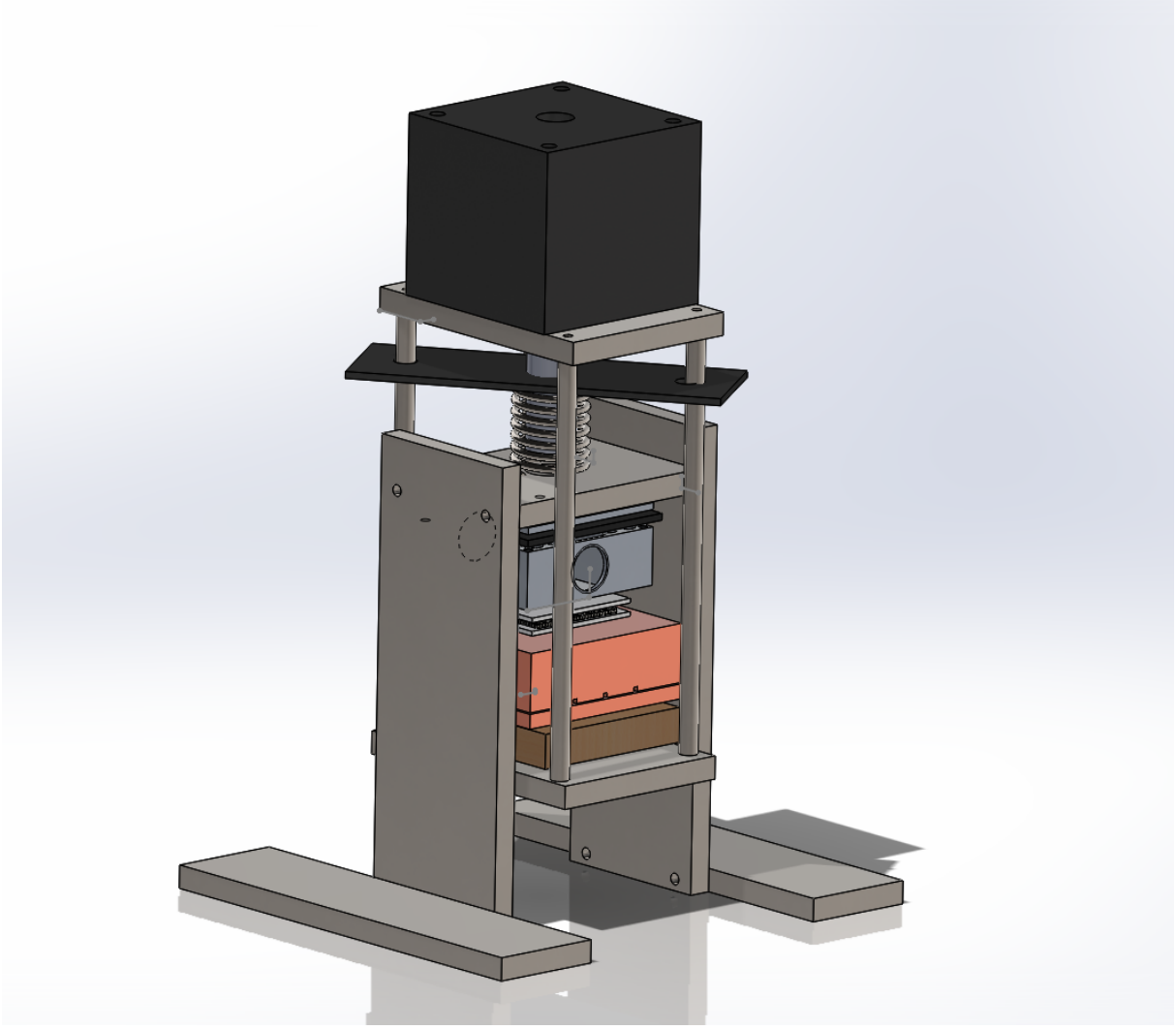

Figure 3.11: Experimental setup

A CAD drawing of the labyrinth design is shown in Figure 3.10. Figure 3.11 details the experimental setup.

The electrical power to the THP is provided by accurate control of an Agilent DC power supply (Agilent N5765). The maximum operating voltage is 30V and 50A; sufficient for testing very large modules, or multiple modules connected in series or parallel. An aluminium heat exchanger is in contact with the hot side of the device, connected to a water tank and with flow metered by a gear pump.

$$Q_{th} = mCp\Delta T \tag{3.11}$$

The temperature difference is a metric used to predict the performance on a heat exchanger. As such, the inlet and outlet temperatures, heat transfer coefficient and total surface area are required. A temperature increase obtained by powering a THP can be converted to thermal energy by analysing the water temperature increase seen across the heat exchanger by applying the steady flow energy equation 3.11).

where Q_{th} is the thermal energy, m is the mass flow of the water, Cp is the specific heat capacity of the water and T_o and T_i are the outlet and inlet temperatures respectively.

It is important to note that the previous equation is independent of heat exchanger type or flow arrangement therefore the energy values can be compared and equated to each other. The total heat transfer rate (Q_{he}) can be determined from the temperature difference between temperature of the THP and mean temperature difference of the water. There is an intrinsic thermal resistance that can be characterised by the overall heat transfer coefficient (U) and is proportional to the surface area of the thermal interfaces (A).

$$Q_{he} = UA\Delta T \tag{3.12}$$

In order to transport the largest possible amount of energy to the water there are several effects to be considered:

- Insulation of the HE from ambient temperatures to ensure only the heat from the THP is transferred to the water

- Thermal conduction between labyrinth chambers is negligible
- Potential and kinetic energy changes are negligible
- Specific heat of the water is constant
- The heat transfer coefficient is constant

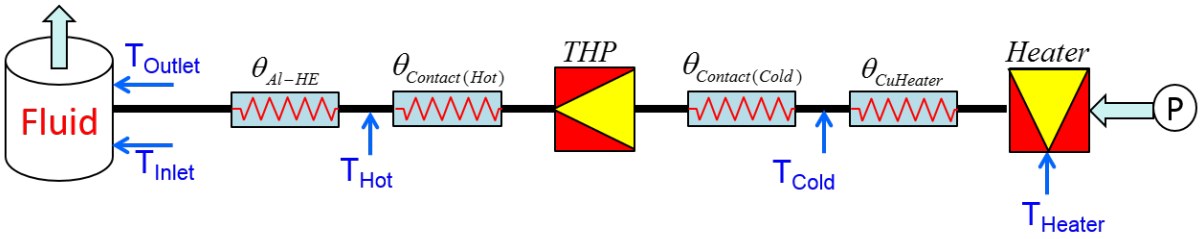

Figure 3.12: Thermal resistance model of the THP characterisation setup

Since the entire test structure was to be manufactured from various metals with high thermal conductivity, special consideration had to be given to ensure that heat flow could only occur in desired path. A thermal resistance model of the losses is presented in Figure 3.12. Aluminium was selected as the main material for manufacture: it has a relatively high heat capacity (910J/kg.K) and excellent conductivity, thereby ensuring that the majority of the thermal energy developed by the THP is transferred to the water with the lowest change in temperature of the heat exchanger itself. Further, if a very simple flow characteristic was used for the HE then the majority of the flow in the heat exchanger would be laminar and have a low Reynolds number, potentially leading to the build-up of hot spots that reduce heat transfer. The aim of a labyrinth heat exchanger design is to encourage turbulent flow and reduce such hot spots.

Radiation losses to the environment were limited by layering glass fibre around the fixture. A cut-out section of mica was placed around the outside of the THP to limit the line-of-sight losses between the heater block and the heat exchanger.

Figure 3.11 details the experimental setup. The heater block is made from Copper and contains two Silicon Nitride heaters. These are surface igniters that are usually used in oil heaters. Each heater is a rectangular in shape providing a large flat surfaces aiding thermal coupling to the copper blocks. These heaters are also capable of being operated

at temperatures in excess of 1200°C which is significantly higher than the temperatures required in THP testing (and indeed the melting point of the copper blocks, but the heat flux through the copper is such that nowhere near this temperature is ever achieved). The present test fixture contains two igniters each rated at 500W / 120V heaters and the very high thermal conductivity of the copper will ensure no local hotspots, even if the heater temperature are slightly mismatched. Figure 3.14 shows the CAD drawing of the heater block. Copper shims are placed between the top face of the igniter and the copper block to ensure the surfaces are in good contact, with care being taken not to excessively compress the heaters which are mechanically hard but not tough. Three thermocouples are located in the copper block: one on each of the faces of the heaters and is the third in contact with the face of the THP being tested. Each heater is controlled independently, but both are controlled in parallel in the Agilent VEE program.

Since the electrical power to the heaters is the 'cold' side to the device and the input power to the THP is also known then the thermal energy at the opposing side of the device is the sum of the THP power and the 'cold' side source power (given by equation 3.13).

$$Q_h = Q_c + P_{THP} \tag{3.13}$$

Figure 3.13 shows a plot of the thermal energy at the heat pumped side of the device and the calculated value for a temperature difference across the THP of 5°C. The blue diamond set of data represents the sum of the electrical power applied to the THP and the electrical power supplied to the heater blocks. A 5% error margin is included to account for measurement inaccuracies at higher temperatures and powers. The red square set of data represents the thermal energy increase measured in the water heat exchanger. A 10% error margin is included to account for an increased degree of scattering at higher temperatures. This is reasonable due to increased irreversibilities caused by raising the temperature of the thermal masses of the heat exchanger and associated pipework used to obtain this measurement. This therefore verifies the relationship in equation 3.13.

A gear pump is used to circulate water from a 20 Litre storage tank to the aluminium heat sink. The flow rate of the water is set by using a variable frequency inverter to

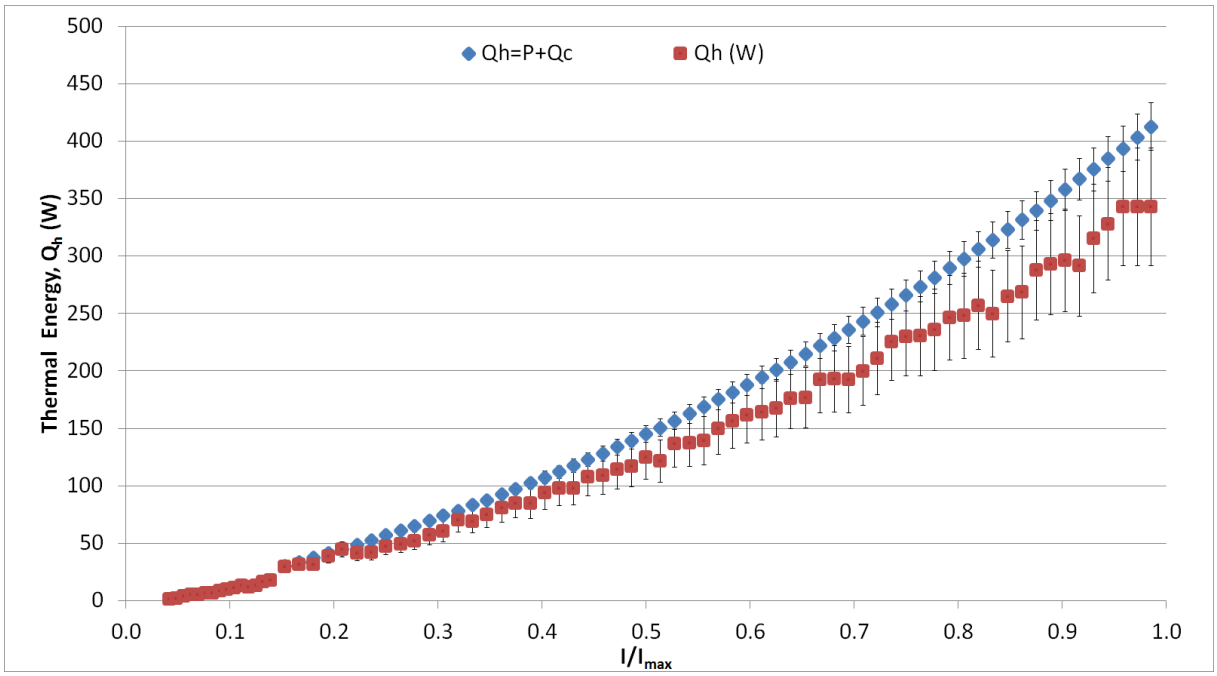

Figure 3.13: Thermal energy at the 'heated' side comparison between the calculated values and experimentally obtained values

drive the pump's induction motor. A sensor is used on the motor's fan to measure the mechanical RPM of the motor (hence pump RPM), to overcome the potential inaccuracy due to induction motor slip, and this is further correlated with an analogue flow meter and a Hall effect digital flow meter. The digital meter is connected to the data logger and the analogue flow meter uses a cone and sight glass to provide an observable reading of the flow and is used primarily to check the apparatus is working as expected.

Mechanical contact between the surfaces of the THP's and the heat sink faces was maintained at the manufacturers recommend a pressure of 1.25MPa to minimise the impact of contact thermal resistances on the thermal efficiency. To achieve this level of mechanical pressure consistently with variable temperature and hence thermal expansion / contraction, the cold side of the test apparatus containing the labyrinth heat exchanger is attached to a mechanical structure and the copper heater blocks are placed on a support column that can be brought in to contact with the heat exchanger by compressing a stiff spring (rate 178.6 kg/cm) on the top the support fixture. The spring preload is controlled by turning an M20 bolt atop the spring and placed on the top surface of the mechanical fixture. This holds the entire test fixture in compression at the desired load. The operating force is measured by a load cell strain gauge and correlated to a weight as

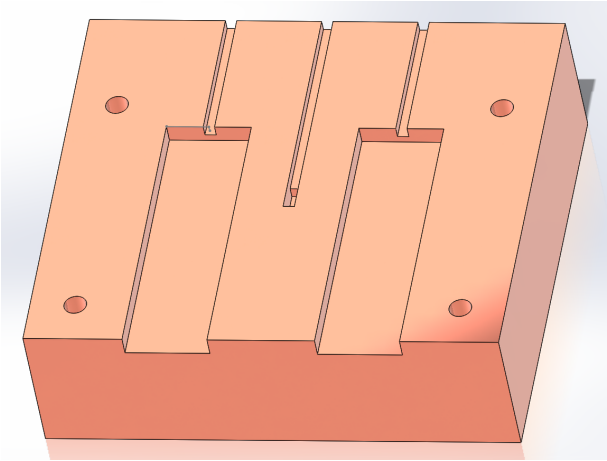

Figure 3.14: CAD drawing of heater block constructed from Copper

shown in Equation 3.14.

$$W = 44.0199\Delta V \tag{3.14}$$

where W is the weight (kg) and ΔV is the measured voltage across the load cell. The strain gauge measures a small displacement in a metal slot cut on the load cell. The metal forming the slot expands and contracts as the cell is loaded and unloaded with force from the spring. Each change in displacement causes a change in the electrical resistance of the metal and this is measured in a Wheatstone bridge configuration where a DC voltage is proportional to the weight. The cell is separately excited by a 5.000V source and is positively located in the test fixture by means of a 0.5mm recess milled in the load spreader plate at the base of the spring.

During early testing it was found that even small expansions in the test fixture due to increased temperature caused relatively large changes in the applied force, despite the inherent spring compliance. In order to maintain a constant pressure an automation system was devised using a stepper motor driven linear actuator. The stepper motor is able to make fixed angular rotations by alternating the power applied to each coil wound to a brushless DC motor. When applied to the linear actuator, each step equates to a small angular turn of a screw in a thread and hence a variation in the clamping force. Haydon Kerk [1] supplied the stepper motor and the motor control driver. The stepper motor has a non-captive Acme-threaded shaft and is capable of a 1.8° step angle. The

[1]Haydon Kerk Non Captive Linear Actuator, 8700 Series, 87F43 `http://www.haydonkerk.com/LinearActuatorProducts`

lead-screw is placed through the centre of the motor which drives the screw in the Z direction. The lead screw is prevented from rotating by the diagonal plate in the fixture, shown in 3.11 and the motor armature rotates about the threaded rod.

3.3.3 Initial Tests

To obtain the COP curve of a thermoelectric device for a specific ΔT the electrical current applied to it is increased in a series of steps from zero to a value where the peak COP has been passed, subject to the constraint that the maximum current (I_{max}) is never exceeded. The input electrical power to the heater providing the thermal energy to be pumped is adjusted at each step to maintain the temperature difference. This procedure is then repeated for a range of ΔT's across the device to obtain a family of curves for the device. The optimum current (I_{opt}) corresponds to the peak value of the COP for the particular ΔT under consideration. Before each measurement is recorded the control program uses a PID control loop to adjust the heater power such that the apparatus is stabilized at the desired ΔT for that step in current. The ratio of input electrical energy to the resultant thermal power flow to the 'hot' side determines the COP.

The actual adjustment and measurement process for COP is rather involved and extensive use of programmable instruments is required for a practical measurement system that is semi-automatic. The following procedural steps are implemented using Agilent VEE Professional and the flow chart for the process is shown in Figure 3.15.

(a) All system components are allowed to reach thermal equilibrium at the ambient lab temperature

(b) The user enters the desired temperature difference across the device, the desired mechanical clamping pressure, the input electrical current increment and maximum current in the control programme. The programme then calculates V_{max} of the device and sets the power supply for the THP to operate in constant voltage mode.

(c) The instruments are programmed and an initial set of measurements at $\Delta T = 0K$ (i.e. when the system is in thermal equilibrium) are taken. These readings are subsequently used to calculate the calibration offset factors for each of the thermocouples used.

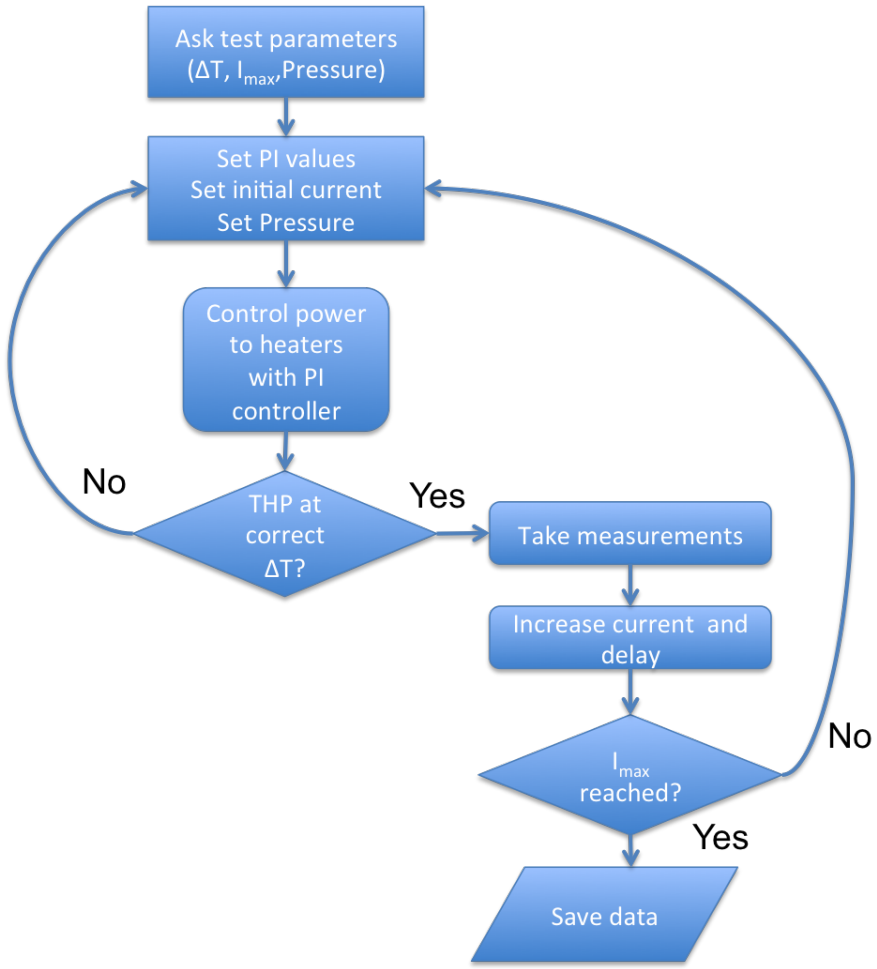

Figure 3.15: Flow chart of the characterisation of a THP programme

(d) The control programme increments the current applied to the THP.

(e) The desired temperature across the device is maintained using a software PID control loop by varying the electrical power supplied to the Silicon Nitride heaters. This provides a source of thermal energy at the 'cold' side for the THP to pump to the heated side. Separate programmable power supplies are used for the heater elements and provide reading of the current, voltage and power.

(f) The control programme then waits until the temperatures have stabilized at the desired temperature difference (determined by obtaining five successive readings at 5 second intervals within the desired temperature tolerance) before recording the temperature of each of the heaters, the heated and cold sides, and the water inlet and outlet temperatures as shown in Figure 3.7.

(g) The control programme calculates the next electrical current value for the THP and

returns to step d) unless I_{max} has been reached.

(h) When the maximum device current is reached the test for this particular ΔT is complete and the programme saves the recorded data in a CSV-format spreadsheet file. All power supplies are reset and the programme terminates.

A set of performance data obtained using this technique is shown in Figure 3.16.

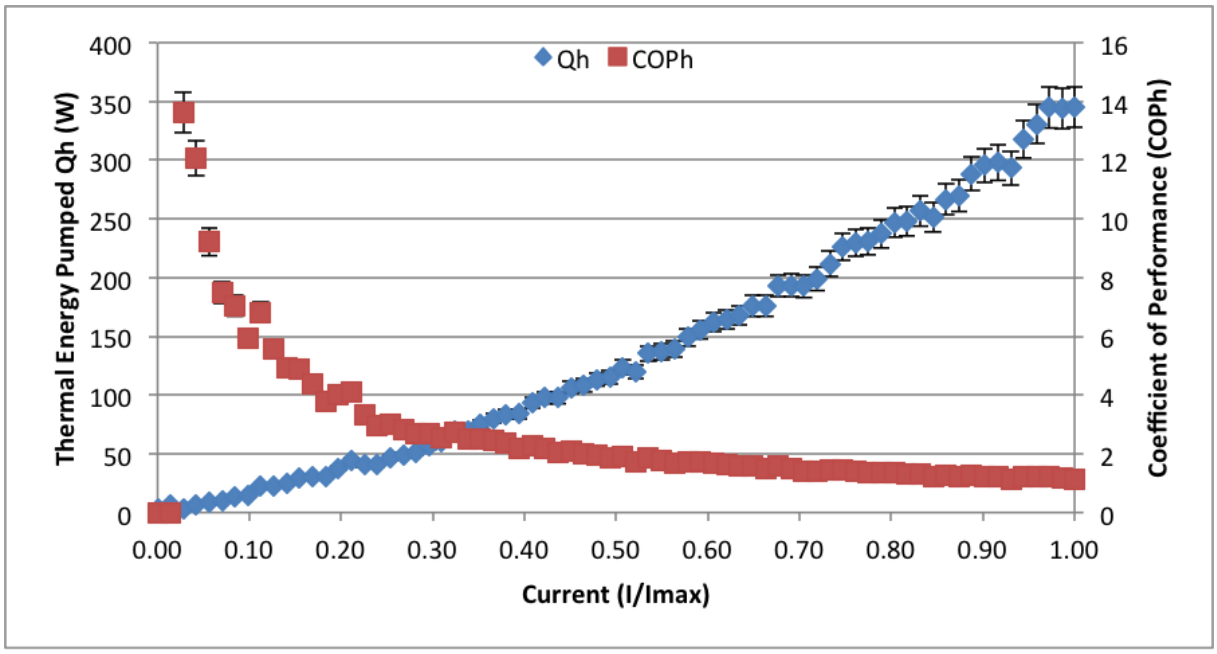

Figure 3.16: COP_h and Q_h plotted against the current ratio I/I_{max} for a $\Delta T = 5$ using a 50mm x 50mm THP

During testing using the water block heat exchanger it was found that for low values of P_{THP} accurately determining the increase in Q_h was exceptionally difficult. The temperature difference in the fluid between the inlet and outlet of the heated water was a few thousandths of a Kelvin, even at low flow rates. This is shown in Figure 3.17.

This is less than the short-term repeatability of the temperature measurement accuracy of the Agilent data-logger and this lack of accuracy was considered unacceptable. In order to overcome this deficiency in the experimental apparatus an alternate test was designed in order to facilitate more accurate measurements at low Q_h values.

In an attempt to reach the desired accuracy at low THP current values, a different test technique was adopted. The method involves recording the temperature change of a pair of thermal masses with known specific heat capacities over a predetermined time

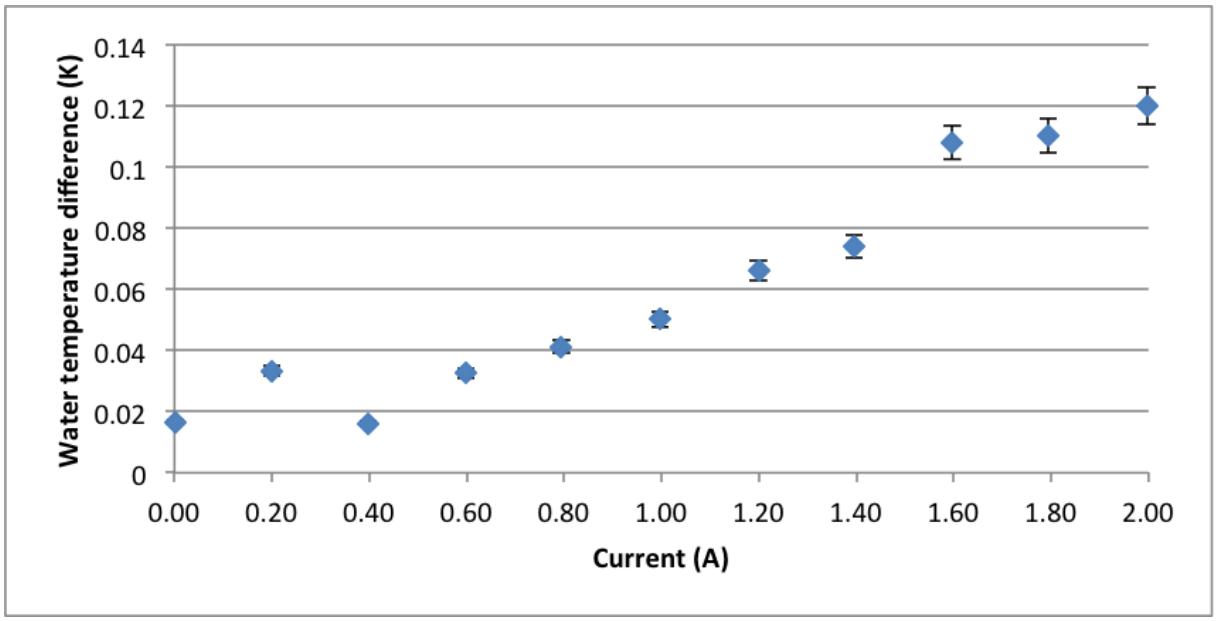

Figure 3.17: Measured water temperature difference as input current to the THP increases to 2A

interval. Two blocks of 99.8% pure copper were accurately weighed and the THP then sandwiched between them. The THP was clamped together using tension springs to provide a compressive force of 0.8MPa. Each spring has a spring rate of 31.8N/mm, with preload of 510N. The spring was extended by 14mm giving an additional force of 1246N. Two springs were used at equal tension resulting in 2492N. 0.8MPa was slightly below the manufacturer's recommended 1MPa but the availability of suitable springs limited what was attainable in a relatively simple fixture. The reduced pressure was considered acceptable in light of prior work by [24] which showed the variation in pressure from 800KPa to 1MPa would have a negligible impact on the results obtained.

After connection of all the wires and thermocouples the whole arrangement was then isolated from ambient temperature fluctuations and draughts by placing it in an insulated box filled with glass fibre. The thermocouple tips were placed in small diameter holes drilled in the copper blocks to ensure their temperature was recorded as accurately as possible. The very low thermal contact resistance between the copper blocks and the faces of the THP combined with the low heat flux through the THP meant that the copper block temperature would be essentially the same as the ceramic surfaces of the THP. This method was judged to be able to provide a greater measurement confidence and repeatability than trying to measure the ceramic surface temperature directly. Before

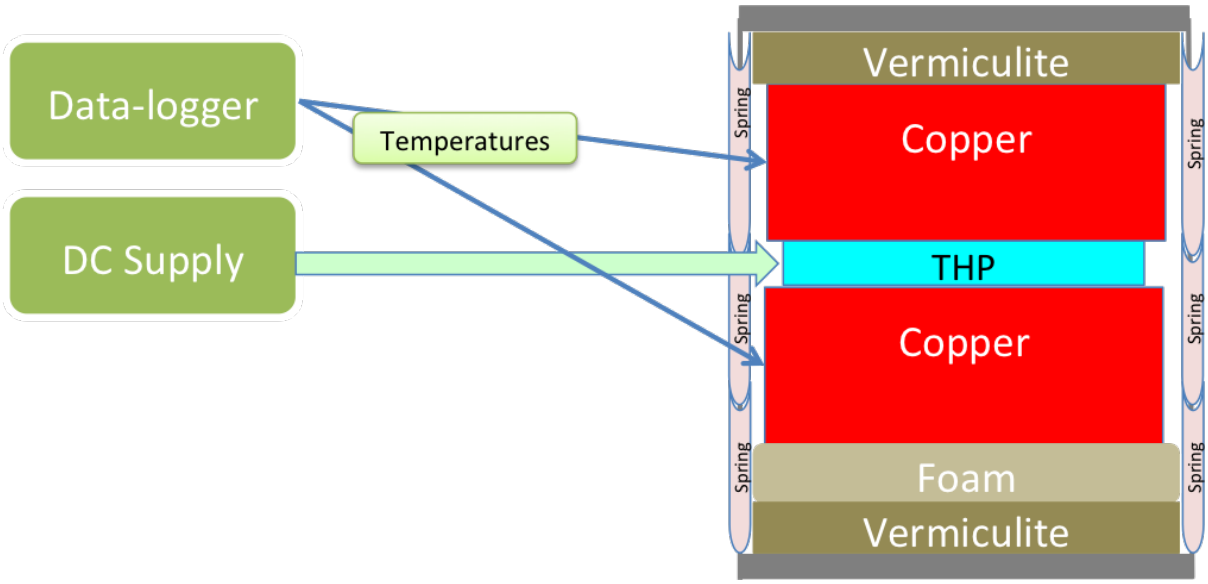

Figure 3.18: Low power characterisation test apparatus

experimental data was recorded, a preliminary set of measurements was taken to confirm that for small ΔTs over a period of 5 minutes the copper blocks were isothermal to the measurement accuracy of the apparatus. Figure 3.18 shows the test apparatus.

A constant current was applied to the THP in 0.1A increments up to a current of 2A. For each step the temperature at both sides of the THP was recorded at ten second intervals. At low THP current the temperature increase between successive measurements is small and to avoid the previous issue of drift in the data logger the running average increase in temperature is calculated using 60 second set of data. This averaging is done when post-processing the data after the measurements for a particular current level had completed.

$$Q = \frac{mCp\Delta T_{Cu}}{\Delta t} \tag{3.15}$$

The rate of energy increase and decrease at the hot and cold sides of the THP can be determined by equation 3.15. where m is the mass of the block, Cp is the specific heat capacity and Δt is the time required to change the block temperature by ΔT_{Cu}.

Table 3.2 provides the masses, dimensions and resultant heat capacities of each block used. Having obtained satisfactory results over the entire operating current range of the THP but by using two different techniques, the final step was to merge the data obtained by both methods to provide a single set of measurements that describe the THP

	Weight	Dimensions	Specific Heat Capacity	Heat Capacity
Copper Block 1	1.7212kg	10cm x 10cm x 3cm	390 kJ/kgK	671.268 kJ/kgK
Copper Block 2	1.6749kg	10cm x 10cm x 2.9cm	390 kJ/kgK	653.211 kJ/kgK

Table 3.2: Various thermoelectric heat pump devices ranging from 20mm x 20mm to 55mm x 55mm

performance. By extracting the COP data at specific ΔT_{THP} and specific current, the COP vs. current curves for a range of ΔT's can be obtained for the device under test from the total data set array.

Unlike the previous test where a constant ΔT can be held, the nature of this test is such that the temperature difference between the thermal masses will be constantly increasing.

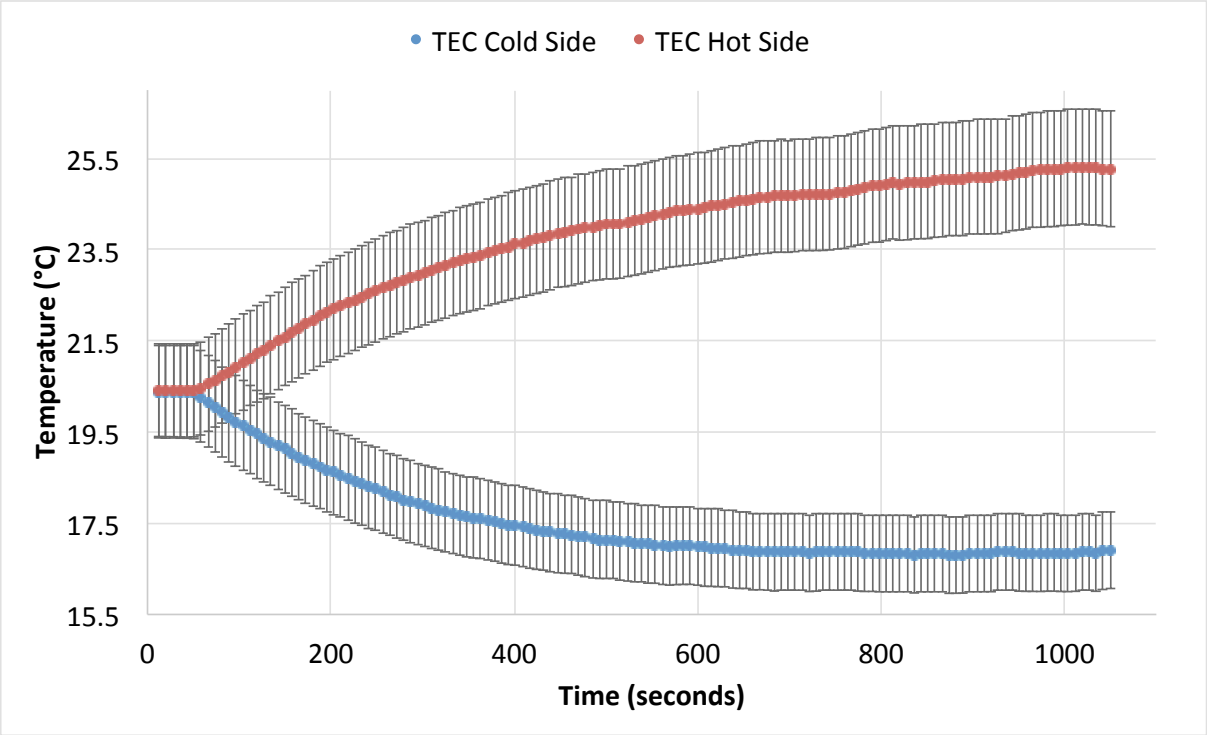

Figure 3.19: Change in temperature at constant current = 1A

Figure 3.19 shows this temperature change for a constant THP current of 1A. Initially the copper blocks are at equal temperature and the apparatus is in thermal equilibrium. As power is applied to the THP the energy extracted from the 'cold' side propagates through the THP to the 'hot' side copper block, along with the THP electrical power.

The test is concluded after 15 minutes. Note that by driving the THP in constant current mode (as opposed to constant voltage), the impact of any changes in the values of the Seebeck and Peltier coefficients resulting from the change in absolute temperature are avoided.

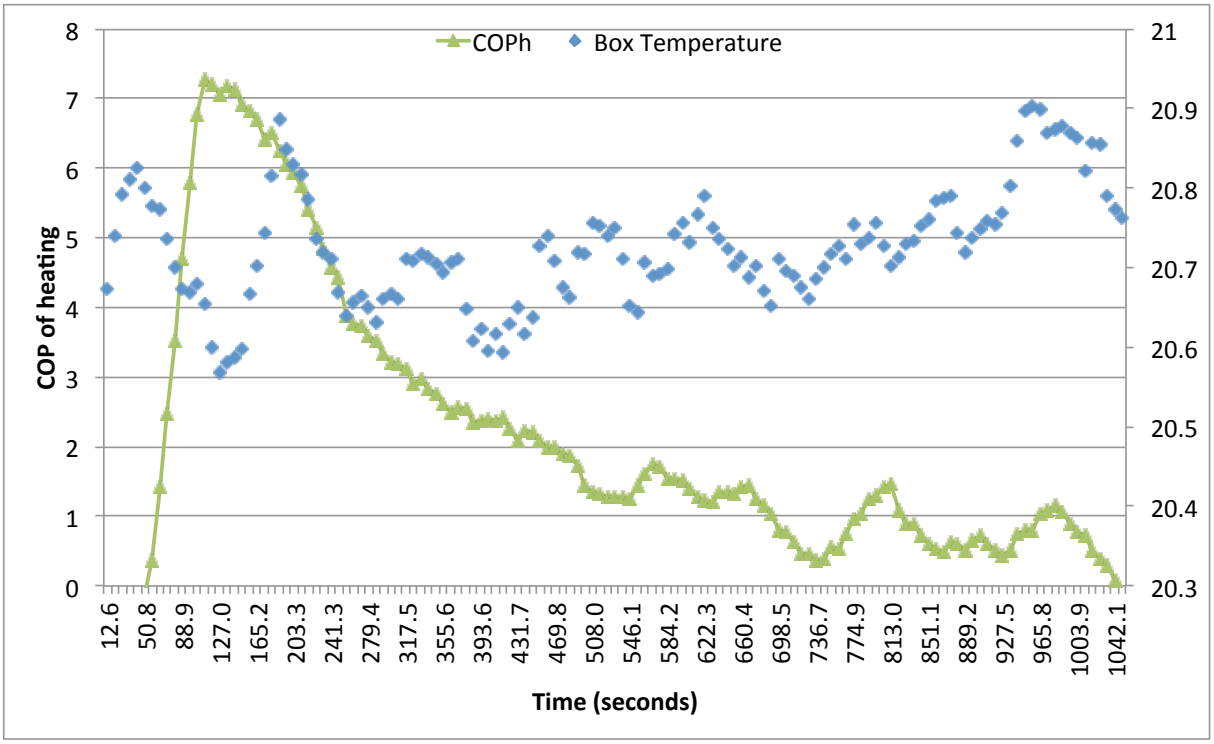

Figure 3.20: Coefficient of performance of heating at a constant current input = 1A

Using the method described, the COP of heating can be calculated from the data sets and an example graph for a THP current of 1A is shown in Figure 3.20. This Figure shows a distinct variation in COP at increasing time points. These peaks and troughs are due to the sensitive temperature measurements and small variations in the ambient temperature over the course of the experiment. The variations in temperature are shown in the 'Box temperature' measurements.

3.3.4 Thermal compound paste comparison

The matter of ensuring a good thermal contact between the surfaces of the THP and copper blocks was mentioned in 3.3.3. Using a gap filler to remove the microscopic air pockets that exist when surfaces are in contact can significantly reduce the thermal contact resistance.

Manufacturer	Part Number	Thermal Compound Type	Material	Electrical Conductor	Thermal Conductivity	Operating Temperature Range
Fischer Elektronik	WLPG05	Paste	Graphite	Yes	10.5 W/mK	-40 °C → 400 °C
RS	7074806	Sheet	Graphite	Yes	16.5 W/mK	-50°C → 150°C
Laird	K52-1	Gap Filler Sheet	Ceramic Based	No	7.1 W/mK	-60°C → 150°C
Arctic	Silver 5	Thermal Paste and Adhesive Compound	Silver	Yes	7.5 W/mK	40°C → 150°C
Graftec	HT 1205	Sheet	Graphite	Yes	10 W/mK	-40°C → 400°C

Table 3.3: Thermal interface material selection

Several thermal compounds are available and were evaluated for use in the test apparatus, detailed in Table 3.3. The following properties were analysed: thermal conductivity, electrical conductivity, operating temperature range and construction material.

The electrical conductivity of the materials was not an important factor in this particular application because the THP devices used have a ceramic on both sides providing the electrical insulation required.

The operating temperature was considered important. In the interests of being able to easily swap different THP devices in and out of the test rig the Laird thermal interface was excluded because the pad changed phase to become a liquid at 52°C. The benefit of this thermal pad is that as it liquidized, any air pockets would be removed eliminating the potential for air pockets to be compressed in a standard sponge-like thermal interface pad. This is ideal for a 'permanent' application, but for test purposes this complicates matters un-necessarily. The Arctic silver paste was excluded as the adhesive nature also compromised the flexibility of the THP test rig. The Fischer Elektronik paste proved very difficult to apply evenly and repeatably to a surface and was eventually discounted, despite its good performance.

The remaining choice between the RS graphite and Graftec thermal interface was decided on the maximum material temperature. The desire to extend the operating range of the test rig for examining the potential of high temperature heat pump testing meant

the Graftec graphite sheet was finally selected. This is now used for all tests.

3.3.5 Minimising experimental error

The measurement of low level electrical signals with high source impedance is particularly susceptible to noise and inaccuracy. For thermal measurement apparatus an additional consideration is the thermoelectric effect which dictates that a Seebeck voltage will be generated when two dissimilar metals are connected together at different temperatures. This can introduce a significant error when measuring small voltages, such as those in the load cell for pressure or from thermocouples whose cables need to be extended. The load cells used in the test rig have a differential output of microvolts per kg.

The effects of mismatch in voltage measurement can be minimised by using cable connections of the same material as the measuring device when extending the device connection to the data-logging unit.

Temperature reading inaccuracies are inherent in the small voltage measurements required in the test rig. The thermocouples are of J- or K-type, and therefore are constructed of different metals according to the temperature range of each thermocouple type. It is not sufficiently accurate to connect the wires of either the J- or K-type to standard copper wire when extending their physical length and wire of the same metal type must be used. For K-type thermocouples with a wide temperature range ($-200°C \rightarrow 1100°$C) Chromel and Alumel is used whereas J-type has a smaller operating range of $-40°C \rightarrow 750°$C using Iron and Constantan. The Agilent data-logging unit also has internal cold-junction-compensation. A block of high heat capacity / high thermal conductivity metal such as Aluminium is contained inside the measurement unit. This block is placed in series with one of the thermocouple cables and held at a constant temperature. This connection acts as another thermocouple and temperature reference to the object whose temperature is being measured. Selecting the internal reference thermocouple and by using the correct extension wire, the remaining errors can be characterized in software and appropriately compensated.

Initially temperature and voltage measurements were made without any filtering in

Integration time	Average Temperature Reading (°C)	Number of Readings in 10 minutes
1 PLC	0.07218	600
10 PLC	0.01327	300
100 PLC	0.04843	50

Table 3.4: Measurement inaccuracy measurements

software.

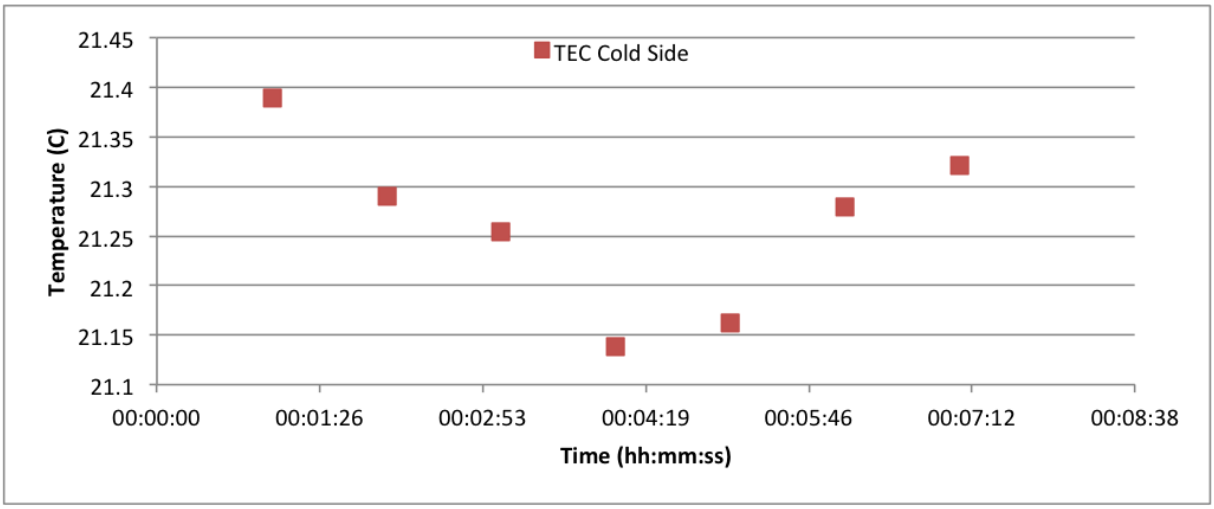

Figure 3.21: Temperature variation of the data logging unit

Figure 3.21 shows the large variation in measurement from a single thermocouple and this is typical of data acquired from the Agilent logging unit. On initial inspection the results look unacceptable but other less expensive digital temperature recorders gave a substantially poorer performance.

Temperature measurement is made by the accurately sensing a small differential voltage change, usually in the region of millivolts. Simply put, an ADC samples the input signal over a set time period. This time period is known as the integration time, whereby longer integration times lead to higher resolution readings but at a cost of speed. The Agilent logging unit specifies this as an absolute interval or can use an integer number of power line cycles (PLC).

The relationship between PLC and acquisition time is described in Table 3.4. As an additional check of the measurement accuracy the offset temperatures measured by the Agilent unit were calibrated against a very accurate mercury thermometer. Both the thermocouples and thermometer were placed in a pipe circulating water from a large

tank which act as a thermal capacitor, attenuating any changes in temperature from the surroundings. The thermocouple channels were offset such that all reported the same temperature.

In addition to offset calibration, the Agilent VEE Professional software developed to control the test apparatus also implemented a simple moving window averaging method. Sequential readings of temperature are loaded into an array $a[4]$. Every fifth reading the contents of a are averaged and used in the remainder of the device calculations. For each new value of temperature recorded the array a shifts one place, removing the oldest value and incorporating the newest value.

This averaging technique has been used throughout the test apparatus to ensure consistent data processing.

3.4 Results

3.4.1 COP curves

The data sets obtained by the low power thermal mass tests and the high power fluid flow rate-based tests are merged to provide a single set of measurements that describe the THP performance over the range of temperatures and currents of interest. By extracting the coefficient of performance data at a specific ΔT and specific current, the COP vs. current curves can be obtained for the device under test.

Both the I_{max} and V_{max} rating of a thermoelectric heat pump are important when defining the highest available COP_h for a given ΔT. Where V_{max} and I_{max} are applied to the THP the result is the maximum possible ΔT_{THP}: these give rise to the largest flow of charge-carriers that cause the heat pumping action and thus the greatest thermal transport. The voltage across the device is directly proportional to the temperature difference, therefore at specific ΔT_{THP}'s the optimum operating point will depend on the current passing through the device. It is important to note that, due to the Seebeck effect, V_{max} will vary with ΔT and therefore the relationship between V_{max} or I_{max} and the COP is a complex one; however, providing the electrical power to the THP is known then the

COP calculation is straightforward.

In THP applications where pumping efficiency (rather than absolute heat pumping capacity) is the primary concern, knowledge of the variation in COP is essential. Unfortunately these COP data are rarely published by device manufacturers and hence are derived from experimental data for the purpose of this research.

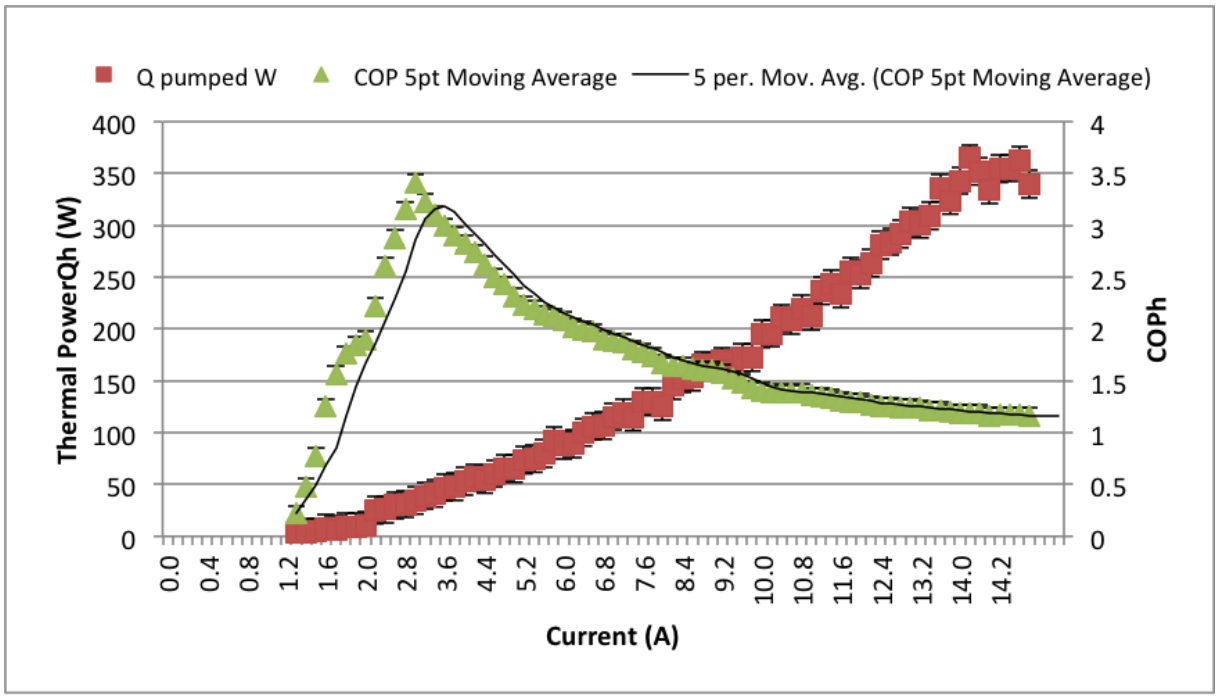

Figure 3.22: Characterisation data for a THP at $\Delta T = 10K$ including results from low power testing and 5-point averaging

Figure 3.22 shows that for a $\Delta T = 10K$ and low input current the COP rises rapidly to a peak value, followed by a decay towards unity. It is important to note that each COP and thermal energy graph starts after 0A, typically around 0.6A for a $\Delta T = 5K$. This is due to the presence of a thermal mass at both the sides of the THP. In order to reach the desired ΔT within the measurement time frame the current and voltage applied to the THP is incremented. For a $\Delta T = 10K$, the minimum operating current is 1.2A; $\Delta T = 15K$ is 1.8A and $\Delta T = 20K$ has a minimum operating current of 2A.

Each temperature difference is measured at opposing sides of the THP and Q_h is a function of the increase in water temperature (ΔT_W). As the ΔT_{THP} increases, so the electrical input power must increase and hence the COP_h curve peak moves to the right along the x-axis, corresponding to an increased value of the ratio of I:I_{max}. As the

limit approaches, the COP_h approaches unity as the I^2R losses dominate the thermal performance.

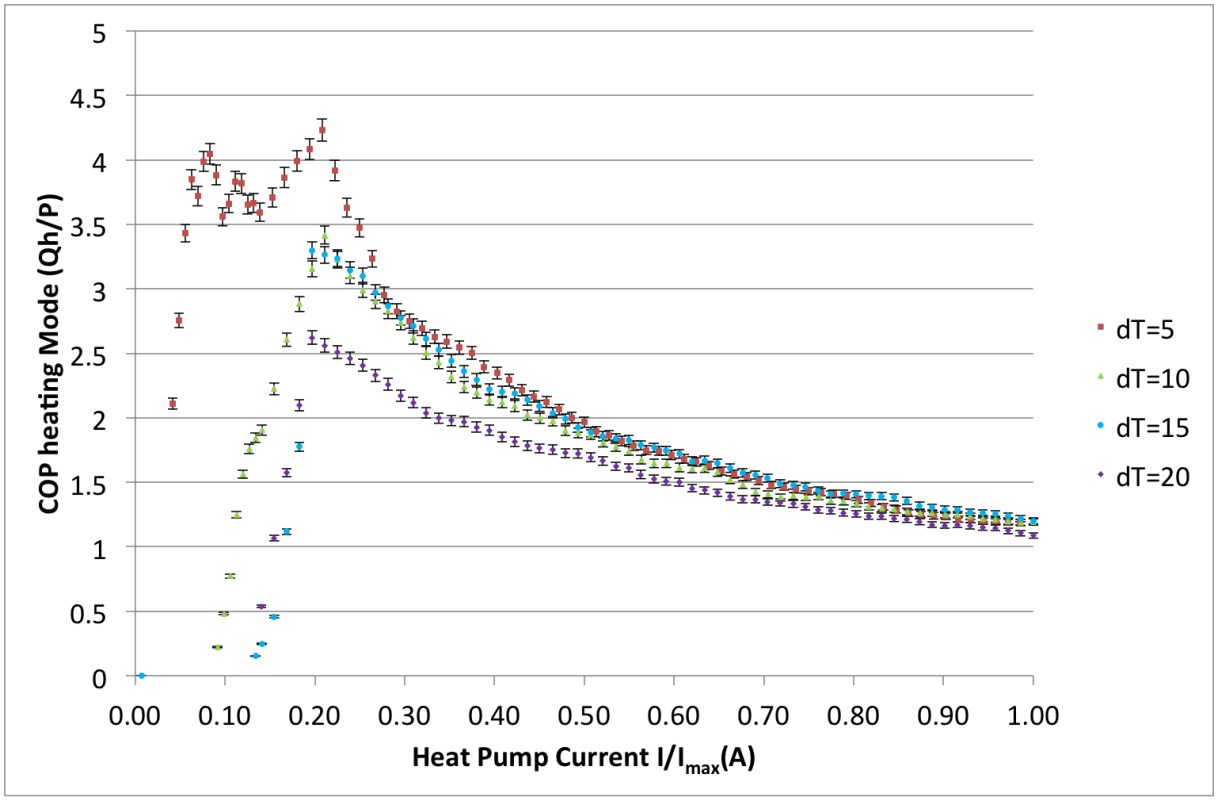

Figure 3.23: Coefficient of performance of heat pumping for a 50mm x 50mm THP

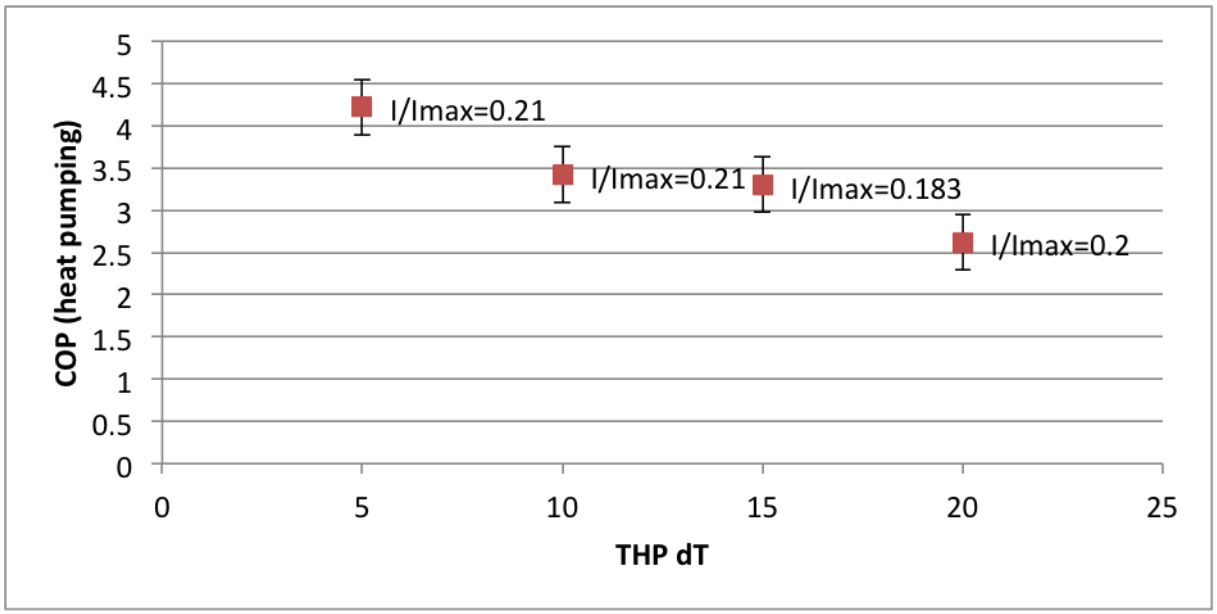

Figure 3.24: Correlation of COP_h to I/I_{max}

The graphs shown in Figure 3.23 and Figure 3.24 show that the greatest COP available from the heat pump is in the region between $0.1I/I_{max}$ and $0.3I/I_{max}$ where I/I_{max} is

the normalized current ratio independent of the maximum heat pumping power achieved in testing. The current ratio is used to enable different THP devices to be compared on the same y-axis.

This correlation confirms and quantifies the COP data not given by device manufacturers to a measurement accuracy described by the error bars in Figure 3.23 and Figure 3.24. More importantly, establishing these data now permits a robust analysis of the actual performance likely to be obtained from commercially available THP's. The scattering of data points below I/I_{max}=0.2 reflects the great difficulty in accurately obtaining these data experimentally.

3.5 Theoretical COP

The theoretical THP performance can be derived from a one-dimensional conduction heat transfer through a single plane, taking into account the Seebeck coefficient, thermal conductivity and electrical resistance. The temperature and heat transfer through the THP is determined by the steady state heat conduction equations. A thermoelectric heat pumping device can be considered in two parts, the heat generation from the cold side and heat extraction through the cold side. Both are proportional to the power applied. As electrical power is applied to the THP, a voltage difference develops across the device characterised by the Seebeck effect. The thermal conductivity determines the amount heat transported due to the temperature gradient developed across the pellet. A graphical representation of this relationship is described in Figure 3.25.

$$Q_h = \alpha I T_h + \frac{1}{2} I^2 R - \kappa \Delta T_{pellet} \tag{3.16}$$

where the thermal energy at the 'hot' side of the device is a combination of the Seebeck coefficient (α), current (I) and absolute temperature at the 'hot' side pellet junction. The Joule heating (I^2R) is additive to the overall thermal energy and further irreversibility is attributed to the thermal conductivity (κ) across the pellet (ΔT_{pellet}). And similarly for

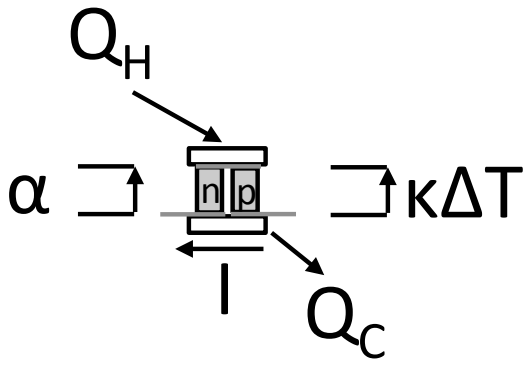

Figure 3.25: Description of the physical effects and relationships that dominate the thermal energy flow in the THP

the cold side,

$$Q_c = \alpha I T_c - \frac{1}{2} I^2 R - \kappa \Delta T_{pellet} \tag{3.17}$$

where the 'cold' side accounts for the energy absorbed ($\alpha I T_c$), Joule heating effects and thermal conductivity across the pellets (ΔT_{pellet}).

At the hot side, the thermal power developed by the THP is found by summing the power developed due to the Seebeck effect and Joule heating. As the THP can be considered as thermal resistance the conductivity is subtracted from the overall thermal power. Similarly for the 'cold' side, the Seebeck effect dominates and the effects of Joule heating are subtracted.

$$\kappa = \frac{\Sigma P}{\Delta T} \tag{3.18}$$

Using these equations a thermal model has been constructed in MATLAB. The data for the Seebeck coefficient, thermal conductivity and electrical resistance are derived from data acquired in testing. The Seebeck coefficient is determined from the material properties and thermal conductivity is calculated from the thermal resistance of the THP module. Since the test apparatus described measures accurately the temperatures at opposing sides of the THP then the thermal resistance is deduced from equation 3.18.

The electric resistance of the THP is measured directly, taking care to exclude the impedance of the intermediate wiring. These values are then used in the MATLAB script to generate the values for the heat pumped. For each temperature gradient the script calculates Q_h values up to the maximum current (14A). Typical data are plotted

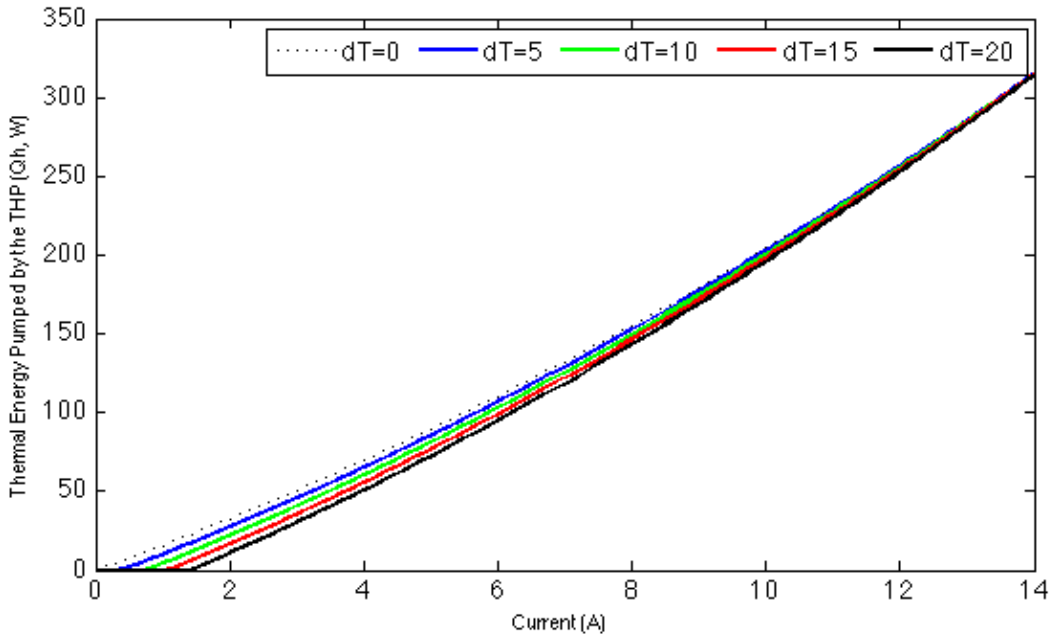

Figure 3.26: Thermal energy pumped by THP

in Figure 3.26. Different temperature gradient values may be selected in a new array and new Q_h values then determined.

The COP data determined by the MATLAB script is generated from device specific characteristics with limited extrapolation of heat conduction beyond the faces of the THP and is therefore far less than expected. Therefore there is known to be a significant mismatch between the thermal energy in the simulation and the thermal energy found in the experimental results.The large COP exhibited is therefore enhanced due to the fact that there is no consideration of the thermal interfaces and thermal loads that would exist in a real system. It is the shape of the COP curve that is of interest in this simulation, rather than the absolute value, and these differences between simulation and the real situation do not have a substantive impact on the conclusions drawn from their use. It is important to note from this graph that for different thermoelectric materials with different ZT values the shape would be the same but the magnitude would change. Figure 3.27 plots the coefficient of performance in heat pumping mode for a range of input currents to 14A.

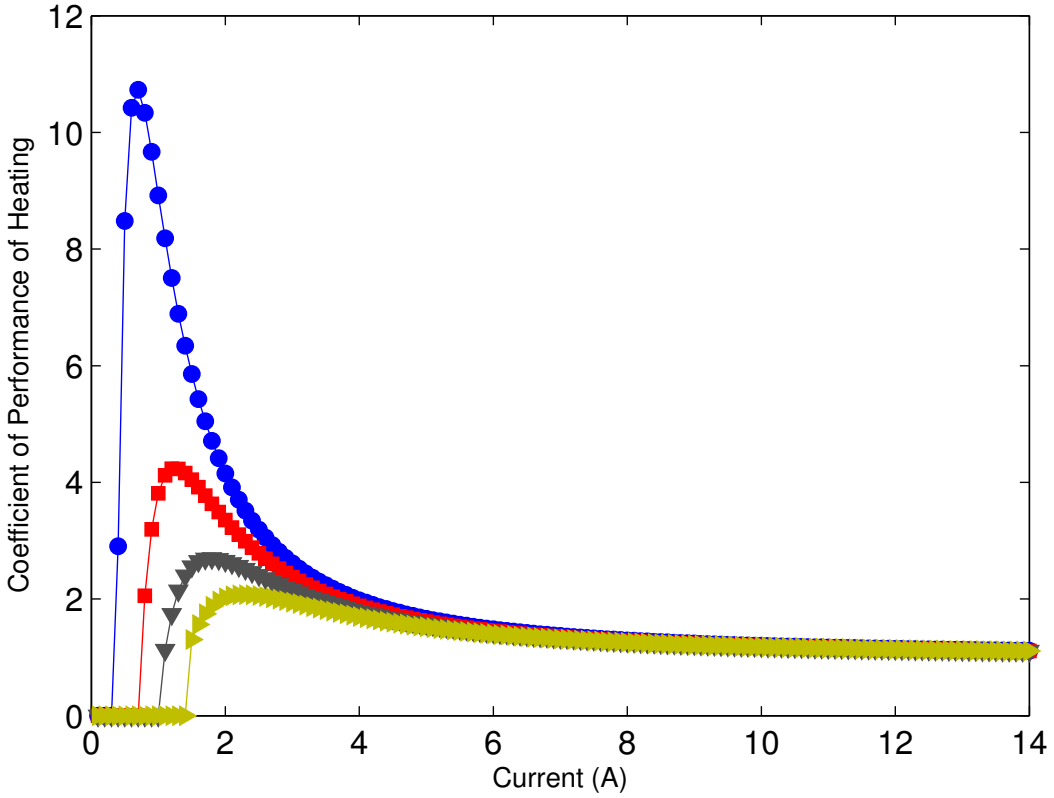

Figure 3.27: Coefficient of performance vs. current

3.5.1 Pellet height effect on temperature and COP of heating

When calculating the thermal energy that can be converted by the THP it is important to consider the effects of the height of the pellets forming the device. Prior work by [113] show how the leg length affects the COP and heat pumping capacity at the single-element scale. Equations 3.19 and 3.20 show the relationship between COP and thermoelectric pellet length.

$$COP_h = \frac{l}{l + 2rl_c}\left(\frac{T_h}{T_h - T_c}\frac{\beta - \frac{T_h}{T_c}}{1-\beta} - \frac{rl_c}{l}\right) \tag{3.19}$$

$$\beta = \sqrt{1 + \frac{lZT_m}{n+l}} \tag{3.20}$$

where l is the pellet length, r is the ratio of thermal conductivity of the thermoelectric device to the solder contact and ceramic layer, l_c is solder and ceramic contact length, Z is the figure of merit, n is electrical contact resistivity between the thermoelectric pellets

and the solder connections, and T_m is the average temperature across the device.

$$Q_h = \frac{\lambda \Delta T_{max} - \Delta T}{l + 2rl_c + \frac{rl_c}{COP_h}} \tag{3.21}$$

where λ is the thermal conductivity of the pellets (W/mK), ΔT_{max} is the maximum temperature difference that can be achieved across the device (K) and ΔT is the modelled temperature difference.

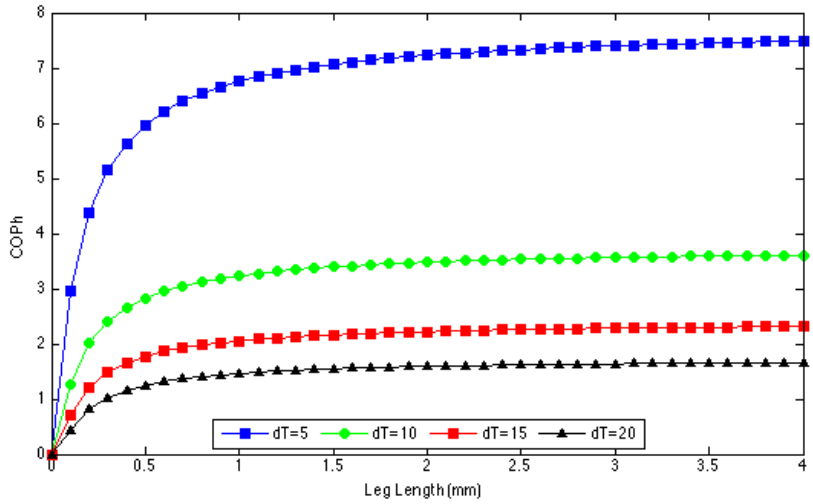

Figure 3.28: Increasing leg length effect on COP_h at increasing ΔT

Based on the parameters in the previous section for thermal conductivity and temperature, the theoretical effect of pellet length on increasing temperature differences across the device is shown in Figure 3.28.

At low temperature gradients the COP_h is large as expected and the COP_h increases as the pellet length increases. This is due to the effect of the thermal conductivity on the overall device performance leading to a higher COP_h at longer pellet leg lengths. Above a leg length of 1.5mm the maximum COP is achieved across all temperature differences (5K, 10K, 15K and 20K). However, while it may appear that the longer pellet length is the only important factor the heat pumping capacity is also affected.

In 3.29 the pellet length is an important factor when considering the heat pumping capacity. The highest heat pumping capacity occurs at the shortest leg length, dropping significantly over the pellet leg length range modeled previously.

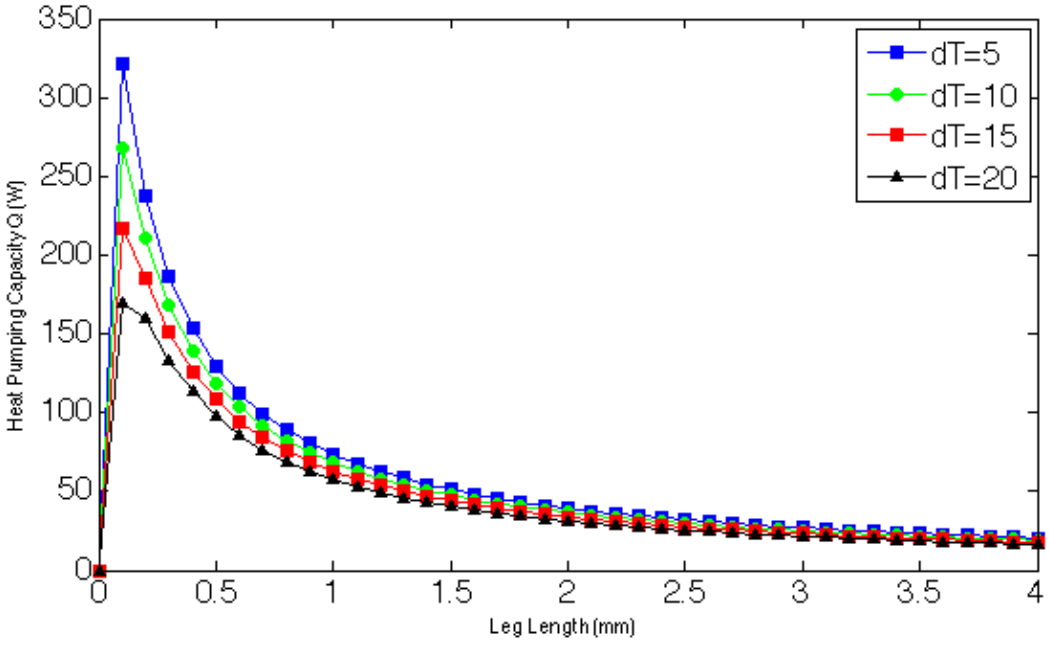

Figure 3.29: Heat pumping capacity at varying pellet leg lengths

Therefore there is a trade-off between obtaining a THP device to provide the largest coefficient of performance and the largest heat pumping power. The device with the largest COP in this model would not be a high-power device as the largest COP occurs when leg length is over 1.5mm. However the heat pumping capacity of a THP at this leg length is significantly reduced when compared to a leg length less than 1mm. Exploration of this trade-off will form part of future work: the device characteristics are key to maximizing both the COP and heat pumping power and suitable selection of these parameters is critical to realizing the highest overall system performance.

3.6 Summary

The preceeding results in this chapter have detailed the theoretical and experimental validation of the performance of a thermoelectric heat pump. The physical effects that underpin the operation of the devices has been presented with a view to describing how each of these impacts the operation of the whole device. From this chapter it is clear that the operating temperature and thermal conditions have a substantial impact on the device performance, showing that the thermoelectric heat pump has higher efficiencies when

operated at low temperatures and temperature differences of 5 or 10 °C in comparison to temperature differences of 15-20 °C.

This chapter has also presented significant work on a method of characterisation. The resultant data from the test apparatus is representative of how the device might be applied to a system and hence of more value to a design engineer. The test apparatus is currently being used as part of wider work by NPL to develop Engineering testing standards for thermoelectric devices that is independent of the device materials. It is key to note that the testing apparatus described in the preceeding chapter is not specific to Bismuth Telluride devices and indeed any other type of thermoelectric device therefore it has significant versatility when it comes to comparing and contrasting the performance of a wider spectrum of thermoelectric devices.

This chapter concludes with an appreciation of current thermoelectric device technology and looks to optimise the structure of the device for heat pumping. It has been shown that a device specifically designed for thermoelectric heat pumping faces two values that must be optimised, namely the heat pumping capacity and the Coefficient of Performance. At larger pellet heights the heat pumping capacity is greatly increased, but the overall Coefficient of Performance drops meaning that the device is less effective at pumping. It was found that a pellet height of 1.5mm proved optimal for heat pumping COP whilst not sacrificing the heat pumping capacity.

The charts and data resulting from this chapter are referenced to frequently throughout the rest of the thesis emphasising the importance of fundamental device performance on the Rankine cycle application. The COP data obtained is used as a reference for determining the performance attainable from the Rankine cycle test apparatus and also how the heat pump application might be expanded which is detailed in Chapter 7.

Chapter 4

Rankine Cycle

This chapter details the theory pertaining to the application of thermoelectric heat pumps to the Rankine cycle.

4.1 Theoretical analysis

The Rankine cycle is the dominant method of electricity generation in the world today. The basic implementation of the cycle was described over 150 years ago and significant advances are still being made to improve its efficiency. This section details the theory behind the cycle and how it can be further adapted to include thermoelectric devices to ultimately increase the net cycle efficiency.

The Rankine cycle (named after William Macquorn Rankine) describes the practical embodiment of the Carnot cycle (shown in Figure 4.1) applied to a steam cycle (Figure 4.2). The working fluid is usually very pure water, retained in a closed loop within the overall process. In operation, thermal energy is added to the process by the heater (Q_{in}), to increase the energy through the latent heat of vapourisation of the working fluid. The resulting vapour is expanded through a series of turbines from which mechanical work is extracted (W_{out}) and used to turn alternators to produce electrical power. Once feasible energy extraction is complete the vapour is re-condensed and the latent heat of vapourisation is released from the process as Q_{out}. The condensate is then returned to the boiler for re-use. The addition and rejection of thermal energy from the working fluid

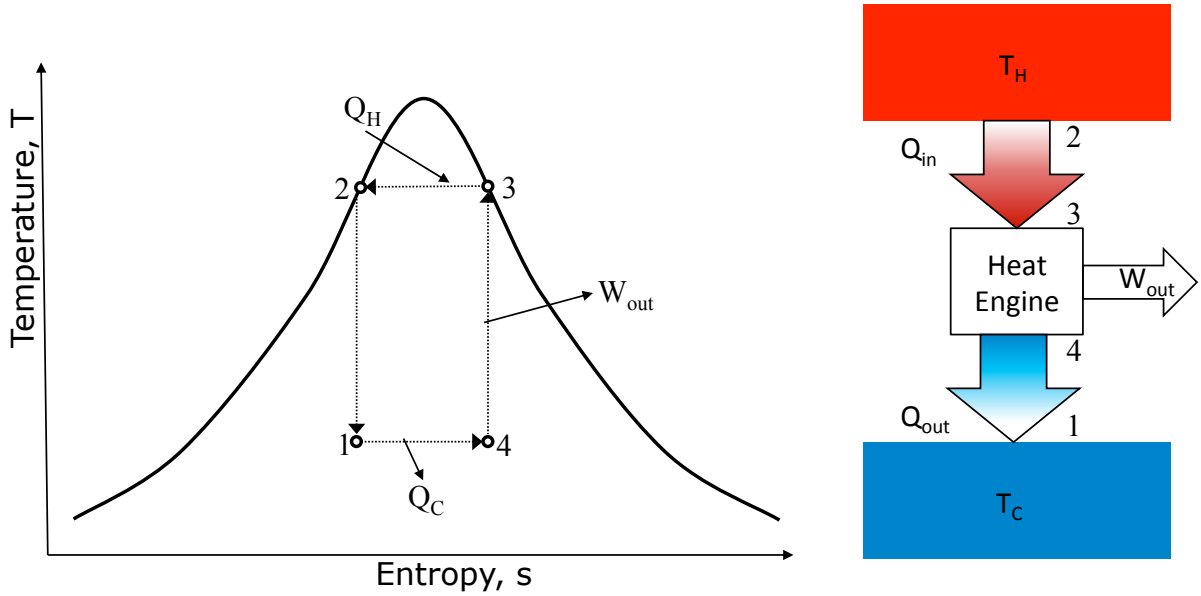

Figure 4.1: Operation of a Carnot cycle and accompanying T-s diagram

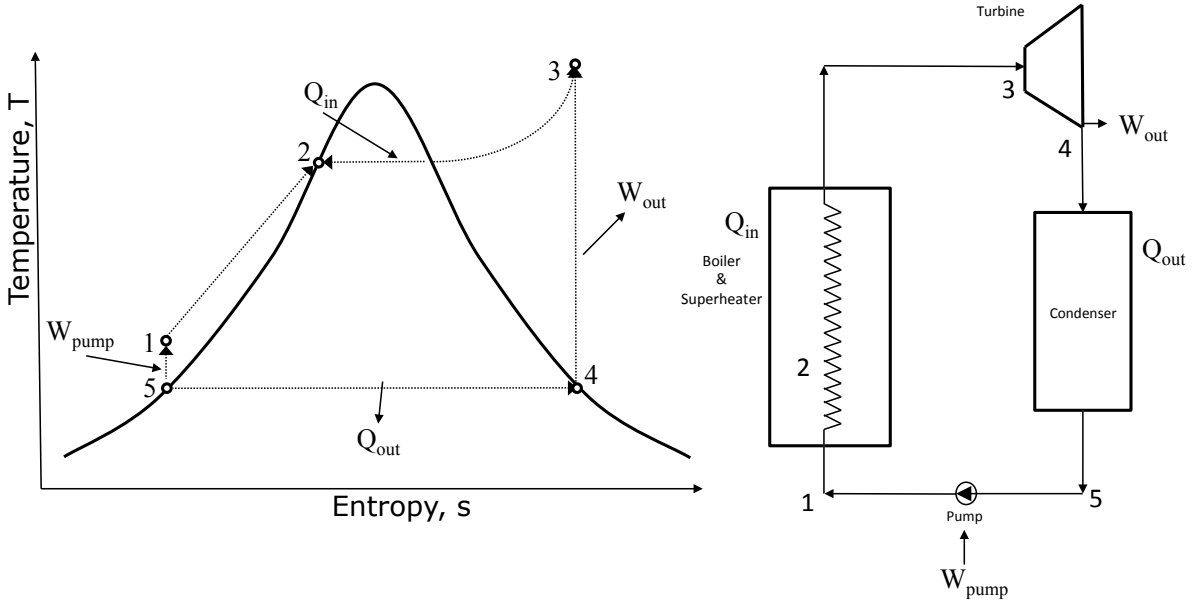

Figure 4.2: Operation of a Rankine cycle and accompanying T-s diagram

is isobaric (occurring at constant pressure) in the Rankine cycle whereas in the Carnot cycle these processes are isothermal this yields an advantage to the Rankine cycle in that injection of a liquid rather than a gas to the boiler has a lower parasitic load on the plant. The temperature and pressure of the condenser are reduced to maximise the work done in the cycle, i.e. the area contained in the T-s diagram. However, despite a large temperature difference the overall ideal Rankine cycle efficiency is below 50% whereas the Carnot efficiency is nearly 70%. This is shown in Figure 4.3.

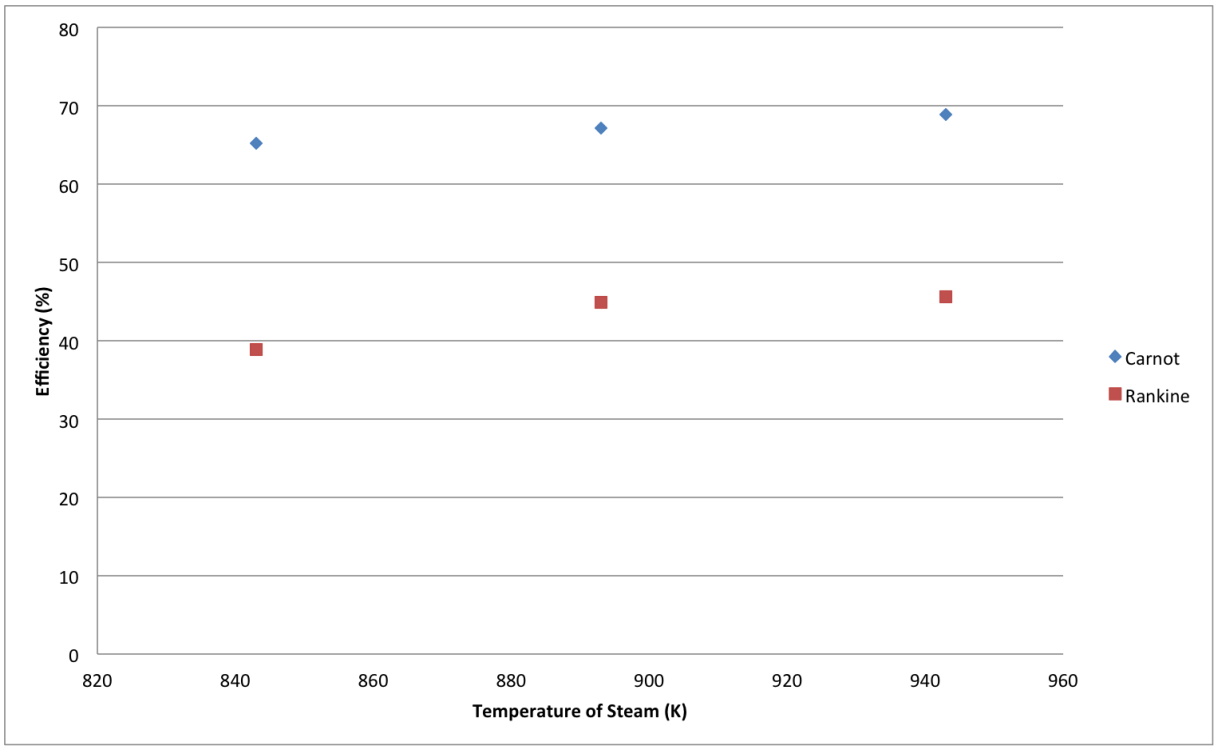

Figure 4.3: Rankine cycle and Carnot cycle efficiency comparison

The Rankine cycle can be described by the consideration of the process through five stages. As part of this explanation the current subcritical power plant at Ratcliffe on Soar is analysed. This plant has four boiling units each capable of generating $521.1MW_e$.

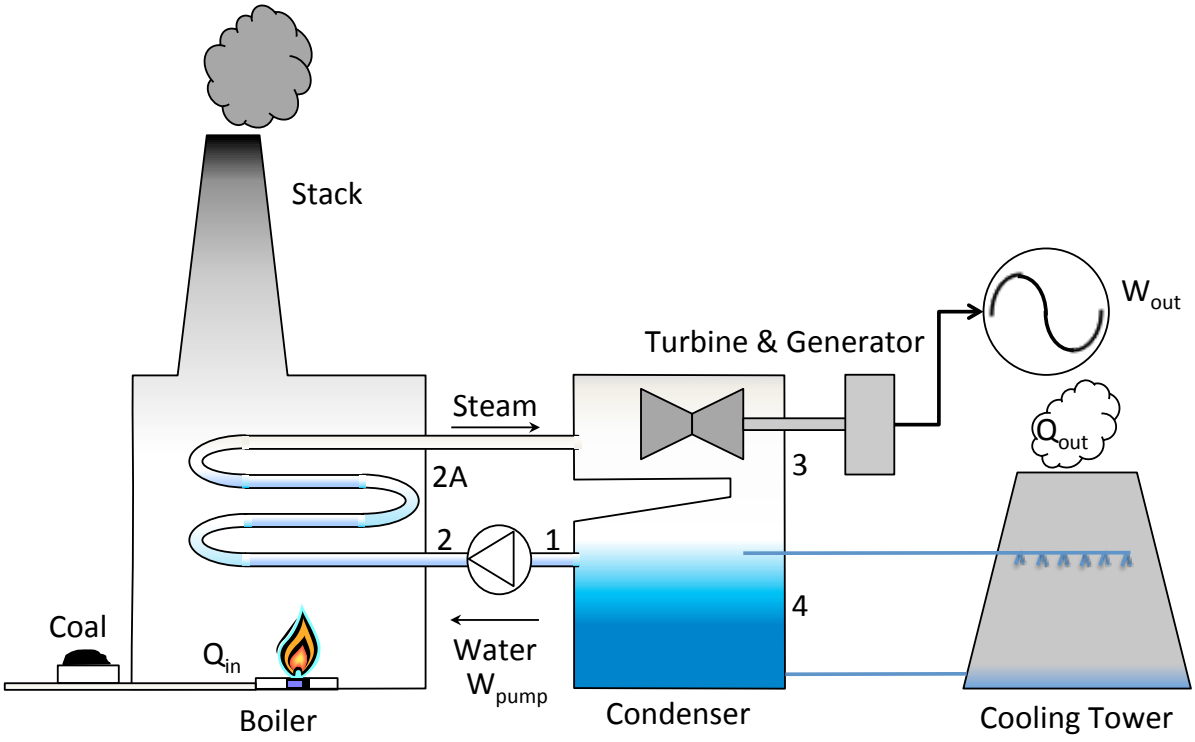

Figure 4.4: Rankine cycle showing each stage

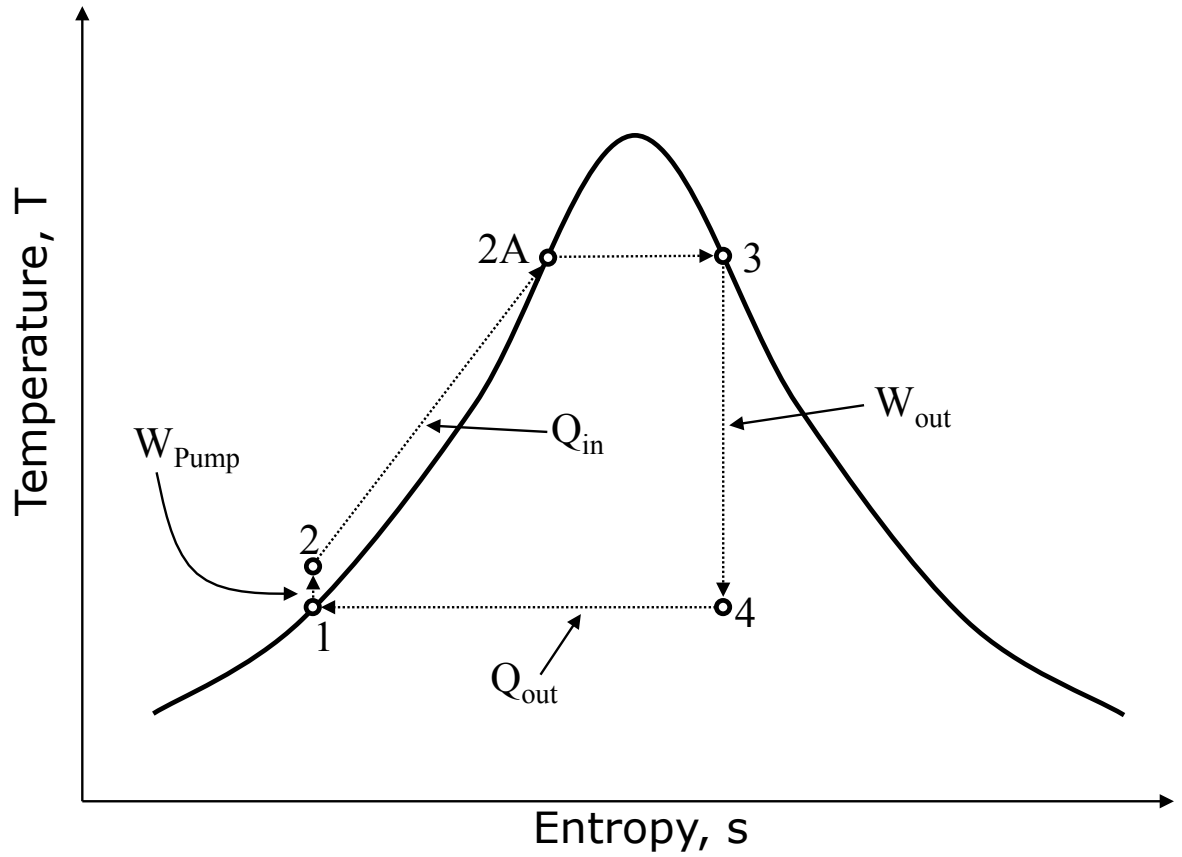

Figure 4.5: Temperature-entropy chart for ideal Rankine cycle

With the aid of Figure 4.4 and Figure 4.5, each stage is described and the thermodynamic conditions defined.

Point 1: Initially water is added to the system at ambient temperatures. The boiling unit raises this temperature by firing fuel, usually coal, oil or gas.

Point 2: The liquid is then subjected to isentropic compression for injection in to the boiling unit (W_{pump}).

Point 2A: The boiling unit produces subcritical steam at high pressure. Subcritical operation means that the water is boiled below the critical point of water (374°C). At atmospheric pressure, the water boils at 100°C, however a subcritical plant will operate at a greater pressure (160bar-abs) meaning the boiling point is much higher. The plant at Ratcliffe achieves 566°C at 160bar-abs in the boiler but despite it being operated above the critical temperature it remains below the critical pressure.

Point 3: Now steam has been generated, work can be extracted through a turbine set. The

amount of energy extracted from the steam is proportional to the enthalpy as shown in equation 4.1. As each turbine extracts energy, the pressure drops as a proportion of the enthalpy. Therefore instead of a single large turbine, multiple stages are implemented to extract as much of the thermal energy as possible.

$$\Delta P = \frac{\Delta H}{T} \tag{4.1}$$

where ΔP is the pressure drop across the turbine, T is the temperature in Kelvin and ΔH is the enthalpy removed in the extraction of work.

For the Ratcliffe plant there are six stages of steam turbine: one high pressure (HP), a double-headed intermediate pressure (IP) turbine and three low pressure (LP) turbines. The HP turbine is designed to accept steam under precise conditions. If the inlet conditions are significantly below or above these then the turbine will not produce the rated mechanical output and may indeed be damaged should water droplets form on the blades. The IP turbine used in the Ratcliffe plant is double-headed meaning that there is a single inlet for the steam, but the expansion occurs laterally on the horizontal plane. A large portion of the enthalpy has now been extracted but in order to remove the remaining useful work the low pressure turbine is employed. These turbine blades are formed differently and cause a large pressure drop by using a reaction type blading. As the steam passes through the reaction blade it is propelled forward causing the rotor of the turbine to spin. This results in a drop in pressure and steam velocity giving very low pressure and temperature steam as the final outlet conditions.

Point 4: After the steam is exhausted from the system it is still in a (mainly) gaseous form, ready to be condensed to water. The steam is passed immediately to the condenser unit, which is formed of a nest of tubes directly in contact with cooling water. This cooling water is in a closed loop which is sprayed down inside the cooling tower on to these tubes containing steam. This allows for the cooling water to absorb the energy from the low pressure and low temperature steam by virtue of being

at a temperature below the steam dew point. The natural air circulation around the cooling tower evaporates some of the coolant which exits the cooling tower in the characteristic steam plume. The water that collects in the cooling tower sump is routed back to the condenser again. The water that evaporated in the air is replenished in the water basin by cold make-up water. In order to ensure purity, the water that collects after is has evaporated in the cooling tower is separate from the steam cycle.

The cooling water for the Ratcliffe plant is sourced from the River Trent and can supply the 14,000 kg/s of water required to condense steam from each of the four boiling units. This large mass flow of water ensures a low river water temperature rise and minimal temperature rise across the condenser process.

Water newly condensed from the steam cycle is reheated on the return path to the boiler where it is reboiled.

There are a number of modifications made to the ideal Rankine cycle which increase the overall efficiency of the physical implementation of the process: The steam generator comprises two separate parts: the economiser, where heat is added to the working fluid in the liquid phase ('sensible heat'; Figure 4.5, point 2), and the steam generator where further heat transfer provides the change of phase to a vapour without further temperature rise ('latent heat'; Figure 4.5, point 3).

The exhaust pressure after the last stage of work extraction by the turbine is maintained below atmospheric pressure. In modern power plants the steam pressure exiting the final stage is typically 45mBara-absolute with a corresponding temperature of 33°C. The effect of doing this is to increase the area of the work done in the T-s diagram of Figure 4.5, but as a result, the quality of the steam exhausting the final turbine stage decreases. In this case, lower quality equates to an increased percentage of liquid water entrained in the steam and passing through the turbine nozzles and blades, which can lead to severe mechanical damage to these components due to the much higher droplet density and therefore momentum. Exhaust quality can be improved by superheating the steam leaving the boiler and also by reheating steam during the expansion stages.

4.1.1 Regeneration with multiple extraction phases

The reduced efficiency of the Rankine cycle with respect to the Carnot cycle is a consequence of the lower average temperature of the heat input to the Rankine cycle. Regeneration is the term used to describe heating within the cycle which would lead to an overall increase in the cycle thermal efficiency. An idealised regenerative Rankine cycle scheme would have the same efficiency as the Carnot cycle, but a variety of physical factors renders this infeasible. These principally include: irreversible heat transfer between the expanding steam in a turbine stage and the feedwater being returned to the economiser, losses due to the heat leakage and fluid friction, and reduced quality in the exhausted vapour from the turbine. Despite being unable to achieve the idealised case, the regeneration concept is applied to good effect by extracting steam from the intermediate turbine stages and using this to preheat the feedwater before the economiser stage. The seven feedwater heaters implemented at Ratcliffe progressively increase the feedwater temperature towards the saturation point and minimise the irreversibilities in the process. The number of extraction stages that are economically viable is determined by the point at which the additional mechanical complexity involved exceeds the return gained in terms of improved cycle efficiency. Hence the use of these feedwater heaters ensures the loss of availability is small.

Physical implementations of the Rankine cycle also requires additional plant components which decrease the overall cycle efficiency. Briefly, these include: Feedwater pumping, Economiser, boiler and superheater inefficiencies.

4.1.2 Feedwater pumping

The final stage of the Rankine cycle requires vapour exhausted from the last turbine to be completely condenser to a saturated liquid before being returned to the economiser via the various regeneration stages. Each stage will require a pump, and will also be subject to fluid friction and heat losses.

4.1.3 Economiser, boiler and superheater inefficiencies

Collectively these are determined by how well the energy released by the combustion of fuel is used to raise the enthalpy of the feedwater passing through each. The principal loss is via the residual energy in combustion products, which eventually leave the process through the chimney (usually less than 20%).

In a multi-megawatt plant the physical size of individual components dictates that there are significant distances between individual components, over which some losses are unavoidable. In addition, throttling is used to maintain constant turbine speed in the presence of variable steam conditions or due to varying mechanical load on the turbine output shaft. Fluid friction present in the expansion process in a turbine stage means the expansion is not isentropic and hence the work output is slightly below the ideal case. The difference between the idealised and actual work output appears as an increase in the enthalpy of the steam leaving the stage, and this has the beneficial side-effect of increasing the quality of the exhaust vapour.

For large-scale power plants, cycle efficiency is of paramount importance. From the preceding discussion it is apparent that, as the turbine inlet pressure (and temperature) is increased, there is a corresponding improvement in the work output and efficiency. Heat rate is defined as the quantity of heat energy supplied to a thermodynamic cycle which yields a corresponding work output from the cycle. The heat rate is effectively the reciprocal of the thermal efficiency if the cycle. Increasing the inlet pressure decreases the heat rate, and therefore the plant efficiency rises. The practical implementation issues described dictate that the heat rate has a minimum value, rather than decreasing monotonically with increasing pressure, and in modern plants this exceeds the critical temperature and pressure of water (374°C/220 bar-abs). A plant operating beyond these limits is said to be supercritical.

4.2 Supercritical plants and THP application

A supercritical power plant based on the Rankine cycle operates at temperatures and pressures greater than 374°C/220bar. There are a number of modifications made to the existing Ratcliffe plant to enable operation at supercritical conditions. The working fluid is very dry steam at 600°C and 290bar-abs ensure it does not contain any water droplets that would normally form wet steam.

The boiler unit and reheater stage are modified to be able to fire to higher operating conditions with the use of materials that could cope with the higher stresses and reduce corrosion and oxidation. The turbine island is significantly altered as the turbines now operate with high-pressure steam. The main benefit is the significant increase in power these turbines can now generate, 576.8MW$_e$ compared to 521.1MW$_e$. With the larger amount of steam generated the cooling load on the condensers also increases, leading to a larger amount of cooling water required to achieve the same condenser conditions.

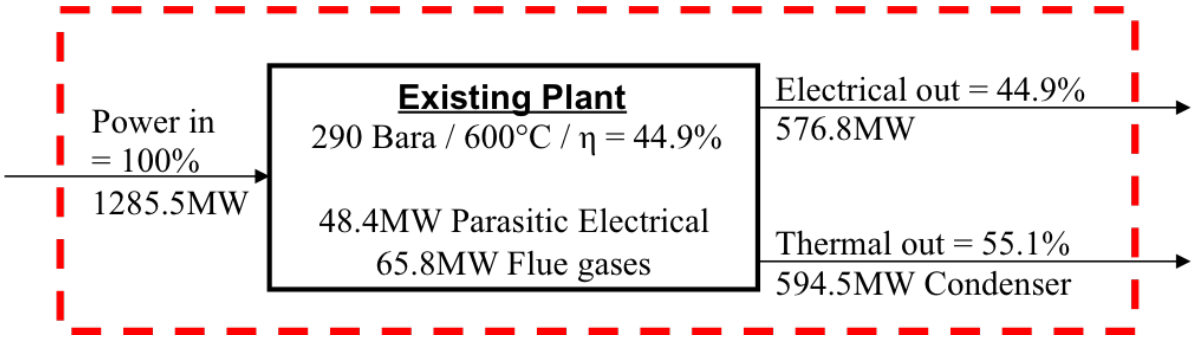

Figure 4.6: Ratcliffe-on-Soar Thermodynamic Properties

Figure 4.6 shows the energy into and out of an advanced supercritical Rankine cycle power plant recently developed in the UK. All the parasitic plant components are contained within the box marked 'Existing Plant'. The gross electrical output from the turbine island is 625.2MW$_e$ however there are several parasitic loads that mean the plant will deliver a net electrical power of 576.8MW$_e$ to the grid. The primary source of this parasitic load of 48.4MW$_e$ is through the turbine-island and running of the cooling system pumps that account for the 7.7% reduction in net output. The thermal losses are 594.5MW$_{th}$ through the condenser cooling towers and 65.8MW$_{th}$ through the flue gases. The total energy lost is 55.1% of the input, therefore the overall coal-to-net-electricity

	Pressure	Temperature
Condenser	45mbara	33°C
FWH1 (after condenser)	21bar	65°C
FWH2	20bar	103°C
FWH3	18bar	130°C
FWH4	15bar	171°C
FWH5	335bar	239°C
FWH6	333bar	282°C
FWH7 (before boiler)	325bar	309°C

Table 4.1: Feedwater reheating temperatures at each stage

conversion efficiency is 44.9%.

4.3 Steam conditions in the condenser

The process is now examined in closer detail. Steam is generated at a rate of 462.73 kg/s at supercritical temperature and pressure. Of this, 273.6 kg/s at 33°C/45mBara-abs reaches the condenser. The remainder is bled off the main transport pipe from each of the HP, IP and LP turbines and is used in the various regenerative and feedwater heating stages. Feedwater leaves the condenser at 273.6kg/s, 33°C as a saturated liquid. It is raised to 309.6°C at 325bar by the end of the feedwater heating process. Assuming a specific heat capacity for water of 4.186 kJ/kgK then the sensible heat power requirement is 1.145MW/K. Table 4.1 summarises the process conditions illustrated in Figure 4.7.

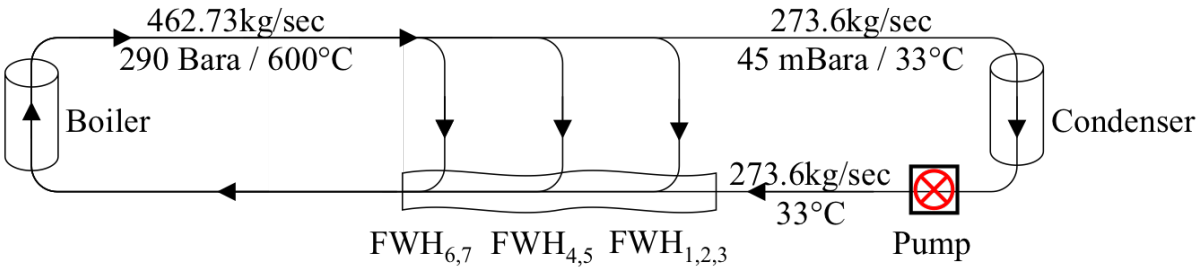

Figure 4.7: Thermodynamic model of Ratcliffe plant with feedwater Heating

A heat pump introduced to the process would supplement FWH1 and reduce the amount of steam required to be bled off from the turbine island into order to achieve the same feedwater heating effect. However, the amount of energy required to give this temperature rise is proportional to the coefficient of performance of the heat pump.

The large portion of energy is rejected from the Rankine cycle is in the condensation of the main steam outlet from the low-pressure turbines. Rather than rejecting this energy from the process through the cooling towers, condensation can be precipitated by electrically powering a THP to achieve a 'cold' side temperature lower than the dew point of the steam. The heat that is pumped to the opposing side would then be used to raise the temperature of the water returning to the boiler. The 'cold' side of the device is placed in the path of the steam entering the condenser and the condensed water returning to the boiler is brought in to contact with the 'hot' side, hence providing the energy transfer from the condenser back into the process.

The dew point is the temperature at which vapour in the air releases the latent heat of condensation at constant pressure. If the steam is to preferentially choose the THP 'cold' side then this must be held below the dew point of the vapour. It is evident from the foregoing discussion that electrical energy is required in order to retain thermal energy within the overall process. However, given that the purpose of the process is the generation of electrical energy, a question that naturally arises is, 'Is this approach viable?' This is determined by the Coefficient of Performance of the heat pump and quantified in the following section.

4.4 Minimum breakeven COP

If a heat pump is introduced into the condenser in such a way that steam will condense on the 'cold' side and feedwater condensate is passed over the 'hot' side of the heat pump, enthalpy released by recondensation can be recovered to the feedwater, rather than rejected to the environment. This will retain a greater amount of energy in the process and hence increase the overall cycle efficiency.

Figure 4.8 illustrates such an arrangement. It is important to note in this diagram that the gross electrical output from the generating set is unchanged and therefore the efficiency gain manifests itself as a reduction in the fuel required to drive the process, albeit with a reduced net electrical output to the grid. The process efficiency may be

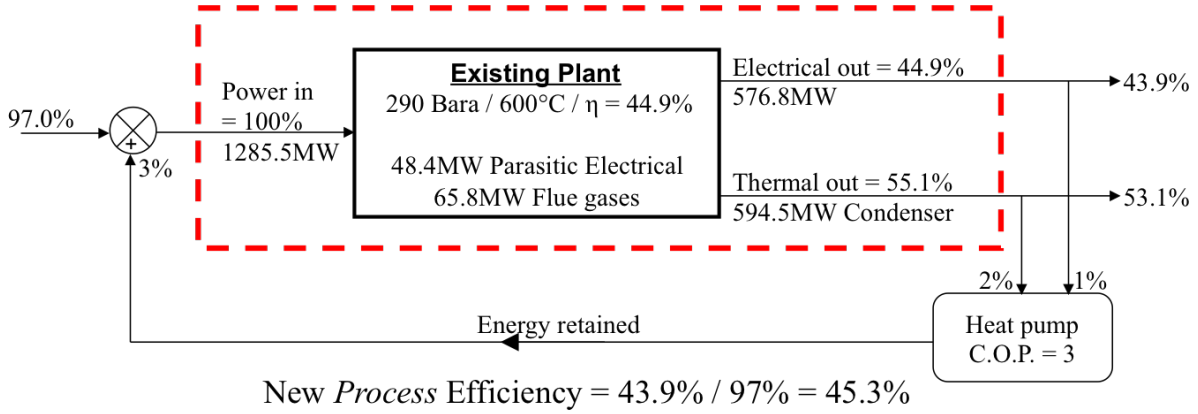

Figure 4.8: Rankine cycle thermodynamic process and efficiency including a THP with a COP_h=3

expressed in equation 4.2 and equation 4.3.

$$\eta_{plant} = \frac{Q_e}{Q_{in}} \tag{4.2}$$

$$COP_h = 1 + \frac{Q_{th}}{Q_e} \tag{4.3}$$

where Q_e is the electrical output power, Q_{th} is the thermal power rejected from the process and Q_{in} is the power input to the process. From Figure 4.6, 100% energy input yields outputs of 44.9% electrical and 55.1% thermal. In Figure 4.8, a heat pump coefficient of performance (COP_h) for heating of 3 is used, thus using 1% of the electrical output will pump a further 2% of the thermal output and this can be added to the 97% of the Figure 4.6 input energy to provide the required 100% level for constant generator output power. The revised process efficiency ($\eta_{process}$)is then given in equation 4.4.

$$\eta_{process} = \frac{43.9\%}{97\%} = 45.3\% \tag{4.4}$$

The limiting COP_h, below which economic recovery is not possible, is when the amount of energy retained within the process equals the energy input necessary to generate the electricity required to drive the recovery process, expressed mathematically as:

$$Q_e = Q_{process}\eta_{process} \tag{4.5}$$

$$Q_{retained} = \Delta Q_e COP_h \tag{4.6}$$

$$Q_{process} = Q_{in} + Q_{retained} \tag{4.7}$$

The process efficiency $\eta_{process}$ is rearranged from 4.5 to 4.8.

$$\eta_{process} = \frac{Q_e}{Q_{retained}} \tag{4.8}$$

$$\eta_{process} = \frac{Q_e - \Delta Q_e}{Q_{process} - Q_{retained}} = \frac{Q_e - \Delta Q_e}{Q_{process} - \Delta Q_e COP_h} \tag{4.9}$$

$$\frac{Q_e}{Q_{process}} = \frac{Q_e - \Delta Q_e}{Q_{process} - \Delta Q_e COP_h} \tag{4.10}$$

$$Q_{process}\Delta Q_e = Q_e \Delta Q_e COP_h \tag{4.11}$$

From equation 4.6, then $COP_h = \frac{Q_{process}}{Q_e}$.

$$COP_h = \frac{Q_{process}}{Q_e} = \frac{1}{\eta_{process}}. \tag{4.12}$$

Then the break-even COP_h is defined in equation 4.12. The minimum economic COP_h is, i.e., the reciprocal of the plant efficiency.

For a plant efficiency of 44.9% this gives a minimum COP_h of 2.2 to make the heat pump configuration beneficial to the plant. A more detailed analysis of the thermodynamic properties of the system to achieve this is presented in Chapter 6. One final observation to make at this stage is that the condenser operation is essentially isothermal and thus the initial stage of the enthalpy recovery will enable the heat pump to operate with a very high COP_h (in other words the steam entering the condenser and the condensed feedwater exiting the condenser are at essentially the same temperature). Heat pump operating at the Carnot cycle efficiency, is demonstrated by equation 4.13 and the COP_h if heating is defined in equation 4.14.

$$\frac{Q_{hot}}{T_{hot}} = \frac{Q_{cold}}{T_{cold}} \tag{4.13}$$

$$COP_h = \frac{T_{hot}}{T_{hot} - T_{cold}} \tag{4.14}$$

where temperatures are expressed in Kelvin.

With T_{hot} and T_{cold} very close to each other, the denominator term in equation 4.14 tends to zero and the overall COP rises dramatically. In practice, there will be a ΔT of a few °C due to a combination of the finite thermal conductance between the steam in the condenser and the feedwater condensate being heated on the 'hot' side, and the thermal resistances in the energy path across the THP.

4.5 Reduced output and Benson load application of THP

The minimum COP defines the breakeven point of operation of the THP applied to the Rankine cycle. However, there are further practical considerations when operating a plant that need to be included in the overall analysis of economic viability. Of paramount importance to the utility provider is the cost at which electricity is supplied to the grid. There may be times at which the cost of running the plant is more expensive and during these periods the facility is placed in a low power state to avoid the heavy duty of turning off the boilers and stopping the turbines. A typical example of such plant operation is its use as a 'spinning reserve' able to be rapidly brought on-line to supply the energy demand peaks associated with the end of popular TV programmes, the conclusion of major sporting events, etc.

Boiler design improvements have enabled operation at high steam temperatures and pressures and the efficiency of the steam cycle relies heavily on the boiler maintaining superheated conditions. Traditionally this was achieved by heating two large drums, one of water and the second containing steam collected from the water drum (shown on the left of Figure 4.9). The benefit of this approach was the steam that collects in the top drum, being less dense that the water, can be heated to a higher temperature in a separate system to generate superheated steam. The water that remains in the base of the drum is circulated and reboiled. In this configuration, the rate at which steam is produced is controlled directly by the fuel-firing rate.

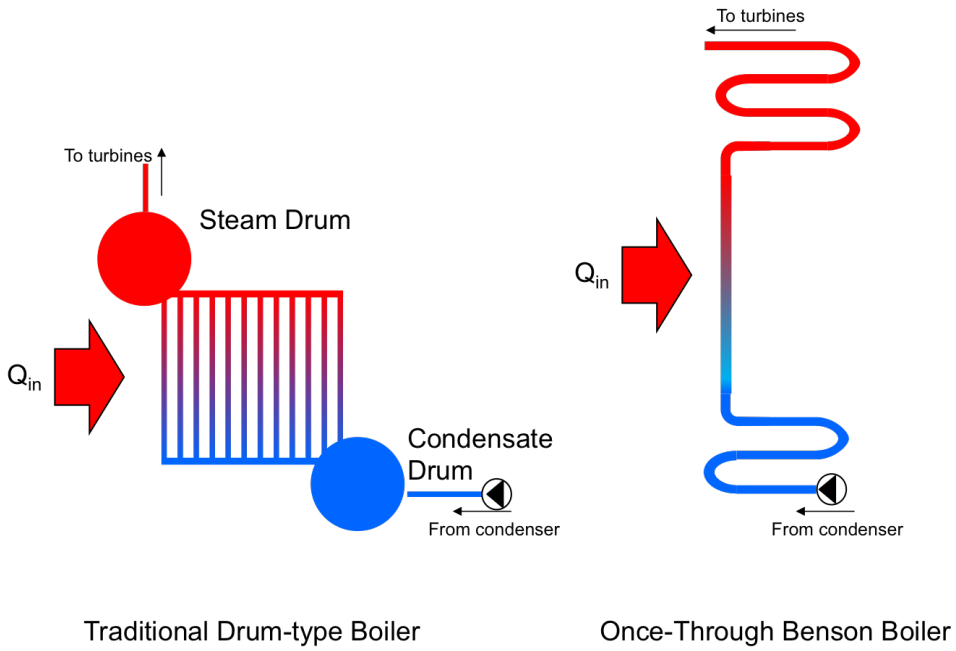

Figure 4.9: Comparison of Boiler technology

The main disadvantage of the drum style of boiler is they must operate at subcritical temperatures and pressures and this limits the efficiency of the Rankine cycle. A super-critical steam plant implements 'once-through' boiler technology that dispense with the drum. This is shown on the right-hand diagram in Figure 4.9 of the 'Benson' boiler.

This approach allows the fluid to be heated to supercritical temperature and pressure immediately on entering the boiler and there is no recirculation. The rate at which superheated fluid is passed to the boiler is controlled by the condensate pump but, the fuel firing rate determines the temperature and pressure of the steam.

These 'once-through' boilers require a minimum flow through the furnace tubes at all times. The exact quantity of this minimum 'once through flow' (which is the definition of the 'Benson Load') is dependent upon the tubes, the wall construction and the heat flux. For the vertical tube furnace design the minimum flow is approximately 30% of full load flow although this can be higher depending on the plant configuration and steam conditions. At loads below the Benson load the water must be circulated back to the inlet of the furnace tubes to avoid stress and fatigue effects that would occur if the boiling region enters the nucleation zone.

The fuel required to keep the plant running in this condition is effectively wasted since there is no electrical power being exported to the National Grid. Application of the

THP in this instance presents a method of substantially reducing the amount of fuel fired to keep the power plant operational. The following example considers use of the THP concept applied to the Rankine cycle when running at the Benson load.

4.5.1 Application of the Benson load to a thermal power plant

The coal-fired thermal power plant is only run to prevent complete shutdown, any reduction in fuel input is beneficial. Assuming the electrical output of the plant is not exported, the plant can be said to be working at 0% efficiency, meaning any $COP_h > 1$ attained by a THP would be beneficial. In other words, the input electrical power to the heat pump can be maximised as it is powered by 'surplus' electricity. The aim is therefore to use the heat pump to reduce the fuel input to the plant to the absolute minimum.

At the Benson load of 30% of the retrofitted plant at Ratcliffe with a net generation capacity of $576.8MW_e$, the electrical output is nominally $173MW_e$. Starting with the assumption of no THP at 30% load the thermal energy required is 30% of $1285.5MW_{th}$, i.e., $385.65MW_{th}$. The associated coal-firing rate is also reduced by 30% or 14.76kg/s.

Assuming the electrical energy generated by the plant is now 35% then this gives $135MW_e$ available to be utilised by a THP. The THP can then operate to recover as much of this thermal energy as possible as the electrical power generated by the plant is typically wasted. Assuming the THP now operates at the maximum $\Delta T = 75K$, then since the $\text{COP}_h \geq 1$ the thermal energy recovered by the THP is $20.55MW_{th}$. Further details and calculations are presented in Appendix A.

$$Q_{retained} = COP_h Q_e \tag{4.15}$$

5% of the thermal energy required for the plant is now supplied by a THP (shown in Figure 4.10) and given by equation 4.15.

Hence the $\text{Q}_{retained}$ in the plant is $20.55MW_{th}$, which represents a 5% drop in the amount of fuel required to maintain the Benson load. Since the new thermal fuel input of coal is now $365.1MW_{th}$, then the new slower rate of coal is 13.98kg/s a net saving of 0.78kg/s of coal.

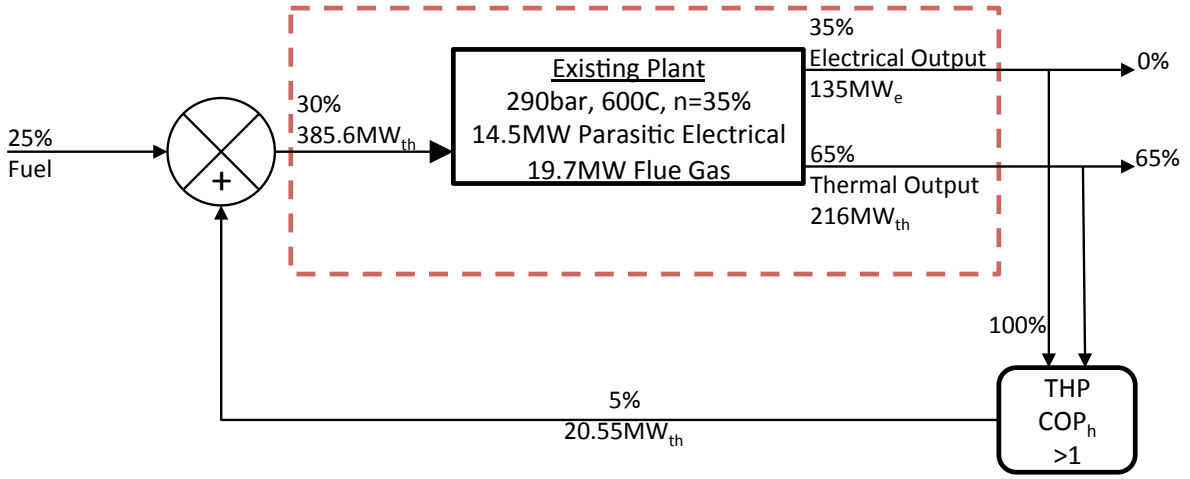

Figure 4.10: Benson load application of THP to supercritical Rankine cycle thermal power plant

Power plants are designed to operate at a rated capacity and duty. Typically they are expected to be available to generate power for 85% of the time over the course of a year. During periods of low utilization, the Benson load applies.

The latest Digest of UK Energy Statistics [3] notes an average plant load factor of 57.1% for UK coal-fired thermal power plants. This metric measures the intensity with which the coal-fired plant is used over the course of a year.

Assuming that the Ratcliffe-on-Soar thermal power plant is typical of these statistics and is operated at full load for 57.1% of the year, then for the remaining 42.1% the plant is operated at the Benson load.

In order to calculate the economic benefit to the plant, the cost of coal must be accounted for. Since the application of a THP to the Rankine cycle results in a lower amount of coal required, the economic benefit is considered as a reduction in coal costs.

Assuming that the price of coal is set at $\frac{£60}{tonne_{coal}}$ ($\frac{6pence}{kg_{coal}}$), then the amount of coal saved by applying a THP is $\frac{£}{kg_{coal}}\frac{kg_{coal}}{s} = \frac{£}{kg_{coal}}0.06\frac{kg_{coal}}{s}0.76 = \frac{£}{s}0.046$, which results in 4.6p saved for every second that the plant is operating at the Benson load with the THP. Taking this over the year when the plant is anticipated to operate at the Benson for 42.1% of the year (153 days), then the overall saving to the plant are over £600,000.

The examination of the Benson load, above, shows there are significant opportunities to reduce the overall running cost of the power plant. The Benson load is seldom considered but is a characteristic of the operation of thermal power plants today. Continued

increase in the penetration of intermittent generation sources such as wind and, in the future, wave power is likely to increase the time plant is required to be run as spinning reserve, simply to assure the continuity of electricity supply. Use of the THP concept can have a significant positive impact on the cost of plant operation through reduced fuel load.

4.6 Summary and conclusions

In this chapter the Rankine cycle has been discussed and the thermodynamic details have been expanded. Current Rankine cycle plant technology has been shown to operate at near 50% efficiency as the pressures and temperatures of the cycle increase to supercritical conditions. These new plant conditions require advances in thermal plant technology, including new efficient boiler designs and turbo-machinery technology. The aim of these systems is to maximise the area of extractable work under the T-s diagram. Numerous steam turbines are implemented in present Rankine cycle power plants specifically designed to extract the maximum amount of enthalpy. The thermal power plant at Ratcliffe-on-soar uses six turbines of varying designs depending on the pressure and temperature of steam. Further, there are several reheat stages that allow for steam to be bled off the main line. These steam bleeds are used to preheat the water returning to boiler and it is this action that is replicated using a thermoelectric heat pump, rather than a bleed of steam diverted.

The thermoelectric heat pump application to the Rankine cycle presents a novel method of improving the thermodynamic efficiency by recovering low-grade energy from the condensation process. The heat source 'cold' side of the THP is placed at the exit of the low-pressure steam turbine to allow steam to condense on extruded fins in contact with the THP and held below the dew point. The opposing side of the THP is interfaced to a liquid heat exchanger that allows for the water temperature to increase as thermal energy develops at the 'heated' side of the THP.

Despite this system using valuable electricity from the plant, it leads to a improvement in the plant efficiency as a reduction in coal or other fuel required to maintain the same

steam conditions in the boiler vital to achieving the optimum energy extracted by the turbine units. Therefore a break-even equation has been developed to show the minimum point at which a THP becomes an improvement to the Rankine cycle.

The remainder of this thesis details an experimental setup of the Rankine cycle in such a configuration as to allow a THP to be included in the condenser and the resultant condensate returning to the boiler via this THP.

The remaining chapters discuss the results showing the operation of the THP above the minimum COP required to make the THP application beneficial to the cycle efficiency.

Chapter 5

Rankine Cycle Test Apparatus

This chapter details the methods and apparatus used for the main experimental work programme undertaken as part of the research presented in this thesis.

The focus of the review of the Rankine cycle in chapter 4 was on large plant implementation. During this, I laid out the theory of a minimum economic COP when a heat pump is applied to the process. In order to develop a practical lab-based system for experimental purposes, the full scale cycle was simplified somewhat and reduced in size to a small fraction of a typical thermal power plant. Importantly, however, the steam conditions in the condenser were replicated in order that the operation of the THP detailed in the previous chapter can be fully investigated. Overall energy input to the experimental process was reduced to $6kW_{th}$ a reduction factor of some 200,000X which exacerbated some effects which are present but would not normally be an issue in the full-scale plant. These limitations are noted in the following discussion.

5.1 Small scale Rankine cycle thermal plant

A small-scale experimental model of a regenerative steam cycle thermal power plant that incorporates a steam expansion stage and condenser-mounted thermoelectric heat pump has been developed to explore thermodynamic modifications to the Rankine cycle. The working fluid is water and the whole system is sealed relative to atmospheric pressure. The purpose of the model shown in Figure 5.1 is to compare a theoretical Second Law

energy analysis with data experimentally determined from the plant. In order to closely approximate larger-scale power plant condenser operation, the model's steam conditions are matched: the operating temperature and pressure at cycle equilibrium are $33°C$ and 45mbar-abs. Of primary interest in this investigation is the behaviour of the heat pump in the steam conditions within the condenser. Hence it is unnecessary for the boiler to mimic the high temperature and pressure of a normal plant. Indeed, by operating the boiler at a much lower temperature, 'wet' steam enters the condenser and this closely matches the vapour state after the final Low Pressure turbine stage of the commercial plant. A photograph of the final experimental apparatus is shown in Figure 5.23.

5.2 Plant model

5.2.1 Rankine cycle operation

With reference to Figure 5.1, for the 'standard' Rankine cycle operation steam is generated in the boiler and exits at point (3). The steam is then expanded through a gate valve and enters the condenser at point (4) at reduced pressure. Within the condenser the latent heat of condensation of the steam is removed by the steam coming into contact with pipes of a refrigeration loop held at a temperature below the dew point, shown in the right of Figure 5.1. The condensate drops by gravity to the bottom of the condenser vessel, leaves the condenser at point (1) and flows to a positive displacement pump located below the base of the condenser. The pressure on the input side of the pump is equal to the vapour pressure in the condenser (45mbar-abs) plus the vertical head between the pump and the condensate level in the condenser (1.5 metres); the head being required to prevent cavitation in the pump. The flow rate is sufficiently low to safely disregard the Bernoulli losses from the head calculation. The pump head of 1.5m and the condensate pressure of 45mbar-abs, results in a pressure at the pump pressure of 140mbar-abs.

A bypass regulator maintains the output head of the pump at 3 bar relative to the input pressure and this differential head can be maintained over the range of flow rates to the boiler for steady-state operation over the available input energy conditions. Of

particular interest in the experimental apparatus is determination of the steady-state operating point for a range of boiler input powers and condenser conditions. Steady-state in this context is defined as the condition where the mass flow of steam leaving the boiler exactly equals the mass flow rate to the boiler, at point (2). A modified internal combustion engine fuel injection system provides the metering of the flow returning to the boiler. Points (1) to (4) also correspond to those shown in the T-s diagram in the previous chapter in Figure 4.5.

5.2.2 Boiler

With reference to Figure 5.1, the water in the boiler is heated using a pair of standard $3kW_{th}$ immersion heater elements fed from a burst controller. This drive mechanism was selected primarily because a) burst control will minimise the electromagnetic interference generated which may subsequently interfere with sensitive readings from other parts of the system, especially thermocouples, and b) the long thermal time constant of the system in comparison with the 50 Hz utility supply will not prevent a stable boiler temperature being held. The boiler is fitted with a sight glass to enable the visible confirmation of adequate water level and a float switch is also fitted approximately half-way up the boiler. If the water level drops below this point the heaters are disabled. Thermocouples are located near the base and approximately 2/3rds up the boiler as an additional safety measure and are used to confirm uniform water temperature.

The system controller uses the temperature and pressure readings from the boiler in a PID control loop (shown in §5.2.8) implemented in Agilent VEE Professional software to adjust the input duty cycle to the burst controller. 0% duty cycle corresponds to $0W_{th}$ input power from the heaters and 100% duty cycle gives $6kW_{th}$ input power. The input power to duty cycle ratio is linear over the operating range. Under normal operating conditions the pressure in the boiler is maintained below atmospheric; typically at 600mbar-abs with a corresponding boiling temperature of $80°C$.

In order to determine the thermal losses from the system a simple experiment was devised to quantify the loss. This entailed measuring the electrical energy required to

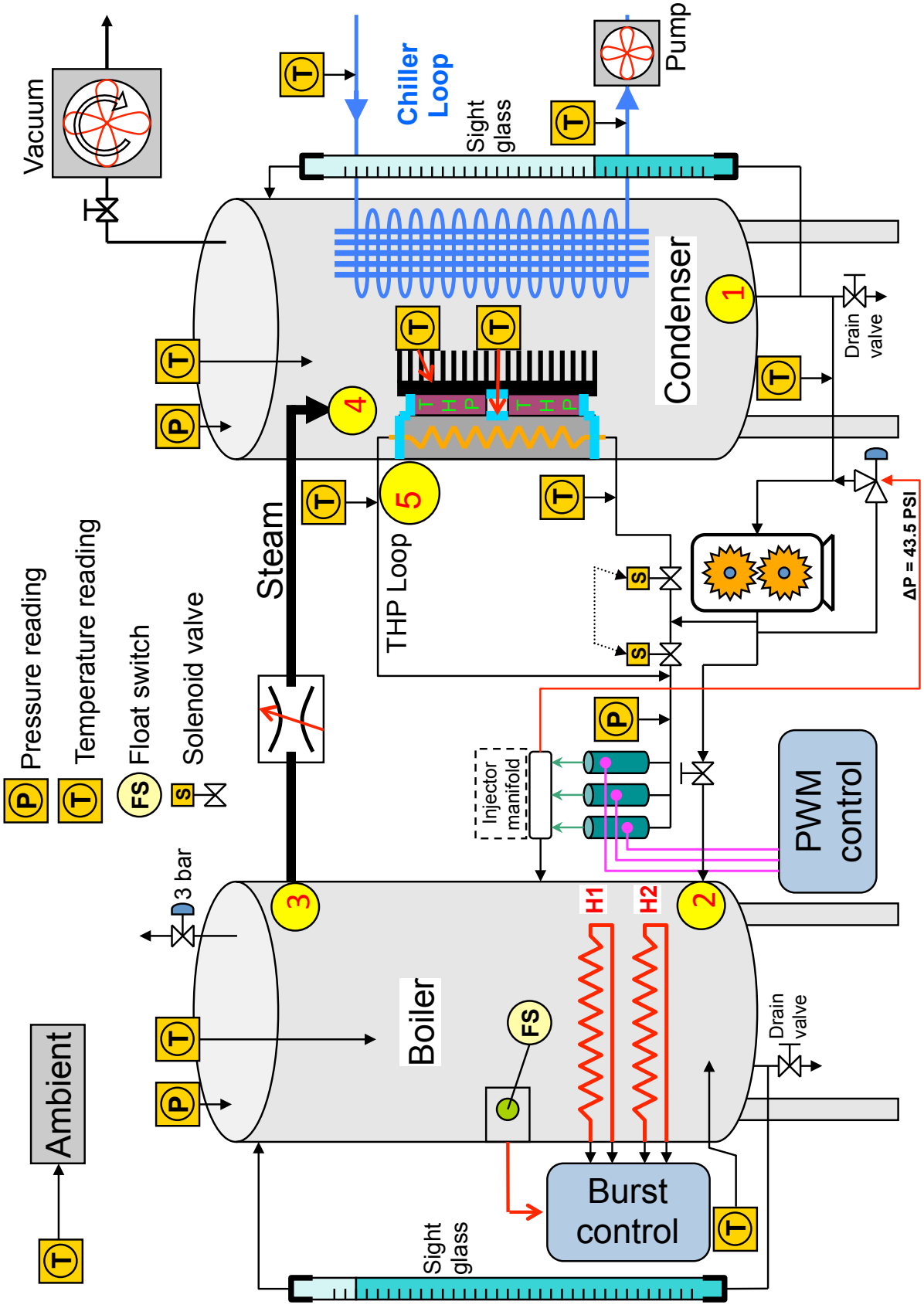

Figure 5.1: Model of the small-scale Rankine cycle

hold the boiler temperature steady for different temperatures above ambient. Initially, the boiler was filled with 60 litres of water and, using the electrical heaters, raised to 50°C at atmospheric pressure. There is no stirring mechanism in the boiler other than from convection currents associated with the heaters, hence the boiler was allowed to stabilise for 15 minutes before measurement commenced, as shown in Figure 5.2. Stabilisation was confirmed by observing the upper and lower thermocouple temperatures to ensure they were providing the same steady values. The heaters are controlled by a zero-crossing

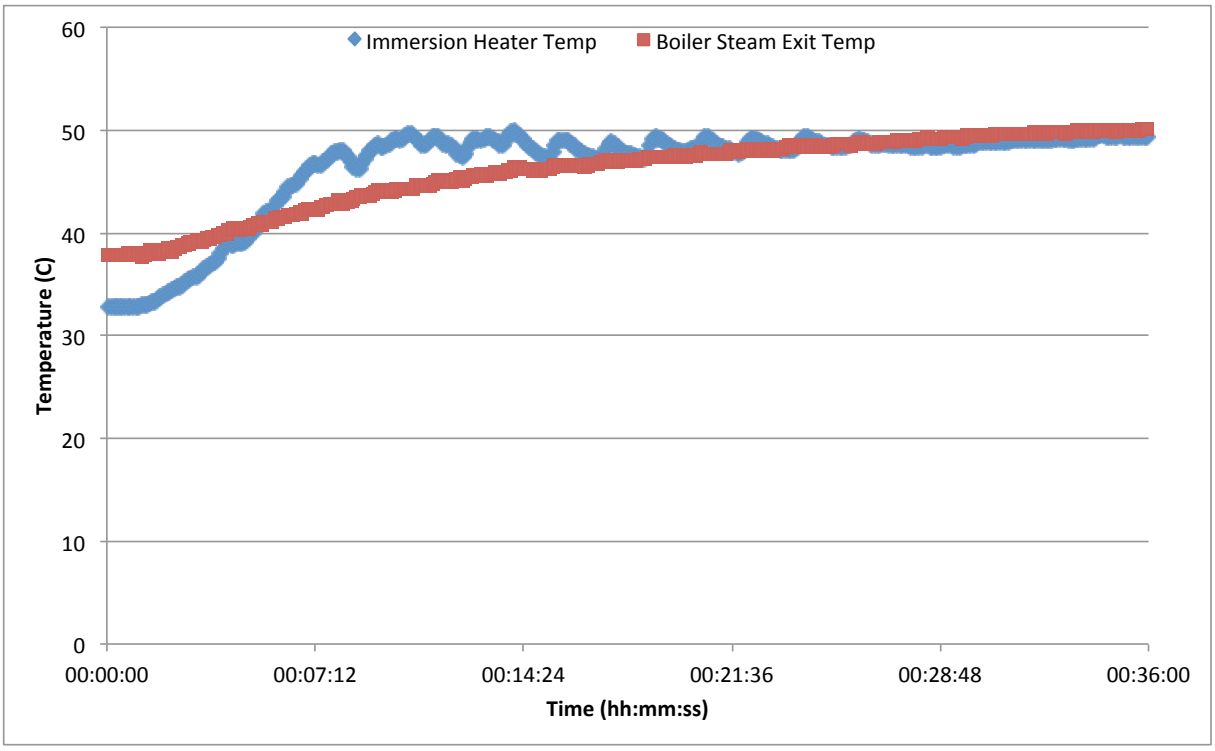

Figure 5.2: Immersion heater and boiler steam exit temperature tracking to ensure a settled temperature

burst fire trigger controller (United Automation FC11BL). The nature of the waveform fed to the heaters makes obtaining an RMS value of the current difficult using a standard ammeter. For this reason, a Voltech PM1000+ single phase Power Analyser was used to integrate the energy flowing to the heaters over a one-hour interval. The reading in Watt-hours directly gives the average power loss from the boiler to its surroundings.

The experiment was repeated at boiler temperatures up to 80°C in 5°C increments and the results obtained are shown in Figure 5.3. A record of the ambient temperature was also taken during the course of the data collection. The error bars presented on the chart represent a 10% uncertainty in reading acquired by the Voltech Power Analyser.

As can be seen, the input power required for thermal equilibrium rises with increasing ΔT, as expected, with a slight rate of change of increase being visible as the temperature difference rises.

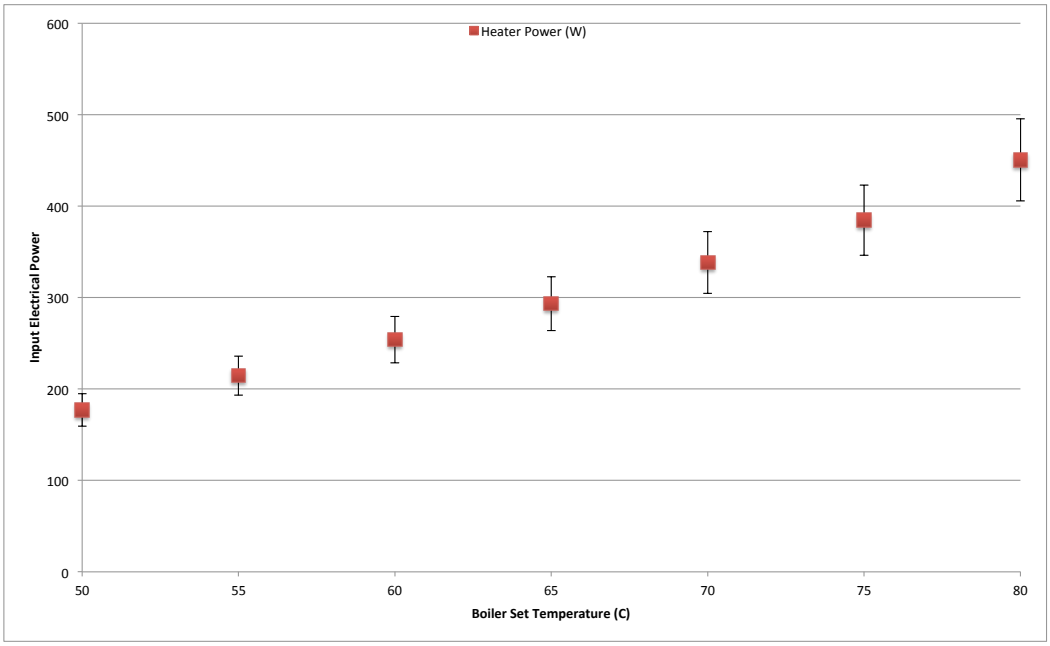

Figure 5.3: Boiler thermal losses at increasing temperatures

With reference to Figure 5.1, steam from the boiler is fed to the condenser via insulated pipework and a gate valve is used as the throttling mechanism. In order to determine the energy transfer to the condenser an accurate knowledge of the boiler energy balance is required. Figure 5.4 shows diagrammatically the method used to establish the values for each energy component. $Q_{electrical}$ represents the electrical input power to the boiler and can be measured very accurately. Q_{steam} is the energy transferred from the boiler to the condenser (which is unknown). $Q_{condensate}$ represents the thermal energy returned to the boiler as saturated liquid, and Q_{loss} is the total heat leakage from the boiler to the surroundings. To avoid the difficulty of directly measuring the mass flow rate of steam leaving the boiler the other values were measured, $Q_{condensate}$ being found using the fluid flow rate, its temperature and the specific heat of water. The energy transfer via steam

to the condenser can be then be deduced. For the condensate equation 5.1 is defined.

$$Q_{condensate} = mC_p\Delta T \tag{5.1}$$

where m is the mass flow of the water (kg/s), C_p is the specific heat capacity (kJ/kgK) and ΔT is the temperature increase in the condensate.

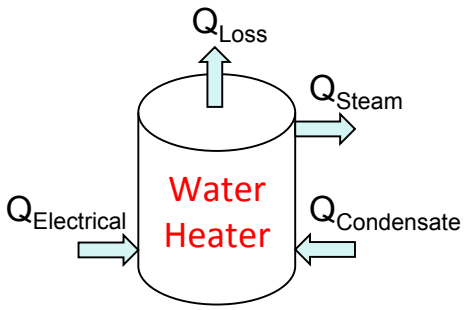

Figure 5.4: Energy transfer in the boiler

$$Q_{steam} = Q_{electrical} - Q_{loss} + Q_{condensate} \tag{5.2}$$

In operation, the experimental apparatus maintains the desired set temperature on the boiler and thus is the primary means of regulating the process. Steam from the boiler expands into the condenser via the gate valve and the differential pressure across the valve determines the rate of transport of steam. The nominal pressure within the condenser is 45mbar-abs giving a saturated steam temperature of $33°C$. The pressure in the boiler determines whether or not steam is produced but the process is inherently stable.

Assume the boiler is maintained at the desired temperature by the heater and the steam valve is shut. The condenser is at a pressure of 45mbar-abs. When the valve is opened, the boiler pressure reduces, steam forms and flows to the condenser. The latent heat of evaporation associated with steam formation leads to a reduction in the temperature of the remaining water in the boiler and this is detected and compensated for by the heater control loop. If the quantity of steam leaving the boiler is reduced and the heater power is left unaltered, the water temperature starts to increase. This is detected

by the controller and the heater power is then reduced.

$$Q = \frac{mCp\Delta T}{t} \tag{5.3}$$

where Q is the thermal energy (kW_{th}), m is the mass of the fluid (kg/s), Cp is the specific heat capacity (kJ/kgK), ΔT is the temperature gradient through which the fluid is raised ($^{\circ}C$) and $'t'$ is the time taken to affect the change in temperature (seconds).

With knowledge of the energy sources, sinks and process parameters and assuming steam production is isothermal, at least to a first approximation and within the experimental accuracy in this experiment, the rate of steam production can be calculated using equation 5.3.

If the boiler maintains a pressure of 200mbar-abs in order to boiler 60 litres of water to $60^{\circ}C$ from $25^{\circ}C$, then the energy required by the boiler to raise this temperature of water is $8792kW_{th}$. However, the energy required to generate steam to balance the system is less than this and given by equation 5.4.

$$Q_{steam} = h_v m \tag{5.4}$$

where h_v is the enthalpy of vapourisation required to change 1kg of water to steam(kJ/kg). The latent heat of vaporisation of water at 200mbar is 2357kJ/kg. Experimental data gave an average thermal power of $3.2kW_{th}$. From Figure 5.3 the energy loss from the boiler when maintaining $60^{\circ}C$ is $254W_{th}$. Assuming water returned to the boiler as condensate is pumped at $1L/min$=$0.0167kg/s$ using the injectors, then the steam energy in the boiler can be determined where the temperature of water returned increases by.

$$Q_{condensate} = mCp\Delta T = 0.0167 * 4.187 * 1 = 0.07kW_{th} \tag{5.5}$$

From equation 5.2 the final Q_{steam} can be deduced in equation 5.6.

$$Q_{steam} = 3.2 - 0.254 + 0.07 = 3.016kW_{th} \tag{5.6}$$

The remaining energy is released in condensation using a combination of the chiller unit and the THP. There is a careful balance between the amount of energy converted to steam and the amount of energy extracted in condensation, as the capacity of the chiller unit is less than what the boiler can generate.

5.2.3 Expansion and Condensation Stages

The condenser and associated apparatus are shown on the right of Figure 5.1. The expansion valve linking the boiler and condenser mimics the work extraction via a turbine in the Rankine cycle power plant. A simple manually controlled gate valve is used for this purpose in the experiment. At start up it is necessary to remove any air and other non-condensing gases from the system. Conventionally this is accomplished using a steam ejector fed from a suitably high-pressure part of the process. In the experimental model the steam pressure is below atmospheric and so instead a vacuum pump is employed to drop the pressure below 20mbar-abs. Once the desired system pressure has been reached the vacuum pump is isolated from the system. The expansion valve controls the pressure drop between the boiler and condenser and the condenser pressure is then maintained at 45mbar-abs, giving a saturation temperature of $33°C$ (306K). Initially several attempts were made to flood the condenser with steam when it was open to the atmosphere in an attempt to displace the air but these proved unsatisfactory, and did not achieve the desired pressure upon condensation. This was done because of the detrimental effect of wet steam passing through the vacuum pump, causing corrosion. Eventually a vacuum pump near the end of its service life was obtained for use with the experiment.

5.2.4 Condenser Cooling Circuit 1

Several iterations were needed to obtain the desired cooling circuit performance. The first attempt at implementing the primary cooling circuit in the condenser used an array of 8mm diameter copper tubes forming heat exchanger elements connected to a large water chiller.

A section of the heat exchanger is shown in Figure 5.5. The input temperature from

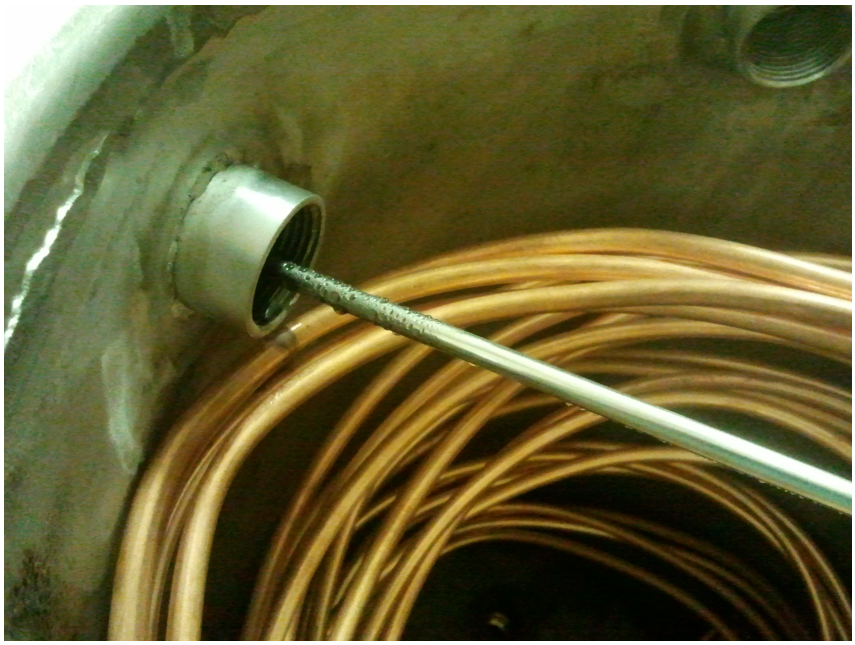

Figure 5.5: Copper cooling loop of 8mm pipe in Rankine cycle condenser

the chiller to the heat exchanger is maintained at $15°C$, i.e., below the dew point of the steam in the condenser. As condensation occurs the latent heat of condensation is released and captured by the chiller loop. This equates to the enthalpy difference between points (4) and (1) in the condenser of Figure 5.1 or the graph shown in Figure 4.5. Only the liquid phase remains after the full condensation and this has an enthalpy of 112kJ/kg. The temperature of the return flow to the chiller loop is also measured, principally to ensure the exit temperature remains at least $3°C$ below the dew point and that isothermal phase change is maintained.

A glass sight tube is also included in the condenser: in the event the condensate level rises such that any part of the heat exchanger is immersed this will lead to additional condensate cooling and cause a significant deviation from true plant operating conditions.

Condensate flows under gravity from the base of the condenser (where its temperature is measured) to the gear pump. In this first iteration the base of the condenser was only 150mm above the entrance to the gear pump. Given the low absolute operating pressure of the condenser and the low head on the pump, severe problems with pump cavitation were experienced. This is once such example of where reducing the size of actual plant yielded what proved to be quite a difficult problem to overcome.

5.2.5 Condenser Cooling Circuit using a Thermoelectric Heat Pump

The condensate path after leaving the gear pump can be switched between either direct boiler injection or via a secondary cooling loop marked 'THP Loop' in Figure 5.1. This is done by selective activation of a pair of solenoid valves, also shown in Figure 5.1.

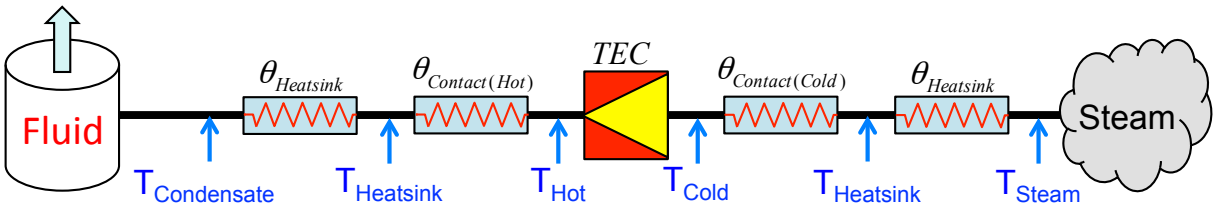

Figure 5.6: Thermal path from condensate fluid to steam through the THP

The thermoelectric heat pump is located in the secondary cooling loop and condensate temperature is measured at the entry and exit of the pump assembly. Various points within the heat pump itself are also measured, including the hot and cold faces of the thermoelectric device. The equivalent thermal circuit with temperatures and resistances for heat flow between the steam and the condensate is shown in Figure 5.6.

When in direct injection mode, condensate is passed through the injector array, discussed shortly, and the flow rate is controlled by varying the injector duty cycle. This, coupled with knowledge of the condensate temperature provides the data necessary to determine the rate of energy transfer to the water heater.

When in THP mode, condensate is passed through a labyrinth heat exchanger on the 'hot' side of the THP. With reference to Figure 5.1 steam in the condenser encounters the 'cold' side heatsink of the heat pump, which is nominally at the same temperature as the primary cooling loop ($26°C$) and condensation occurs.

The THP COP falls with increasing ΔT across the device and hence the heat-sink and contact thermal resistances shown in Figure 5.6 are minimised to keep the COP as high as possible. The condensate receives the thermal energy transferred by released enthalpy and electrical power is used to operate the THP. After passing through the labyrinth, condensate is then injected into the water in the usual way. Several thermocouples are

used in this cooling loop to measure condensate temperature at various stages of the pre-heat process.

5.2.6 Pump Flow Characteristics

The main condensate pump was selected to be able to provide the injectors with the required pressure to operate on the outlet of the pump, while maintaining a low pressure on the inlet of the pump. The pump selected is manufactured by Micro Pump Ltd [1] and is a geared positive displacement pump meaning that the liquid is sucked in the inlet pipe and is trapped between two gears before ejection at the outlet. The pump is fitted with an N21 sized gear giving 0.316ml per revolution, a minimum speed of 500RPM and a maximum speed of 4600RPM. This equates to an operating flow range of 2.6ml/s to 24.3ml/s. In order to ensure correct operation the pump performance was experimentally

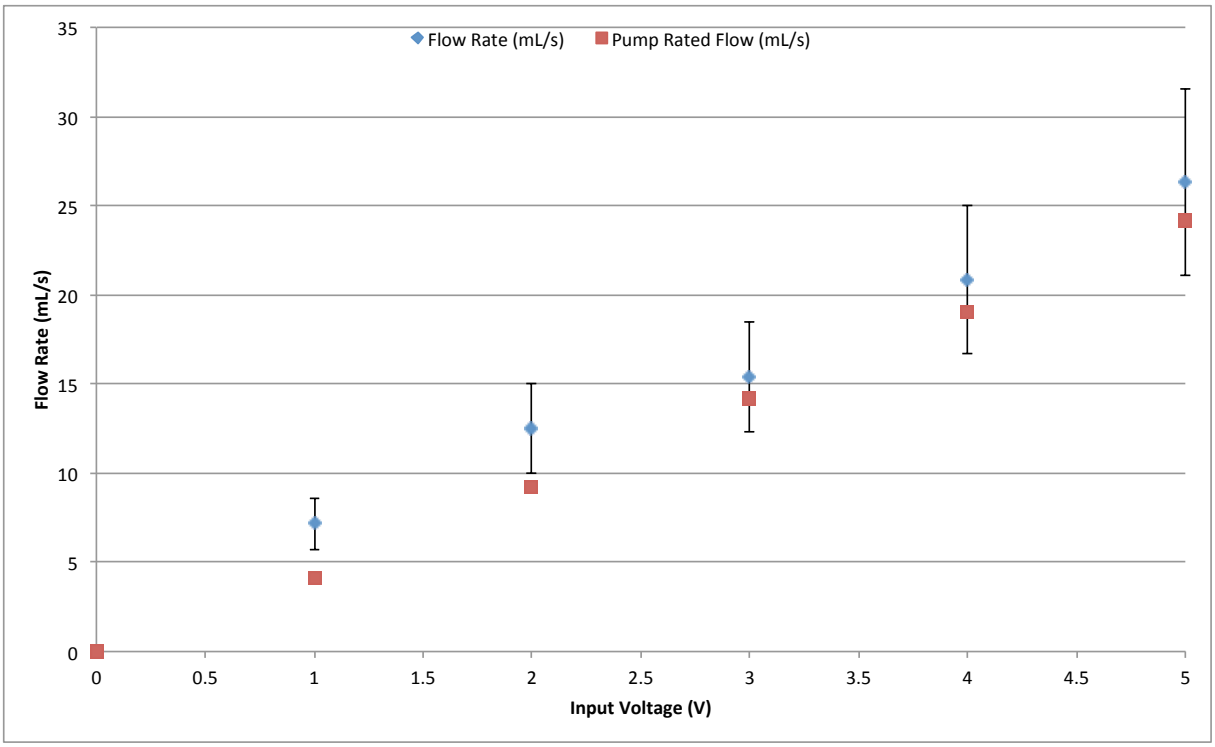

Figure 5.7: Geared pump performance

validated. The time taken for 100ml to be pumped was measured by a stopwatch as the input voltage to the pump was increased in 1V steps. The chart in Figure 5.7 plots the flow rate calculated from the datasheet in red squares and the flow rate when pumping

[1] Micro Pump Ltd, Gear Pump, GC Series `www.micropump.com`

100ml water is plotted in blue diamonds. There is a margin of error in the measured data as the stopwatch was slightly delayed in starting and stopping to compensate for the pump motor running up to speed and coming to a rest, however, the data is a reasonably close match and it was therefore surmised that pump performance matched the datasheet. The

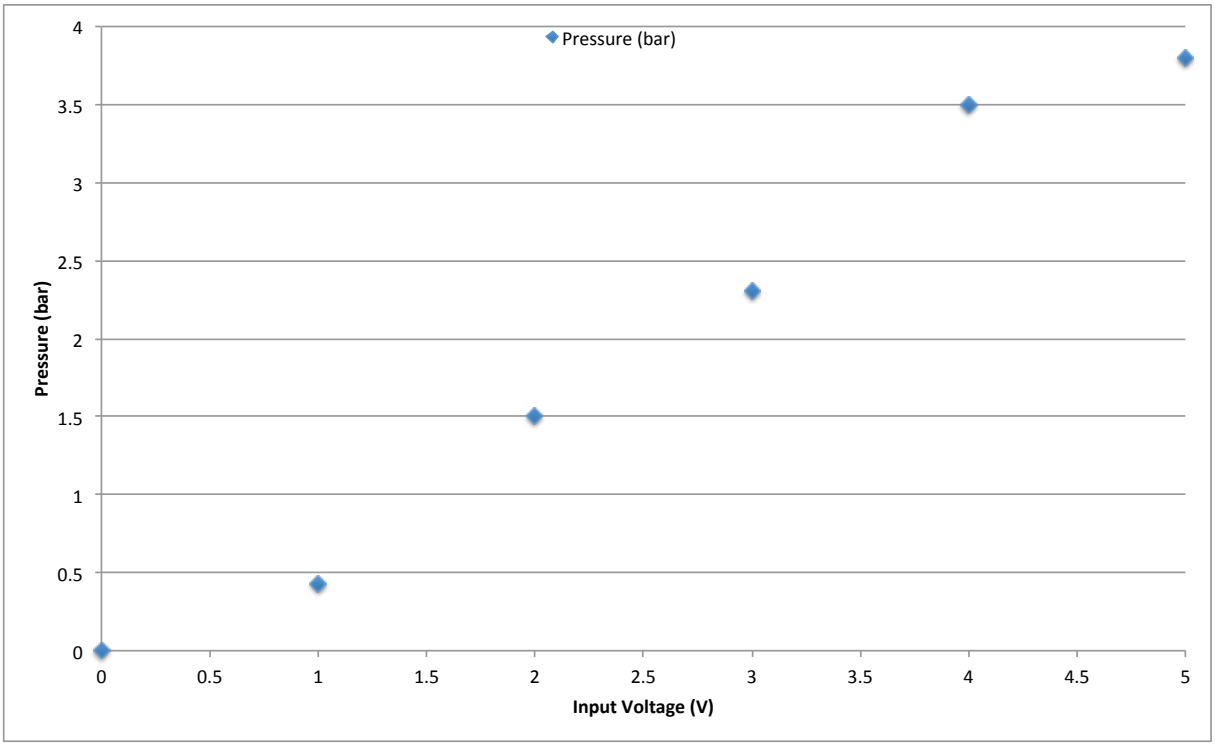

Figure 5.8: Thermal path from condensate fluid to steam through the THP

other aspect of this pump is the ability for it to provide the minimum pressure required for the injectors. In order to characterise the performance, the system was left at ambient pressure and the input voltage to the pump incremented in 1V steps. The injectors were operated at their maximum duty cycle and to meet their published flow characteristics a differential pressure of 3bar must be maintained on the high pressure injector manifold. The pressure at the outlet of the pump was measured by a pressure transducer and is plotted in Figure 5.8.

As Figure 5.8 shows, at input voltages lower than 4V the pump cannot maintain the pressure required for the injectors, therefore the minimum input voltage is 4V to ensure correct operation at any injector flow rate.

5.2.7 Injector Characterisation and Flow Rate

Very early in the design of the experiment it was determined that accurate metering of the flow rate of condensate returning to the boiler was required in order to be able to calculate the energy balance for the system. Accurate flow meters for very low flow rates are exceptionally expensive and an alternative method had to be found. Automotive fuel injection systems are capable of very accurate metering of fuel to the combustion cylinder and what is effectively an engine fuel injection system has been implemented to provide the necessary flow control and metering of condensate returning to the boiler.

The final stage of the feedwater loop in the experimental Rankine cycle apparatus is the re-injection of the condensate to the water heating unit. The injectors are of the 1000cc type meaning that $1L/minute$ can be passed, and doing so requires a nominal pressure of 43.5psi of gasoline at $52°C$. Gasoline is less dense than water and the flow and pressure characteristics will differ. The injectors operate by the movement of a small solenoid at the tip. A large voltage and current in a high-speed pulse train causes the solenoid to move and this has the effect of atomising the liquid.

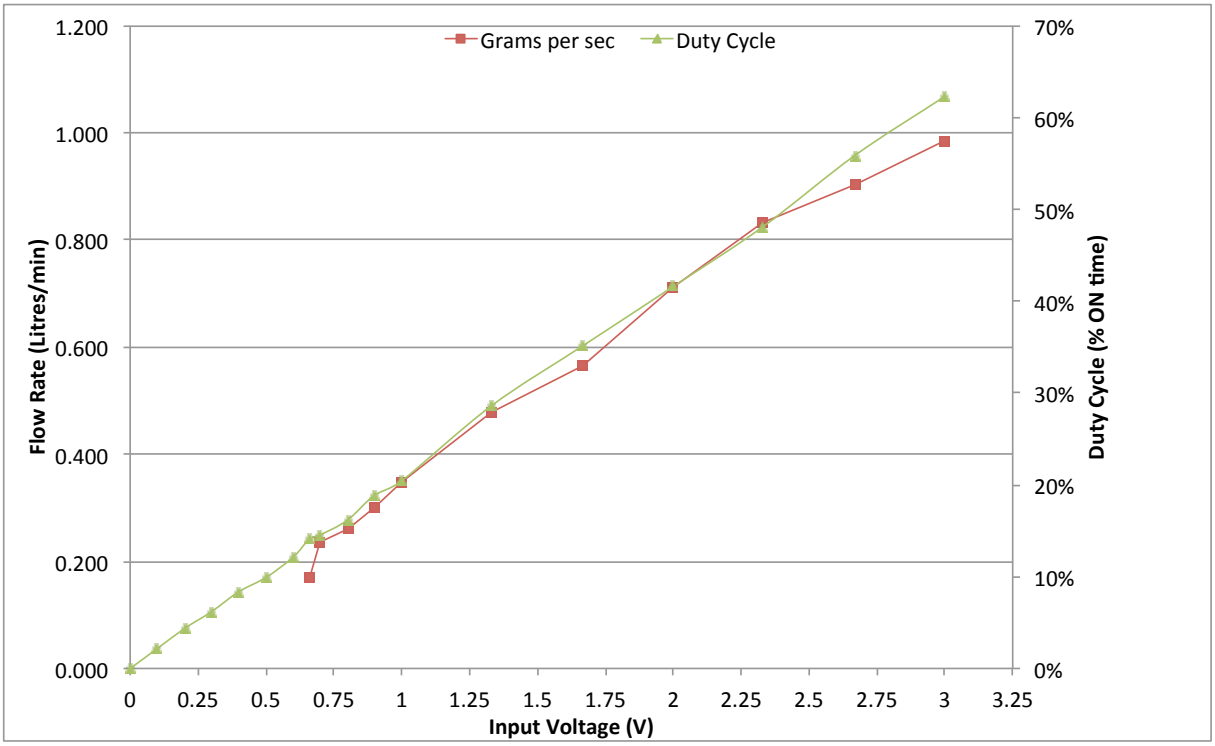

Figure 5.9: Injector performance as a function of input voltage and duty cycle

Regardless of the feedwater route taken (direct or via the THP), condensate at the injectors is maintained at 3bar (43.5 psi) relative to the point of entry to the water heater by the use of a pressure regulator in the bypass loop. The regulator operates to ensure a constant pressure is set at the pump outlet regardless of the inlet pressure (subject to the minimum pump voltage of 4V being adhered to). The control system (described in §5.2.8) provides a 0→5V analogue output to a microprocessor-based converter which translates the analogue voltage to a PWM waveform for the injectors. Due to the different viscosity of water at $25°C$ and gasoline at $52°C$ the flow rate of the inject system had to be accurately remapped according to the operating duty cycle of the injectors. The relationship between the control voltage, PWM duty cycle and flow rate for ΔP of 3bar is shown in Figure 5.9.

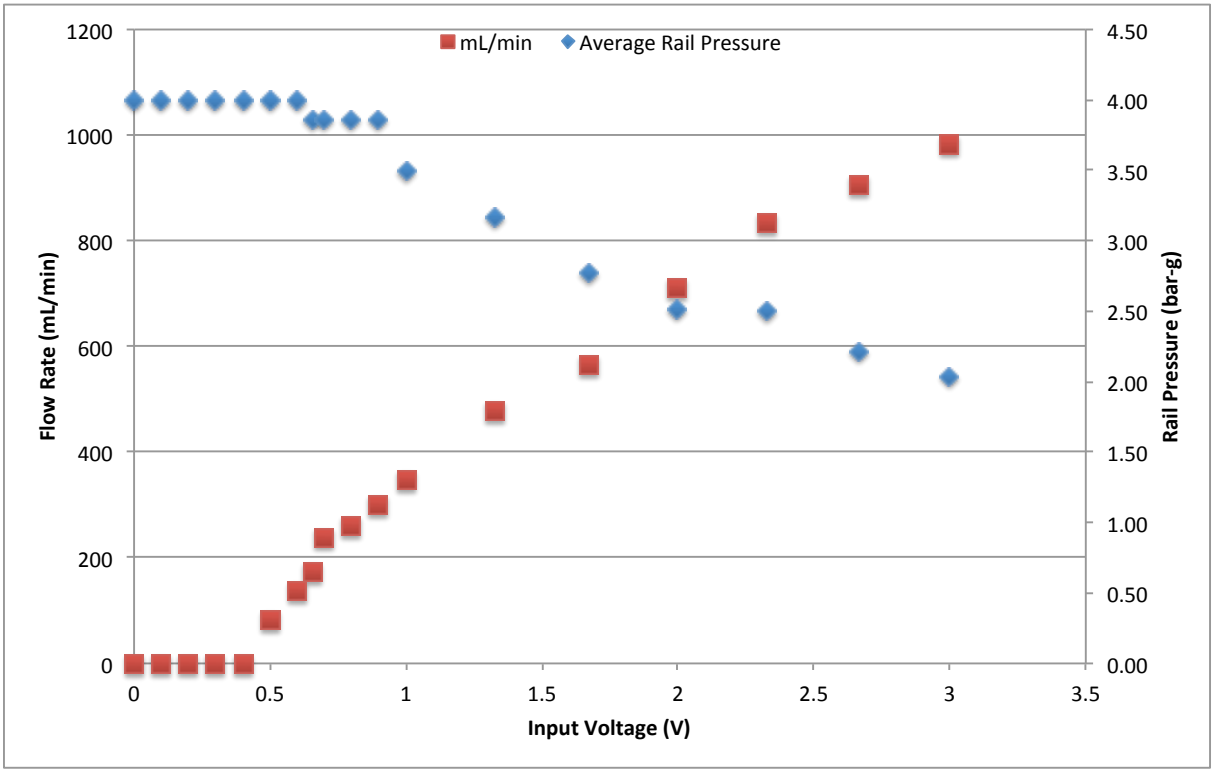

Figure 5.10: Variation of rail pressure with increased duty cycle and the increase in flow rate

Figure 5.10 shows the relationship between the input pressure to the injectors and flow rate as the input duty cycle is increased. The red square line in Figure 5.10 shows a threshold of $0.2g/s$ of water flow at 0.66V, 10% duty cycle. This represents the limit of the operation of the injector as the subsequent flow rates follow linearly with increasing duty

cycle. The pressure on the injector rail drops as the capability of the injectors outweighs the pumping capacity at the required ΔP and this sets the upper limit for 'calibrated' operation. At input voltages of greater than 1.66V the pressure drops below the 3bar threshold for guaranteed injector operation, however Figure 5.9 shows that only voltages above 2.5V result in a departure from the expected flow rate. Therefore the injectors can be operated to 2.33V and maintain the correct flow rate. Higher injector duty cycle was used under some circumstances, e.g. simply pumping condensate back to the boiler if the condenser had to be drained for some reason.

5.2.8 Control Program and Software PID

An Agilent data-logger (34972A) was used to measure and control all of the inputs and outputs on the experimental plant using Agilent VEE Professional control software. In addition, all of the instruments are controlled using the IEEE-488 interface and many additional instrument readings are returned to the control software for use in the control programme. All plant data are checked every five seconds and each value archived in a Microsoft Excel spreadsheet file for subsequent analysis. Some 22 separate parameters are logged.

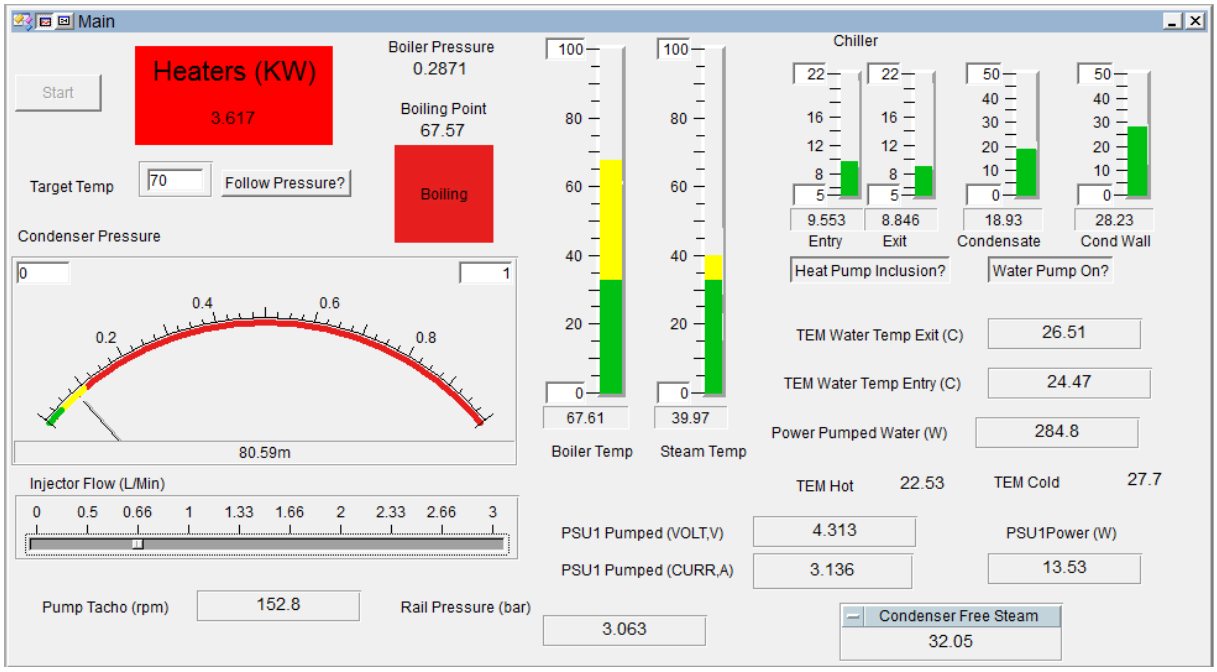

Figure 5.11: Rankine cycle plant control software

The software allowed the plant to be monitored in real time and values from the various power supplies and the data-logging unit were displayed on computer screen. A snapshot of the control panel for the computer programme is shown in Figure 5.11.

The operation of the software is as follows:

The desired boiler temperature is set in the 'Target Temp' text box at the top left hand side in Figure 5.11. Depending on the prevailing temperature the immersion heater power is ramped up to $6kW_{th}$ to match the desired value. Since there is no sight window on the boiler itself, the software relies purely on the temperature and pressure readings to determine if the system has reached the saturation temperature of the water. (In fact when the boiling point is reached the boiler tends to vibrate quite obviously, accompanied by audible boiling noises.) If the saturation temperature is reached or exceeded, the system notifies the user. It is possible to let the software automatically reach boiling conditions by having the programme track the boiler pressure and to always aim for a desired boiler temperature above the saturation temperature.

Simultaneously, the condenser was isolated from the boiler by shutting the gate valve and using the vacuum pump to reduce its pressure to below 20mbar-abs. Periodically the gate valve connecting the boiler and condenser was opened, primarily to remove the uncondensable air trapped at the top of the boiler and also to reduce the pressure of the boiler to generate steam at the required conditions. Finally, the gate valve was adjusted to maintain a pressure differential balance between the boiler and condenser resulting in steam being present in the condenser at 45mbar-abs.

The cooling loop inlet and exit temperatures were monitored to determine the amount of energy rejected by the chiller when condensing the steam.

The solenoid valves that direct the flow (denoted 'S' in Figure 5.1) are operated in tandem by the button 'Heat Pump?'. When the button is pressed the solenoid valve operating the heat pump loop is opened and the short return loop is closed. At this point, the 'Water Pump ON' button is switched on to supply 5V to the tachometer input on the geared positive displacement pump. The rail pressure is monitored in real time and when the required pressure is met the injector slider bar can be increased.

The thermoelectric heat pump input power is monitored by the program, recording

the DC voltage and current applied to the device.

5.3 First Iteration of Complete Apparatus

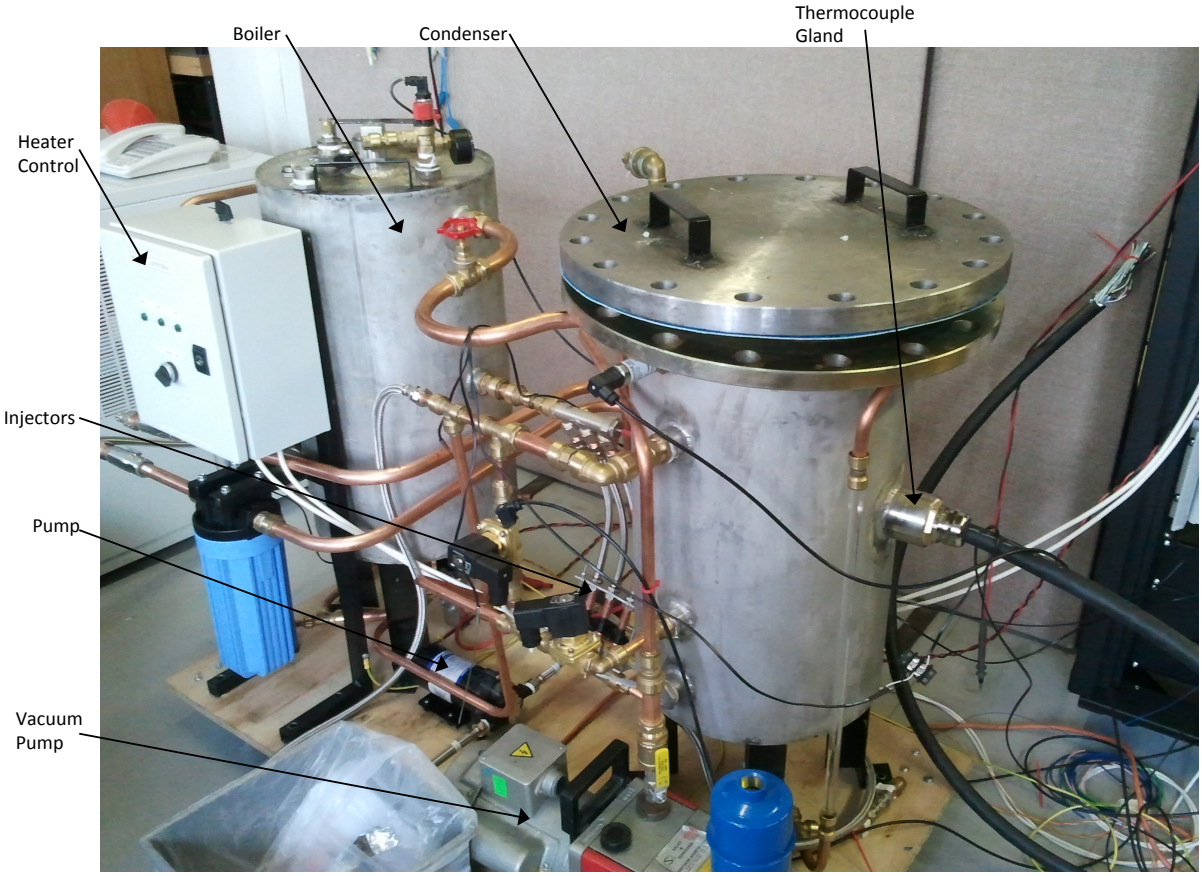

Figure 5.12: First iteration of the small-scale Rankine cycle test apparatus

The first version of the complete system is shown in Figure 5.12. The condenser is the vessel on the right with the large lid and black handles. To get some idea of the scale of the experiment, this lid is 18" in diameter and weighs 70 kg. The boiler is on the left in the picture with the immersion heater controller shown in the grey box in front of the boiler. Thermocouples were passed in to the condenser using the gland shown on the right at the side of the condenser and the vacuum pump is shown in the bottom right. The injectors and pump are shown in the centre between the boiler and condenser. The control electronics and data-logging unit are shown in Figure 5.13.

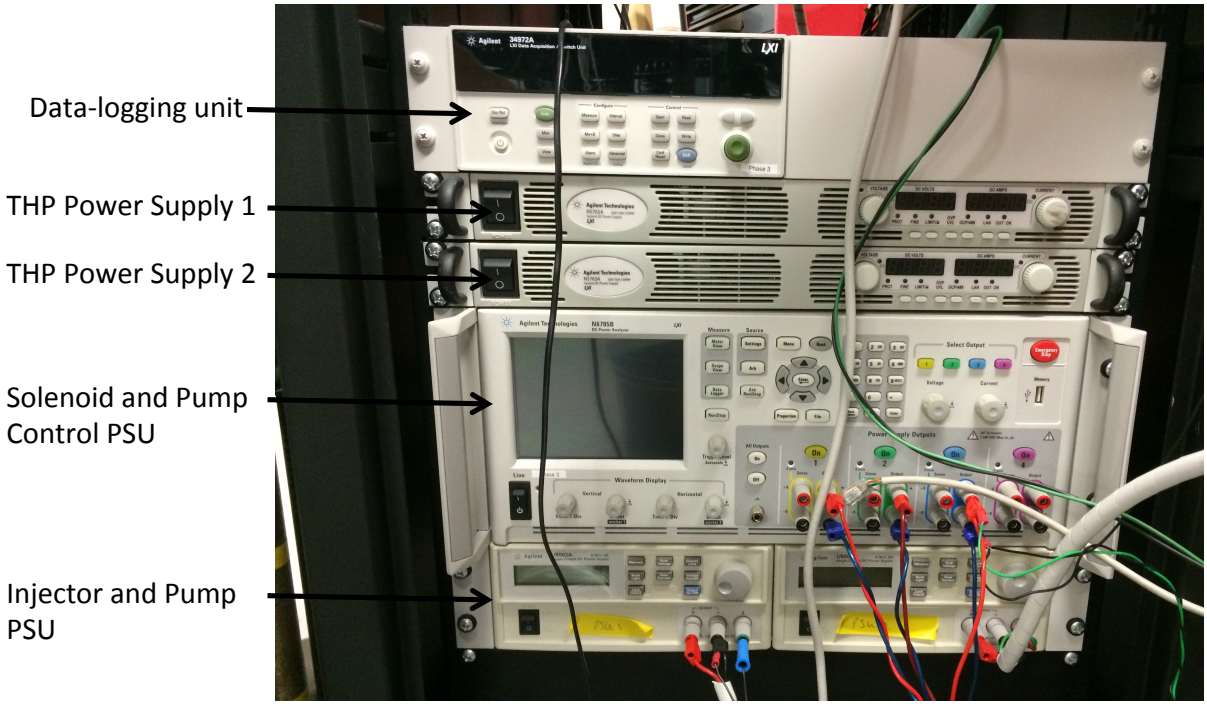

Figure 5.13: Control electronics, power supplies and data-logging units

5.3.1 Immersion Heater

A pair of standard 3kW domestic immersion heaters were used to heat the water in the boiler, although their use has not been without problems. One immerser failure occurred when the mounting flange and heating element mechanically separated. This was attributed to operating the unit at negative pressure relative to ambient during system pump down. Under normal operation the immerser is subject to positive pressure and hence the heater element is forced against the flange in the mounting boss. Several air leaks were subsequently traced to the immerser flanges and in order to combat this during system startup the boiler temperature was raised prior to evacuation of the air at the top of the system, hence the pressure never dropped below about 0.6 bar-abs. In addition a liberal application of bath sealant was applied to the heater flanges to aid leak suppression.

5.3.2 Pump Testing

As shown in Figure 5.12, the system was laid out on a horizontal plinth with the boiler and condenser located beside each other. In this configuration the steam outlet pipe from the boiler could be placed inline with the condenser, reducing the piping distance

and reducing thermal losses to the environment. The base of the condenser has four pipe connections to other parts of the system: the sighting tube; drain; reference for the pressure regulator; and inlet for the pump. The drain plug was the lowest point in the system and the remaining connections were placed above this point.

The system was tested by dropping the pressure in the condenser to the design point of 45mbar-abs. The pump tachometer input operates from a $0 - 5V_{DC}$ signal and the flow rate and pressure are proportional to this pressure. The pump failed to achieve the pressure difference of 3bar at $5V_{DC}$. The cause was eventually found to be that the level of water in the condenser had to be sufficient to cause a large enough pressure to develop at the inlet port. The pump cavitation was caused when the low-pressure water effectively boiled as the pump operated. The result was that the flow rate was unpredictable and the pressure at the outlet did not reliably reach 3bar.

Cavitation has the potential to destroy pump impeller blades so this situation must be avoided. The only solution was to place the pump at a sufficient depth below the base of the condenser to avoid cavitation by the addition of a gravity head of water. This is typical of the type of issues encountered in trying to scale down the real plant.

5.3.3 Cooling Capacity

The cooling capacity of the system is based on the supply of chilled water. The surface area of the looped coils totals $0.503m^2$, spread across 4 lengths of copper tubing each 8mm diameter. The chiller unit in use is capable of $4.3kW_{th}$ of cooling. By measuring the temperature difference at the inlet and outlet of the chiller unit the performance of the coiled copper pipe can be determined from the mass flow rate of the chiller which is fixed at $12L/min$ (0.2kg/s) and filled with a glycol/water mixture with a resultant heat capacity of 4 kJ/kgK.

Figure 5.14 shows the amount of thermal energy transferred to the coolant loop and condenser pressure as a function of time. As the thermal energy in the condenser increased, the temperature gradient across the coolant loop increased until the condenser saturated with steam. The full cooling capacity of the chiller was $4.3kW_{th}$ and the ex-

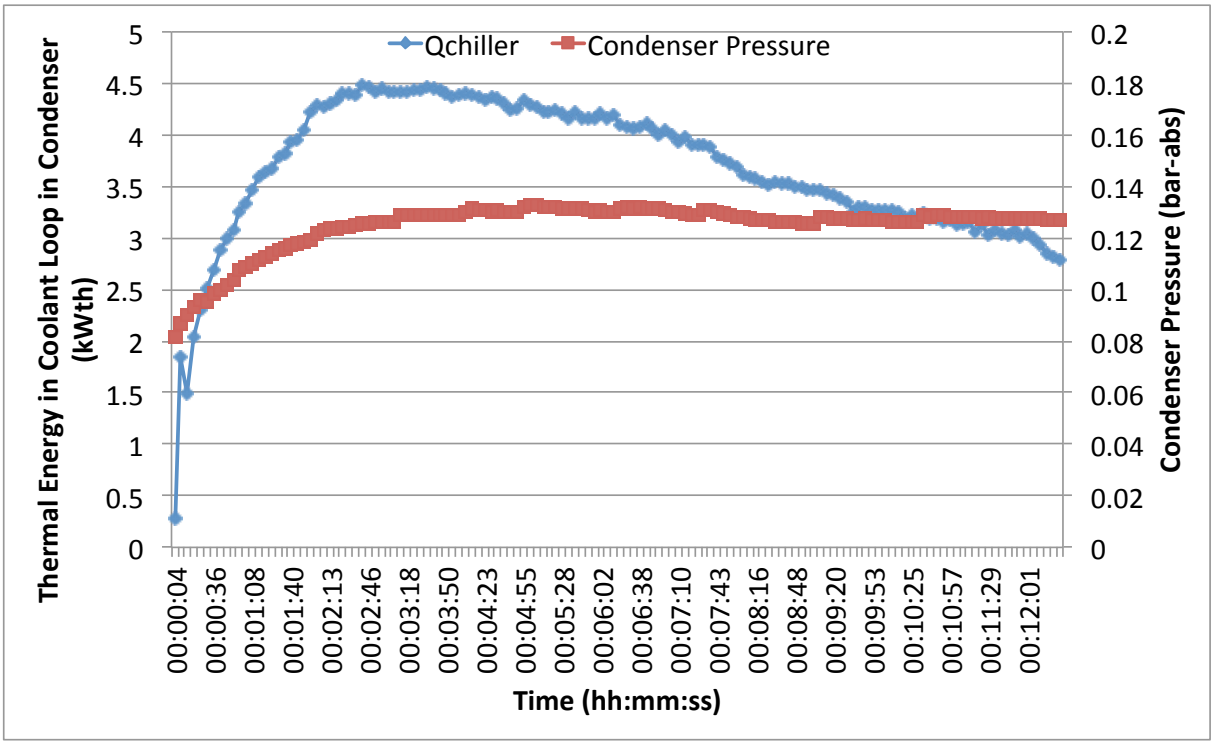

Figure 5.14: Thermal energy rejected by the condenser and condenser pressure

periment reached $4.5kW_{th}$ over an extended period of time. This meant that the THP loop was overcome with higher temperature steam causing an elevated condenser pressure. A conclusion drawn for this observation was that the primary cooling loop was not of sufficient size, therefore a new condensing coil was required to increase the available surface area. Another issue factored into the design at this point was a redesign of the THP module in the condenser: in this iteration the primary coolant loop was arranged as a helix near the outer wall of the condenser, leaving a cylindrical shape within the centre volume of the condenser for access and THP heat exchanger placement. It was felt necessary that the redesigned experiment should restrict the THP loop to the region near steam entry at the top of the condenser. One final practical point was the great difficulty in reaching the bottom of the condenser to make pipe connections because of the number of pipes and wires in the way.

5.3.4 Vacuum and Air Ingress

As noted in the introduction to this chapter, a basic requirement of the experimental apparatus was its ability to recreate actual steam conditions found in the condenser of a

thermal power plant, albeit at reduced scale. This requires the condenser to operate near to a vacuum to maximise the area of the T-s curve. There were significant difficulties encountered in properly sealing the condenser and boiler to operate at the desired operating pressures. Issues with the immerser units have already been discussed; pipe and cable feedthroughs were also initially troublesome.

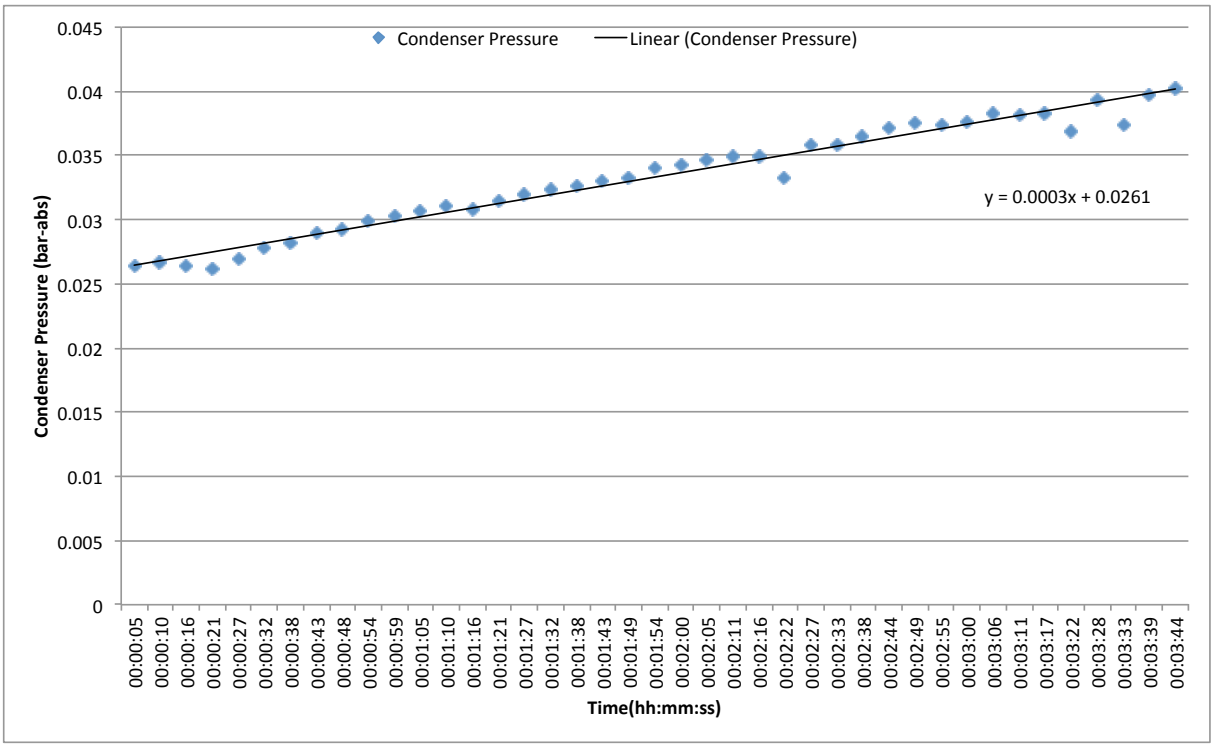

Figure 5.15: Condenser pressure drift

After system evacuation, the chart in Figure 5.15 shows a rapid increase in pressure in the condenser. The amount of drift is calculated as a linear equation where the gradient of the line over a course of 37 minutes was calculated. Clearly there was considerable leakage of air back into the system which is unacceptable.

The pipework of the entire system was completed using push-fit fittings. These fittings are rated to 3 bar internal positive pressure but, as was discovered, not rated for a negative pressure. The pipe plumbing was rebuilt using compression fittings with Loctite 542 thread sealant which solved one source of air ingress.

Both the negative and the positive pressures were tested (Figure 5.16 and Figure 5.17) to test if the system was air-tight. The equation of the straight line was used to assess the relative improvement made in the seal of the system c.f. Figure 5.15. The improvement is

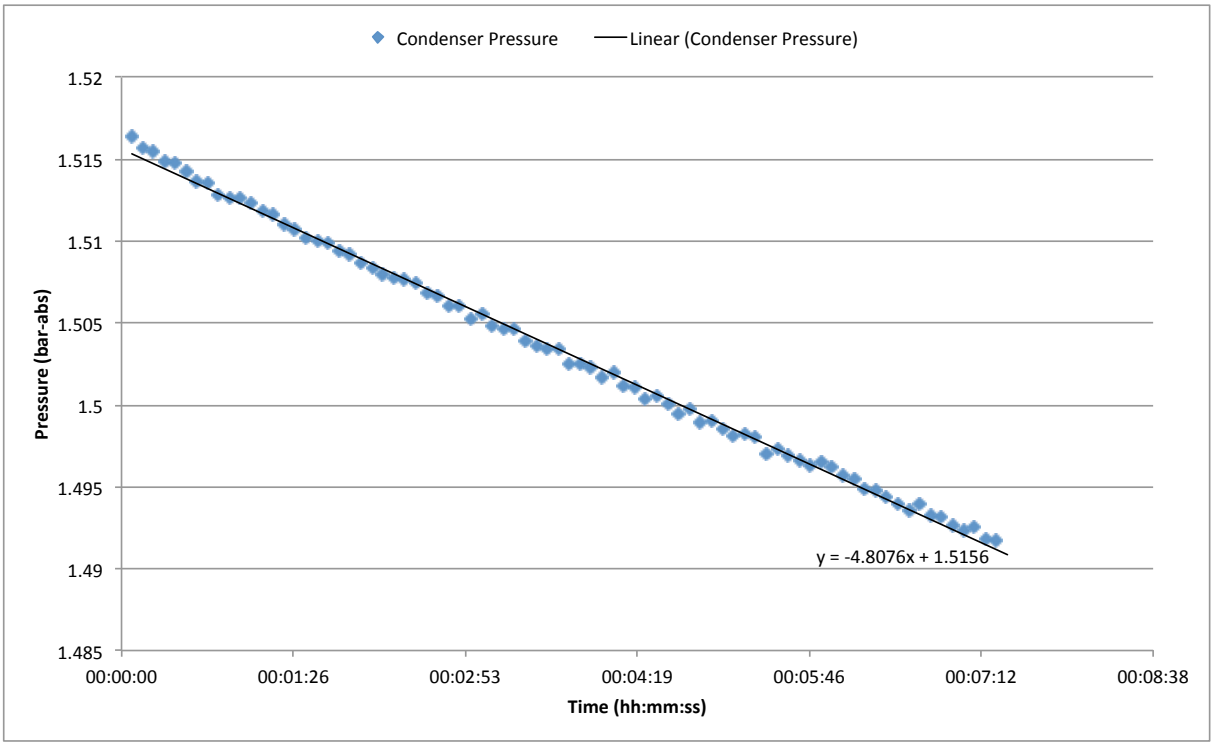

Figure 5.16: Condenser positive pressure test showing a large leak rate

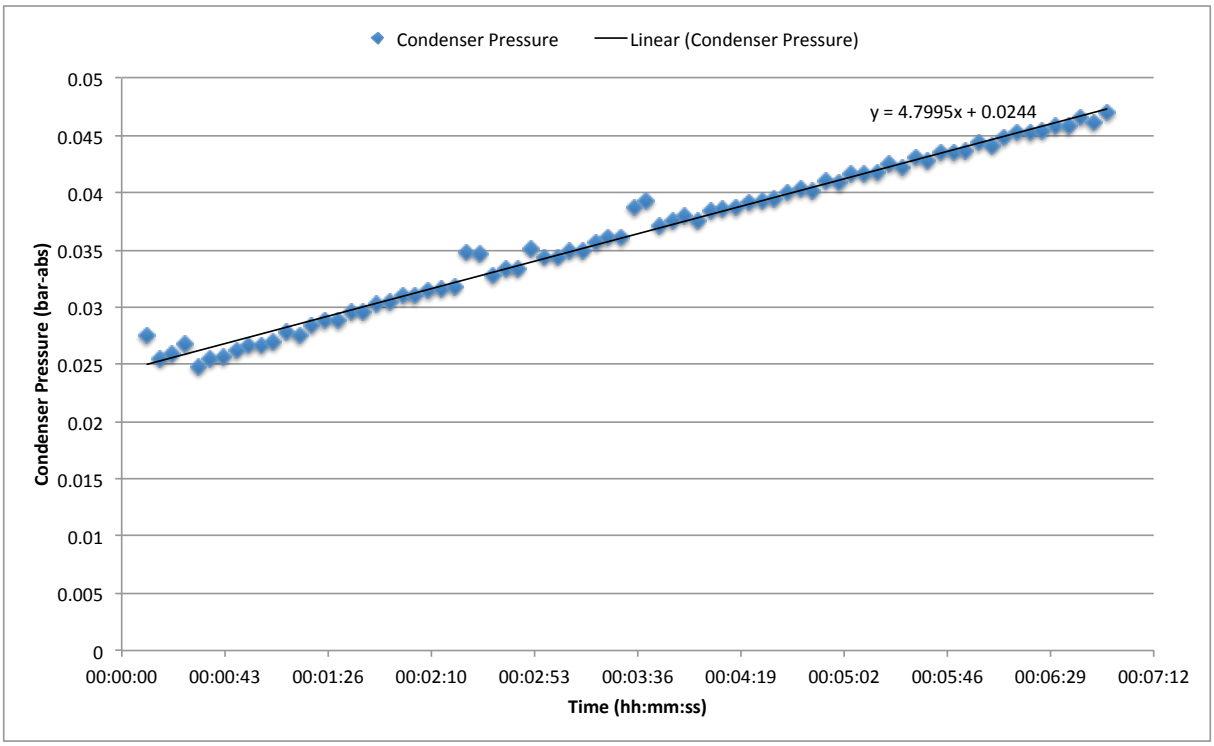

Figure 5.17: Condenser negative pressure test showing a large leak rate

obvious, however, still unsatisfactory. Figure 5.16 and Figure 5.17 show the same slope, indicating the leak rate is the same regardless of the direction of the pressure differential.

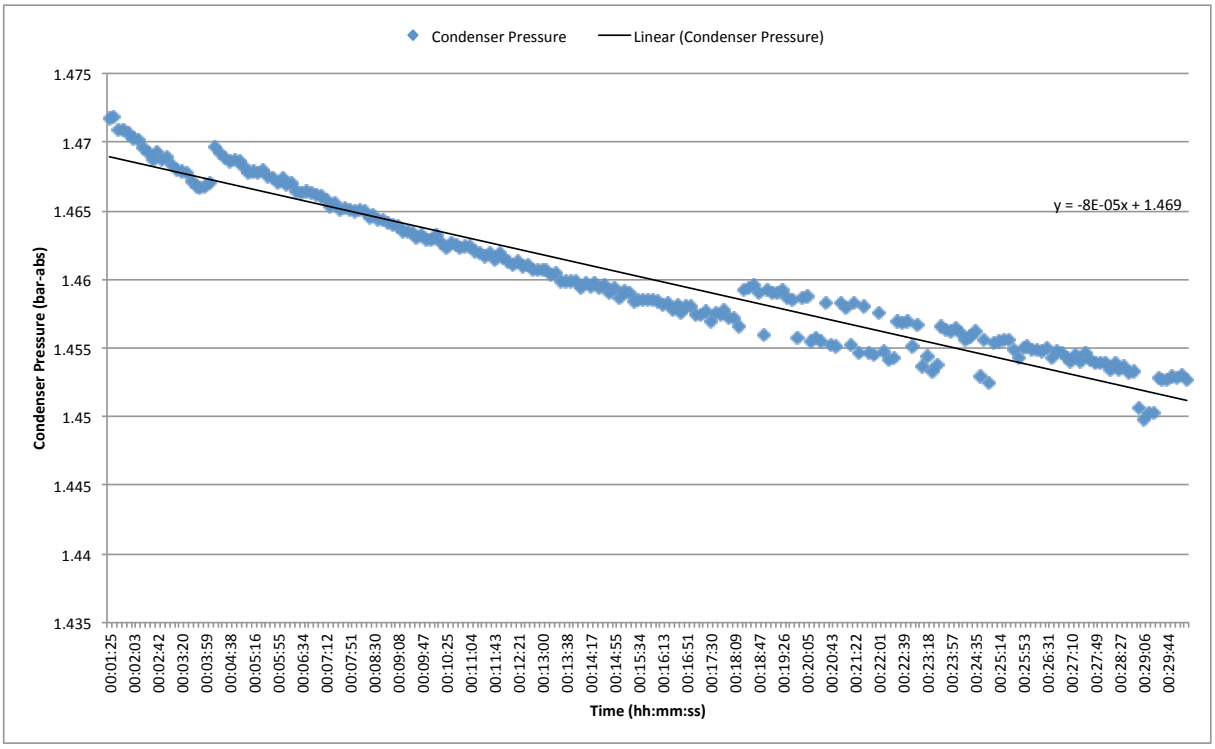

Figure 5.18: Condenser positive pressure test showing a reduced leak rate

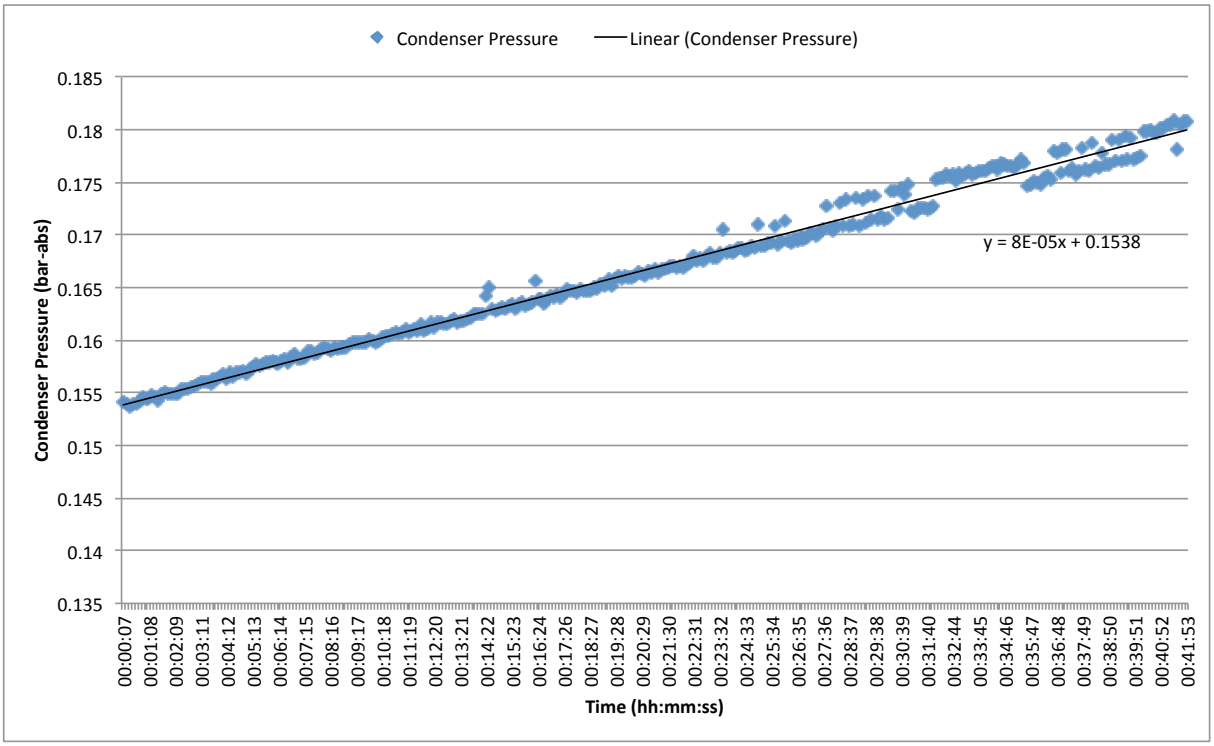

Figure 5.19: Condenser negative pressure test showing a reduced leak rate

Figure 5.18 and Figure 5.19 shows the final result achieved when the system was finally sealed. The condenser could satisfactorily hold a vacuum for extended periods of time and allow the steam experiments to progress over a period of several hours without a

Figure 5.20: Sealed thermocouple feed-through port in to the condenser

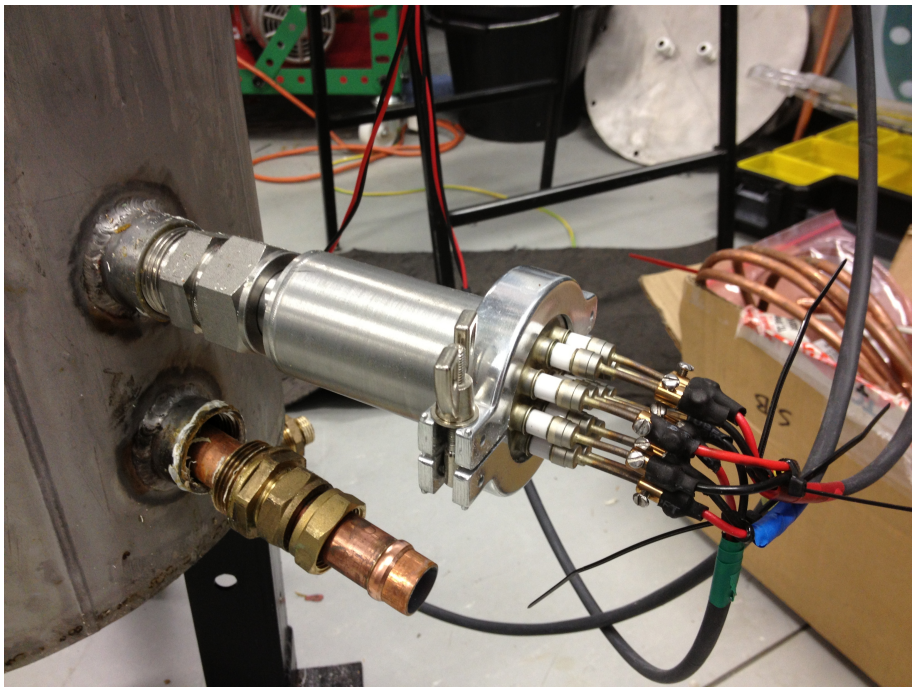

Figure 5.21: Thermoelectric heat pump power supply conductors feed-though

significant change in the steam conditions being experienced.

The remaining leak was finally traced to the cabling into the system for the thermocouples and thermoelectric power supply which had a small cavity in between the conductors and the insulating sheath. To solve this, two separate feed-through ports were designed and are shown in Figure 5.20 and Figure 5.21.

5.3.5 Vertical THP Mounting and Droplet Formation

The 'cold' side of the THP should be in good thermal contact with the steam environment within the condenser. It was known from previous work that a THP is capable of pumping relative large amounts of heat (100's of Watts), and therefore some form of heat-sinking would be required.

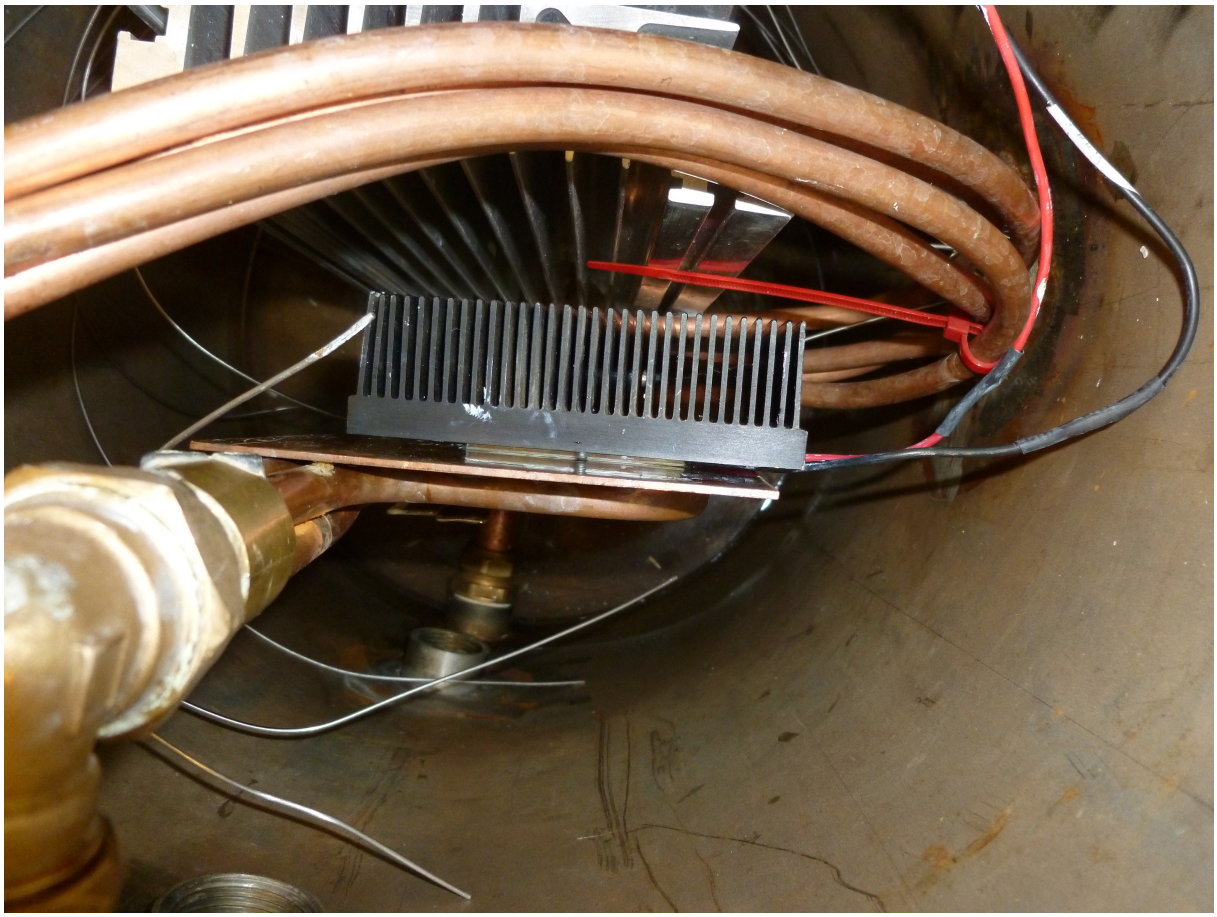

Figure 5.22: Vertical mounted THP with heatsink and pipework

The 'hot side' heat exchanger used was formed by a loop of copper pipes soldered to the back of a copper plate, shown in Figure 5.22. The THP is attached to this plate

and a large heat sink is attached to the opposing face of the THP (the 'cold' side) and is secured to the copper plate with screws. This configuration was chosen because the loops of pipework bonded to the copper allowed for easy connection to 15mm copper pipe through which the condensate flow can be directed. During subsequent experiments it was discovered that the level of the condensate in the condenser covered the exit pipe of the THP loop (nearest the base of the condenser), and that since the pipework was not insulated then the temperature of the water from the THP was being altered by this immersion.

As noted in §5.3.3 the unreliable results from this version led to the development of a horizontally mounted version at the top of the condenser. This is described in §5.4.3.

5.3.6 Clamping Force

In the first iteration, the heat-sink was attached to the THP using a high thermal conductivity thermal paste as detailed in Chapter 3 to ensure good thermal conductivity between the parts. The necessary clamping force was achieved using screws between the heat-sink and the heat exchanger, tightened to the required torque to achieve the force required. However, the screws acted as a thermal short circuit between the source and the sink leading to inaccurate determination of the heat pump performance.

The foregoing discussion in this section condenser summarises some 2 years of experimental work in developing the experiment and gradually refining its operation. In reviewing progress it was determined that the control system and boiler were working satisfactorily but that the condenser, THP and feedwater retun circuit required a complete redesign if accurate results were ever to be achieved. This redesign is summarised in §5.4

5.4 Second Iteration

The most significant system alteration for the revised experiment was placing the condenser above the boiler in order to achieve a sufficient head on the condensate gear pump. The height of the condenser placement was limited by the ceiling tiles in the laboratory.

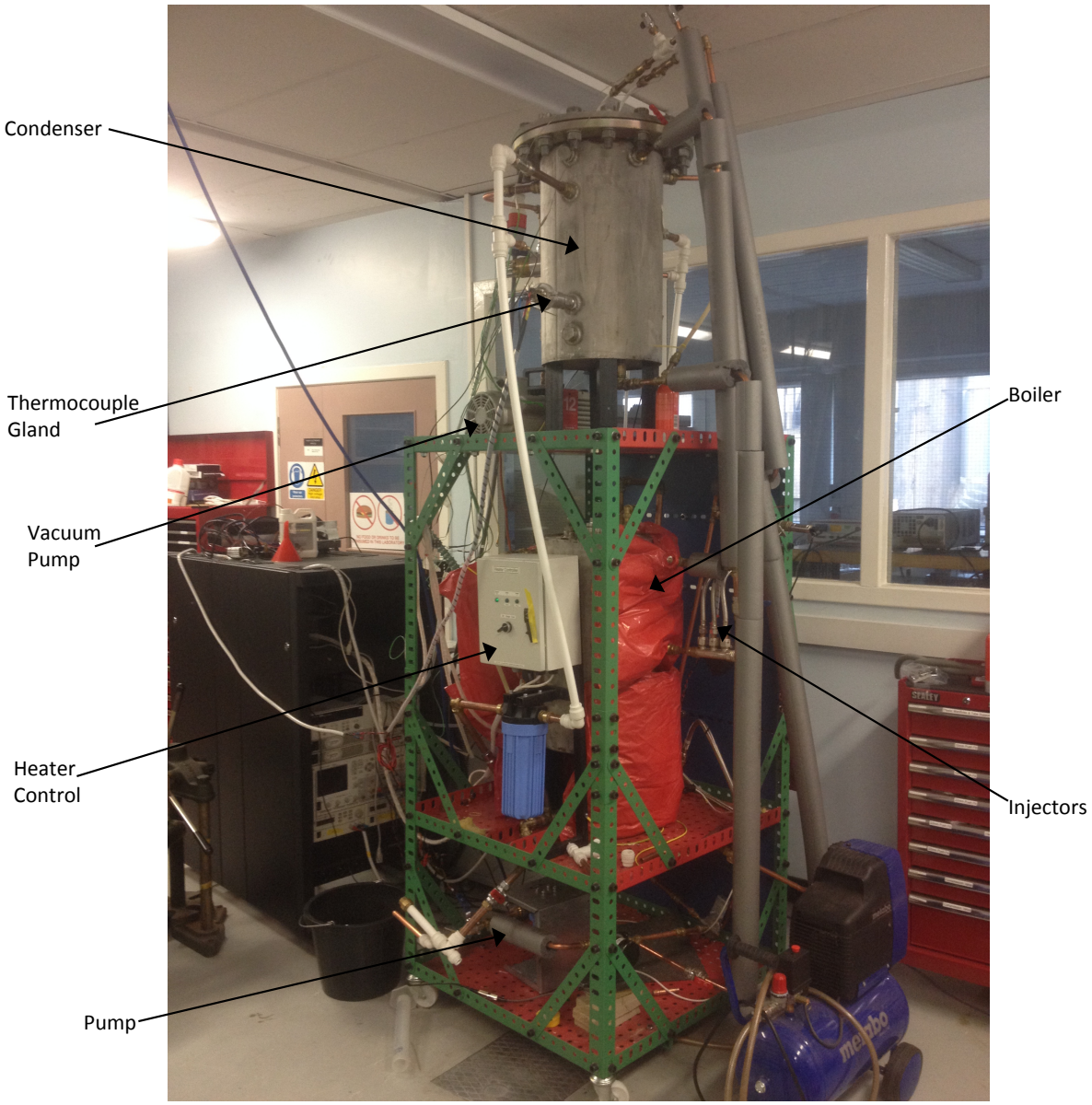

Figure 5.23: Rankine cycle test apparatus in its final form

Giant 'Meccano' parts were purchased to fabricate a strong, stable framework. Figure 5.23 shows the configuration used.

The top of the picture in Figure 5.23 shows the condenser vessel, the centre section shows the boiler and the pump is housed in the bottom section. The electrical power and control instrumentation is held in the black 19" equipment rack on the left side. Both the boiler and condenser are heavily insulated during normal operation but this has been removed for the purpose of obtaining the picture. The chiller unit is not visible in the picture but is located behind the black rack.

5.4.1 Cavitation elimination by vertical mounting

With the vertical arrangement the total head of water on the pump is 1.5 metres, plus whatever the depth of water in the condenser is and also taking into account the condenser absolute pressure. This completely eliminated pump cavitation issues.

5.4.2 Cooling capacity

5.4.2.1 Version 2

Since the cooling capacity of the first set of condensing coils was insufficient, a second iteration was designed.

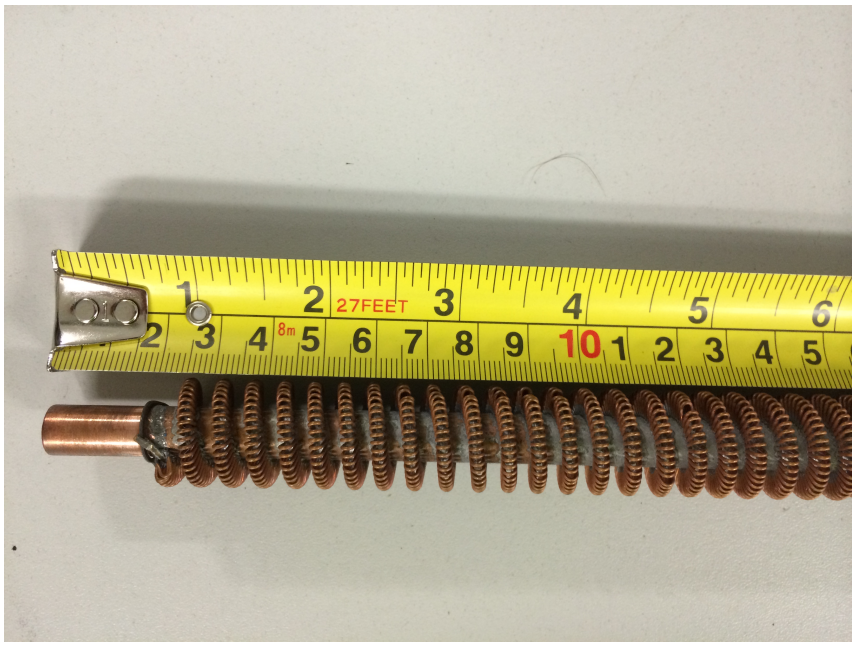

Figure 5.24: Condensing oils supplied by Thermex used in version 2 and 3 of the design

This used commercial heat exchanger shown in Figure 5.24.

These were formed of 20cm sections of copper pipe with a helically wound copper wire formed into a second coil around the central pipe. The two parts are solder together to provide and excellent thermal contact between them. The calculation for the total surface area is split into two sections: the coil surface area and the pipe surface area. The coil surface area (A_{coil}) is $0.00539m^2$, and the pipe surface area (A_{pipe}) is $0.0324m^2$ giving a total of $0.03779m^2$ shown in equation 5.7. The configuration used, shown in Figure 5.25

Figure 5.25: Condensing coils using Thermex coils for version 2

used 16 pipes (N), $0.60464m^2$. The chamber surface areas are: $0.113m^2$ and $0.125m^2$ leading to a total of $0.8426m^2$.

$$A_{total} = N(A_{coil} + A_{pipe}) \tag{5.7}$$

The original intention was to use push fit connections at either end of the central pipe section to connect to the manifolds, noting that this part of the plumbing is at a positive pressure relative to the condenser. However, no suitable parts could sources and compression fittings had to be used. The assembly of the device proved difficult because the closeness of the adjacent pipework prevented the compression fittings from being properly tightened around each of the Thermex pipes - there was insufficient space between each of the pipes to allow spanner to be used. After several attempts at sealing the unit had failed it was abandoned in favour of a revised manifold design.

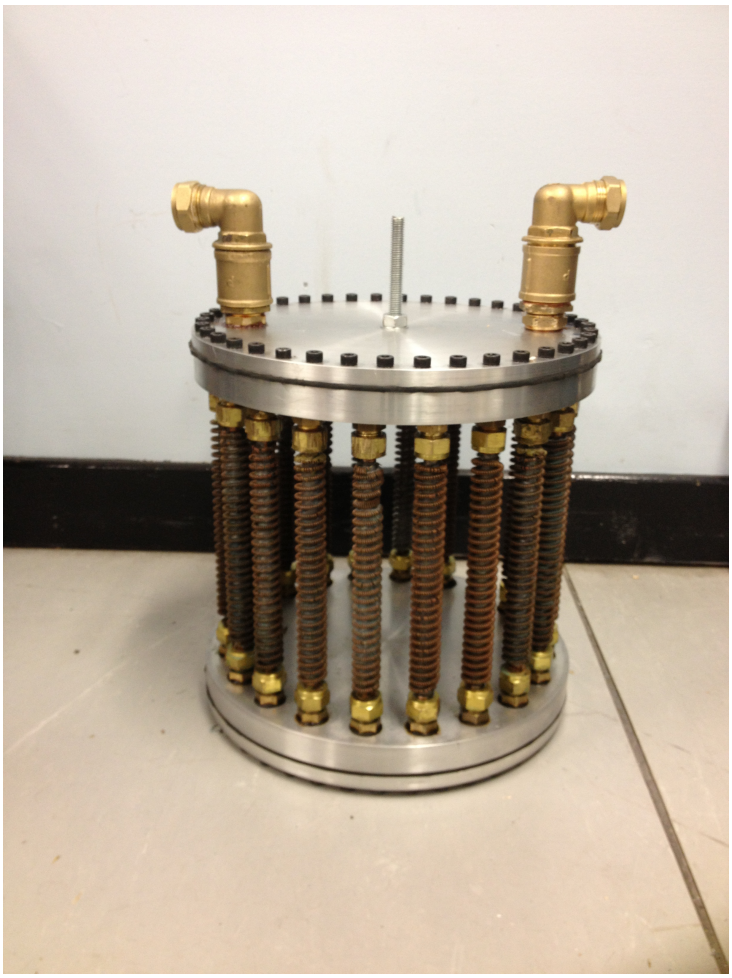

Figure 5.26: Condensing coils using Thermex coils for version 3

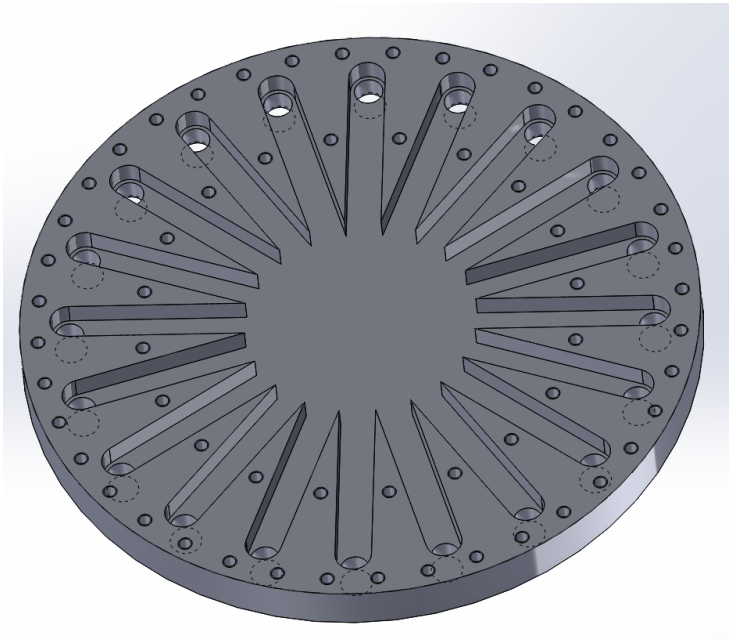

Figure 5.27: Bottom chamber CAD design

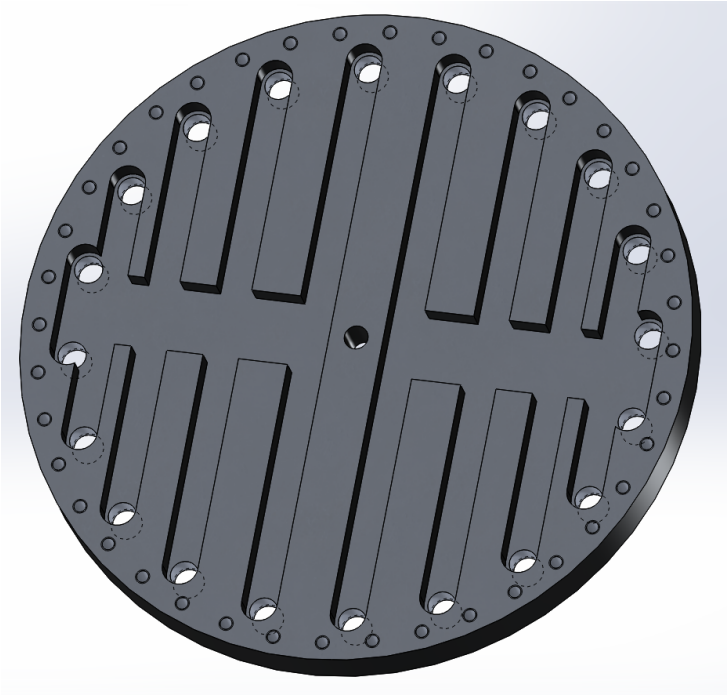

Figure 5.28: Top chamber CAD design

5.4.2.2 Version 3

A third iteration of the condensing coils was designed and assembled and is shown in Figure 5.26. The same Thermex coiled pipes used in the second iteration were reused. The total surface area of this system was calculated from the single length of coil having a surface area of $0.03779m^2$, and then for 20 single loops the total is $0.7558m^2$. Further, the surface area of the bottom and top chambers in Figure 5.27 and Figure 5.28 ($0.3236m^2$ and $0.3336m^2$ respectively) gives a total cooling surface area of $1.413m^2$. Before assembly, each element has a hydrophobic coating applied to minimise the post-condensation cooling that occurs before the condensate droplets reach the pool in the base of the condenser. As discussed in §5.3.3, in order to overcome the difficulty of connections in the base of the condenser both the inlet and outlet of the cooling circuit are located at the top of the unit. Figure 5.26 shows the split manifold design keeping the inlet and outlet separate at the top and Figure 5.27 shows how the flow from the inlet is directed to the return part of the circuit in the base. Figure 5.28 also shows the very large number of large bolts used to hold the manifold parts together and the thickness of the material used. The large central bolt was used to prevent 'hogging' of the plates, potentially leading to the

gasket leaking and primary coolant (which contains glycol) escaping into the feedwater circuit. The pressure in the primary coolant loop is substantially above 1 bar and the condenser is close to a vacuum, hence the internal force on the manifolds is over 30kN. This cooling unit worked as intended and without any issues for the remainder of the research programme.

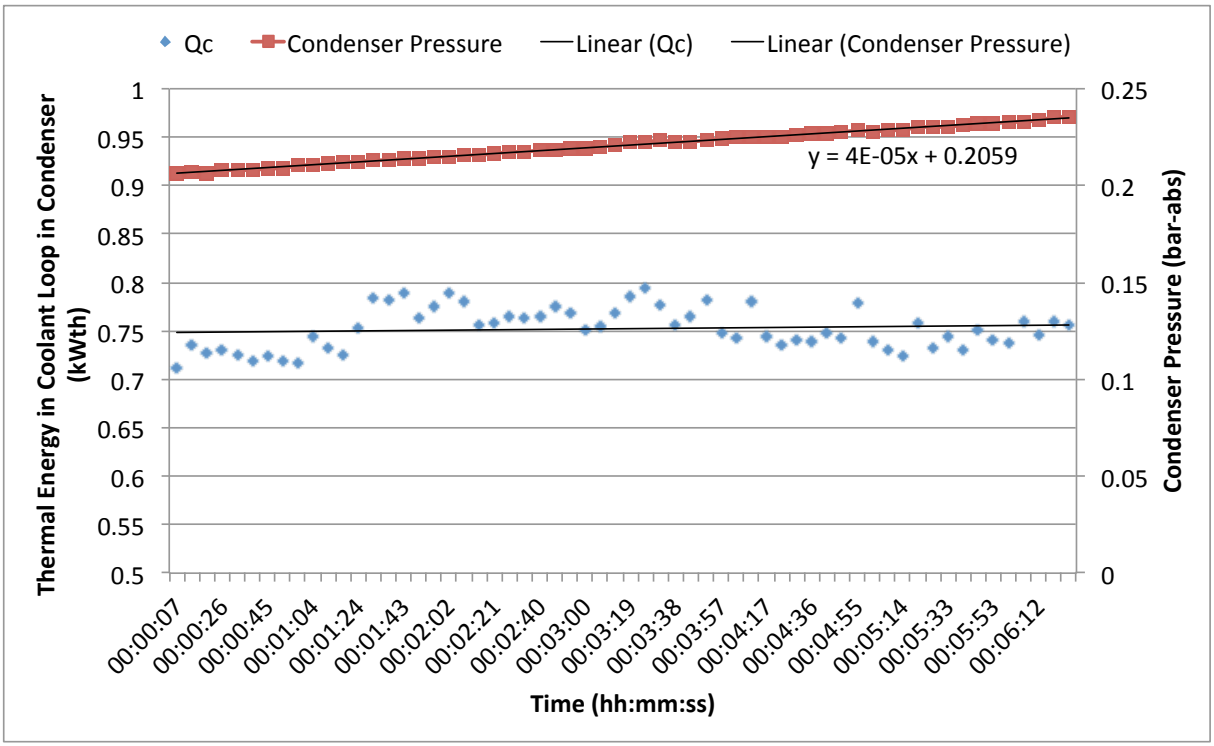

Figure 5.29: Thermal energy in coolant loop and condenser pressure with v3 Condensing Coils

The resultant thermal energy in the condenser is shown in Figure 5.29. The larger number of coils in the condenser cooling loop allows for more steam to be condensed. The pressure of the condenser then is steady in comparison to Figure 5.14 as there is no longer a build up of steam causing the internal pressure to rise.

5.4.3 Horizontal THP mounting and Silicone coating

The aluminium labyrinth heat exchanger used to transfer the thermal energy from the THP 'hot' side to the condensate returning to the boiler is shown in Figure 5.30.

A thermocouple was placed in the centre of the heat exchanger to permit the THP's ceramic surface temperature to be measured. The inlet and outlet temperatures of the

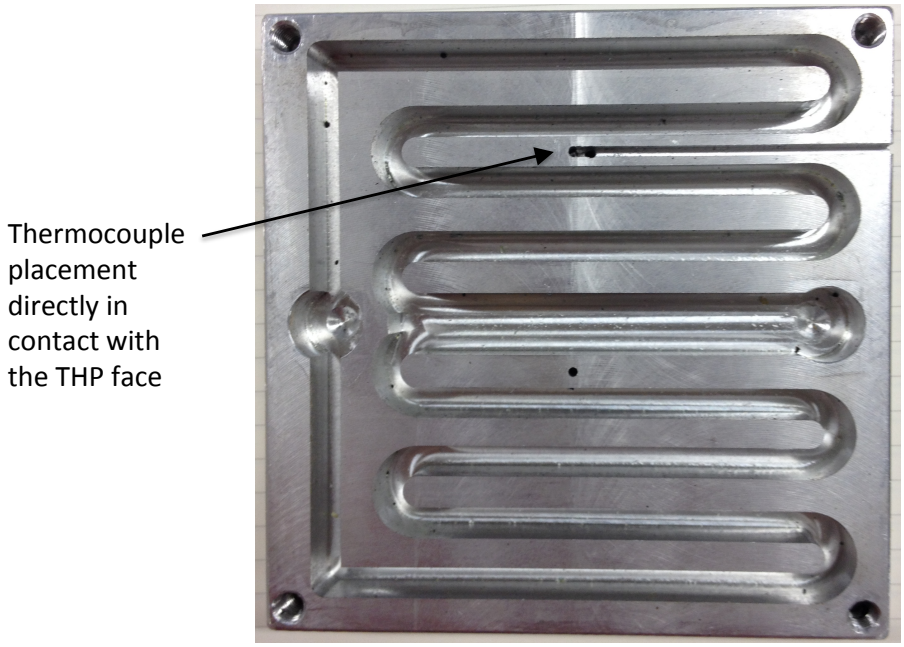

Figure 5.30: Labyrinth heat exchanger design

condensate were monitored by thermocouples placed in the water channel, shown in Figure 5.31. Figure 5.30 and Figure 5.32 shows the placement of an additional thermocouple in the side of the heat-sink to enable reading of the 'cold' side of the THP.

Horizontal mounting of the THP allowed steam to rise up to the top, preferring to condense on the fins of the heatsink attached to the THP. In Figure 5.32 the THP assembly is inverted; normally the black heatsink is facing downwards with the fins vertical. Droplets form on the fins and fall into the condenser where they are collected in the base. A hydrophobic coating (silicone) was liberally sprayed on to the fins of the heatsink to ensure droplets which formed there did not accumulate.

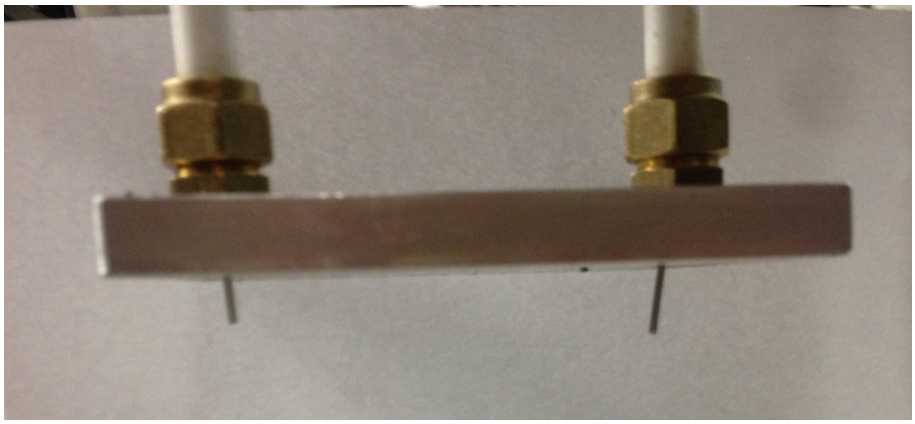

Figure 5.31: Mineral-insulated thermocouples placed in the pipework attached to the lid of the heat exchanger on the THP

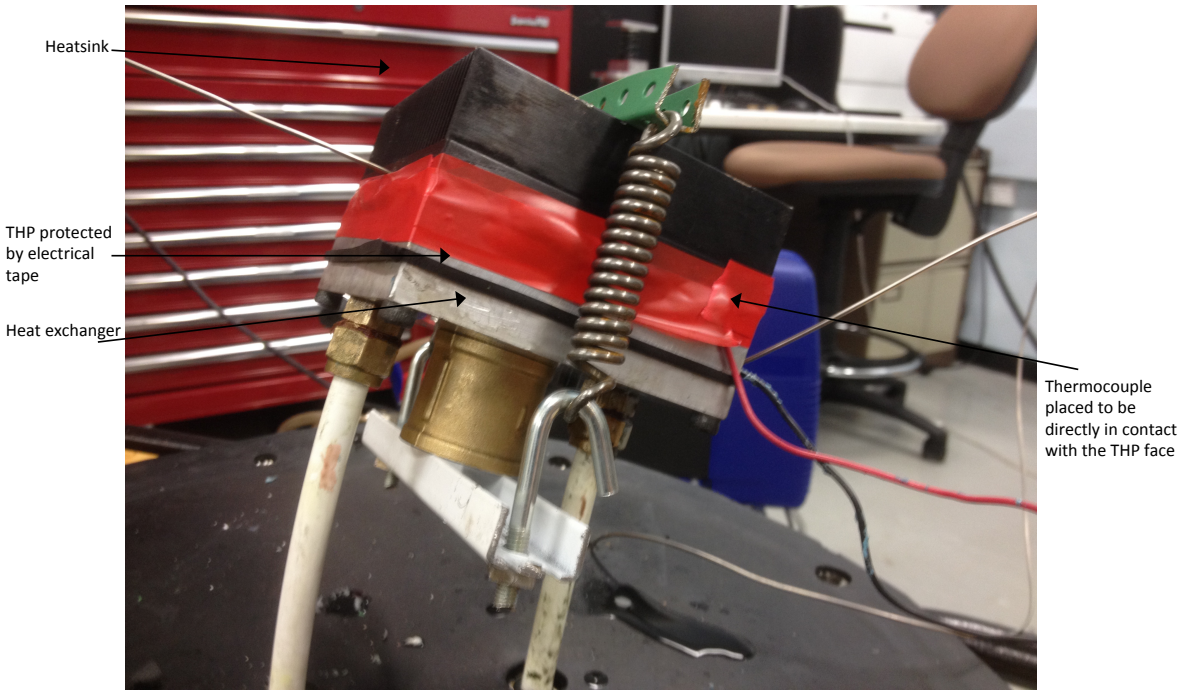

Figure 5.32: The result of the springs applied to the THP, heat-sink and heat exchanger to be mounted inside the condenser

Figure 5.33 shows the insulation placed around the heat exchanger and pipework. This ensured that the aluminium block was protected as far as possible from direct steam contact that could affect the water return temperature. Ideally only the 'cold' side of the THP would be present within the condenser, but the mechanical complexity of the system required to achieve this was considered too great to be in scope for this PhD project. Extraneous energy leakage to the THP hot side has been minimised as far as is practical and, as will be seen in Chapter 6, the experimental results support this belief.

5.4.4 Clamping Force

Considerable attention is paid to minimise stray energy loss paths and the un-insulated heat pump assembly is shown before and after in the photographs in Figure 5.34 and Figure 5.32 respectively. The spring selected has properties summarised in Table 5.1. With the use of a pair of springs the resultant force is 1971.8N compressing a square THP of dimensions 50mm x 50mm ($0.003025m^2$) with a pressure of 652kPa.

Springs are used in the final version (compared with bolts in the first iteration) for two reasons. Firstly, the bolts presented a thermal short-circuit and when the springs are

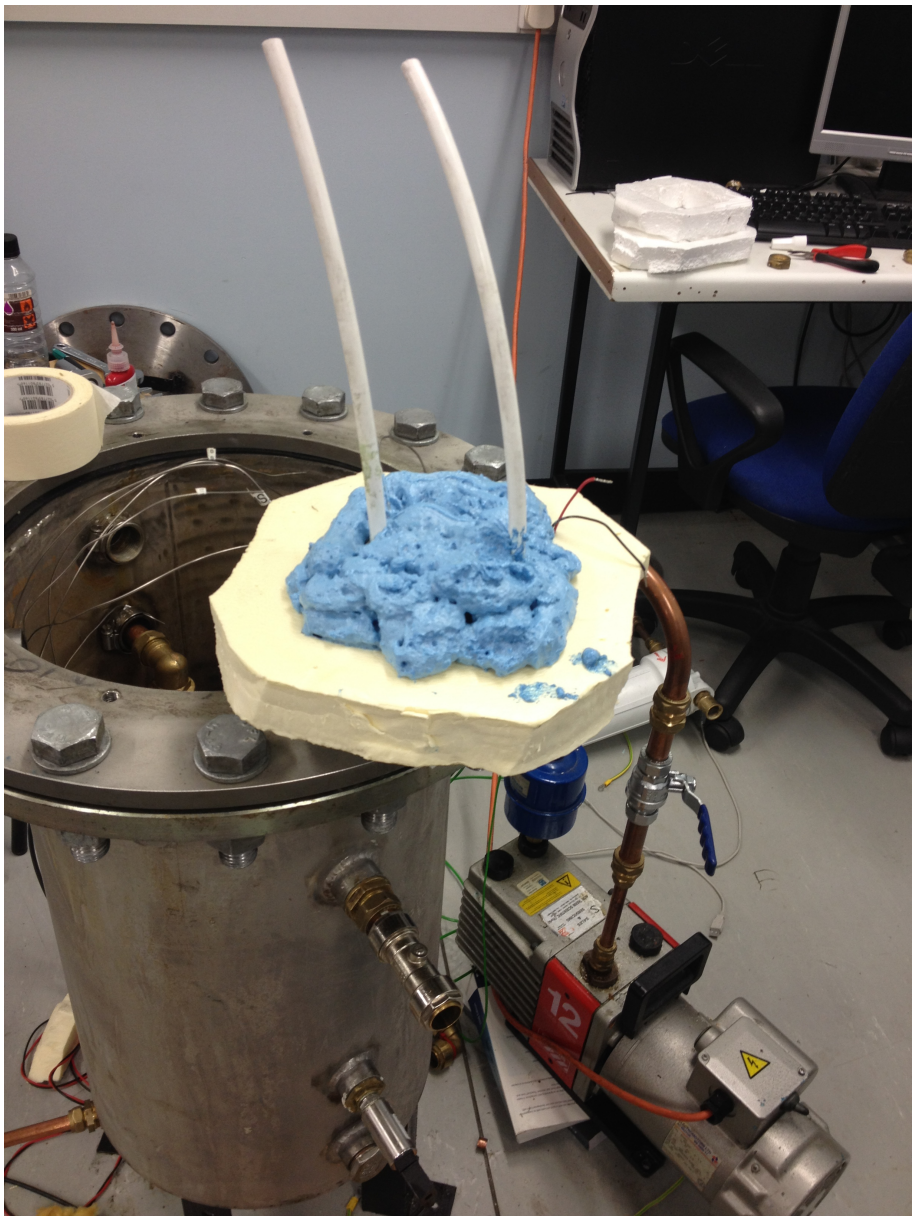

Figure 5.33: Insulation moulded around the heatsink, heat exchanger and THP. The two white tubes are the water flow and return pipes for the THP loop

stretched as shown in Figure 5.34, the thermal path length from the hot to cold sides is long, resulting in very low thermal flux across the spring. The second reason for using the spring concerns mechanical compliance. Aluminium has a fairly high (for a metal) coefficient of linear thermal expansion of $22.2\mu m/mK$. A quick calculation predicted that the expansion of the 'hot' side would be almost matched by a contraction of the cold' side, thus the two would more or less cancel out. However, the average temperature of the assembly is higher when in use in the condenser and hence to avoid the danger of mechanically crushing the THP so form of mechanical compliance is needed. In operation,

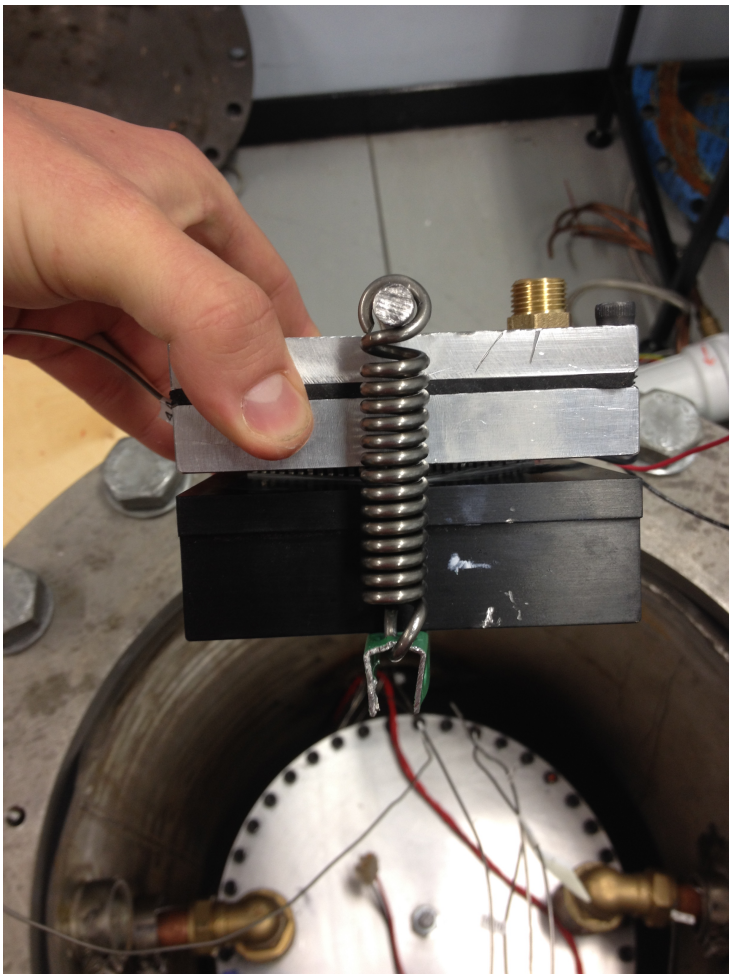

Figure 5.34: Springs exerting a clamping force on the THP sandwiched between the heat-sink and the heat exchanger

the springs' compressive force rises slightly, leading to enhanced thermal conductivity in the THP assembly and therefore reducing the overall ΔT and assisting the COP. The effect is small, however.

Preload Force	400N
Spring Rate	33N/mm
Extension	21mm
Resultant Force	985.9N

Table 5.1: THP Clamping Force and Spring Properties

5.4.5 Characterisation of the Heat Exchanger Thermal Resistance

An aluminium heat exchanger was mounted to the opposing side of the THP to allow for the return water feed to the boiler to be brought in to contact with the THP, shown in Figure 5.32. The aluminium heat exchanger was tested using the test apparatus described in Chapter 3 and characterised separately to the remainder of the Rankine cycle test apparatus. The setup was as follows: the heat exchanger was attached to a chiller unit to provide a constant temperature of water flowing through the heat exchanger. The copper heater block was then mounted and used to vary the temperature to the face of the heat exchanger. Thermocouples were placed at the faces of the heat exchanger, the water inlet and outlet.

$$\Theta_{heatsink} = \frac{T_{hot} - T_{THPhot}}{\Sigma P} \tag{5.8}$$

The system can be simplified to a series of thermal resistances, shown in Figure 5.6 and the thermal resistance of the heat exchanger is defined in equation 5.8.

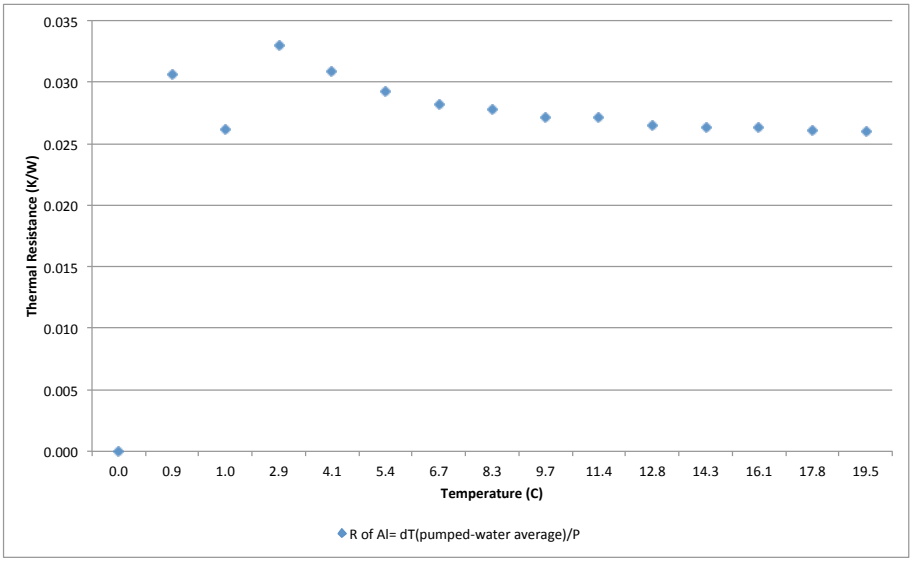

Figure 5.35: Thermal resistance of Aluminium heat exchanger at increasing temperature

Electrical power was varied to the copper block and the temperature increase in the water flowing in the heat exchanger was recorded. Figure 5.35 plots the thermal resistance at increasing heater powers. At increasing temperature differences the thermal resistance

of the Aluminium remains constant.

$$R_{Al} = \frac{x}{A\kappa} \tag{5.9}$$

Equation 5.9, where R_{Al} is the thermal resistance of the Aluminium heatsink (W/K), x is the depth of the slot cut for the water path in the heatsink (m) and κ is the thermal conductivity of Aluminium (W/mK).A further experiment was conducted to measure the volume of the heat exchanger by accurately measuring the amount of water that can be held in the enclosed unit. The outlet port was sealed using a blanking plug and 110ml of water was poured into the heat exchanger giving a volume of $110cm^3$. Since the height of the heat exchanger is measures as 22.5mm then the resultant surface area is $48.9cm^2$. The thermal resistance of the heat exchanger can be calculated from the heat equation 5.9. Given that the thermal conductivity of Aluminium is 205W/mK then the resulting thermal resistance is 0.025K/W.

The matches the thermal resistance measured in the test apparatus.

5.5 Discussion and Conclusions

This chapter has reviewed the trials and tribulations experienced in the design and construction of a substantially scaled-down Rankine cycle experiment. By necessity much of the experimentation undertaken that did not contribute to the final result has been omitted from this thesis. However, despite the difficulties encountered, the final result is a sophisticated piece of apparatus that permits the accurate experimental analysis of the THP performance. A short design guide is given in Appendix B.

Following this review of the experiment system in Chapter 5, the experimental results obtained using the apparatus are presented in Chapter 6.

Chapter 6

Experimental Results Using Rankine Cycle Test Apparatus

This chapter details the experimental results obtained from operation of the Rankine cycle test apparatus described in Chapter 5. Operation with and without the thermoelectric heat pump is discussed and conclusions drawn from the measured performance. This is compared to the theoretical performance required at a system level to demonstrate a viable application of the THP.

6.1 Energy Balance

The energy transfer in a power plant can be accounted for in all aspects of the system. The chemical energy released by the combustion of fuel is then transferred to the feedwater to raise its temperature and generate steam. A portion of the thermal energy is rejected from the stack. The steam generated is expanded through a turbine to turn a shaft and generate mechanical work, which is converted to electrical power by an alternator. Residual energy in the working fluid is rejected to the environment as the feedwater re-condenses. During each of these conversion processes energy is lost from the overall cycle. Although energy can never be destroyed, it is converted into other forms that are not immediately useful and usually of higher entropy. For example, the energy released in burning coal manifests as light and not just heat. A portion of the energy transferred the

Location	Adjustment
Immersion Heater	+0.692°C
Boiler Steam Exit	+0.369°C
Free Air in Room	−1.341°C
THP Loop Top	−0.219°C
THP Loop Bottom	−0.128°C
Condenser Wall	−0.406°C
Steam Inlet	−0.044°C
THP Hot Side	−0.121°C
Chilling Loop Bottom	−0.349°C
Condensate Exit	−0.179°C
Chiller Loop Top	−0.041°C
Condenser Free Steam	−0.204°C
THP Cold Side	+0.245°C

Table 6.1: List of adjustments

turbines will be used to overcome friction losses and be converted into kinetic energy in the form of vibrations. I^2R losses in the alternator windings is rejected as waste heat.

The energy consumption in the Rankine cycle test apparatus is quantified by how much the process water changes in energy and enthalpy at each point in the system. A MATLAB model has been constructed of the plant which is able to determine the process values for pressure, temperature, entropy, enthalpy and mass flow based on the operating conditions. In the following discussion this model is correlated to the system based on its two operating states: no heat pumping; and with heat pumping.

6.1.1 Operation Without THP

The system is brought to steady state conditions as detailed in chapter 5 and the numerous thermocouple temperatures were calibrated using an accurate mercury/glass thermometer. The component temperatures shown in Figure 6.1 were measured over a twelve hour period to allow the system to settle to thermal equilibrium. The majority of the temperatures settled to between 19°C and 20°C and this matched the ambient temperature of 19.5°C measured using the thermometer. The temperatures were normalised from the average temperature of 19.5°C ambient by an offset factor.

Table 6.1 shows the values used to offset each of the temperature readings and Figure 6.2 shows the resultant normalized temperature with their offsets incorporated.

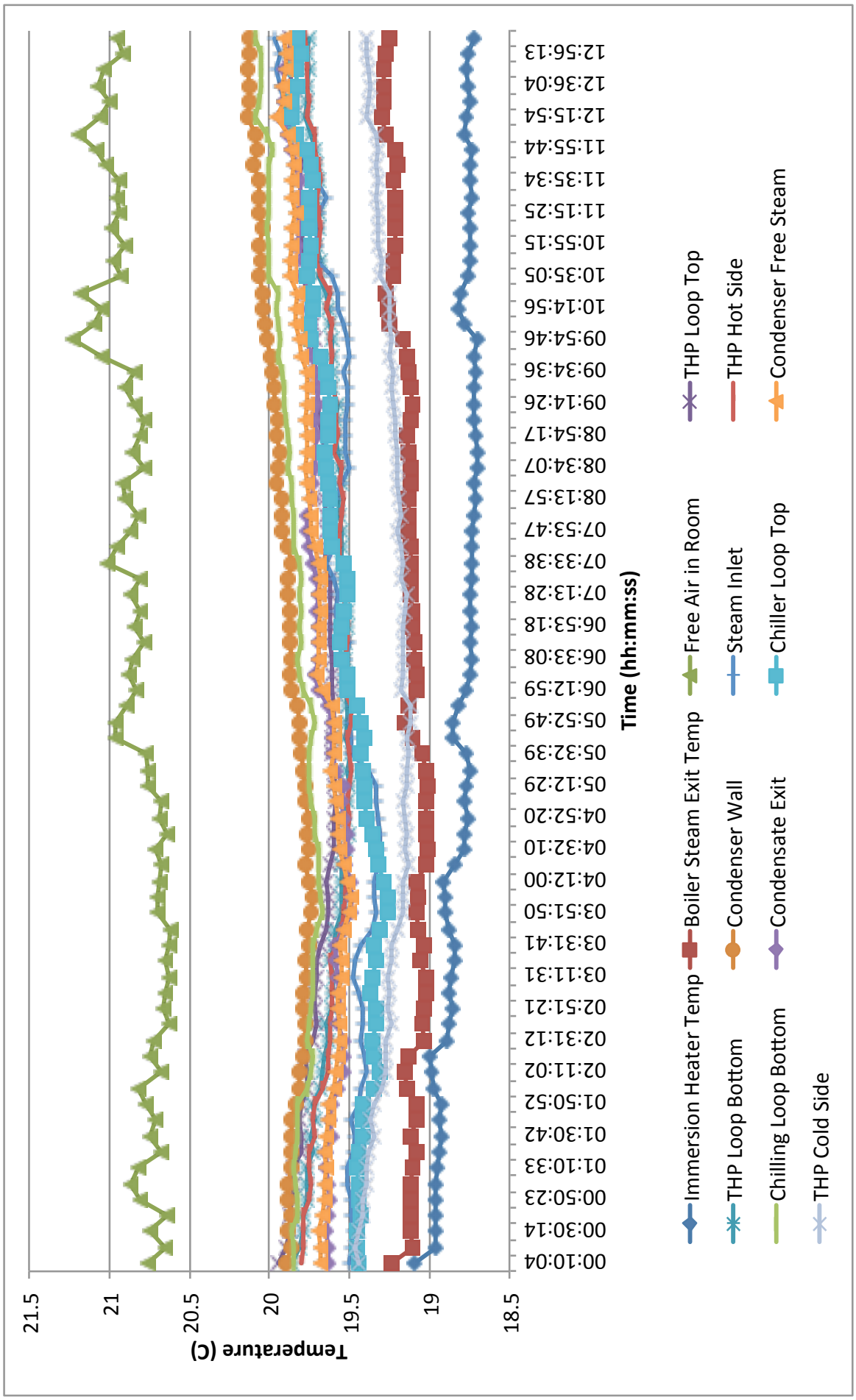

Figure 6.1: Temperature measurement over 12 hours

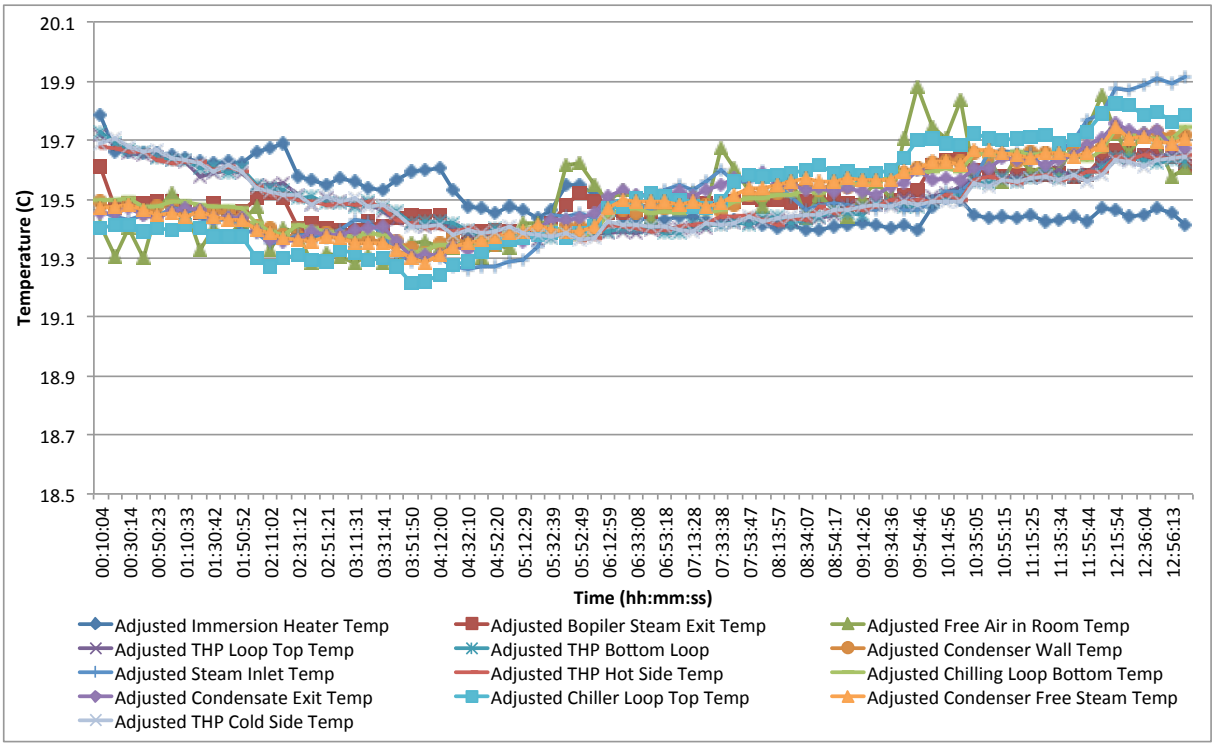

Figure 6.2: Adjusted temperature measured over 12 hours

The system was brought to steady state and pressure. The boiler conditions were 96°C, 900mbar-abs. The condenser was held at 60mbar-abs giving a water condensation temperature of 40°C .

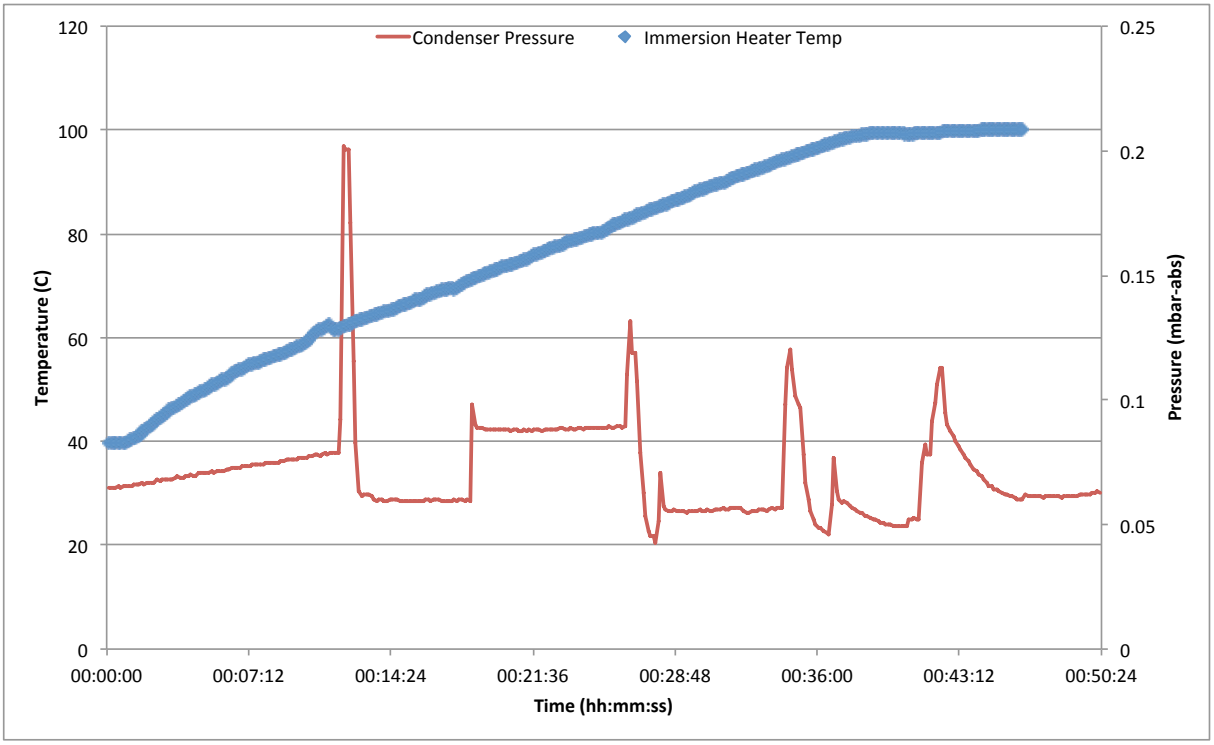

Figure 6.3: Time to raise boiler temperature

Location	Pressure	Saturation Temperature	Actual Steam Inlet Temperature
Boiler	900mbar-abs	96.7°C	98.6°C
Condenser	60mbar-abs	45.8°C	34.6°C

Table 6.2: Temperature and Pressure Conditions in the Boiler and Condenser

Figure 6.3 shows the warm-up phase which lasted approximately 50 minutes. The spikes in the condenser pressure correspond to venting non-condensibles from the boiler to the condenser for removal by the vacuum pump as described in Chapter 5 to 60mbar-abs as shown in the figure. The values presented in Table 6.2 are dependent on the mass of water in the boiler, temperature measured and pressure.

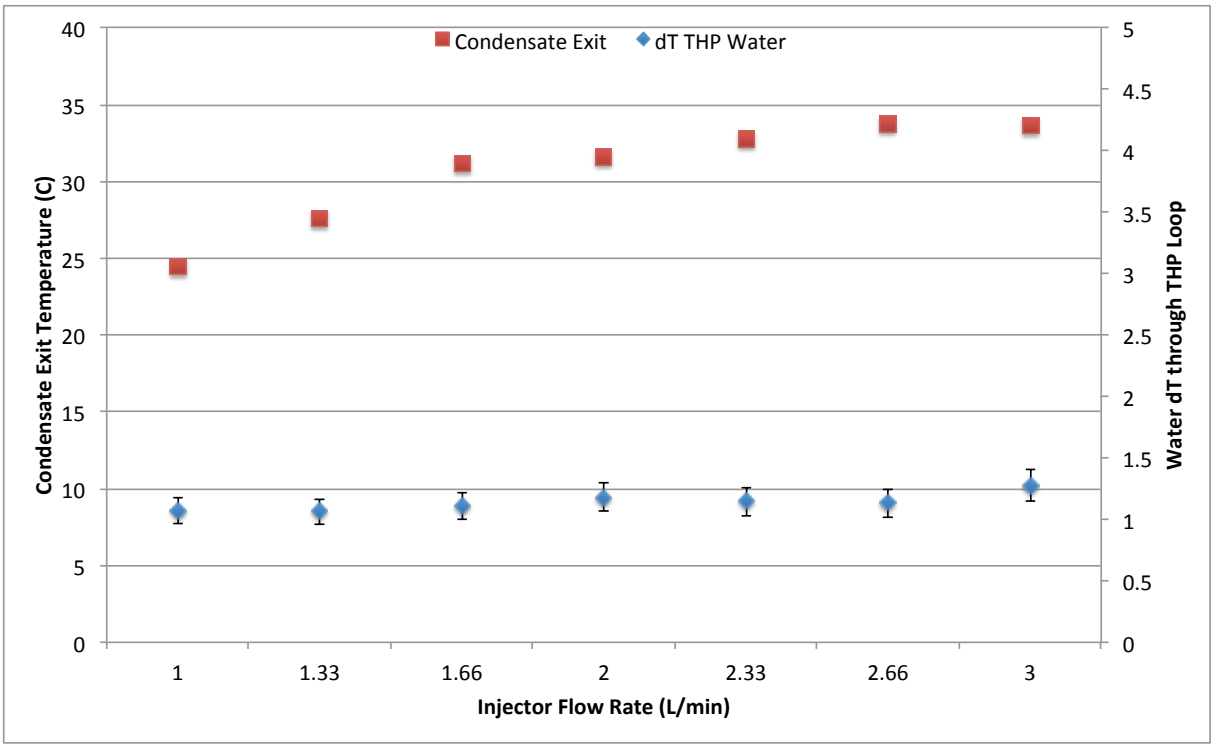

Figure 6.4: Increasing flow rate with the THP disconnected

At this point, the heat pump fluid circuit was switched in but the THP itself remained off. The aim in doing this was to characterise the temperature rise in the THP loop for various flow rates as a consequence of thermal energy from the condenser leaking into the loop. The tests were repeated several times and then averaged. The resultant data is presented in Figure 6.4.

At low injection rate values the water temperature at the condensate exit (which feeds the THP loop directly) remains constant around 23°C therefore any rise in THP loop can

be attributed to thermal energy leaking inside the condenser to the pipework supporting the THP. The chart of water temperature difference in the THP loop (Water outlet-Water inlet) shows the presence of an offset of 1°C ±5% and shows a sight decrease as the injector flow rate increases.

The condensate exit temperature at the base of the condenser is measured as a reference for the increase in water temperature in the THP loop is fed directly using water at this temperature.

6.1.2 Operation With Thermoelectric Heat Pump

For the duration of these tests the boiler was brought to temperature and pressure of 63°C at 230mbar-abs to generate steam which was then expanded in to the condenser. The condenser was maintained at 55mbar-abs for a condensing temperature of 34.5°C. As testing progressed the boiler and condenser pressure rose slightly, due to small amounts of air ingress to the apparatus over a long time period in the order of hours to allow for THP measurements to take place.

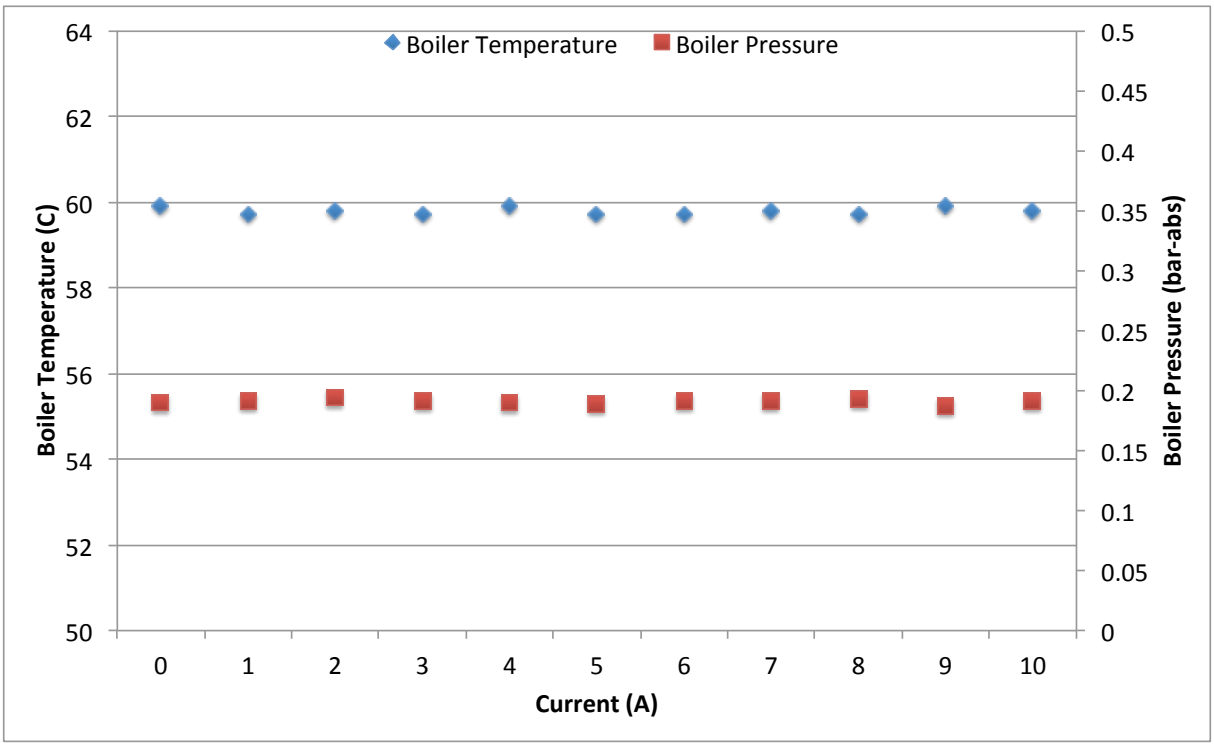

Figure 6.5: Boiler temperature and pressure at increasing THP input current

The pressure and temperature of the boiler is plotted (Figure 6.5) at each of the THP

currents. The temperature and pressure of the boiler remains constant throughout the testing phases.

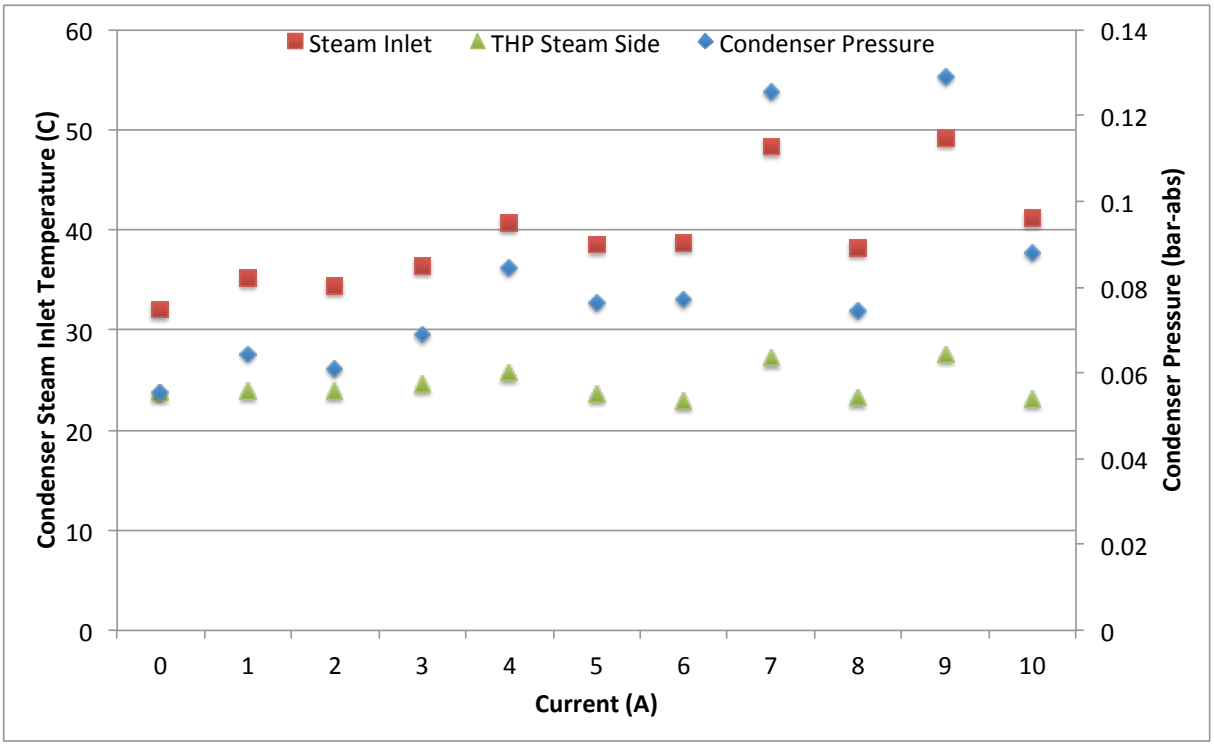

Figure 6.6: Condenser temperature and pressure at increasing THP current

The THP loop was then enabled and the input power to the THP was incremented in steps of 1A up to 10A. Figure 6.6 shows the prevailing conditions for condenser pressure, steam inlet temperature and the steam side (the 'cold' side) temperature of the THP for each current value.

Steam is condensed on to the fins of the heat-sink and the heat pump is driven at increasing input powers. The energy picked up by the heat-sink can be correlated to the condenser temperature and from Figure 6.6 the temperature of the steam side of the THP varies with the change in condenser pressure and steam inlet temperature.

Table 6.3 shows the increase in water temperature between entering and exiting the THP heat exchanger in the top of the condenser. The energy is calculated from the energy equation based on the mass flow of the water, a heat capacity of 4.187kJ/kg and the temperature difference in the heat exchanger.

In order to cancel the effects of the additional energy picked up by the heat exchanger in the system (determined by operating the system without the THP energised) the initial

Current	Water Δ T	$Q_{pumped} = mC_p\Delta$ T(W_{th})	Temperature Offset (°C	$Q_{adjusted} = mC_p\Delta$ T W_{th}
0	0.426°C	28.4	0°C	0
1	0.725°C	48.43	0.299°C	19.97
2	0.8896°C	59.42	0.46°C	30.97
3	1.215°C	81.2	0.78°C	52.7
4	1.655°C	110.6	1.23°C	82.1
5	2.05°C	136.7	1.62°C	108.2
6	2.7°C	179.4	2.26°C	150.9
7	3.35°C	223.5	2.92°C	195.1
8	4.32°C	288.4	3.89°C	259.92
9	5.8°C	385.3	5.341°C	356.78
10	6.22°C	415.5	5.8°C	387.04

Table 6.3: Energy increase in water at increasing THP currents

temperature reading is treated as an offset and subtracted from the corresponding previous values. The thermal energy is then recalculated based on this value and shown in the final column of Table 6.6.

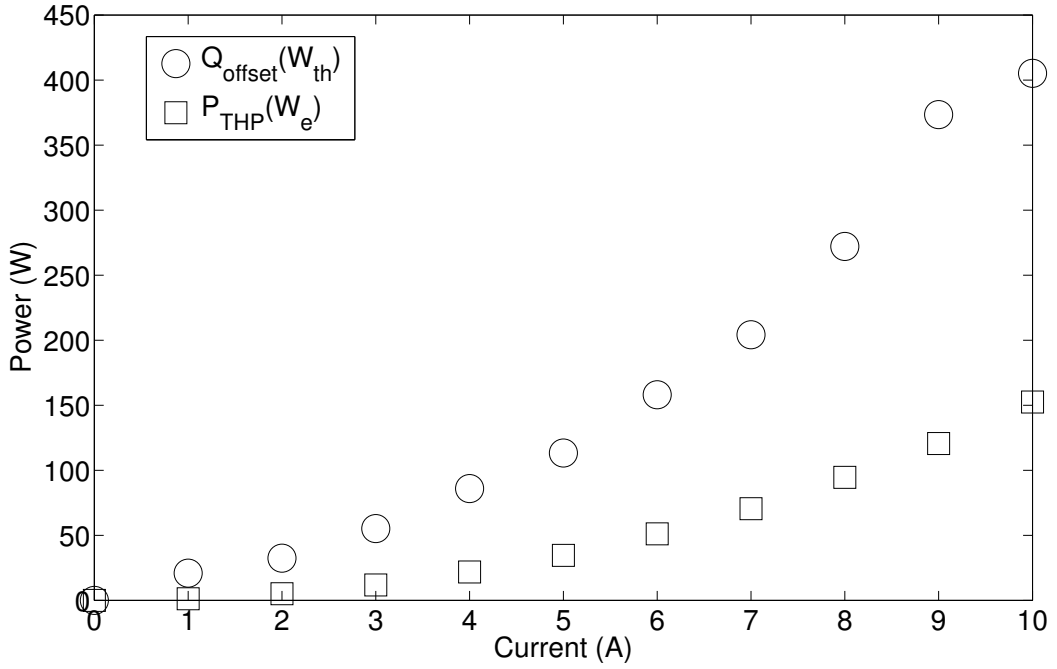

Figure 6.7: Thermal energy and applied power as a function of increasing current

Figure 6.7 plots the thermal energy increase of the water (left axis) and the electrical power applied to the THP (right axis). As expected the thermal energy in the water exiting the THP stage rises as the applied electrical power to the device is increased. The rate of increase is not linear, however.

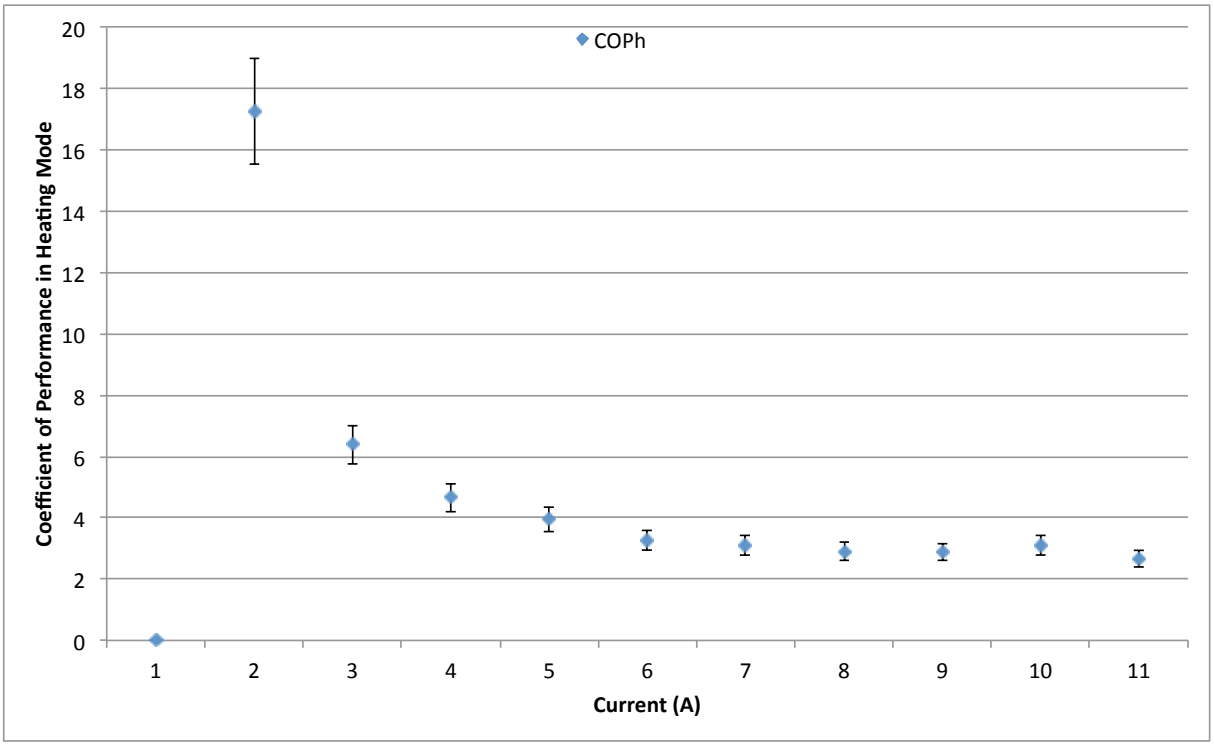

Figure 6.8: Coefficient of performance in heating mode at increasing applied heat pump currents

Using the data in Figure 6.7, the apparent coefficient of performance can be calculated and plotted (Figure 6.8) as the ratio between the thermal energy increase in the water and the applied electrical power. However, the COP calculated by these experimental results is uncalibrated and therefore artificially high. In order to calibrate the data, the water temperature from the tests with no THP is combined with the offsets presented in Table 6.3 and subtracted from the measured water temperature in the THP tests where current is applied. The equation used to factor in the corrections is shown in equation 6.1.

$$\Delta T = \Delta T_{water} - \left(\frac{\Delta T_{THP=0A} - T_{offset}}{2}\right) \tag{6.1}$$

The corrected data set gives a lower temperature difference, but crucially it is more accurate. The final column of Table 6.4 shows the corrected COP and the corresponding graph is shown in Figure 6.9. The data show the characteristic peak of high COP at low current and a gradual decay to a COP_h of unity at high heat pump input power where Joule heating dominates the behaviour.

Current	Offset	Averaged Offset	Q	COP
0	0°C	0°C	$0W_{th}$	0
1	0.299°C	0.08°C	$5.27W_{th}$	4.36
2	0.46°C	0.16°C	$11.04W_{th}$	2.18
3	0.78°C	0.32°C	$22.42W_{th}$	1.89
4	1.23°C	0.54°C	$37.8W_{th}$	1.74
5	1.62°C	0.74°C	$51.46W_{th}$	1.49
6	2.26°C	1.05°C	$73.84W_{th}$	1.45
7	2.92°C	1.39°C	$96.9W_{th}$	1.38
8	3.89°C	1.87°C	$130.86W_{th}$	1.38
9	5.341°C	2.59°C	$181.55W_{th}$	1.51
10	5.8°C	2.82°C	$197.4W_{th}$	1.29

Table 6.4: Adjusted readings for water temperature based and resultant thermal energy and COP

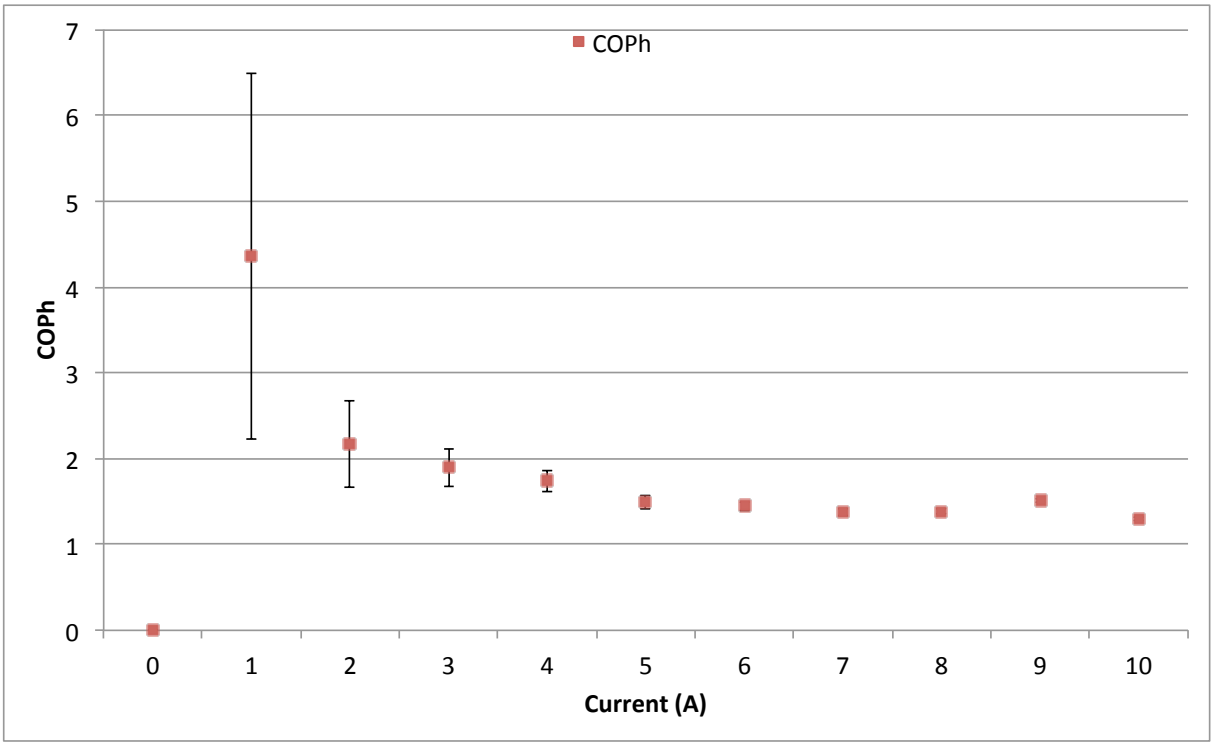

Figure 6.9: COP in heating mode with adjusted temperature difference measured across the water at flow rate $1L/min$

Figure 6.9 shows a large error margin for the low input current calculation of COP_h. This is attributed to inaccuracies in water temperature measurement as the system was susceptible to ingress from the temperature of the steam present in the condenser.

Despite this, these results represent a first attempt to validate the process and importantly, the equipment worked and the reasons for the COP of heating not being attained have been detailed.

6.2 MATLAB Script for Energy Balance

A script has been written in MATLAB that performs a Second Law thermodynamic analysis on the system by calculating the energy changes occurring at each point of the system. By this method the performance of the heat pump in the condenser can be modeled. This is also shown in Appendix C.

The system is designed to calculate the temperature, pressure, vapour fractions, enthalpy and entropy of the water in the system by extracting the values from steam tables. Figure 6.10 details these parameters at each of the points in the Rankine cycle T-s diagram of Figure 4.5. Points 1, 2, 3 and 5 denote the usual paths of water flow in the cycle. Points 4a and 4b denote the THP included in the system. T_x, p_x, s_x and h_x denote the temperature, pressure, entropy and enthalpy at the respective x points.

Initially the temperature and pressure in the boiler are defined and the values of entropy and enthalpy are interpolated from tables of Water and Steam (IAPWS-IF97). For a boiler temperature of 63°C and a saturation pressure of 228mbar-abs the entropy of the system is 7.86kJ/kgK and the enthalpy is 2614.3kJ/kg. The condenser pressure of 0.055bar-abs dictates that the steam will have a saturation temperature of 34.6°C , presuming that the expansion phase is 100% efficient.

At this pressure and temperature in the condenser, the conditions are such that the steam condenses to water and therefore two phases exist at the same time. Despite the expansion phase there has been no drop in the entropy of the system, but the entropy value at this stage is a portion of liquid and vapour. The fraction is calculated from the entropy values of the liquid state and the vapour state as at the condenser pressure of 55mbar-abs the liquid entropy is 0.499kJ/kgK and the vapour entropy is 8.36kJ/kgK. The difference between these values is the same the entropy of the original steam. The portion of steam is given as a vapour fraction shown in Equation 4.2.

$$x_2 = \frac{s_2 - s_{2f}}{s_{2g} - s_{2f}} = \frac{7.86 - 0.499}{8.36 - 0.499} = 86.3\% \tag{6.2}$$

For enthalpy, the fraction of vapour to liquid dictates the amount of energy that can

be extracted by the THP system and by the chilling loop. The enthalpy value for the liquid phase is 114.9kJ/kg and the vapour phase is 2563kJ/kg.

This enthalpy is removed by a phase change in the chiller loop in the condenser, up to $4.3kW_{th}$. The chilling loop is maintained at around 10°C, which is below the dew point of the steam entering the condenser at 34.6°C therefore the steam will prefer to condense on the coils at lower temperature. However, the steam side of the heat pump is also maintained below the dew point at 23°C. The heat-sink with the THP attached is mounted in the direct path of the steam exiting the boiler, so initially steam will condense as directed on the steam side of the THP.

$$Q_{chiller} = mC_p\Delta T_{(outlet-inlet)} = 384W_{th} \tag{6.3}$$

$$Q_{condenser} = Q_{2g} - Q_{chiller} = 1.88kW_{th} \tag{6.4}$$

The energy rejected by the chiller is calculated from the known mass flow and the temperature difference measured in the water entry and exit (equation 6.3). The final condenser energy is given by the total enthalpy subtracted by the energy rejected by the chiller ($Q_{chiller}$) (equation 6.4).

The MATLAB model is then split in to two sections as the THP can be included or excluded. With the THP loop excluded the water is fed directly back to the boiler with no increase in temperature. In this case points 4a and 4b are skipped and 3 and 5 are the same values. The system performance is then evaluated by how much energy is required to raise the water to steam in the boiler.

The THP has raised the water temperature by 0.16°C. This equates to an energy increase of $11W_{th}$.

These results show that there is a distinct increase in thermal energy returning to the boiler as a result of using a thermoelectric heat pump. The MATLAB model presented in Figure 6.10 uses a single thermoelectric device based on currently available technology validated using experimental apparatus detailed in chapter 3.

The result of an increase of $11W_{th}$ can be compared to the experimental apparatus however the model does not account for thermal energy leaking in to the THP loop as

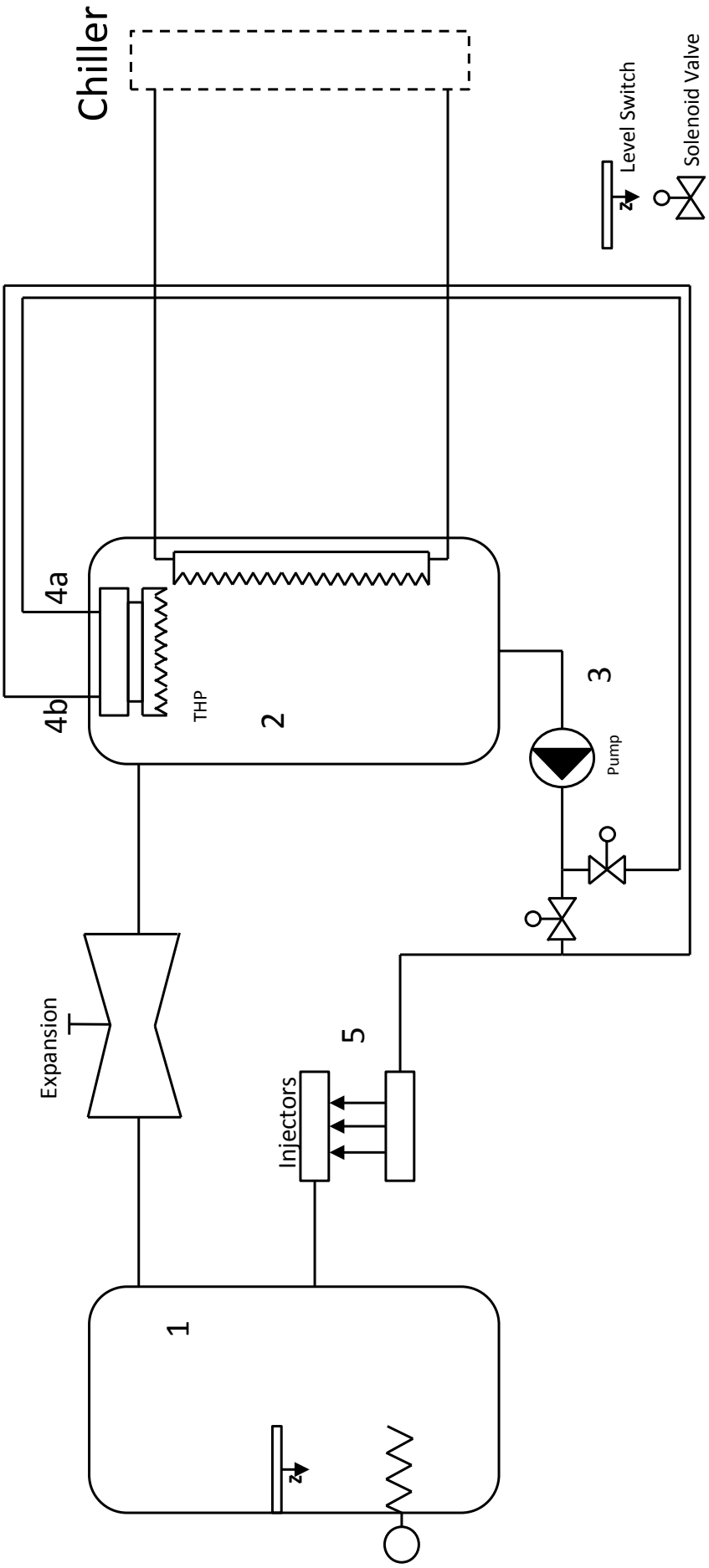

Figure 6.10: Rankine Cycle model used in the MATLAB simulations

was experienced in the actual running of the system. The model verifies the operation of the THP in the Rankine cycle and the resultant thermal energy increase as shown in the comparison at COP_{opt} in Table 6.4, the thermal energy increase (Q) of $5W_{th}$ is recorded at 1A.

6.3 THP Performance Summary

In this section the values for the coefficient of performance are compared at different flow rates of $0.66L/min$ and $1L/min$ through the THP loop. At the flow rate increases the temperature rise on the hot side of the THP should reduce due to the increased volume of water to be heated.

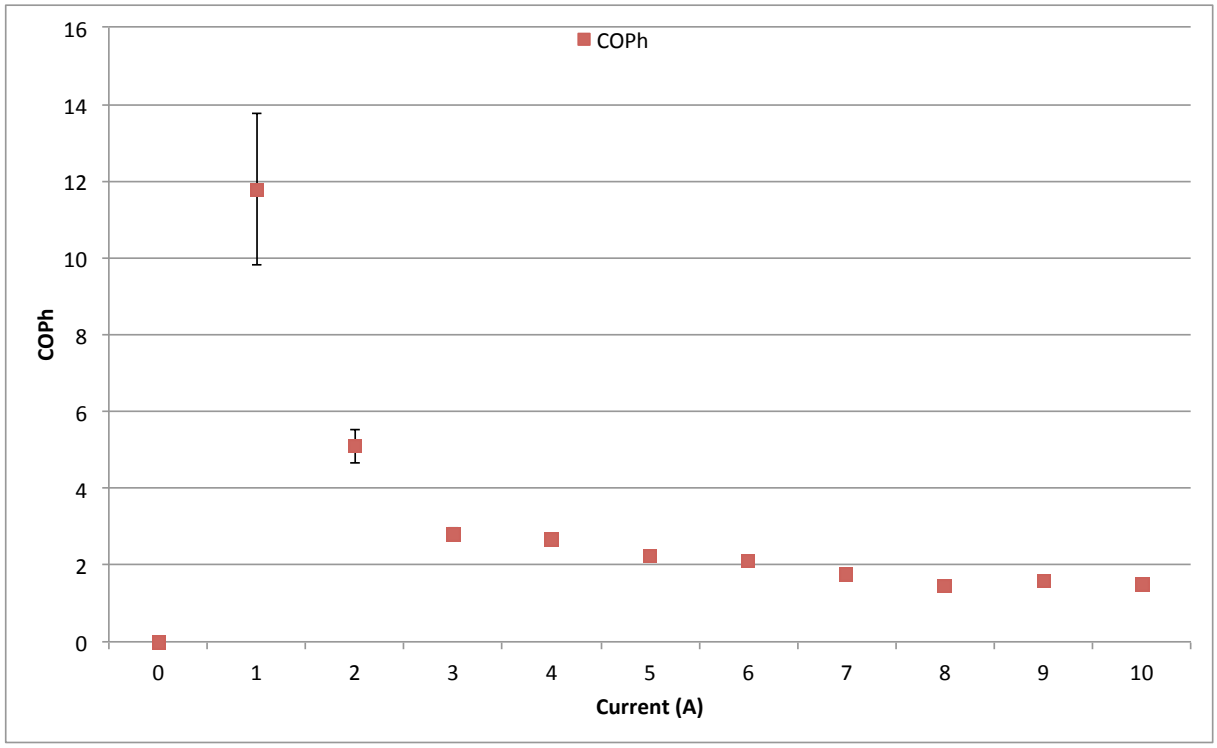

Figure 6.11: $0.66\frac{L}{min}$ flow rate COP with error bars

For the data for a flow rate of $0.66\frac{L}{min}$ shown in Figure 6.11, at low current, around 1A, the COP remains artificially high at 11.78, but lowers to values around 2.3 at 2A. The water temperature difference increases as the input power increases, but the maximum COP remains at low values of input current.

The data also shows that at a water flow rate of $0.66\frac{L}{min}$ there is a large percentage

error in the temperature reading. Despite various statistical averaging techniques used to generate the graph of Figure 6.11 (and similarly Figure 6.9) the COP at low values of current remains high – too high to be considered representative of the actual performance likely present in the system.

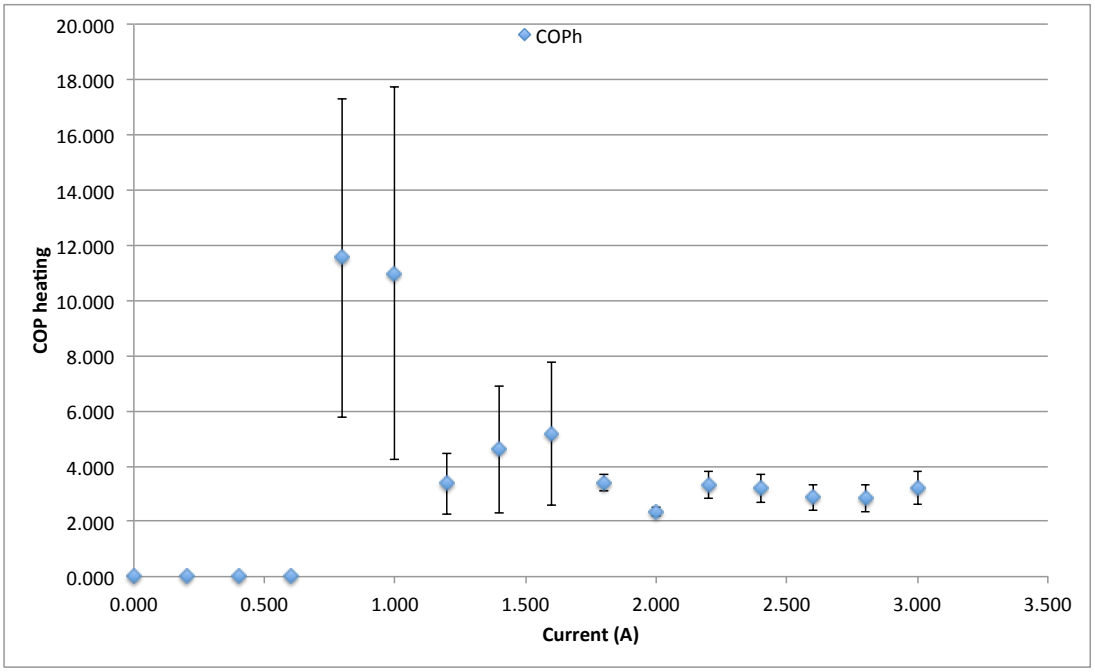

Figure 6.12: THP COP of heating at low currents (0-3A)

This is attributed to the behaviour of the apparatus at lower THP loop flow rates. The thermal energy increase of the water is more sensitive to increases in condenser temperature. Therefore, the higher flow rate of $1\frac{L}{min}$ is likely to be more accurate because the impact of the steam on the overall temperature of the heat exchanger is limited. Previous characterisation data has shown that the optimum coefficient of performance occurs at an I/I_{max} ratio of 0.2. These data shows that the highest COP occurs at lower values of input power and for lower flow rates the maximum COP occurs between 1A and 2A. Therefore the tests were repeated in an attempt to obtain additional values between 0A and 3A. These are presented in Figure 6.12.

6.4 Theoretical Analysis to Prove COP=1/η

The COP chart of Figure 6.12 follows the general shape of the COP curves shown in Figure 3.22 in chapter 3. The absolute values are somewhat different but the trend remains the

same. The primary finding of importance is that in order to meet the minimum COP which dictates if the THP would be beneficial to the plant, the COP_h must remain above 2.2.

At the low currents depicted there is a significant margin of error when compared against the chart in Figure 6.9, therefore the breakeven COP of heating has not been met. However the point lies within the error bars in the Figure. We cannot conclusively say with complete confidence that the breakeven condition has been satisfied therefore a scale-up is required to verify this. Steps to improve this result are noted in §6.5 and in the Chapter 8 conclusions.

6.5 Conclusions

Despite careful attempts to mitigate errors and unwanted effects introduced by the extreme scale reduction of the test apparatus there is a deviation from ideal performance in the results obtained. The principal causes of error are attributed to the proximity of the condenser coils and the THP system and the difficulty if thermally isolating the THP loop from the steam supply. The effects are exacerbated by the great difficulty experienced in reliably maintaining a constant state of steam equilibrium between the boiler and condenser for such low mass flow rates. These effects would be much less problematic at larger scales and therefore the next step in this project would be to have a large steam boiler and larger condenser. Finally, the COP calculation is particularly sensitive to the denominator term which tends towards zero at low THP input current.

To overcome these difficulties will require a much larger input power level. Negotiations are underway to use a $100kW_{th}$ steam plant in a local research establishment and the future work will focus solely on the design of the condenser system to more accurately characterise the THP loop. A large energy company has been approached with a view to establishing a commercial basis for this work. The work presented in this thesis does, however, show that the use of thermoelectric heat pumps can be applied to the Rankine cycle at an industrial scale and will result in an overall process efficiency gain. As such, the primary objective of the research programme has been achieved.

Chapter 7

Vision and Further Work

A fundamental requirement for economic use of condenser heat pumping is to ensure that the input power required for the pumping does not exceed the point at which use of the system detracts from the cycle efficiency. Prior work has determined theoretically that the point at which the heat pump becomes beneficial is when the COP exceeds the reciprocal of the cycle efficiency i.e. $COP_h = \frac{1}{\eta_{cycle}}$ ($COP_h = 2.2$ for $\eta_{cycle} = 44.9\%$ base plant efficiency).

However, this COP_h threshold calculation does not take into account the temperature at which heat pumping occurs and it is therefore of great interest to determine the largest increase in feedwater temperature returning to the boiler that still ensures the minimum COP_h requirement is met. In a typical $600MW_e$ generating set each 1°C temperature rise in the feedwater returned to the boiler equates to approximately 1MW of thermal power not required from fuel combustion.

7.1 Cascaded Heat Pumps

To maximize the energy recovered from the condenser a number of heat pumps will be used in series with the output of one stage feeding the input to the next.

Figure 7.1 illustrates such an arrangement with the use of three cascaded stages. Each stage will require a separate electrical power arrangement and will operate with a different ΔT_{THP} and corresponding COP_h. In reality due to the scale of thermal energy to

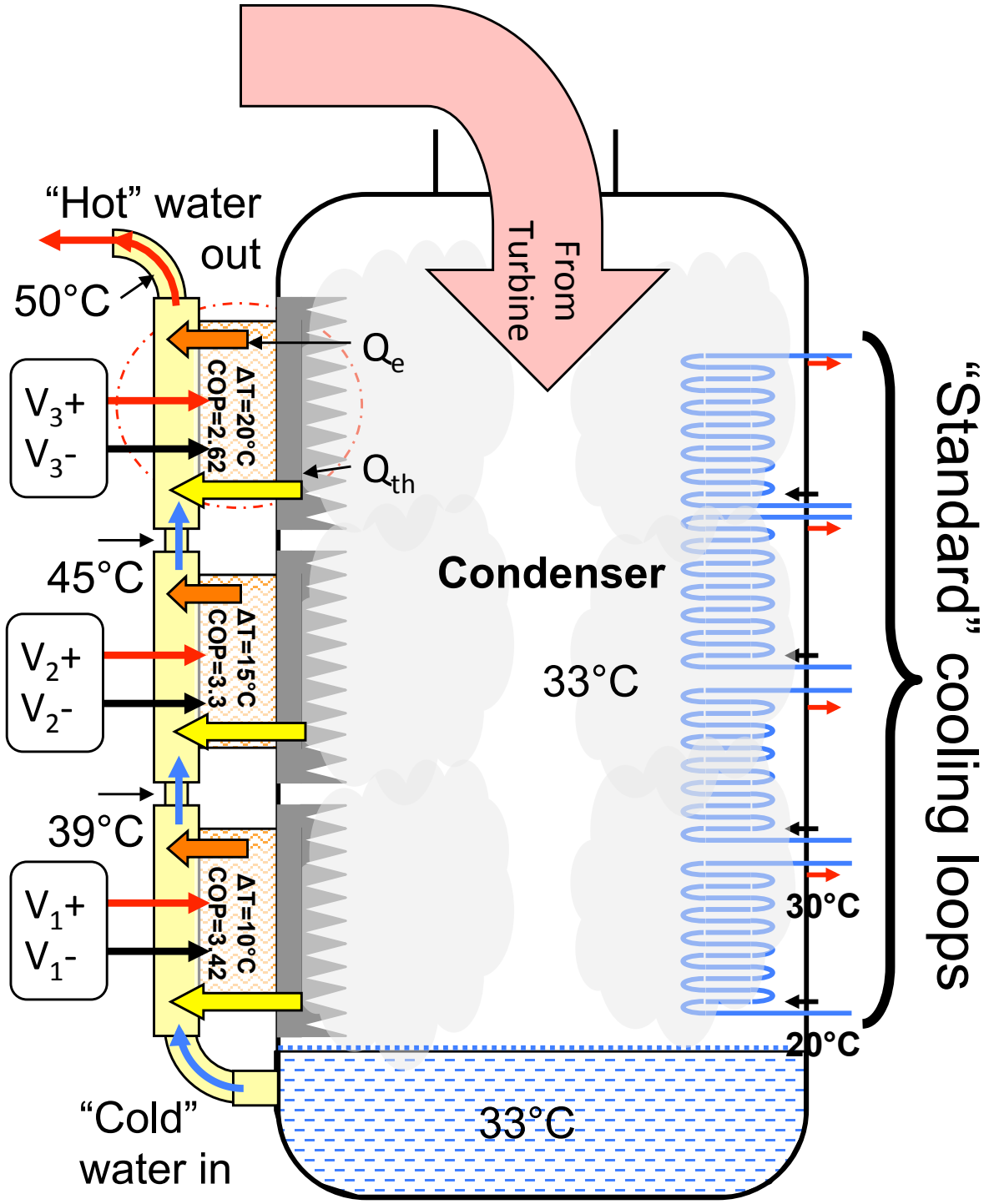

Figure 7.1: Triple stage cascaded THP application in the condenser

be shifted, many heat pumps will also be used in parallel for each temperature increment.

The internal temperature of the condenser remains constant (due to the rejection of latent heat occurring isothermally) on the "cold" side of each stage and hence the condensate temperature feedback to the boiler through the THP hot sides must progressively increase to absorb the sensible heat captured. Each THP will operate at the optimum

Stage	T_{Win} °C	T_{Wout} °C	ΔT °C	T_{THPhot} °C	$T_{THPcold}$ °C	ΔT_{THP} °C	COP_{opt}	I/I_{max}	$Q_h W_{th}$	m (kg/s)
1	33	39	6	42	32	10	3.42	0.21	34.6	0.0013
2	39	45	6	47	32	15	3.3	0.183	29.9	0.0013
3	45	50	5	52	32	20	2.62	0.2	28.7	0.0013

Table 7.1: Thermal energy analysis at each stage of the thermoelectric heat pump installed in the condenser

COP and therefore each stage of the cascade of heat pumps will require different voltages and currents to be applied for best efficiency.

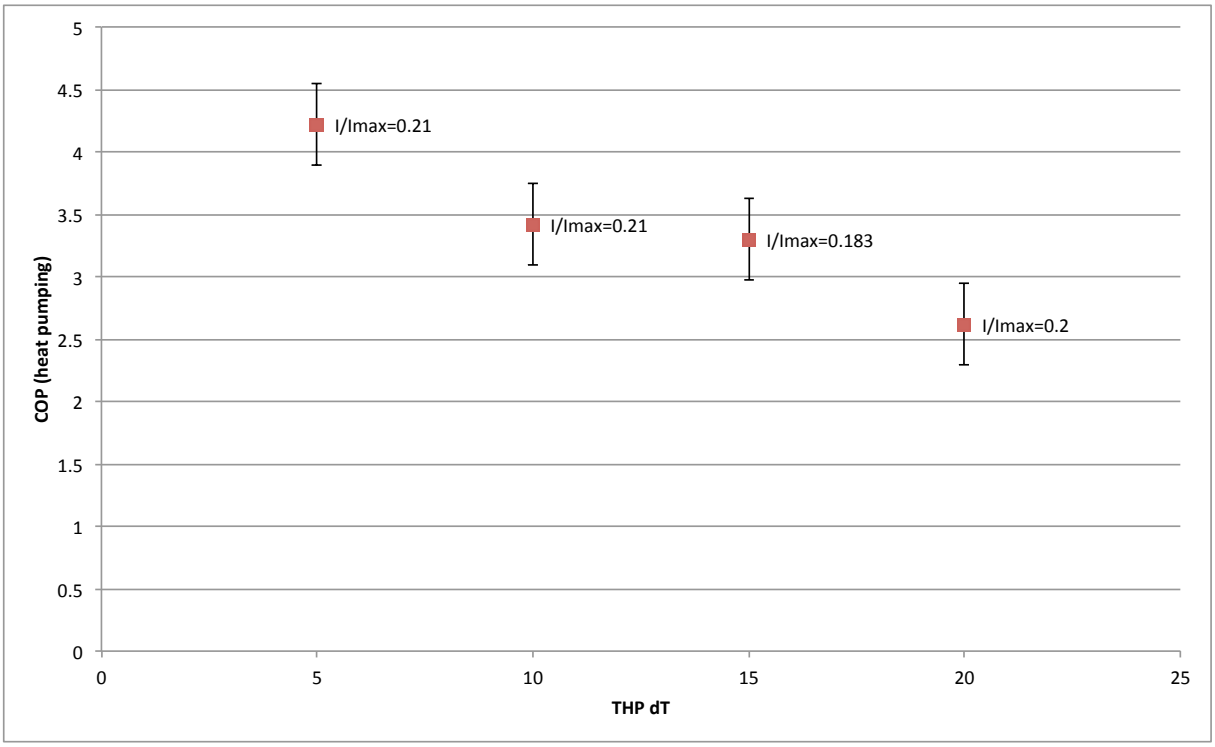

Figure 7.2: Optimum COP_h for ancreasing ΔT at the maximum I/I_{max}

Steam in the condenser encounters the "cold" side heat sink of the THP. The steam is at low pressure and hence low temperature (nominally 33°C, 45mbar-abs). Holding the THP below the dew point of the steam forces condensation and hence releases enthalpy. Figure 7.2 shows the optimum current ratio to I_{max} to drive the THP characterized in this work for a specific ΔT In previous chapters it has been noted that the COP is particularly sensitive to the thermal gradient across the THP, hence the need to minimize thermal resistance at the mechanical interfaces. This includes the heat transfer gradients from the steam to the THP and from the THP to the feedwater.

In Figure 7.1 the heat pump cascade is shown when split in to three stages. The

temperature of the feedwater increases with each stage and the cold-to-hot sides temperature difference across successive stages increases. The following conditions are met: $\Delta T_{w3} < \Delta T_{w2} < \Delta T_{w1}$, while for the actual device: $\Delta T_{THP3} > \Delta T_{THP2} > \Delta T_{THP1}$. For each successive stage the attainable COP_h is reduced in comparison with the previous stage, but it is still above the theoretical economic minimum.

In order to present a preferential condensation site in the condenser, the 'cooled' side temperature of the heat pump must be below that of the ambient steam conditions. For a typical large thermal plant operating at 33°C, 45mbar-abs a THP cold side of 32°C is sufficient to achieve this. It is assumed in this work that there will always be a surplus of steam in the condenser relative to the quantity that can be used for economic feedwater heating. This is likely to remain the case for foreseeable heat pump technologies and attainable COPs. The aim of the system presented here is to increase the temperature of the water returning to the boiler to 50°C, i.e., a 17°C temperature rise. This is achieved in three stages by increasing the operating temperature difference of the heat pump (ΔT_{THP}) while maintaining the optimum operating conditions (COP_{opt}) obtained from Figure 7.2 for that stage, summarized in Table 7.1.

At stage 1, the water enters the base of the THP loop at the condensate exit temperature of 33°C. In order to achieve a water exit temperature of 39°C then the required "heated" side temperature of the THP is 42°C. Using Figure 7.2, for a $\Delta T_{1THP} = 10$°C the maximum COP_h is 3.42 at $I/I_{max} = 0.21$. Using the modules previously characterised in this thesis, this equates to supplying $10.1W_e$ (3.37V at 3A), and producing a resultant $Q_h = 34.6W_{th}$.

At stage 2, water enters at 39°C and exits at 45°C giving a required $\Delta T_{2THP} = 15$°C ($T_{hot} = 47$°C and $T_{cold} = 32$°C). At this value, the maximum COP_h is 3.3 at $I/I_{max} = 0.183$. The resultant thermal energy increase to the water feed is $29.9W_{th}$ which is achieved by supplying $9W_e$ (3.5V at 2.6A) to the THP.

For the final stage, the water enters the heat exchanger at 45°C and increases by 5°C, exiting at 50°C. Since the THP_{cold} side remains at 32°C, the ΔT_{3THP} must be 20°C in order to achieve the 52°C required. The optimum COP_h of 2.62 can be obtained by driving the THP at the optimum $I/I_{max} = 0.2$. This gives an equivalent THP input power

Stage	V_{THP}	Devices per chain	Chains required	Total Electric Power	Total Thermal Power
1	3.4	172	1,224	$2.12MW_e$	$7.21MW_{th}$
2	3.6	162	1,299	$1.9MW_e$	$6.29MW_{th}$
3	4	146	1,442	$2.32MW_e$	$6.04MW_{th}$

Table 7.2: Layout of THP chains and number of devices dependent on the voltage

of $11W_e$ (3.9V at 2.8A) producing a thermal energy increase to the water of $28.7W_{th}$.

These figures are also summarized in Table 7.1.

The overall Coefficient of Performance of the cascade system averages to 3.11, an electrical input power of $30.1W_e$ and an overall increase in thermal power of $93.2W_{th}$. With these proven experimental results the scaling up of the system to very large energy levels can be explored.

7.2 Series and Parallel Connections

Energy to drive the THP system is a parasitic load on the electrical output of the plant. There are many other such loads in the plant: fans, pumps, conveyors systems etc. and to cater for different load requirements a variety of 3-phase(ϕ) supplies at different voltages are available throughout the plant. In the case of the THP system a DC supply is needed to ensure unidirectional heat pumping in the heat pump modules. Using the data presented in Figure 3.24, a putative design for the electrical system to power the condenser heat pump system is now considered. The 3-stage cascade system is replicated in parallel to the required level to provide the energy necessary to raise the feedwater return temperature to 50°C.

This is presented schematically in Figure 7.3 and with the numerical detail provided in Table 7.2. For the purpose of this example, assume a pair of $415V_{AC}$ supplies capable of providing power of $72kW_e$ is available in the plant from a transformer with electrical outputs 30° apart electrically (a star- and a delta- wound secondary). $415V_{AC}$ is preferred over higher voltages, mainly to reduce the electrical insulation requirements and creepage and clearance distances otherwise needed. A 12-pulse rectifier is used to convert the $415V_{AC}$ to a nominal $585V_{DC}$. A single chain of thermoelectric heat pump devices is used

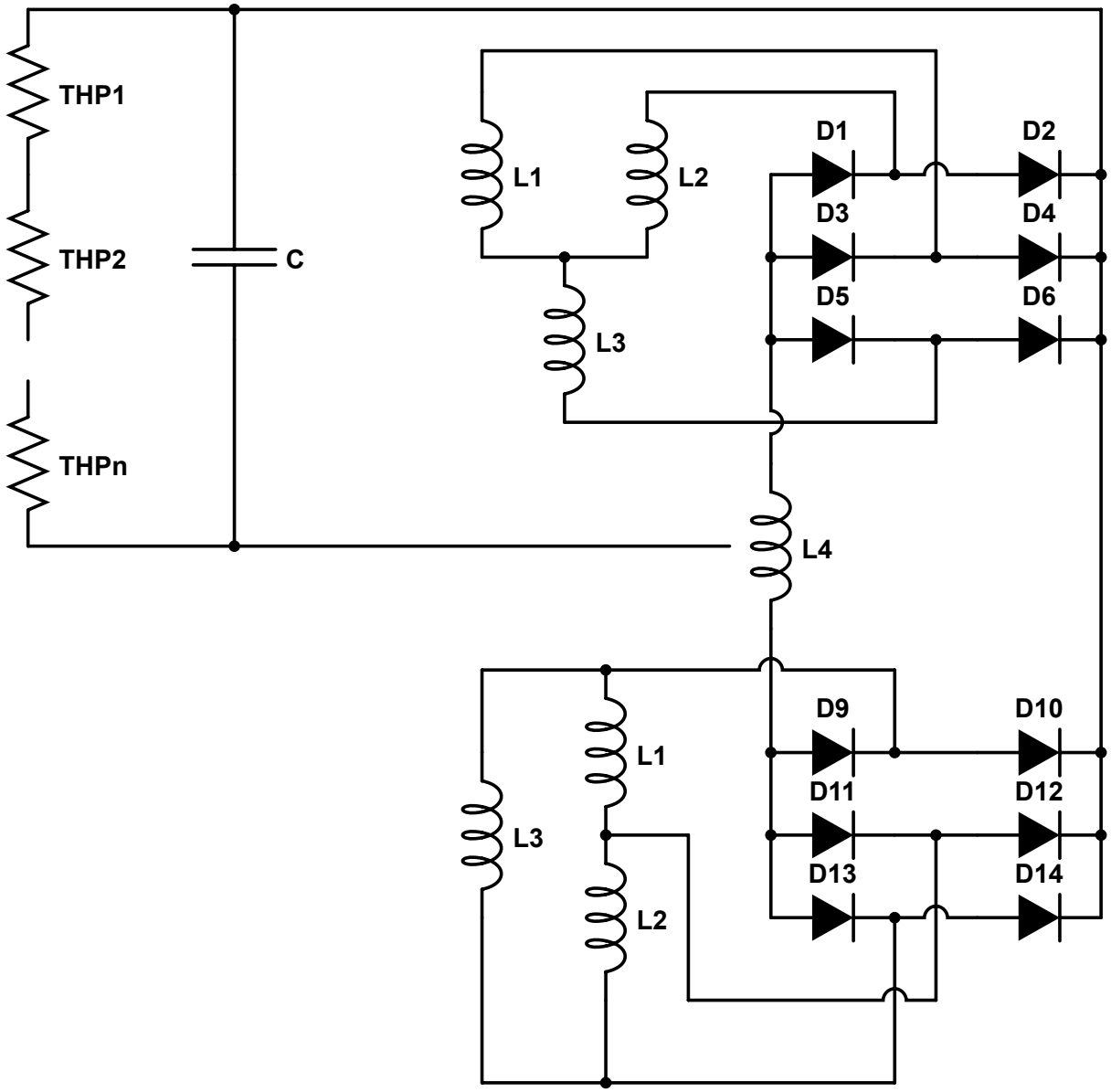

Figure 7.3: 12-Pulse AC/DC Rectifier with THP chain

with each 12-pulse rectifier and a constant current load of 100A will require a capacitor to reduce the ripple voltage. With no capacitor the ripple voltage is 20V assuming the conduction angle of each diode pair is 30°. Adding a suitable smoothing capacitor reduces this ripple voltage to 6V or approximately 1% of the string voltage. This is considered sufficiently smooth for the array of THPs connected to the supply to operate satisfactorily. The ripple frequency is 12X the supply frequency (50 or 60 Hz), i.e. a couple of milliseconds, and this is orders of magnitude less than the thermal time constant of the THP assembly.

Many THPs are connected electrically in a series – parallel array to an individual

power supply but are mounted thermally in parallel in the condenser wall. Since each stage of the heat pump cascade operates at a different ΔT the voltage across each stage varies and requires a difference number of THP's fed from each $415V_{AC}$ pack. This has the additional benefit of being modular: if a chain develops a fault, the remaining chains and other cascades can continue to operate unaffected and plant performance is not severely degraded. Note that in this example a uniform plant operation is assumed, but the diodes in the rectifier circuits can be replaced with thyristors if variable voltage is required.

In order to meet the mass flow requirement of the feed water returning to the boiler multiple THP arrays will be required. The plant described in this thesis has a return water feed of 273.6kg/s from the condenser with each THP capable of attaining the desired heat energy transfer at a mass flow of 0.0013kg/s. Therefore a total of 210,462 devices are required. This calculation assumes a standard 50mm x 50mm module but in reality a much larger module would be used. The low operational temperature difference will alleviate the mechanical stresses that would otherwise occur, especially in the corners of the module. 200mm x 200mm is thought feasible, requiring some 13,000 such modules.

The electrical resistance of the semiconductor pellets in the THP have a resistance of a couple of ohms, therefore over the large number of devices envisaged there will be a significant voltage drop in the interconnecting wiring. To compensate, the voltage of each THP is slightly increased, giving the voltages for each THP at each stage shown in Table 7.2.

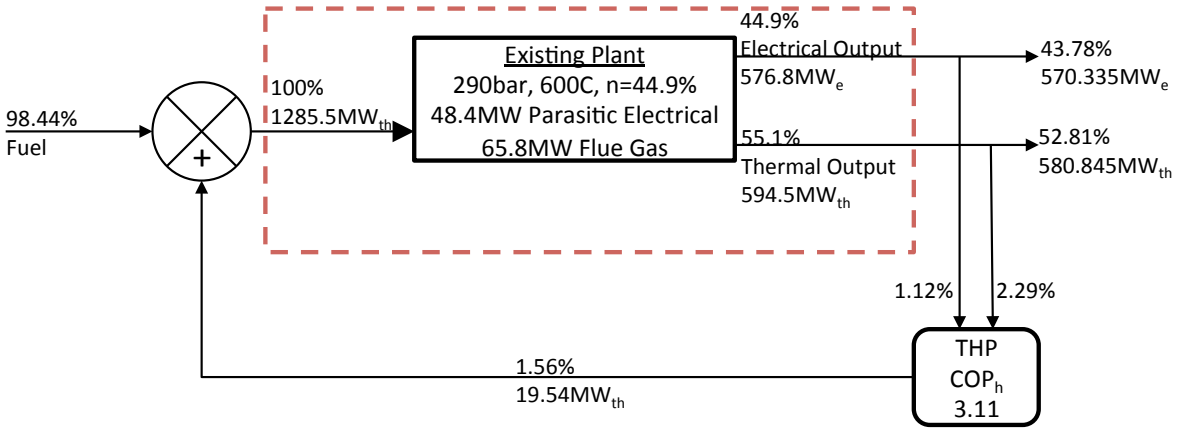

Figure 7.4: THP applied to the Rankine plant

Within a particular THP array the temperature difference across each THP element

will be constant, meaning the internally generated Seebeck voltage and internal impedance will be equal, at least to the manufacturing consistency of the devices. Empirical data obtained from testing several nominally identical devices has shown the a consistency of better than 1%. The load current will thus be equal in each device within the same stage and this permits the series/parallel array to be created with convenient electrical drive current and voltage requirements.

An application of such a set of THP arrays to a $600MW_e$ Rankine cycle plant is demonstrated in Figure 7.4. The sum of the electrical powers to the THP is $6.34MW_e$, which 1.12% of the net electrical output of the plant. Further, we can calculate that the large-scale thermal output of the THP is $19.54MW_{th}$. Hence the overall coefficient of performance of heating when applied to the plant = 3.1. As previously shown, this is well above the minimum threshold for the application of a THP to be beneficial to this plant, the threshold being $\eta_{cycle} = 1/44.9\% = 2.22$.

7.3 Economics

The preceding theoretical analysis and experimental results have demonstrated favourable operating conditions for implementing a THP cascade in the Rankine cycle. In order to quantify this economic advantage its impact on a coal-fuelled thermal plant is examined. In the following analysis the additional cost-benefit of the reduction in carbon dioxide emissions is excluded for clarity.

7.3.1 Cost of Electricity

Assuming the generating cost of electricity is 3.5p/kWh and that the plant as a load factor of 85% and a capacity of $600MW_e$ then a saving of £5.1 million per year can be made for a thermal energy addition of $19.54MW_{th}$ to the plant. If the plant sells electricity at a cost of 4p/kWh (£40/MWh) then a THP reduces the income to the plant by £1.89 million per year. This assumes that $6.334MW_e$ is supplied to the THP from the plant.

Year	Y0	Y1	Y2	Y3	Y4	Y5
THP System	(£12.62)	£0	£0	£0	£0	£0
Coal Reduction	£0	£5.1	£5.1	£5.1	£5.1	£5.1
Electricity Revenue	£0	(£1.89)	(£1.89)	(£1.89)	(£1.89)	(£1.89)
Difference Total	(£12.62)	(£9.41)	(£6.2)	(£2.99)	£0.22	£3.43

Table 7.3: Payback period for THP. All figures in £millions

7.3.2 Thermal Plant Equipment CAPEX

For a THP system that consists of 210, 462 devices for each stage, it equates to 631,386 devices. Assuming a cost price per THP of £10 then the initial capital cost of only the devices is £6.313 million. The infrastructure and other capital expenditures are estimated at double the cost of the devices totalling to £12.62 million.

Table 7.3 shows the interval between the initial capital cost and the payback period, taking into account both the reduced fuel expenditure and lost revenue for decreased sales of kWh of electricity due to the THP system parasitic load.

This equates to a payback of a little over 4 years compared with an expected service life of some 30 years for the THP system. This system thus clearly gives a reduced operating cost and, even using today's available standard parts, is economically attractive.

7.4 Final Remarks

As noted in §6.5, the extreme difficulty in obtaining accurate experimental data from such a massively scaled-down Rankine cycle plant has made it difficult to determine with absolute certainty the available COP and hence the potential temperature rise on the feedwater return. The numbers used in this chapter are conservative and take into account the lower limits on the error bars from the various results presented. The next step will require an increase to an estimated 100kW thermal in a larger condenser. Physically this will be a much easier experiment to manage and a commercial partner is being sought to continue the work.

In reflecting on the accomplishments presented in this thesis, the other major area for consideration of heat pumping is the flue gas. Today's plant designs retain significant thermal energy in the combustion products ($> 60MW_{th}$) to ensure they rise quickly

from the stack and properly disperse in the atmosphere. It may be economically feasible to recycle some of this thermal energy back into the process by using heat pumps and providing addition flue gas momentum by the use of large blowers (and the electrical energy converted to heat by the associated motors will be entrained in the flue gases). So long as there is a net gain in the total cycle efficiency this would be worthwhile.

Chapter 8

Conclusions

This thesis has shown that there is scope to improve the cycle efficiency of a thermal power plant operating on the Rankine cycle by harvesting thermal energy normally rejected by the condenser. Today's thermoelectric materials have attained the performance level that makes them a viable technology in this application. This has been explored theoretically and demonstrated experimentally in the work presented here. Although the THP's exhibit a lower COP than their vapour-compression alternatives at high pumping power, their reliability and simplicity of operation makes them an attractive option. Each of the multistage cascade heat pumps is electrically driven to maximize the COP for the required temperature difference across the array of devices – of the order of an I/I_{max} ratio = 0.2. Heat pumping power densities of the order of 1MW/m^3 are attainable and their low mass makes them suitable for condenser walls in both retrofit and new designs.

The technical feasibility of using a large number of thermoelectric heat pumps has been investigated. Each stage of the heat pump cascade requires a different operating voltage and current, therefore there are distinct advantages in using large numbers of devices in parallel arrays. Electrical power to control the arrays from $415V_{AC}$/3-ϕ supplies allows for cost-effective implementation using standard power conversion circuitry.

The economic case at the plant level has been examined and despite the large number of devices, the costs are recoverable in 4 years using a pessimistic estimate of both costs and savings. A more detailed analysis would depend on the particular plant, retrofit versus new build costs, the prevailing efficiency incentives and subsidies, carbon trading

costs, future fuel and electricity unit selling costs, etc.

Further work will detail the implementation of a thermoelectric heat pump in a small-scale Rankine cycle experiment that replicates power plant steam conditions and will examine the mechanical implementation required for the their successful use.

After a relatively long period where little improvement in thermoelectric materials has been made, rising energy costs and stringent emissions regulations are motivating massive investment in semiconductor processes and materials work and this is yielding dividends: thermoelectric devices are being produced using commonly available materials and their performance is improving. This strengthens the case for their application in what is already a viable enhancement to the Rankine cycle.

This work has detailed several research contributions. Initially the application of the heat pump to the Rankine cycle is described and the potential cycle efficiency improvement is presented. A breakeven Coefficient of Performance is detailed showing the dependence on the cycle efficiency of the plant. At lower cycle efficiencies the thermoelectric heat pump application becomes increasingly attractive.

In order to determine the performance of such a thermoelectric heat pump, testing apparatus has been developed. Importantly this setup is capable of testing and characterising a thermoelectric device independent of material used (i.e. independent of Bismuth Telluride TE devices). This testing apparatus is now the focus of work by NPL in determining engineering standards for such TE devices.

The test setup for the Rankine cycle is also a significant contribution and the ability of the apparatus to generate the condenser entry thermodynamic conditions. Further, a design guide (in Appendix B) notes the individual component choice for the Rankine cycle and includes notes on the assembly.

From an economic perspective, the potential savings to the plant have been investigated. Initial data is given for a THP applied to the plant and the costs of installation and operation of these devices is provided. This data shows shows the costs can be recovered in less than 5 years. Further, the Benson load implications have been detailed and initial calculations have been provided. However, this could have a greater impact on the plant when varying availability of such a plant is considered.

Bibliography

[1] BP, "BP Energy Outlook 2035," Tech. Rep. January, 2014.

[2] Y. F. Wang, K. P. Li, X. M. Xu, and Y. R. Zhang, "Transport energy consumption and saving in China," *Renewable and Sustainable Energy Reviews*, vol. 29, pp. 641–655, Jan. 2014.

[3] I. MacLeay, K. Harris, and A. Annut, *Digest of United Kingdom Energy Statistics*. 2013.

[4] DECC, "Transport energy consumption in the UK between 1970 and 2012," tech. rep., 2013.

[5] R. Weijermars, P. Taylor, O. Bahn, S. R. Das, and Y.-M. Wei, "Review of models and actors in energy mix optimization – can leader visions and decisions align with optimum model strategies for our future energy systems?," *Energy Strategy Reviews*, vol. 1, pp. 5–18, Mar. 2012.

[6] S. Pacala and R. Socolow, "Stabilization wedges: solving the climate problem for the next 50 years with current technologies.," *Science (New York, N.Y.)*, vol. 305, pp. 968–72, Aug. 2004.

[7] European Commission, "A Roadmap for Moving to a Competitive Low Carbon Economy in 2050," tech. rep., 2011.

[8] O. Badr, S. Probert, and P. O'Callaghan, "Rankine cycles for steam power-plants," *Applied Energy*, vol. 36, pp. 191–231, Jan. 1990.

[9] J. M. Beér, "High efficiency electric power generation: The environmental role," *Progress in Energy and Combustion Science*, vol. 33, pp. 107–134, Apr. 2007.

[10] B. Hoffmann, S. Häfele, and U. Karl, "Analysis of performance losses of thermal power plants in Germany – A System Dynamics model approach using data from regional climate modelling," *Energy*, vol. 49, pp. 193–203, Jan. 2013.

[11] Y. Zhao, S. Wang, L. Duan, Y. Lei, P. Cao, and J. Hao, "Primary air pollutant emissions of coal-fired power plants in China: Current status and future prediction," *Atmospheric Environment*, vol. 42, pp. 8442–8452, Nov. 2008.

[12] H. Hou, J. Mao, Y. Yang, and N. Luo, "Solar-Coal Hybrid Thermal Power Generation — an Efficient Way to Use Solar Energy in China," *Journal of Energy Engineering*, vol. 2, pp. 137–142, 2012.

[13] T. Kyono, R. Suzuki, and K. Ono, "Conversion of unused heat energy to electricity by means of thermoelectric generation in condenser," *IEEE Transactions on Energy Conversion*, vol. 18, pp. 330–334, June 2003.

[14] S. I. Kim, K. Ahn, D.-H. Yeon, S. Hwang, H.-S. Kim, S. M. Lee, and K. H. Lee, "Enhancement of Seebeck Coefficient in Bi0.5 Sb1.5 Te3 with High-Density Tellurium Nanoinclusions," *Applied Physics Express*, vol. 4, p. 091801, Sept. 2011.

[15] J. R. Buckle, a. Knox, J. Siviter, and a. Montecucco, "Autonomous Underwater Vehicle Thermoelectric Power Generation," *Journal of Electronic Materials*, vol. 42, pp. 2214–2220, Apr. 2013.

[16] G. Min and D. M. Rowe, "Ring-structured thermoelectric module," *Semiconductor Science and Technology*, vol. 22, pp. 880–883, Aug. 2007.

[17] R. O. Suzuki and D. Tanaka, "Mathematic simulation on thermoelectric power generation with cylindrical multi-tubes," *Journal of Power Sources*, vol. 124, pp. 293–298, Oct. 2003.

[18] F. Stabler, "Automotive Thermoelectric Generator Design Issues," pp. 1–26, 2009.

[19] S. Lineykin and S. Ben-Yaakov, "Modeling and Analysis of Thermoelectric Modules," *IEEE Transactions on Industry Applications*, vol. 43, no. 2, pp. 505–512, 2007.

[20] D. T. Crane and L. E. Bell, "Progress Towards Maximizing the Performance of a Thermoelectric Power Generator," *25th International Conference on Thermoelectrics*, pp. 11–16, 2006.

[21] E. Sandoz-Rosado and R. J. Stevens, "Experimental characterization of thermoelectric modules and comparison with theoretical models for power generation," *Journal of electronic materials*, vol. 38, pp. 1239–1244, Mar. 2009.

[22] X. Gou, H. Xiao, and S. Yang, "Modeling, experimental study and optimization on low-temperature waste heat thermoelectric generator system," *Applied Energy*, vol. 87, pp. 3131–3136, Oct. 2010.

[23] C.-T. Hsu, G.-Y. Huang, H.-S. Chu, B. Yu, and D.-J. Yao, "Experiments and simulations on low-temperature waste heat harvesting system by thermoelectric power generators," *Applied Energy*, vol. 88, pp. 1291–1297, Apr. 2011.

[24] A. Montecucco, J. Buckle, J. Siviter, and A. R. Knox, "A New Test Rig for Accurate Nonparametric Measurement and Characterization of Thermoelectric Generators," *Journal of Electronic Materials*, vol. 42, pp. 1966–1973, Mar. 2013.

[25] A. Montecucco, J. Siviter, and A. Knox, "Simple, fast and accurate maximum power point tracking converter for thermoelectric generators," *ECCE 2012*, pp. 2777–2783, 2012.

[26] J. Siviter, A. Knox, J. Buckle, A. Montecucco, and M. Euan, "Megawatt scale energy recovery in the Rankine cycle," in *ECCE2012*, pp. 1374–1379, 2012.

[27] J. Siviter, A. Montecucco, and A. Knox, "Rankine Cycle efficiency gain using Thermoelectric Heat Pumps," *Applied Energy*.

[28] A. Montecucco, J. Siviter, and A. Knox, "Practical Design Considerations for Automotive Thermoelectric Exhaust Energy Recovery Systems," *Applied Energy (under review)*.

[29] A. R. Knox, J. Buckle, J. Siviter, A. Montecucco, and E. McCulloch, "Megawatt-Scale Application of Thermoelectric Devices in Thermal Power Plants," *Journal of Electronic Materials*, 2013.

[30] O. Maganga, N. Phillip, K. J. Burnham, A. Montecucco, J. Siviter, A. Knox, and K. Simpson, "Hardware Implementation of Maximum Power Point Tracking for Thermoelectric Generators," *Journal of Electronic Materials*, Feb. 2014.

[31] J. Siviter, "Stirling Engines and Thermoelectric Devices for Heat Scavenging in Oxyfuel and PCCC," tech. rep., 2010.

[32] A. R. Knox, E. McCulloch, and J. Siviter, "Method and Apparatus for Improvement of Efficiency of Thermal Cycles WO 2012 085551 A2," 2011.

[33] United Nations Department of Economic and Social Affairs, "World Population Prospects The 2012 Revision, Highlights and Advance Tables," 2012.

[34] H.-x. Zhao and F. Magoulès, "A review on the prediction of building energy consumption," *Renewable and Sustainable Energy Reviews*, vol. 16, pp. 3586–3592, Aug. 2012.

[35] BP, "BP Energy Outlook 2030," Tech. Rep. January, 2013.

[36] V. K. Arora, J. F. Scinocca, G. J. Boer, J. R. Christian, K. L. Denman, G. M. Flato, V. V. Kharin, W. G. Lee, and W. J. Merryfield, "Carbon emission limits required to satisfy future representative concentration pathways of greenhouse gases," *Geophysical Research Letters*, vol. 38, pp. 3–8, Mar. 2011.

[37] M. Azhar Khan, M. Zahir Khan, K. Zaman, and L. Naz, "Global estimates of energy consumption and greenhouse gas emissions," *Renewable and Sustainable Energy Reviews*, vol. 29, pp. 336–344, Jan. 2014.

[38] B. Metz and O. Davidson, *Climate Change 2007 Mitigation of Climate Change*. 2007.

[39] D. Victor and D. Zhou, "Climate Change 2014 Working Group III Mitigation of Climate Change," tech. rep., 2014.

[40] P. Capros, L. Paroussos, P. Fragkos, S. Tsani, B. Boitier, F. Wagner, S. Busch, G. Resch, M. Blesl, and J. Bollen, "European decarbonisation pathways under alternative technological and policy choices: A multi-model analysis," *Energy Strategy Reviews*, pp. 1–15, Jan. 2014.

[41] A. F. Ghoniem, "Needs, resources and climate change: Clean and efficient conversion technologies," *Progress in Energy and Combustion Science*, vol. 37, pp. 15–51, Feb. 2011.

[42] United Nations, "Kyoto Protocol to the United Nations Framework Convention on Climate Change," tech. rep., 1998.

[43] IEA and OECD, "Monthly Electricity Statistics," tech. rep., 2013.

[44] J. r. Bugge, S. Kjæ r, and R. Blum, "High-efficiency coal-fired power plants development and perspectives," *Energy*, vol. 31, pp. 1437–1445, Aug. 2006.

[45] S. Kjaer and S. Kjæ r, "Status and future of advanced PF power plants," *Energy conversion and management*, vol. 37, no. 95, pp. 897–902, 1996.

[46] H. Yang, Z. Xu, M. Fan, R. Gupta, R. B. Slimane, A. E. Bland, and I. Wright, "Progress in carbon dioxide separation and capture: a review.," *Journal of environmental sciences (China)*, vol. 20, pp. 14–27, Jan. 2008.

[47] B. Li, Y. Duan, D. Luebke, and B. Morreale, "Advances in CO2 capture technology: A patent review," *Applied Energy*, vol. 102, pp. 1439–1447, Feb. 2013.

[48] R. S. Panesar, M. R. Lord, and S. T. Simpson, "Emerging Energy Technologies," *Coal-Fired Advanced Supercritical Retrofit with CO2 Capture*, pp. 1–83, 2008.

[49] S. J. Goidich, "Technology on the March Steady Progress in Supercritical Once-through Technology," *COAL-GEN, Chicago*, 2001.

[50] S. J. Goidich, R. J. Docherty, K. P. Melzer, F. Wheeler, and N. America, "The World's First Supercritical FW-BENSON Vertical PC Boiler - The 750 MWe Longview Power Project," tech. rep., 2011.

[51] J. M. Klara and J. E. Plunkett, "The potential of advanced technologies to reduce carbon capture costs in future IGCC power plants," *International Journal of Greenhouse Gas Control*, vol. 4, pp. 112–118, Mar. 2010.

[52] A. W. Bhutto, A. A. Bazmi, and G. Zahedi, "Underground coal gasification: From fundamentals to applications," *Progress in Energy and Combustion Science*, vol. 39, pp. 189–214, Feb. 2013.

[53] J. Oexmann and A. Kather, "Minimising the regeneration heat duty of post-combustion CO2 capture by wet chemical absorption: The misguided focus on low heat of absorption solvents," *International Journal of Greenhouse Gas Control*, vol. 4, pp. 36–43, Jan. 2010.

[54] A. S. Bhown and B. C. Freeman, "Analysis and status of post-combustion carbon dioxide capture technologies.," *Environmental science & technology*, vol. 45, pp. 8624–32, Oct. 2011.

[55] D. T. Hountalas, G. C. Mavropoulos, and K. B. Binder, "Effect of exhaust gas recirculation (EGR) temperature for various EGR rates on heavy duty DI diesel engine performance and emissions," *Energy*, vol. 33, pp. 272–283, Feb. 2008.

[56] S. M. Mousavian and M. T. Mansouri, "Conceptual feasibility study of retrofitting coal-fired power plant with oxy-fuel combustion," *Proceedings of the Institution of Mechanical Engineers, Part A: Journal of Power and Energy*, vol. 225, pp. 689–700, Aug. 2011.

[57] L. Chen, S. Z. Yong, and A. F. Ghoniem, "Oxy-fuel combustion of pulverized coal: Characterization, fundamentals, stabilization and CFD modeling," *Progress in Energy and Combustion Science*, vol. 38, pp. 156–214, Apr. 2012.

[58] J. Hong, R. Field, M. Gazzino, and A. F. Ghoniem, "Operating pressure dependence of the pressurized oxy-fuel combustion power cycle," *Energy*, vol. 35, pp. 5391–5399, Dec. 2010.

[59] B. Metz, O. Davidson, H. de Coninck, M. Loos, L. Meyer, and H. de Coninck, "Carbon Dioxide Capture and Storage Special Report from The IPCC," tech. rep., 2005.

[60] C. Chen and E. S. Rubin, "CO2 control technology effects on IGCC plant performance and cost," *Energy Policy*, vol. 37, pp. 915–924, Mar. 2009.

[61] E. S. Rubin, H. Mantripragada, A. Marks, P. Versteeg, and J. Kitchin, "The outlook for improved carbon capture technology," *Progress in Energy and Combustion Science*, vol. 38, pp. 630–671, Oct. 2012.

[62] A. Bejan, "Theory of heat transfer-irreversible power plants," *International Journal of Heat and Mass Transfer*, vol. 31, no. 6, 1988.

[63] A. Geete and A. I. Khandwawala, "Thermodynamic analysis of 120MW Thermal Power Plant with Combined Effect of Constant Inlet Pressure (124.61bar) and Different Inlet Temperatures," *Case Studies in Thermal Engineering*, vol. 1, pp. 17–25, Aug. 2013.

[64] Y.-S. Wang, B.-C. Xie, L.-F. Shang, and W.-H. Li, "Measures to improve the performance of China's thermal power industry in view of cost efficiency," *Applied Energy*, vol. 112, pp. 1078–1086, Dec. 2013.

[65] S. Bekdemir, R. Ozturk, and Z. Yumurtac, "Condenser Optimization in Steam Power Plant," *Journal of Thermal Science*, vol. 12, no. 2, 2002.

[66] E. Yasni and C. G. Carrington, "Off-design exergy audit of a thermal power stations," *Journal of Engineering for Gas Turbines and Power*, vol. 110, 1988.

[67] M. Richardson, Y. Kidera, and Y. Shimogori, "Supercritical Boiler Technology Matures," in *Coal Gen*, pp. 1–24, 2004.

[68] J. M. Salazar, U. Diwekar, E. Constantinescu, and V. M. Zavala, "Stochastic optimization approach to water management in cooling-constrained power plants," *Applied Energy*, vol. 112, pp. 12–22, Dec. 2013.

[69] CANADA and USA, "Final Report on the Implementation of Task Force Recommendations," tech. rep., 2006.

[70] W. Wang, D. Zeng, J. Liu, Y. Niu, and C. Cui, "Feasibility analysis of changing turbine load in power plants using continuous condenser pressure adjustment," *Energy*, Dec. 2013.

[71] O. M. Al-Rabghi, M. Beirutty, M. Akvurt, Y. Najjar, and T. Alp, "Recovery and utilization of waste heat review paper," *Heat Recovery Systems and CHP*, vol. 13, no. 5, pp. 463–470, 2002.

[72] T. Borrnert, "Organic Rankine Cycle Based Power Plant to Utilize Low-Grade Waste Heat Sources," in *Cement Industry Technical Conference*, pp. 1–10, 2011.

[73] G. Angelino, C. Invernizzi, and G. Molteni, "The potential role of organic bottoming Rankine cycles in steam power stations," *Proceedings of the Institution of Mechanical Engineers, Part A: Journal of Power and Energy*, vol. 213, pp. 75–81, Jan. 1999.

[74] R. S. Murugan and P. M. V. Subbarao, "Efficiency enhancement in a Rankine cycle power plant: combined cycle approach," *Proceedings of the Institution of Mechanical Engineers, Part A: Journal of Power and Energy*, vol. 222, pp. 753–760, Dec. 2008.

[75] C. Wang, B. He, S. Sun, Y. Wu, N. Yan, L. Yan, and X. Pei, "Application of a low pressure economizer for waste heat recovery from the exhaust flue gas in a 600MW power plant," *Energy*, vol. 48, pp. 196–202, Dec. 2012.

[76] A. Borsukiewicz-Gozdur, "Exergy analysis for maximizing power of organic Rankine cycle power plant driven by open type energy source," *Energy*, vol. 62, pp. 73–81, Dec. 2013.

[77] K. M. Mohamed, M. C. Bettle, A. G. Gerber, and J. W. Hall, "Optimization study of large-scale low-grade energy recovery from conventional Rankine cycle power plants," *International Journal of Energy Research*, vol. 34, no. 12, pp. 1071–1087, 2009.

[78] B. Liu, P. Rivière, C. Coquelet, R. Gicquel, and F. David, "Investigation of a two stage Rankine cycle for electric power plants," *Applied Energy*, vol. 100, pp. 285–294, Dec. 2012.

[79] Y. Ying and E. J. Hu, "Thermodynamic advantages of using solar energy in the regenerative Rankine power plant," *Applied Thermal Engineering*, vol. 19, pp. 1173–1180, Nov. 1999.

[80] K. Chua, S. Chou, and W. Yang, "Advances in heat pump systems: A review," *Applied Energy*, vol. 87, pp. 3611–3624, Dec. 2010.

[81] E. Neal, "Heat pumps - applications for heating conservation and heat recovery," *Progress in Energy and Combustion Science*, vol. 9, no. 2, 1983.

[82] P. Byrne, J. Miriel, and Y. Lenat, "Experimental study of an air-source heat pump for simultaneous heating and cooling – Part 2: Dynamic behaviour and two-phase thermosiphon defrosting technique," *Applied Energy*, vol. 88, pp. 3072–3078, Sept. 2011.

[83] P. Byrne, J. Miriel, and Y. Lenat, "Experimental study of an air-source heat pump for simultaneous heating and cooling – Part 1: Basic concepts and performance verification," *Applied Energy*, vol. 88, pp. 1841–1847, May 2011.

[84] S.-H. Yang and J. Y. Rhee, "Utilization and performance evaluation of a surplus air heat pump system for greenhouse cooling and heating," *Applied Energy*, vol. 105, pp. 244–251, May 2013.

[85] D. Antonijevic and R. Heckt, "Heat pump supplemental heating system for motor vehicles," *Proceedings of the Institution of Mechanical Engineers, Part D: Journal of Automobile Engineering*, vol. 218, pp. 1111–1115, Oct. 2004.

[86] S. B. Riffat and X. Ma, "Thermoelectrics: a review of present and potential applications," *Applied Thermal Engineering*, vol. 23, pp. 913–935, June 2003.

[87] M. Zebarjadi, K. Esfarjani, M. S. Dresselhaus, Z. F. Ren, and G. Chen, "Perspectives on thermoelectrics: from fundamentals to device applications," *Energy & Environmental Science*, vol. 5, no. 1, p. 5147, 2012.

[88] R. J. Mehta, Y. Zhang, C. Karthik, B. Singh, R. W. Siegel, T. Borca-Tasciuc, and G. Ramanath, "A new class of doped nanobulk high-figure-of-merit thermoelectrics by scalable bottom-up assembly.," *Nature materials*, vol. 11, pp. 233–40, Mar. 2012.

[89] K. Biswas, J. He, I. D. Blum, C.-I. Wu, T. P. Hogan, D. N. Seidman, V. P. Dravid, and M. G. Kanatzidis, "High-performance bulk thermoelectrics with all-scale hierarchical architectures.," *Nature*, vol. 489, pp. 414–8, Sept. 2012.

[90] F. Felgner, L. Exel, and G. Frey, "Model-Based Design and Validation of Waste Heat Recovery Systems," in *IEEE Advances in Energy Conversion*, pp. 265–270, 2012.

[91] D. M. Rowe, "Applications of nuclear-powered thermoelectric generators in space," *Applied Energy*, vol. 40, pp. 241–271, 1991.

[92] E. D. Case, "Thermal Fatigue and Waste Heat Recovery via Thermoelectrics," *Journal of Electronic Materials*, vol. 41, pp. 1811–1819, Apr. 2012.

[93] Y. Hikage, S. Masutani, T. Sato, S. Yoneda, Y. Ohno, Y. Isoda, Y. Imai, and Y. Shinoharam, "Thermal Expansion Properties of Thermoelectric Generating Device Component," in *International Conference on Thermoelectrics*, pp. 1–5, 2007.

[94] J. D'Angelo, T. Hogan, and J. D'Angelo, "Long term thermoelectric module testing system.," *The Review of scientific instruments*, vol. 80, p. 105102, Oct. 2009.

[95] F. Ritz and C. Peterson, "Multi-mission radioisotope thermoelectric generator (MMRTG) program overview," *Aerospace Conference, 2004. ...*, 2004.

[96] G. Min and D. M. Rowe, "Experimental evaluation of prototype thermoelectric domestic-refrigerators," *Applied Energy*, vol. 83, pp. 133–152, Feb. 2006.

[97] T. Furue, T. Hayashida, Y. Imaizumi, T. Inoue, K. Nagao, A. Nagai, I. Fujii, and T. Sakurai, "Case study on thermoelectric generation system utilizing the exhaust gas of interal-combustion power plant," in *Thermoelectrics, 1998. Proceedings ICT 98. XVII International Conference on*, no. 1, pp. 473–478, 1998.

[98] K. Yazawa, Y. R. Koh, and A. Shakouri, "Optimization of thermoelectric topping combined steam turbine cycles for energy economy," *Applied Energy*, vol. 109, pp. 1–9, Sept. 2013.

[99] S. Yamaguchi, N. Kondoh, I. Yonenaga, Y. Hasegawa, and T. Eura, "New Proposal of High Temperature Thermoelectric Conversion In Power Plant," in *1999. Eighteenth International Conference on Thermoelectrics*, pp. 1–4, 2004.

[100] N. Kondo and S. Yamaguchi, "New proposal of medium temperature thermoelectric conversion in power plant," in *Thermoelectrics, 1999. Eighteenth International Conference on*, no. 1 999, pp. 88–91, 1999.

[101] C. Wu, "Analysis of Waste-Heat Thermoelectric Power Generators," *Applied Thermal Engineering*, vol. 16, no. 1, pp. 63–69, 2003.

[102] H. Xiao, K. Qiu, X. Gou, and Q. Ou, "A flameless catalytic combustion-based thermoelectric generator for powering electronic instruments on gas pipelines," *Applied Energy*, vol. 112, pp. 1161–1165, Dec. 2013.

[103] V. Leonov and R. J. M. Vullers, "Wearable electronics self-powered by using human body heat: The state of the art and the perspective," *Journal of Renewable and Sustainable Energy*, vol. 1, no. 6, p. 062701, 2009.

[104] L. Francioso, C. De Pascali, I. Farella, C. Martucci, P. Cretì, P. Siciliano, and a. Perrone, "Flexible thermoelectric generator for ambient assisted living wearable biometric sensors," *Journal of Power Sources*, vol. 196, pp. 3239–3243, Mar. 2011.

[105] R. Richter and A. Eder, "Vehicle Having A Thermoelectric Generator," 2009.

[106] K. Nakajima and N. Wakabayashi, "Waste heat recovery system and thermoelectric conversion system," 2006.

[107] R. K. Stobart, A. Wijewardane, and C. Allen, "The Potential for thermo-electric devices in passenger vehicle applications," *SAE*, 2010.

[108] Y. Hsiao, W. Chang, and S. Chen, "A mathematic model of thermoelectric module with applications on waste heat recovery from automobile engine," *Energy*, vol. 35, pp. 1447–1454, Mar. 2010.

[109] H. Nagayoshi and T. Kajikawa, "Mismatch Power Loss Reduction on Thermoelectric Generator Systems Using Maximum Power Point Trackers," *2006 25th International Conference on Thermoelectrics*, pp. 210–213, 2006.

[110] H. Nagayoshi, K. Tokumisu, and T. Kajikawa, "Evaluation of multi MPPT thermoelectric generator system," *2007 26th International Conference on Thermoelectrics*, pp. 318–321, June 2007.

[111] C. Yu and K. T. Chau, "Thermoelectric automotive waste heat energy recovery using maximum power point tracking," *Energy Conversion and Management*, vol. 50, pp. 1506–1512, June 2009.

[112] F. J. Lesage, R. Pelletier, L. Fournier, and E. V. Sempels, "Optimal electrical load for peak power of a thermoelectric module with a solar electric application," *Energy Conversion and Management*, vol. 74, pp. 51–59, Oct. 2013.

[113] G. Min and D. M. Rowe, "Improved model for calculating the coefficient of performance of a Peltier module," *Energy conversion and management*, vol. 41, pp. 1–9, 1999.

[114] M. Hodes, "Optimal pellet geometries for thermoelectric refrigeration," *IEEE Transactions on Components and Packaging Technologies*, vol. 30, pp. 50–58, Mar. 2007.

[115] C.-W. Cho, H.-S. Lee, J.-P. Won, and M.-Y. Lee, "Measurement and Evaluation of Heating Performance of Heat Pump Systems Using Wasted Heat from Electric Devices for an Electric Bus," *Energies*, vol. 5, pp. 658–669, Mar. 2012.

[116] S. Hava, R. Hunsperger, and H. Sequeira, "Monolithically Peltier-cooled laser diodes," *Journal of Lightwave Technology*, vol. 2, pp. 175–180, Apr. 1984.

[117] J. Li, B. Ma, R. Wang, and L. Han, "Study on a cooling system based on thermoelectric cooler for thermal management of high-power LEDs," *Microelectronics Reliability*, vol. 51, pp. 2210–2215, Dec. 2011.

[118] P. E. Phelan, V. A. Chiriac, and T. Y. T. Lee, "Current and future miniature refrigeration cooling technologies for high power microelectronics," *IEEE Transactions on Components and Packaging Technologies*, vol. 25, no. 3, pp. 356–365, 2002.

[119] I. Sauciuc, R. Prasher, J.-y. Chang, H. Erturk, G. Chrysler, C.-p. Chiu, and R. Mahajan, "Thermal Performance And Key Challenges for Future CPU Cooling Technologies," *IPACK*, pp. 1–12, 2005.

[120] Z. Tian, C. Chen, K. D. Choquette, and D. V. Plant, "30 Gb/s Direct Modulation of Holey VCSELs with Thermoelectric Cooling," *Conference on Lasers and Electro-Optics 2010*, vol. 2, p. CME3, 2010.

[121] D. Kondratiev and L. Yershova, "TE coolers computer simulation: incremental upgrading of rate equations approach," *6th European Workshop on Thermoelectrics*, pp. 1–8, 2001.

[122] H. Y. Zhang, Y. C. Mui, and M. Tarin, "Analysis of thermoelectric cooler performance for high power electronic packages," *Applied thermal engineering*, vol. 30, pp. 561–568, May 2010.

[123] I. Chowdhury, R. Prasher, K. Lofgreen, G. Chrysler, S. Narasimhan, R. Mahajan, D. Koester, R. Alley, and R. Venkatasubramanian, "On-chip cooling by superlattice-based thin-film thermoelectrics," vol. 4, no. April, pp. 235–238, 2009.

[124] H. Böttner and G. Chen, "A spects of Thin-Film Superlattice Thermoelectric Devices , and Applications," *Materials Science and Engineering: R: Reports*, vol. 31, no. March, pp. 211–217, 2006.

[125] D. Letz, "Semiconductor Device for Comprising an In-Chip Active Heat Transfer System," 2010.

[126] J. Jiang, G. V. Kaigala, H. J. Marquez, and C. J. Backhouse, "Nonlinear Controller Designs for Thermal Management in PCR Amplification," vol. 20, no. 1, pp. 11–30, 2012.

[127] E. Kotlyarov, P. D. Crom, and R. Voeten, "Some Aspects of Peltier-Cooler Optimization Applied for the Glove Box Air Temperature Control," pp. 1–5, 2011.

[128] M. Russel, D. Ewing, and C. Ching, "Characterization of a thermoelectric cooler based thermal management system under different operating conditions," *Applied Thermal Engineering*, vol. 50, pp. 652–659, Jan. 2013.

[129] S. Yamaguchi, "Power Plant," 2013.

[130] Y. Awashima and H. Yoshimoto, "Thermoelectric Power Generating Device and Power Generating System Using Said Thermoelectric Power Generating Device," 2010.

[131] J. Bass, "Stove Pipe Thermoelectric Generator," 2000.

[132] S. Chakraborty, "Industrial Thermoelectric Generator," 2008.

[133] S. Chakraborty and R. Karschnia, "Pipeline Thermoelectric Generator Assembly," 2008.

[134] P. Watts, "Thermoelectric Generator," 2009.

[135] M. Taheer, R. Dupree, P. Dong Fei, and D. Garner, "Thermoelectric Generator," 2007.

[136] J.-Y. Jang, Y.-C. Tsai, and C.-W. Wu, "A study of 3-D numerical simulation and comparison with experimental results on turbulent flow of venting flue gas using thermoelectric generator modules and plate fin heat sink," *Energy*, vol. 53, pp. 270–281, May 2013.

[137] K. Murata, "Exhaust Heat Power Generation Apparatus," 2004.

Appendices

Appendix A

Benson Load Calculation

This appendix details the Benson load calculations.

The Benson load for a thermal power plant assumes that the 30% of the rated input is required to maintain the plant and avoid complete plant shutdown. The calculations presented start by using the values for 100% and then back-calculate to obtain 30%.

At 100% load, the plant consumes 49.2kg/s of fuel producing $1285.5MW_{th}$ of thermal energy as the fuel has an assumed specific heat capacity value of 27MJ/kg.

$$Q_{in-Benson} = 0.3Q_{in} \tag{A.1}$$

$$Q_{in-Benson} = 1285.5 * 0.3 = 385.65MW_{th} \tag{A.2}$$

The flue gas exhaust energy is assumed to reduce along with the electrical parasitic load giving $19.74MW_{th}$ and $14.52MW_e$ respectively. The overall cycle efficiency of the plant drops to 35%. Hence the electrical power generated by the plant can be calculated in equation A.5.

$$Q_{plant} = Q_{in-Benson} - Q_{parasitic-electrical} - Q_{flue} \tag{A.3}$$

$$Q_{plant} = 385.65 - 14.52 - 19.74 = 351.4MW_{th} \tag{A.4}$$

$$Q_{electrical} = 0.35Q_{in-benson} = 135MW_e \tag{A.5}$$

From A.5, the thermal energy rejected from the plant can be deduced from equation A.6.

$$Q_{cond} = Q_{plant} - Q_{electrical} \tag{A.6}$$

$$Q_{cond} = 216MW_{th} \tag{A.7}$$

Since the original steam flow rate of the plant operating at 100% efficiency =273kg/s then the final steam flow rate with operating at the Benson load is assumed to be 30% giving 81.9kg/s.

A thermoelectric device driven at maximum power to obtain a temperature difference across the device of 75K is applied to the condenser. Assuming this results in a tem-

perature increase in the feedwater returning to the boiler of $60°C$ (since a portion of the temperature is lost in thermal resistance) then equation A.8 presents the thermal energy now returning to the boiler.

$$Q_{feedwater} = mCp\Delta T \tag{A.8}$$

$$Q_{feedwater} = 81.9 * 4182 * 60 = 20.55MW_{th} \tag{A.9}$$

Since the specific heat capacity of the fuel (C_{coal} supplied is 27MJ/kg then the reduction in fuel is shown in equation A.10.

$$m_{fuel-rate} = \frac{Q_{feedwater}}{C_{coal}} = 0.76kg/s \tag{A.10}$$

The conversion follows equation A.11 and then multiplied by the percentage of the year the plant is expected to run at the Benson load of 42.9%.

$$\frac{60£}{tonne} \rightarrow 3600seconds \rightarrow 24hours \rightarrow 365days \rightarrow 42.9\% \tag{A.11}$$

Hence, the final cost saving to the plant over the course of a year is therefore £622,331 per year. Over the course of a thirty year plant life the savings total to over £18 million. This figure does not account for the reduction in CO_2 as a result of less fuel being fired in the boiler.

Appendix B

Rankine Cycle Design Guide

The following section represents a design guide for the Rankine cycle test apparatus. Each of the components of the test apparatus are detailed and the operation of each part is explained.

B.1 Rankine Cycle Apparatus

This section is split into several subsections that describe the operation of system. The following parts are described: boiler, expansion valve, condenser, condensing coils, THP assembly and pump.

B.1.1 Boiler

The boiling unit is formed of a 300mm diameter vessel, 600mm length. There are nine ports placed on the vessel: 2 of $2\frac{1}{4}$" diameter for immersion heaters; 3 of 1" diameter for placement of sensors (temperature, float switch, pressure); 3 of 1" diameter for flow entry, exit and drain; and one of 1" diameter for a pressure relief valve (set to release at 3bar). This is shown in Figure B.1.

In order to generate steam from a water tank, standard immersion heaters were used due to their simplicity and it being a commonly available part. The immersion heater thermostat was removed and replaced with a large thermocouple connected to a heater controller to enable customised control over the heater. In the first iteration of the boiling unit,an immersion heater failed due to negative pressure causing the flange to crack.

B.1.2 Expansion Valve

In order to mimic the turbine stage of the Rankine cycle, restriction in the steam flow was introduced. This was achieved by using a gate valve in line with the boiler and condenser. The gate valve was selected as it allowed a greater aperture for steam flow adjustment in comparison to a ball valve.

Figure B.1: Boiler showing the expansion valve in red.

B.1.3 Condenser

Similar to the boiling unit construction, the condenser vessels is over 300mm diameter and 600mm length. There are eight ports on the vessel of 1" diameter: 2 for the chiller unit entry and exit, 2 for the vertical THP entry and exit, one for condensate exit and drain, 1 for power connections to be passed through, 1 for connection of the vacuum pump and one for connection of the pressure transducer. A ninth port is of $2\frac{1}{4}$" diameter size and provides connections into the condenser for thermocouples. On the second iteration of the condenser a further 2 ports were added to the lid for horizontal mounting of the THP to allow the entry and exit pipes to pass through. This is shown in Figure B.2.

In the first iteration of the Rankine cycle test apparatus there were several issues noted after analysis of the results. Initially it was clear that the condenser was not capable of

holding a constant pressure and there was an air leak. To counter this, all pipe fittings were switched to use compression fittings as the system contained fluid flow at both positive and negative pressures. The push-fit fittings used allowed air the leak in to the system from the atmosphere and therefore had to be replaced. Loctite thread sealant was also used to further reduce leaking. A neoprene gasket was added to the lid to ensure uniform seal. Thermocouple and power cabling was also identified as a source of leaking as air was sucked in over the lengths of cable that were fed inside both condenser and boiler. To remedy this a bespoke thermocouple feedthrough was designed and a specialised power feedthrough connector was purchased.

Sight tubes were also added to both the boiler and condenser units to allow for visual verification of system balance.

The vacuum pump used to reduce the pressure in the system was found to drop performance as vapour caused oil contamination. Regular replacement of oil is required to ensure optimum pump operation.

During pump-down of the system it is important to ensure all air is purged from the system. The system pressure should be reduced with the expansion valve open to connect both the boiler and the condenser. The pressure can be reduced to allow water to boil at $60°C$. The vacuum pump can now be switched off and isolated, and the boiler and condenser can be isolated from each other. The boiler can now be brought up to temperature to generate steam. In tandem, the condenser can further reduce in pressure by operating the vacuum pump. Once the condenser pressure has reached 45mbar-abs the pump can again be isolated from the condenser. The expansion valve between the boiler and condenser can be opened again and the system will further reduce in pressure and force any remaining air from the boiler and condenser to be removed.

B.1.4 Condensing Coils

The condensing coils were initially formed of 4x8mm diameter Copper pipes welded into a manifold at either end. The pipes were coiled together to enabled 20 meters of pipework to be placed inside the condenser. After initial tests thermal fatigue was found on the manifold this led to leakage from the loop into the condenser. This led to a temperature and pressure increase in the condenser and moving the system away from the desired operating conditions. To improve this, the condensing coils were redesigned using Thermex coiled brass pipes that drastically increased the surface area and improved the cooling capacity. The new design of coils also allowed for an alternate configuration of THP in the condenser from vertical to horizontal mounting.

Figure B.2: Condenser

B.1.5 THP Assembly

The first assembly of the THP system used a simple heat exchanger formed of soldered Copper pipes on the back of the flat plate. The soldering was done at uniform temperature in an Aga. To improve the heat transfer and from the heat exchanger to the THP a new labyrinth heat exchanger was designed however the design was improved to account for a gasket to be included as the combination of the condenser pressure being negative and the flow in the heat exchanger being positive the heat exchanger leaked.

At high steam temperatures and input powers to the THP, the assembly became unsoldered. Specifically, the cable connecting the positive lead to the first THP pellet was subjected to higher than expected temperatures and hence broke the contact. This was eliminated by sufficient insulation and control of the condenser temperature. To

achieve this insulation a quantity of Polyurethane foam was applied liberally to the THP assembly.

B.1.6 Pump

The first iteration of the Rankine cycle apparatus had the pump placed on a horizontal plane on the same level as the condensate exit loop from the condenser. However when the system was operating a sub-atmospheric pressure, cavitation occurred and the pump did not attain the positive pressure required. The issue was solved by moving the pump to below the condenser and the current test setup iteration has a pump head height of 2m. This solved the pump cavitation problem.

Further issues were found after the condenser was moved to top of the system. Since the new setup used a horizontal mounting of the THP and therefore the pipes for water flow and return had to be raised further above the system to connect to the pump at the base of the apparatus. This is shown in Figure B.3. It was found that an air lock developed at the top of the system as the pump didn't have enough capacity to displace the bubble. Ball valves were installed to relieve the trapped bubble and allow for the system to operate as desired.

Figure B.3: Top of condenser showing the placement of ball valves to remove air locks.

Appendix C

MATLAB Model for Rankine Plant

```
function rankine_model(t1,p2)

% saturation pressure for minimum
% superheated steam production
p1=XSteam('psat_T',t1);
t1=t1+0.1;
s1=XSteam('s_pT',p1,t1);
h1=XSteam('h_pT',p1,t1);

% saturation temperature of water
t2=XSteam('Tsat_p',p2);
% get saturated vapour entropy
s2g=XSteam('sV_p',p2);
% get saturated liquid entropy
s2f=XSteam('sL_p',p2);
% find x2 - portion of wet steam
% s2 = s2f + x2*(s2g-s2f)
x2=(s1-s2f)/(s2g-s2f);
% now for enthalpy
% h2 = h2f + x2*(h2g-h2f)
h2g=XSteam('hV_p',p2);
h2f=XSteam('hL_p',p2);
h2=h2f + x2*(h2g-h2f);

% Enthalpy to be removed in condenser
h_cond=h2-h2f;

% h4 is saturated liquid at
```

```
% condenser pressure
h4=h2f;

% determine TEG properties

t_water_in=17.5;
t_water_out=38.7;
teg_hot=46.3;
teg_cold=35.7;
mass_flow=0.0055;
p_elec_teg=20;
q_total=mass_flow*4.187*(t_water_out-t_water_in);
q_chiller_removed=0.2*4000*(10.19-9.71);
condenser_energy=h_cond-q_chiller_removed;



t_cold_teg=20; % cold temperature should be
% below saturation of condensate
dT_teg4a=10;
COP4a=4.90;
t4a=t_cold_teg+dT_teg4a;
s4a=XSteam('sL_T',t4a);
h4a=XSteam('hL_T',t4a);
CP4a=XSteam('CpL_T',t4a);
h4a2=(CP4a*(t4a-t2));
P4a=h4a2/COP4a;

dT_teg4b=20;
COP4b=2.90;
t4b=t_cold_teg+dT_teg4b;
s4b=XSteam('sL_T',t4b);
h4b=XSteam('hL_T',t4b);
CP4b=XSteam('CpL_T',t4b);
h4b2=(CP4b*(t4b-t4a));
P4b=h4b2/COP4b;

dT_teg4c=30;
COP4c=2.16;
```

```
t4c=t_cold_teg+dT_teg4c;
s4c=XSteam('sL_T',t4c);
h4c=XSteam('hL_T',t4c);
CP4c=XSteam('CpL_T',t4c);
h4c2=(CP4c*(t4c-t4b));
P4c=h4c2/COP4c;

t5=t4c; % assuming perfect coupling to water
CP=XSteam('CpL_T',t5);
% h5 is heat required from TEG to increase
% FW temperature by condensate +
% Thot of teg
h5=(CP*(t5-t2));
% Can now determine the Power input from
% TEG at COP
%P=h5/COPh;

% enthalpy to be removed in cooling loop
h_ct=h_cond-h5;

Qin_no_teg=CP*(t1-t2);
Qin_teg=CP*(t1-t5);
disp(Qin_no_teg);
disp(Qin_teg);

function cycle_efficiency=rankine_example(t1,p1)

clear all;
% set up initial conditions
t1=98.7;
p1=0.9;
s1=XSteam('s_pT',p1,t1);
h1=XSteam('h_pT',p1,t1);

% stage 2
% assume turbine is 100% efficient, s1=s2
s2=s1;
% define condenser pressure
p2=0.035;
```

```
% get saturated vapour entropy
s2g=XSteam('sV_p',p2);
% get saturated liquid entropy
s2f=XSteam('sL_p',p2);
% find x2 - portion of wet steam
% s2 = s2f + x2*(s2g-s2f)
x2=(s2-s2f)/(s2g-s2f);
% now for enthalpy
% h2 = h2f + x2*(h2g-h2f)
h2g=XSteam('hV_p',p2);
h2f=XSteam('hL_p',p2);
h2=h2f + x2*(h2g-h2f);

% First Expansion stage
% get pressure 8
% determine h8, assume s1=s2
p8=10;
h8=XSteam('h_ps',p8,s2);
% throttling at points 12 and 13
% only saturated liquid
h12=XSteam('hL_p',p8);

% Second Expansion stage
% get pressure 9
% determine x9, portion of wet steam
% s9 = s9f + x9*(s9g-s9f)
p9=1.1;
% saturdated liquid and vapour
s9f=XSteam('sL_p',p9);
s9g=XSteam('sV_p',p9);
x9=(s2-s9f)/(s9g-s9f);
% similarly for enthalpy
h9g=XSteam('hV_p',p9);
h9f=XSteam('hL_p',p9);
h9=h9f + x9*(h9g-h9f);
h6=h9f;h10=h9f;h11=h9f;

% Feedwater Heater 1
% comprises of streams 6,7,8,12
```

```
% sum of all streams =0
h7=h12;
y1=(h7-h6)/(h8-h12);

% Feedwater Heater 2
% h3 is saturated liquid at condenser pressure
h3=h2f;
% neglect pump work
h4=h3;
% full return flow through TEG
t4=XSteam('Tsat_p',p2);
% set dT of TEG
teg_dT=20;
% set COPh of TEG
COPh=2.90;
% set cold side of TEG
tc_teg=17;
% assume T5 is hot side of TEG, no losses in
% heat exchange
t5=tc_teg+teg_dT;
%t5=t4; % do not include teg
CP5=XSteam('CpL_T',t5);
% h5 is heat required from TEG to increase
% FW temperature by condensate +
% Thot of teg
h5=(CP5*(t5-t4));
% Can now determine the Power input from
%  TEG at COP
P=h5/COPh;

% now calculate FWH2
% comprises of 5,6,9,10,13
h13=h12;
y2=((h6-h5)-y1*(h13-h10))/(h9-h10);

% Condenser Energy Balance
% now determine h removed in condenser
% h in condenser= sum of 2 + 11
h_condenser=(1-y1-y2)*h2+(y1+y2)*h11;
```

```
Q_ct=h_condenser-h5;

% now calculate cycle efficiency
cycle_efficiency=((h1-h8)+(1-y1)*(h8-h9)+
(1-y1-y2)*(h9-h2)+P)/((h1-h7)+h5);
```